Università degli Studi di Ferrara

DOCTORAL COURSE IN

"EARTH AND MARINE SCIENCES (EMAS)"

CYCLE XXXVII

COORDINATOR: Prof. Paolo Ciavola

Halimeda bioherms from the pre-evaporitic Messinian successions of the Mediterranean area: a paleoenvironmental archive

Scientific/Disciplinary Sector (SDS) GEO/02

Candidate

Dr.ssa Passaseo Chiara

Supervisor

Prof. Michele Morsilli

Years 2021/2024

Table of contents

Extended abstract (English version)

Halimeda bioherms have recently garnered significant scientific attention, as they serve as valuable stratigraphic and paleoecological archives, similar to the more extensively studied coral reefs. *Halimeda*, a genus of calcareous green algae, abundant in tropical settings and also found in temperate ones, plays a crucial role in the production of $CaCO_3$-rich sediments through its rapid calcification process, driven by its unique internal structure. *Halimeda* bioherms are particularly notable for their discontinuous distribution, both in the modern oceans and in the stratigraphic record. While *Halimeda* is well-documented across contemporary reefs in the tropical belt, large bioherms are restricted to certain regions, such as the Indonesian K-Bank, the Caribbean, and, notably, the Great Barrier Reef (GBR) in Australia, where they span over 6,000 km^2. *Halimeda* thrives across depths of 2 to 150 meters but is most prolific between 20 and 65 meters, where it builds bioherms that can tower up to 140 meters. While it prefers low-energy environments, it is also found in intertidal zones, often alongside seagrass and macroalgae, on sandy lagoon floors, and in deeper slope areas. A similarly discontinuous distribution is observed in the Miocene, with *Halimeda* bioherms documented exclusively in the lower pre-evaporitic Messinian of the Mediterranean Basin. The restricted occurrence of *Halimeda* bioherms in the Mediterranean during the Messinian raises the question of whether this unique distribution results from insufficient documentation in other regions or is driven by specific geological factors. Another underexplored aspect concerns the internal structure of these bioherms, as existing literature primarily focuses on their general size and locations. Detailed analyses of their taphonomy and sedimentological characteristics remain largely absent.

To answer these key questions, the study involved a comprehensive review of existing literature on *Halimeda* bioherms, from Modern to the Oligocene, integrated by new data on sedimentological and taphonomic features of three key regions in the Mediterranean: the Salento Peninsula on the Apulia Carbonate Platform, the Neogene Sorbas and Nìjar Basins in Spain, and the Neogene Heraklion Basin in Crete. These regions were strategically selected based on their geographical distribution—eastern, central, and western Mediterranean—forming a natural transect that captures variability across different areas.

The study aimed to investigate the presence and development of *Halimeda* bioherms during the Messinian, with particular focus on their depositional environments, facies distribution, taphonomic characteristics and internal organization. Field campaigns across these regions involved detailed stratigraphic measurements, reconstruction of depositional geometries and systematic sample collection. Successively, a comparison was also carried out with similar deposits from other time intervals. The main goal of this thesis was to

investigate how *Halimeda* bioherms, predominantly found in the mesophotic zone and deeper waters during both the Messinian and the Modern, are influenced by their relative position within specific depositional settings, and to identify the key factors governing their formation and distribution.

Field observations revealed that *Halimeda* bioherms in southeastern Spain and the Heraklion Basin developed in similar mixed carbonate-siliciclastic depositional settings, forming both large, isolated mounds and extensive beds on ramp systems. In contrast, the smaller *Halimeda* bioherms in the Salento Peninsula formed in a pure carbonate-dominated environment along the slope of a fringing to barrier reef system. The *Halimeda* bioherms across all three regions exhibited similar facies, predominantly characterized by *Halimeda* rudstone-floatstones, and scattered *Halimeda* boundstones, along with encrusting organisms such as coralline algae, serpulids, and acervulinids.

In the comparison of the three study areas distinct environmental and geological factors were identified as key influences on the development of *Halimeda* bioherms and *Halimeda*-rich beds during the pre-evaporitic Messinian. In this context, we explore the connection between the presence of *Halimeda* bioherms and nutrient inputs, driven by both geological and hydrodynamic factors. This association has been widely documented in modern analogues, such as the Great Barrier Reef.

For the *Halimeda* bioherms of the Salento Peninsula, the present data suggest that their development is linked to external nutrient inputs, likely derived from upwelling currents influenced by the occurrence of internal waves. Upwelling currents were extensively documented throughout the Tortonian in the Mediterranean, particularly through the deposition of phosphatic hardgrounds. In the Salento area, the hardground "Aturia level" records upwelling conditions during the Tortonian. Although no direct evidence for such currents exists in the Messinian, we hypothesize that nutrient-rich upwelling could have continued, influencing the development of *Halimeda* bioherms. Given that the Salento area was located at the southernmost tip of the Apulia Carbonate Platform, far from the continental area, external nutrient inputs—likely driven by upwelling or internal waves—were necessary to support the flourishing of the bioherms. However, as the Messinian Salinity Crisis (MSC) approached, the availability of these external nutrient sources gradually diminished, leading to more restricted environmental conditions, also influenced by temperature and salinity fluctuations.

Fieldwork in southeastern Spain primarily focused on comparing and analyzing existing *Halimeda* accumulations, rather than on the collection of new data. Unlike in the Salento Peninsula, *Halimeda* accumulations in Spain are more abundant and significantly

larger in scale. Two distinct occurrences of *Halimeda* were identified along the Messinian ramps, including both mounds and *Halimeda*-rich beds. The textures observed in these beds are similar to those found in Salento, including rudstone, floatstone, and boundstone lenses, with a mixed carbonate and terrigenous matrix. In addition, numerous thin clayey and marly layers were recorded within the measured sections. The observed differences compared to the Salento Peninsula can be attributed to the proximity of prominent mountain chains in Spain, which resulted in a considerable influx of freshwater and siliciclastic material into the depositional environment. Furthermore, the input of nutrient-rich waters from the Atlantic, channeled into the Mediterranean via the Betic Corridor, likely enhanced the local hydrodynamic conditions, further contributing to the development of these accumulations.

In Crete, previous literature only documented a small, isolated *Halimeda* mound along a ramp system. The new stratigraphic sections measured in Crete revealed additional *Halimeda* bioherms, significantly enriching the existing fossil documentation of these bioconstructors. In fact, recent fieldwork played a crucial role in discovering new outcrops and uncovering differences across the deposits. It became clear that *Halimeda*-rich beds are much more common and abundant than mounds. The textures are similar to those observed in Spain, with rudstone, floatstone, and lenses of boundstone. The matrix is mixed, carbonate-siliciclastic, with frequent occurrences of thin marl and clay layers. Similarly, to Spain, the tectonic context plays a key role in controlling bioherm development. The Heraklion Basin, a graben surrounded by pre-existing mountain chains, facilitated a substantial influx of terrigenous sediments, enriching the nutrient supply and creating favorable conditions for the development of *Halimeda* bioherms.

In conclusion, in southeastern Spain and Crete, the nutrient supply for *Halimeda* bioherms seems to have been more strongly influenced by regional tectonics and the surrounding geological context than by hydrodynamic interactions, as in the Salento Peninsula. The new outcrops discovered in Crete have provided valuable insights into their distribution and development during the Messinian, contributing to a deeper understanding the role of *Halimeda* in past marine ecosystems.

The concentration of *Halimeda* bioherms in the Mediterranean during the lower Messinian is probably due to the region's semi-enclosed nature, which created favorable conditions for growth, including restricted oceanic connection, optimal temperature and salinity ranges, and high salinity levels that may have acted as refugia for some organisms like *Halimeda*. The onset of the Messinian Salinity Crisis (MSC) further intensified these conditions, contributing to the decline of *Halimeda* bioherms. Moreover, the apparent absence of *Halimeda* bioherms outside the Mediterranean in this stratigraphic interval is

probably due to limited documentation and research in other regions, which could have led to an underestimation of their presence.

These findings highlight the importance of continued research on *Halimeda* bioherms, given their critical role in carbonate production in both modern and fossil settings. Gaining deeper insight into these systems is essential for reconstructing past marine environments and their dynamics.

Abstract esteso (versione italiana)

Le bioerme ad *Halimeda* hanno recentemente attirato l'attenzione della comunità scientifica, poiché rivestono il ruolo di preziosi archivi stratigrafici e paleoecologici, similmente alle più studiate biocostruzioni a coralli. *Halimeda*, un genere di alghe verdi calcaree abbondante in ambienti tropicali e comune anche in quelli temperati, svolge un ruolo cruciale nella produzione di sedimenti ricchi di $CaCO_3$, attraverso un rapido processo di calcificazione che avviene nella sua peculiare struttura interna. Le bioerme ad *Halimeda* sono particolarmente notevoli per la loro distribuzione discontinua, sia negli oceani moderni che nel record stratigrafico. Sebbene Halimeda sia ben documentata nei reef tropicali, le grandi bioerme sono circoscritte a determinate regioni, come la K-Bank indonesiana, i Caraibi e, in particolare, la Grande Barriera Corallina (GBR) in Australia, dove si estendono su oltre 6.000 km². *Halimeda* si sviluppa a profondità che vanno da 2 a 150 metri, trovando il suo habitat ideale tra i 20 e i 65 metri, dove forma bioerme che possono raggiungere i 140 metri di altezza. Sebbene prediliga ambienti a bassa energia, si trova anche in zone intertidali, spesso accanto a praterie di fanerogame marine e macroalghe, sui fondali sabbiosi delle lagune e nelle aree più profonde delle scarpate.

Una distribuzione altrettanto discontinua si osserva nel Miocene, con bioerme ad *Halimeda* documentate esclusivamente nel Messiniano inferiore, prima della fase evaporitica, nel Bacino Mediterraneo. La limitata diffusione delle bioerme ad *Halimeda* nel Mediterraneo durante il Messiniano solleva la questione se questa distribuzione unica sia il risultato di una documentazione insufficiente in altre regioni o se sia causata da specifici fattori geologici. Un altro aspetto ancora poco indagato riguarda la struttura interna di queste bioerme, poiché la letteratura esistente si concentra principalmente sulla loro dimensione e localizzazione generali. Le analisi dettagliate della loro tafonomia e delle caratteristiche sedimentologiche sono ancora largamente assenti.

Per rispondere a queste domande chiave, questo lavoro ha comportato una revisione completa della letteratura esistente sulle bioerme ad *Halimeda*, dal periodo moderno all'Oligocene, integrata da nuovi dati sulle caratteristiche sedimentologiche e tafonomiche in tre regioni chiave nel Mediterraneo: la Penisola Salentina sulla Piattaforma Carbonatica Apula, i Bacini Neogenici di Sorbas e Nìjar in Spagna, e il Bacino Neogenico di Heraklion a Creta. Queste regioni sono state selezionate strategicamente in base alla loro distribuzione geografica—Mediterraneo orientale, centrale e occidentale—costituendo un transetto naturale che riflette la variabilità tra le diverse aree.

L'obiettivo di questo studio è stato quello di esaminare la presenza e lo sviluppo delle bioerme ad *Halimeda* durante il Messiniano, con particolare attenzione agli ambienti

deposizionali, alla distribuzione delle facies, alle caratteristiche tafonomiche e all'organizzazione interna. Durante le campagne sul campo effettuate in queste regioni sono state eseguite misurazioni stratigrafiche dettagliate, con particolare riguardo alla ricostruzione delle geometrie di deposizione e alla raccolta sistematica di campioni. Successivamente, è stata eseguita una comparazione con depositi simili di altri intervalli temporali. L'obiettivo principale di questa ricerca è stato indagare come le bioerme ad *Halimeda*, che si trovano principalmente nella zona mesofotica e in acque più profonde durante sia il Messiniano che l'epoca moderna, siano influenzate dalla loro posizione relativa all'interno di ambienti deposizionali specifici e identificare i fattori chiave che regolano la loro formazione e distribuzione.

Le osservazioni sul campo hanno rivelato che le bioerme ad *Halimeda* nel sud-est della Spagna e nel Bacino di Heraklion si sono sviluppate in ambienti deposizionali misti carbonatico-silicoclastici, formando sia grandi mound isolati che letti estesi in sistemi di rampa. Al contrario, le piccole bioerme ad Halimeda della Penisola Salentina si sono formate in un ambiente puramente carbonatico lungo la scarpata di un sistema di *fringing to barrier reef*. Le bioerme ad *Halimeda* in tutte e tre le regioni hanno presentato facies simili, caratterizzate prevalentemente da tessiture *rudstone-floatstone* e da lenti di *boundstone*, associate a organismi incrostanti come alghe coralline, serpulidi e acervulinidi.

Nel confronto delle tre aree di studio, sono stati identificati i principali fattori di controllo, sia ambientali che geologici, nello sviluppo delle bioerme e dei *rich beds* durante il Messiniano pre-evaporitico. In questo contesto, esploriamo la connessione tra la presenza di *Halimeda* e gli apporti di nutrienti, guidati sia da fattori geologici che idrodinamici. Questa associazione è ampiamente documentata negli analoghi moderni, come la Grande Barriera Corallina.

Per le bioerme della Penisola Salentina, i dati attuali suggeriscono che il loro sviluppo sia legato a input esterni di nutrienti, probabilmente trasportati da correnti di risalita influenzate dalla presenza di onde interne. Le correnti di risalita sono state ampiamente documentate durante il Tortoniano nel Mediterraneo, in particolare attraverso la deposizione di *hardgrounds* fosfatici. Nell'area del Salento, l'*hardground* "Livello ad Aturia" registra le condizioni di risalita durante il Tortoniano. Sebbene non vi sia evidenza diretta di tali correnti nel Messiniano, si ipotizza che la risalita di acque ricche di nutrienti possa essere proseguita, influenzando lo sviluppo delle bioerme in questione. Poiché l'area del Salento era situata all'estremo sud della Piattaforma Carbonatica Apula, lontano dalle aree continentali, gli apporti esterni di nutrienti—probabilmente generati da risalita o onde interne—erano necessari per sostenere la crescita delle bioerme. Tuttavia, con l'avvicinarsi della Crisi di

Salinità Messiniana (MSC), la disponibilità di queste risorse esterne è diminuita gradualmente, portando a condizioni ambientali più restrittive, ulteriormente influenzate da fluttuazioni di temperatura e salinità.

Le ricerche sul campo nel sud-est della Spagna si sono principalmente focalizzate sul confronto e l'analisi dei depositi ad *Halimeda*, piuttosto che sulla raccolta di nuovi dati. A differenza della Penisola Salentina, in Spagna sono più abbondanti e di scala significativamente maggiore. Sono state identificate due distinte occorrenze di Halimeda lungo sistemi di rampa messiniane, che includono sia *mound* che *rich beds*. Le tessiture osservate in questi letti sono simili a quelle riscontrate nel Salento, tra cui *rudstone*, *floatstone* e lenti di *boundstone*, con una matrice mista carbonatico-silicoclastica. Inoltre, sono state registrati numerosi sottili livelli argillosi e marnosi all'interno delle sezioni misurate. Le differenze osservate rispetto alla Penisola Salentina possono essere attribuite alla vicinanza di catene montuose prominenti in Spagna, che hanno determinato un considerevole afflusso di acqua dolce e materiale silicoclastico nell'ambiente deposizionale. Inoltre, l'apporto di acque ricche di nutrienti dall'Atlantico, canalizzate nel Mediterraneo tramite il Corridoio Betico, ha probabilmente migliorato le condizioni idrodinamiche locali, contribuendo ulteriormente allo sviluppo di questi accumuli.

Per quanto riguarda Creta, la letteratura precedente documentava un unico mound di *Halimeda* lungo un sistema di rampa che, tuttavia, veniva interpretato come risedimentato. Le nuove sezioni stratigrafiche misurate a Creta hanno rivelato ulteriori bioerme, arricchendo significativamente la documentazione fossile di questi biocostruttori. Il recente lavoro sul campo ha avuto un ruolo cruciale nella scoperta di nuovi affioramenti e nel chiarire le differenze tra i depositi. È stato evidente che i *rich beds* sono molto più comuni e abbondanti rispetto ai *mound*. Le tessiture osservate sono simili a quelle documentate in Spagna, con *rudstone*, *floatstone* e lenti di *boundstone*. La matrice è mista, carbonatico-silicoclastica, con frequenti strati sottili di marne e argille. Similmente alla Spagna, il contesto tettonico gioca un ruolo chiave nel controllo dello sviluppo delle bioerme. Il Bacino di Heraklion, un *graben* circondato da imponenti catene montuose, ha facilitato un notevole afflusso di sedimenti terrigeni, arricchendo la disponibilità di nutrienti e creando condizioni favorevoli per la proliferazione algale.

In conclusione, nel sud-est della Spagna e a Creta, la disponibilità di nutrienti per lo sviluppo di *Halimeda* sembra essere stata maggiormente influenzata dalla tettonica regionale e dal contesto geologico circostante, piuttosto che dalle interazioni idrodinamiche, come nel caso della Penisola Salentina, sebbene non si possano escludere completamente. I nuovi affioramenti scoperti a Creta hanno fornito informazioni cruciali sulla distribuzione e lo

sviluppo di *Halimeda* durante il Messiniano, contribuendo a una comprensione più approfondita del suo ruolo negli ecosistemi marini del passato.

La concentrazione delle formazioni a *Halimeda* nel Mediterraneo durante il Messiniano inferiore è probabilmente legata alla paleogeografia dell'area, che ha creato condizioni favorevoli alla crescita di questi biocostruttori. In particolare, fattori come uno scambio oceanico limitato, temperature e salinità ottimali hanno contribuito a configurare un ambiente ideale per il loro sviluppo. Inoltre, alti livelli di salinità potrebbero aver rappresentato un rifugio per questi organismi, causandone successivamente il loro declino con l'inizio della Crisi di Salinità Messiniana (MSC).

Questi risultati sollevano interrogativi sulla distribuzione delle bioerme ad Halimeda al di fuori del Mediterraneo durante il Messiniano inferiore. La loro presunta assenza potrebbe riflettere una limitata documentazione e ricerca in altre regioni, con una conseguente sottovalutazione della loro effettiva diffusione.

L'analisi condotta sottolinea la necessità di approfondire ulteriormente lo studio delle bioerme a *Halimeda*, il cui contributo alla produzione di carbonato risulta fondamentale sia negli ambienti moderni che in quelli fossili. Comprendere in dettaglio la distribuzione, la paleoecologia e le dinamiche di crescita di questi biocostruzioni è essenziale per affinare le ricostruzioni paleoambientali e i modelli deposizionali del Messiniano. Inoltre, una prospettiva comparativa con contesti extra-mediterranei potrebbe rivelare nuove evidenze sulla loro effettiva diffusione e sul loro ruolo negli ecosistemi marini del passato.

1. State of the Art

1.1 *Halimeda*: from algae to bioherms

Halimeda (J.V. Lamouroux, 1816), a green calcareous macroalgae belonging to the order Bryopsidales, plays a significant role in modern tropical marine environments. It is known for its ability to precipitate calcium carbonate ($CaCO_3$) in its segmented thalli, contributing substantially to carbonate sediment production. This capacity positions *Halimeda* as a crucial element in the development of marine bioherms, especially in tropical and subtropical waters.

Halimeda bioherms are biogenic structures formed predominantly by the accumulation of *Halimeda* segments, often interspersed with other carbonate-producing organisms like foraminifera and coralline algae. These bioherms serve as important contributors to carbonate platforms and reef systems, shaping the sedimentary architecture of tropical marine environments. In modern oceans, they are primarily distributed across the Indo-Pacific and Caribbean regions, where they contribute to the growth of carbonate sediments and influence the local geomorphology.

Halimeda (Lamouroux, 1812) is a genus of green algae belonging to the order of Bryopsidales, commonly found in shallow tropical marine environments (Fig. 1.1). This alga plays a crucial role in the production of sediments rich in calcium carbonate ($CaCO_3$), essential for the formation of coral reefs. *Halimeda* is characterized by a flexible body (thallus) from which numerous small, flattened leaf-like structures (segments) emerge. After the alga dies, these segments disaggregate and settle on the seafloor, forming thick accumulations called bioherms (Davies and Marshall, 1988). These structures can grow both vertically and laterally, forming substantial carbonate banks.

The significant contribution of *Halimeda* to carbonate sediment production (sand and mud) is largely due to the rapid calcification of its segments, followed by the filling of inter-utricular spaces with aragonite crystals (Multer, 1988a). Although *Halimeda* occupies a wide depth range, from 2 to 150 meters (Multer, 1988b), it finds optimal conditions between 20 and 65 meters, where it forms bioherms that can range from a few meters to an impressive 140 meters in height, as documented in the southwestern Caribbean (Hine et al., 1988).

This alga thrives in low-energy environments, though it is also found in the intertidal zone, often associated with seagrass and other macroalgae, on sandy lagoonal bottoms, and in deeper slope areas (Drew, 1983; Littler et al., 1985). In addition to being a primary producer

of carbonate sediment, *Halimeda* is an important food source for many herbivorous fish. For example, parrotfish primarily feed on *Halimeda*, although their preference depends on the alga's $CaCO_3$ content (Overholtzer and Motta, 1999; Hay et al., 1988; Paul and van Alstyne, 1988; Pennings and Paul, 1992).

Halimeda is unusual among macroalgae because it is both coenocytic (lacking cross-walls in its siphons) and calcareous. The coenocytic thallus suggests that *Halimeda* and other members of the Bryopsidales represent a distinct branch within the algal evolutionary tree. Additionally, having a calcified thallus gives *Halimeda* a richer fossil record compared to most benthic algae, which, due to their soft thalli, have left relatively few fossil traces (Hillis et al., 2001).

The term "bioherm" broadly refers to lenticular bodies or in-situ accumulations of organisms—typically invertebrates—that create a topographic relief compared to the surrounding seafloor and may display stratification. Specifically, *Halimeda* bioherms, are extensive carbonate accumulations dominated by the alga *Halimeda*. When describing the structures associated with *Halimeda* proliferation, various terms are used depending on the discipline involved. For example, "meadows" refer to a thin layer of living shrub-like algae, 10 to 30 cm high, densely or irregularly distributed at the water-sediment interface. This term is commonly used by biologists, ecologists, and phycologists to describe the algal community within its benthic habitat. The algae that form these structures are known as psammophytic, and they have a globular holdfast that anchors them within soft, unconsolidated sediment (Hillis-Colinvaux, 1980). In contrast, lithophytic species of *Halimeda* prefer hard substrates (Hillis-Colinvaux, 1980; Hillis, 1988) and are more common in reef facies. Both types shed aragonite segments that contribute to sediment production, but only psammophytic species build bioherms. While active modern bioherms are always covered by an algal meadow, not all algal meadows are necessarily associated with bioherms (Hillis, 1988).

Fig. 1.1. Living *Halimeda* individuals and *Halimeda* meadows on the outher shelf of Great Barrier Reef (Australia) (McNeil et al., 2016).

1.2 *Halimeda* bioherms distribution in present-day

Halimeda bioherms attracted significant scientific interest, particularly from geologists, during the 1970s and 1980s when seismic surveys in the Great Barrier Reef, Indonesia, and the Caribbean revealed their occurrence and associated internal structures.

Holocene bioherm descriptions were provided by Drew (1983), Drew and Abel (1985), Davies and Marshall (1985), Orme (1985), Drew and Abel (1988), Marshall and Davies (1988), Orme and Salama (1988), Searle and Flood (1988), Davies (2011), Webster et al.

(2012), McNeil et al. (2016, 2021, 2022), Webster et al. (2023), Szilagy et al. (2023), Reolid et al. (2024) for the Australian Great Barrier Reef, by Heyward et al. (1997), for Timor Sea (Australia), by Roberts et al. (1987, 1988) and Phipps and Roberts (1988) for the Indonesian K-Bank area, and by Hine et al. (1988) for the Caribbean (Fig. 1.2).

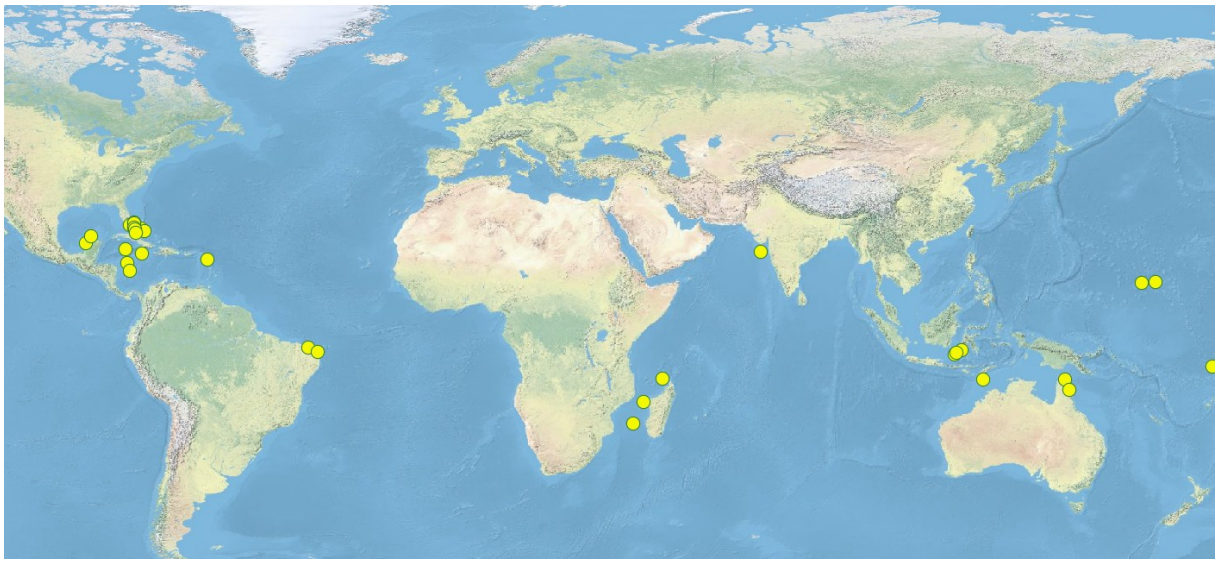

Fig. 1.2. Modern *Halimeda* bioherms global distribution from literature (yellow spots)

Kalukalukuang bank (K-bank), Indonesia

In the Indonesian K-Bank, Phipps and Roberts (1988) describe seismic profiles that reveal the presence of *Halimeda* bioherms, which appear as transparent units with clearly defined internal structures (Figs. 1.3, 1.4). These bioherms rest on a Pleistocene carbonate surface and exhibit significant variability in thickness and depth depending on their location. In the northern region of the bank, the bioherms are thinner, measuring approximately 20-30 meters, and occur at shallower depths of around 20 meters. In contrast, bioherms located along the southern margins are much thicker, reaching up to 50 meters or more, and are submerged at depths exceeding 100 meters.

In deeper waters, isolated bioherms have been observed at depths greater than 160 meters on the southeastern edge of the bank (Fig. 1.4). These features, however, may have become inactive due to insufficient light penetration at such depths. Along the western and southeastern margins of the bank, larger composite bioherms, formed by extensive *Halimeda* meadows that developed during the Holocene, can be observed. These broader bioherms are typically 10-15 meters thick, although some examples in the southwestern region can reach between 20 and 30 meters.

Seismic profiles indicate that the initial bioherms started as small, isolated mounds that later coalesced into larger, composite features. Signs of erosion from waves and currents are evident within the bioherms' internal reflectors. Despite the evidence of sediment transport and dynamic conditions, Phipps and Roberts (1988) found no evidence of coral reef development at these depths.

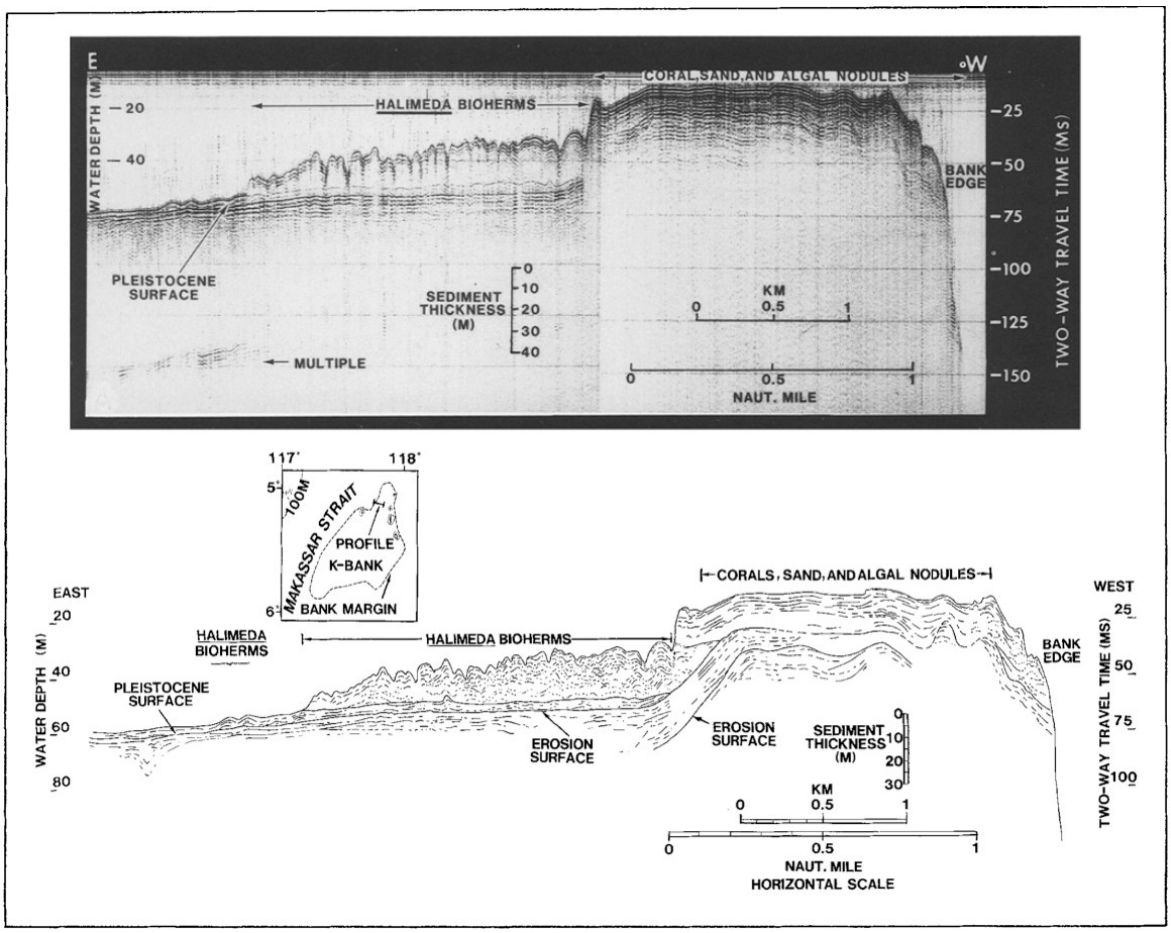

Fig. 1.3. Seismic profiles illustrating *Halimeda* bioherms in the northern sector of K-Bank, with thickness ranging from 20 to 30 meters. These bioherms are located at relatively shallower depths (Phipps and Roberts, 1988).

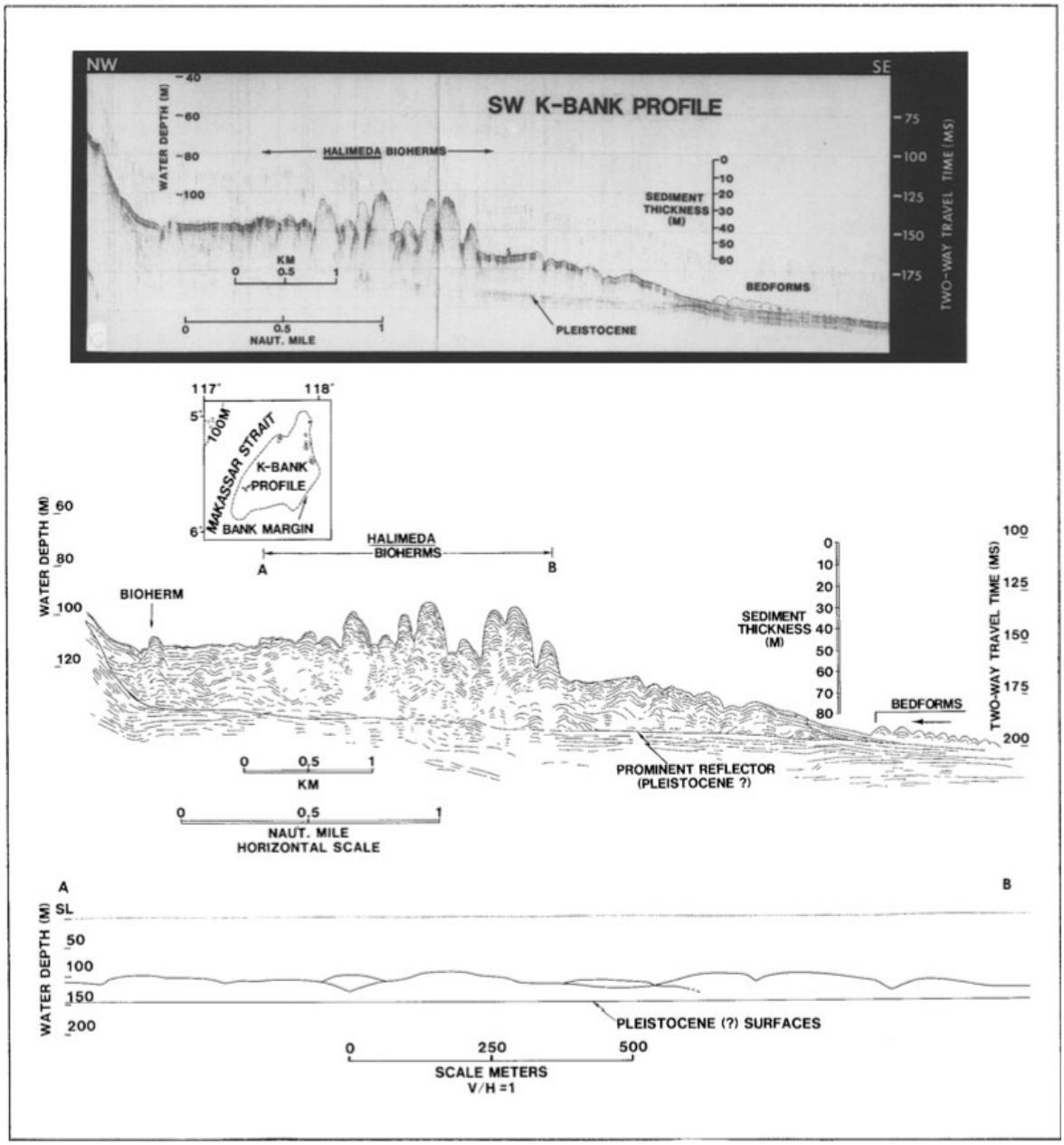

Fig. 1.4. Seismic profiles showing *Halimeda* bioherms in the southwestern part of K-Bank, where the thickness of the bioherms can exceed 50 meters. This variation in thickness is related to the depth and distribution within the bank's structure (Phipps and Roberts, 1988).

Miskito Channel (Nicaragua)

In the Miskito Channel, Nicaragua, Hine et al. (1988) discovered exceptional *Halimeda* bioherms, revealing the presence of numerous carbonate structures located on the Miskito Bank in the southern Caribbean Sea (Fig. 1.5). Interpretations of seismic reflection data indicate that some of these bioherms exceed 140 m in relief, marking the first documented occurrence of these green algal buildups in the Caribbean/Bahama Bank region.

The bioherms examined by the authors, form a nearly continuous band that borders the margins of the Miskito Channel, a shallow and open passage that is 125 km long. This channel, approximately 220 m deep, bisects the Miskito Bank, an important carbonate platform. In seismic profiles, the bioherms appear acoustically "soft" and reveal a local relief of 20-30 m, with the tops of these features located at a depth of about 40-50 m (Fig.1.5).

Facies consist of coarse, poorly cemented packstones/grainstones, dominated by largely intact, disarticulated *Halimeda* segments set in a poorly sorted sandy matrix. The significance of these bioherms and their overall extent in the Caribbean are not yet fully understood. This documentation adds to other Holocene evidence regarding *Halimeda* bioherms, providing valuable insights into the depositional patterns and environmental dynamics of carbonate platforms in the Caribbean context.

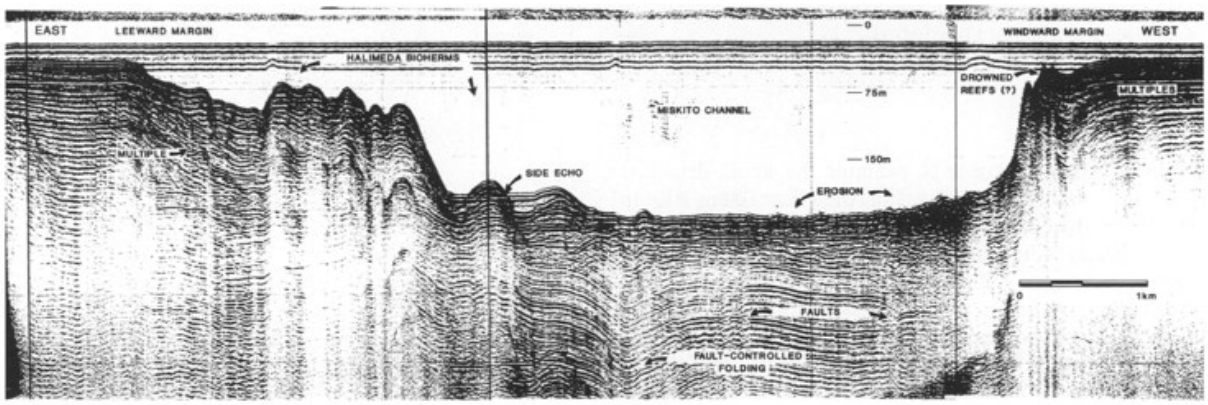

Fig. 1.5. This seismic profile line running E-W across the southern portion of the Miskito Channel, illustrates the low-gradient, eastern side with well-developed *Halimeda* bioherms and the steeper-gradient western side supporting reefal structures of unknown origin. The floor of the channel appears to be erosional along the western side (Hine et al., 1988).

Great Barrier Reef (Australia)

Concerning the Great Barrier Reef, the region where the presence of extensive *Halimeda* bioherms has been most thoroughly documented across the tropical belt, earlier seismic profile data from initial studies and mappings (Drew and Abel, 1985, 1988) have been supplemented by more recent data (McNeil et al., 2016). This approach ensures a continuously updated record of the areal extent of these *Halimeda* bioherms. To achieve this, McNeil et al. (2016) employed various methods to accurately map and redefine not only the bioherms distribution but also their morphology. Bathymetric data from airborne lidar (ALB) and multibeam surveys were used, integrated with existing seismic profiles and sediment sampling. A digital elevation model (DEM) was created using 3D visualization and GIS software to analyze the morphology of the bioherms, calculate the spatial extent,

and distinguish geomorphological features from corals and inter-reef channels. The historical distribution was compared with the new data to assess variations.

The work of McNeil et al. (2016) has provided significant updates on the morphology of *Halimeda* bioherms, revealing through bathymetric analysis that the forms and patterns do not correspond to the previous representation of parallel ridges and valleys prevalent in the literature (Fig. 1.6). According to the authors, previous descriptions have been compared to the lenticular morphology of Late Paleozoic phylloid algal mounds (Wray 1977; Drew and Abel 1988) and to the *Halimeda* deposits of the Upper Miocene coral reefs in the Sorbas Basin (Braga et al. 1996; Martín et al. 1997), which are considered analogous to their Holocene counterparts in the Great Barrier Reef (GBR). However, the *Halimeda* bioherms in the northern GBR appear to exhibit much more complex and variable morphologies over large spatial scales. They identified and described three new morphological subtypes, whose boundaries gradually blend into one another (Fig. 1.7). According to McNeil et al. (2016) these reticulate/annular patterns resemble the morphology of patch reefs observed in shallow lagoons, which are thought to be influenced by antecedent topography (e.g., Purdy 1974; Purdy and Winterer 2006) along with hydrodynamic influences (Fig. 1.8).

Sub-type	Description	Spatial Distribution	Proportion (%)	Example
Reticulate	High-relief, irregular ridges with sharp sinuous crests, complex honeycomb rugosity, non-circular	Proximal to reef and shelf break to east, grading into annulate zone	16	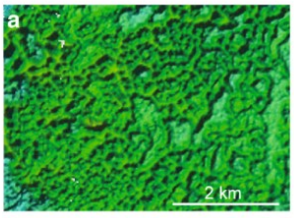
Annulate	Smooth, circular ring shapes, hollow centred with or without central pinnacle, often coalescing together with shared boundaries. Typically 200 to 250 m across from crest to crest, but can be up to 500 m across	More distal to reefs and shelf break, generally increasing in size westward	16	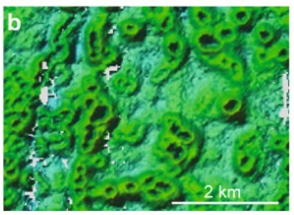
Undulate	Sinuous and wave-like, smooth crests, with low relief above surrounding sediment	Between and around annulate and reticulate zones, grading into surrounding inter-reef sediment	68	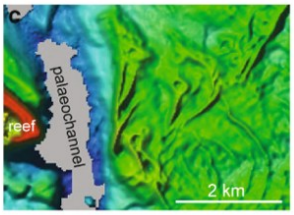

Fig. 1.6. Nomenclature, descriptions, spatial distributions, and representative examples of three morphological sub-types: (a) reticulate, (b) annulate, and (c) undulate (McNeil et al., 2016).

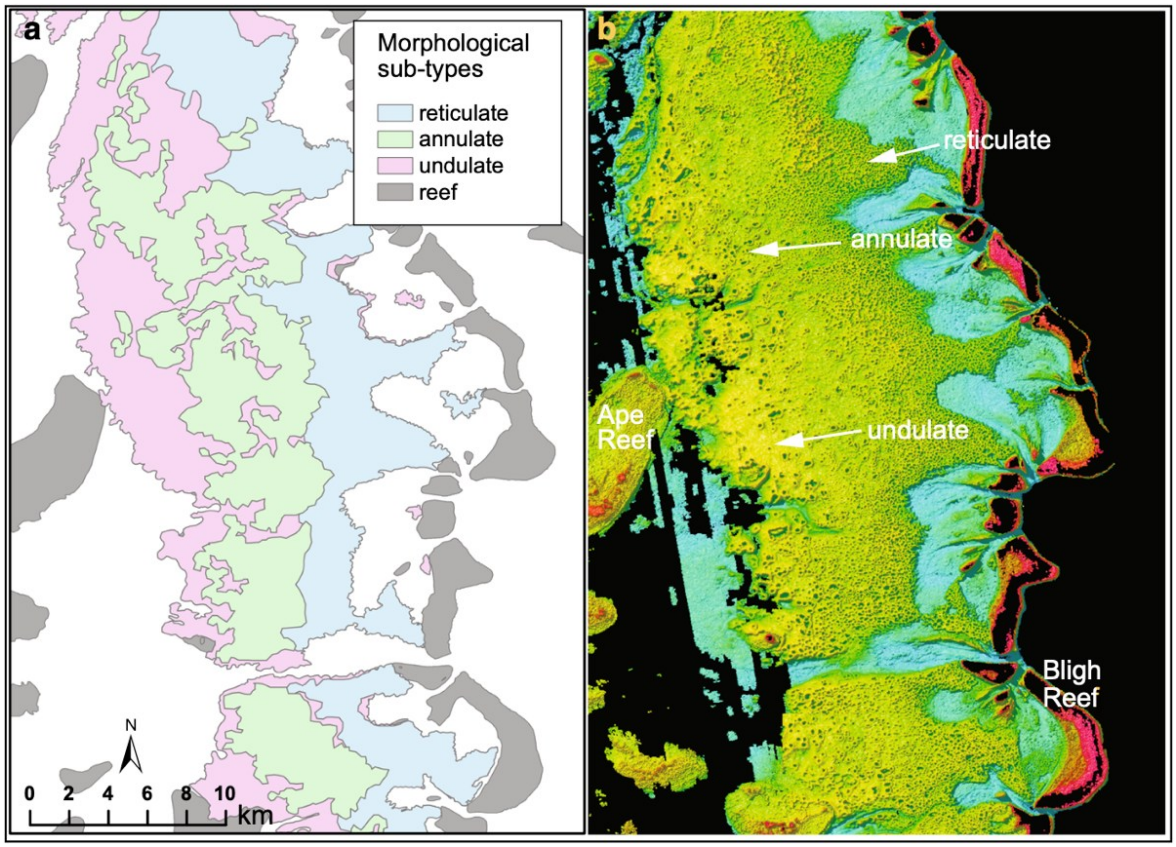

Fig. 1.7. The distribution of morphological sub-types on a large bioherm area in the GBR region shows that complex reticulate morphology is prevalent near reefs, transitioning into an annulate zone where the morphology becomes simpler and ring sizes increase westward. Additionally, smooth, low relief undulating morphology connects and encircles the reticulate and annulate sub-types, as depicted in the 25 m lidar data for the same area (McNeil et al., 2016).

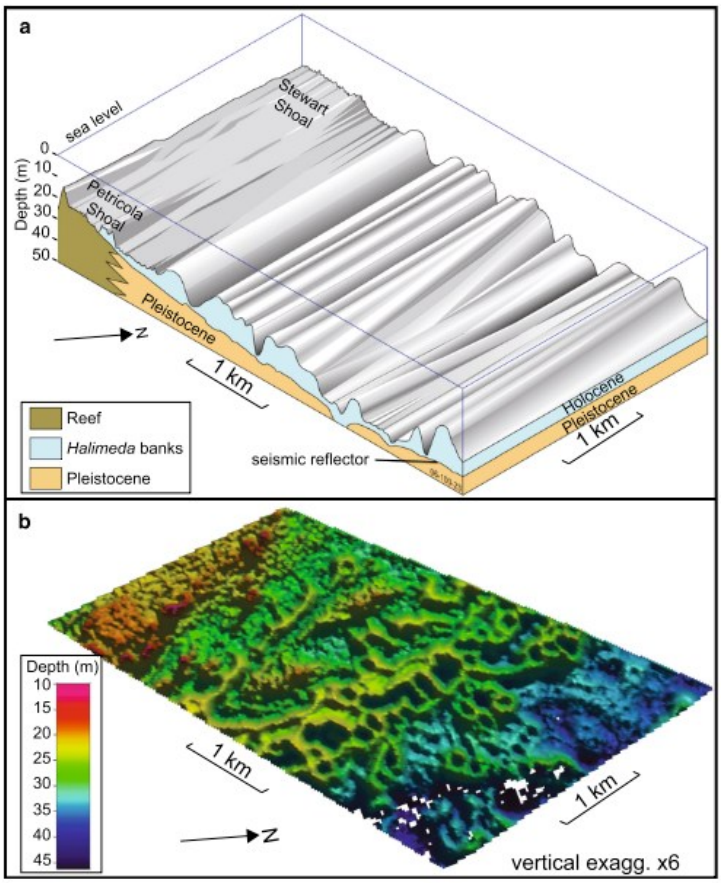

Fig. 1.8 - a) old concept diagram of bioherm morphology based on Mathews et al. (2007); b) new 3D view of lidar bathymetry for the same area illustrating their complex reticulate morphology (McNeil et al., 2016).

Recent studies on the reticulate patterns of Holocene coral reefs have shown that these morphologies can also form on flat erosional surfaces devoid of karst topography (Blakeway and Hamblin 2015; Schlager and Purkis 2015). These authors suggest that at small to intermediate scales (from meters to kilometers), reticulate patterns may be biologically controlled rather than substrate-controlled, with access to nutrients and protection from predation and erosion cited as possible driving factors of "biotic self-organization" (Schlager and Purkis 2015). For instance, modeling conducted by Blakeway and Hamblin (2015) demonstrated that collapsing organisms, such as branching *Acropora*, produce "cellular" (i.e., reticulate) reefs similar to the reticulate and annular morphology of the bioherms described here. However, according to McNeil et al. (2016) the relationship between the origin of *Halimeda* bioherms, accumulation, morphological variation, and the underlying antecedent topography remains poorly understood due to a lack of detailed geophysical surveys and sediment core data throughout the distribution of the bioherms. The bioherms are accumulating above a prominent seismic reflector (Fig. 3b), interpreted as the Pleistocene erosional unconformity ("Reflector A"; Orme et al. 1978; Davies and Marshall, 1985; Marshall and Davies, 1988), but the available data are insufficient to clarify any unequivocal relationship with antecedent topographic highs or pinnacles, or to test Blakeway and Hamblin's (2015) self-organization model against the growth and collapse of living *Halimeda*. Regardless of the processes controlling the origin of these morphological subtypes, it remains to be established whether these patterns are unique to the GBR; however, high-resolution bathymetric data from other locations in the modern context (e.g.,

Kalukalukuang Bank, Indonesia; Nicaraguan Rise; Big Bank Shoals, Timor Sea) are necessary.

These findings are crucial, as they not only enhance our understanding of modern bioherms but also provide insights for interpreting past models, suggesting that the complexity of *Halimeda* bioherms may reflect ecological and geomorphological processes that have occurred throughout geological history.

Recently, Reolid et al. (2024) updated the documentation on the morphotypes of *Halimeda* bioherms present in the Great Barrier Reef (GBR), in Tregrosse Bank. In addition, these authors described for the first time the internal organization of these mesophotic bioconstructions, providing essential information for comparison with the fossil bioherm systems addressed in this thesis (Fig. 1.9).

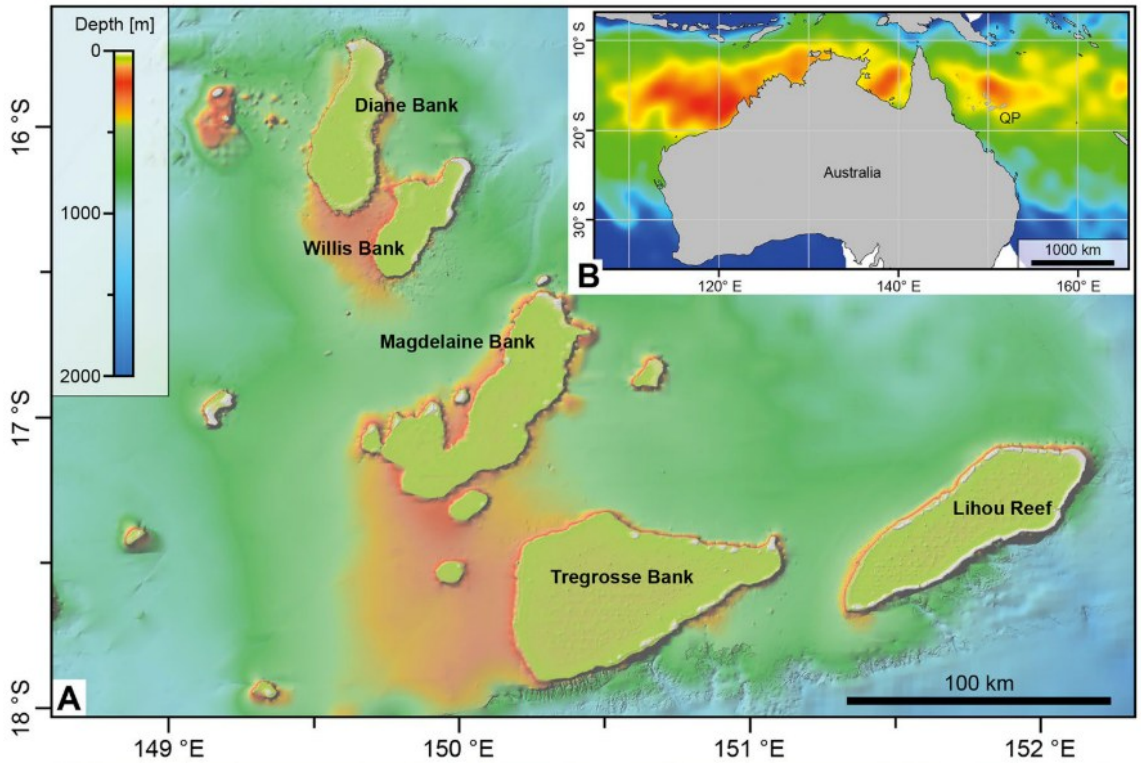

Fig. 1.9. Large emergent reefs and banks of the Queensland Plateau, northeastern Australia. B Cyclone intensity around Australia and the Queensland Plateau (warm colours: strong; blue colours: weak) (Reolid et al., 2024).

According to the authors, this work presents the morphology, internal structure, and in situ facies distribution of mesophotic *Halimeda* bioherms from the Queensland Plateau (NE Australia) and proposes the definition of a new bioherm morphotype. The studied *Halimeda* bioherms consist of cone-like buildups that can reach up to 500 m in diameter and heights

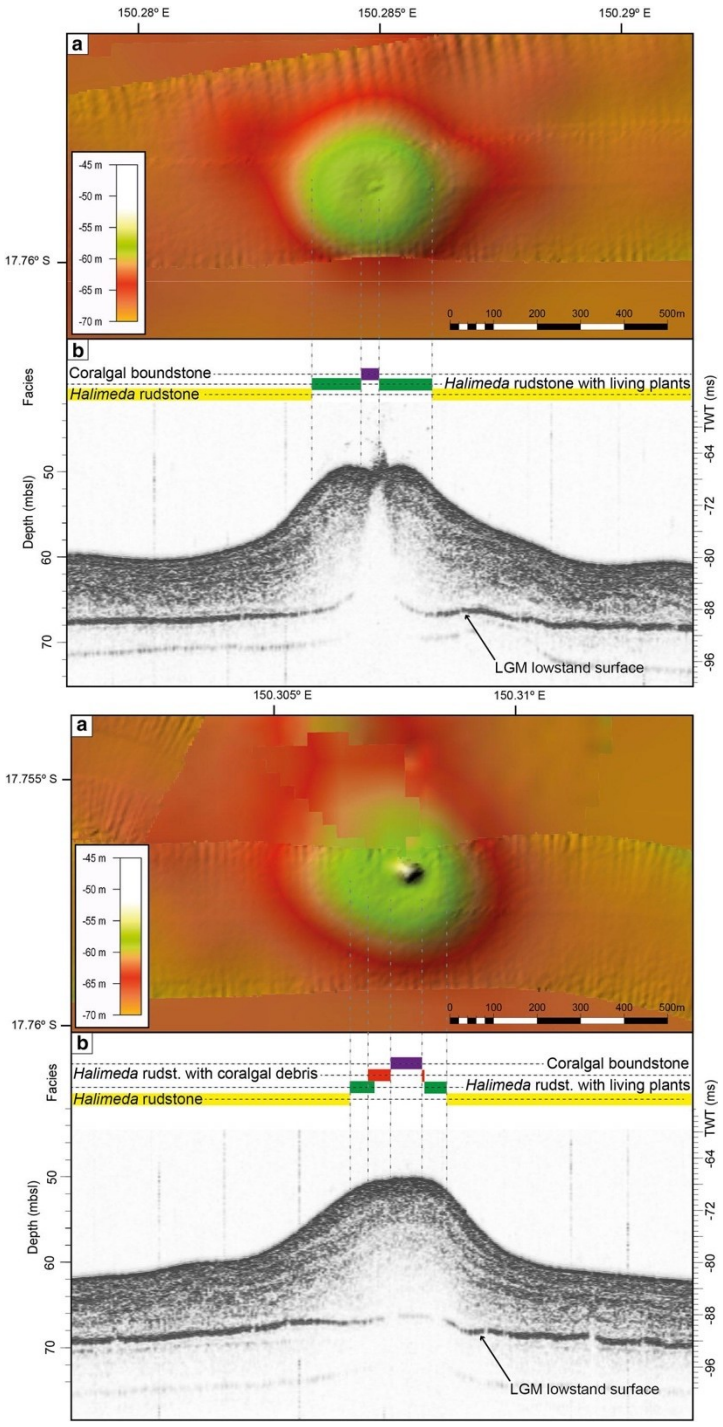

Fig. 1.10. Bioherm profiles East and West. A) Multibeam bathymetry map. B) Parasound profile with surface facies distribution. LGM: last glacial maximum (Reolid et al., 2024).

between 3 and 10 m relative to the local baseline, occurring at water depths between 10 and 70 mbsl, particularly abundant between 50 and 65 mbsl (Fig. 1.10).

Their internal structure consists of aggrading low-amplitude reflections at the core of the bioherm, interfingering with high-amplitude reflections to the flanks. The surface facies may be exclusively colonized by living *Halimeda* plants or exhibit up to four facies belts (Fig. 1.11), ranging from distal to proximal: *Halimeda* rudstone, *Halimeda* rudstone with living plants, *Halimeda* rudstone with coralgal debris, and coralgal boundstone (when present, it occupies the top of the bioherm). The *Halimeda* rudstone dominating the facies is recent but strongly reworked in its upper decimeters, with an average age of only a few decades. The development of *Halimeda* bioherms in the nutrient-poor waters of the Queensland Plateau is therefore unique compared to other *Halimeda* bioherms worldwide. Due to their distinct depth, geomorphology, complex internal structure, and surficial facies distribution, as well as their oligotrophic origin, the buildups of the Queensland Plateau represent a new *Halimeda* bioherm morphotype.

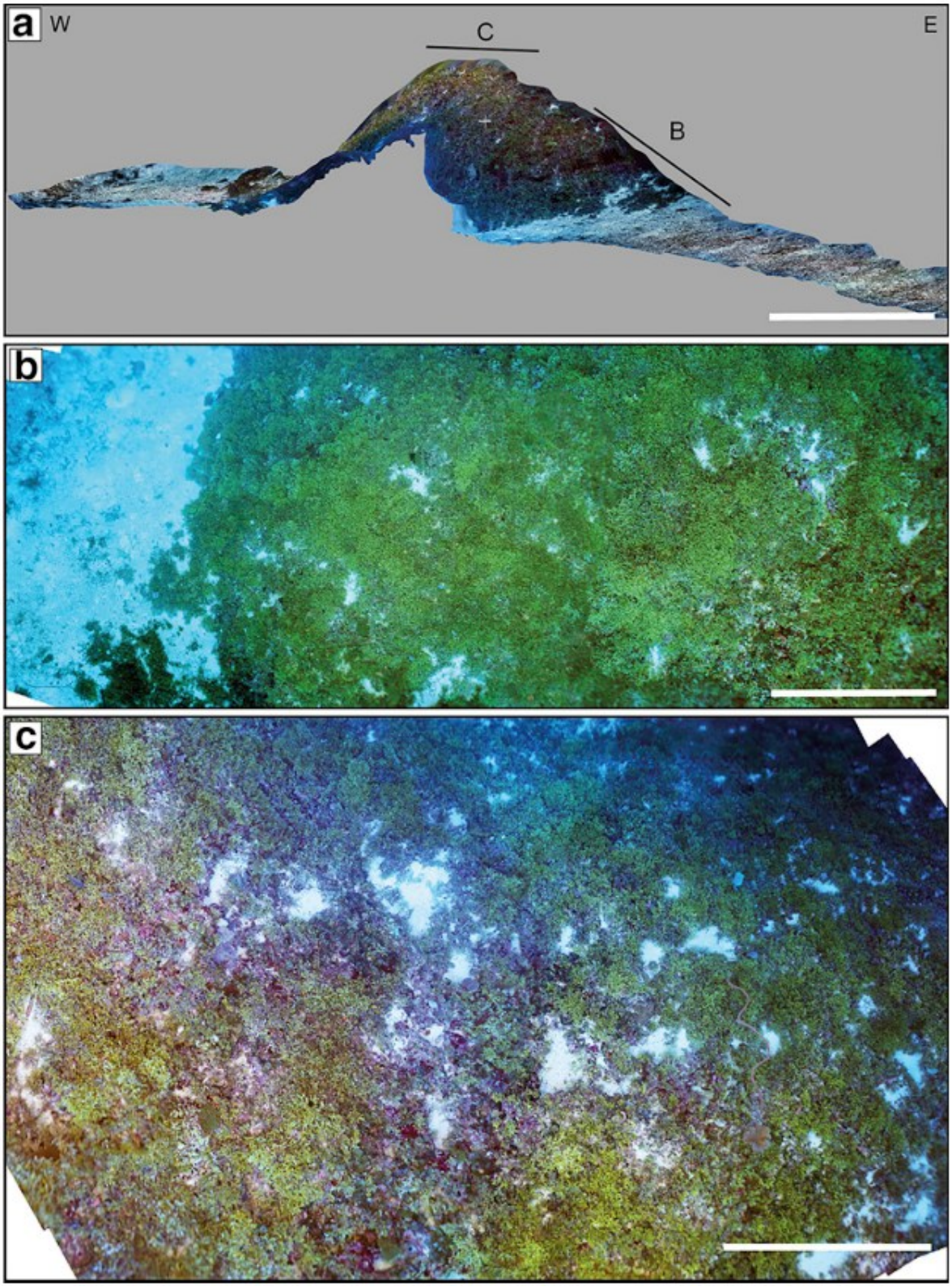

Fig. 1.11. The *Halimeda* Bioherm at Tregrosse Bank (Queensland Plateau). A) Photogrammetric model of the bioherm covered with living *Halimeda* plants. Scale bar: 5 m. B) Panorama showing the base of the bioherm, highlighting the transition from green living Halimeda plants to white-colored *Halimeda* rudstone sediment. C) Panoramic view of the top of the bioherm. Scale bar: 1 m (Reolid et al., 2024).

1.3 The Role of *Halimeda* in carbonate sediment production

An estimate of the Global Carbonate Budget has become necessary since the correlation between carbon dioxide levels and global temperatures in ice core records was established. Therefore, quantifying the components of the global carbon cycle has become a priority for defining climate system models (Rees, 2006). For this purpose, calculating the rate of production and accumulation of carbonate sediment from *Halimeda* bioherms since the Holocene is essential to quantify the total carbonate budget (Rees et al., 2007).

It is estimated that coral reefs have accumulated about 7.97 Gt of CaCO3 every 1000 years (0.8 Gt per year) over the last 10,000 years. Since *Halimeda* also contributes to carbonate production especially in shallow marine tropical facies, it is crucial to determine its contribution to the global carbonate budget. The first attempts were made in the early 1990s, estimating that current *Halimeda* bioherms produce around 0.15 Gt of $CaCO_3$ per year, assuming an aerial coverage of 5×10^4 km² (Milliman, 1993). Subsequently, this value was increased to 0.4 Gt per year based on estimates (Smith and Kinsey, 1976, Hillis, 1997), corresponding to about 83% of the production from coral reefs.

Currently, *Halimeda* bioherms in the Great Barrier Reef (GBR) grow vertically from 1 to 3 meters every thousand years over the last 5000 years and consist of about 75% $CaCO_3$, with the remaining 25% made up by terrigenous sediment (Marshall and Davies, 1988). These bioherms, confined to the outer platform, have thicknesses and growth rates comparable to those of coral reefs, but with a higher $CaCO_3$ content (Flood, 1984; Hillis, 1997).

To quantify the relationships between sediments from coral reefs and those from *Halimeda* bioherms, data from seismic profiles and cores previously published were used (Orme et al., 1978; Davies and Hopley, 1983; Davies et al., 1985; Davies and Marshall, 1985; Orme, 1985; Marshall and Davies, 1988; Orme and Salama, 1988; Wolanski et al., 1988; Rees et al., 2007).

The volume of $CaCO_3$ in *Halimeda* bioherms compared to the rest of the northern portion of the GBR has been estimated considering the areal extent and thickness of the bioherms, along with the density and porosity of the $CaCO_3$, and the percentage of carbonate present. Rees et al. (2007) argue that *Halimeda* bioherms contain carbonate sediment volumes comparable to those recorded in adjacent coral ribbon reefs, with a ratio of 1:1 for Cooktown and 1:4 for Lizard Island, with differences due to the thicknesses and extents of the bioherms between the two regions. This finding aligns with what was reported by Flood (1984), Hillis-

Colinvaux (1986), Marshall and Davies (1988), and Freile and Hillis (1997), who concluded that *Halimeda* bioherms contain more carbonate than the adjacent carbonate platforms.

In conclusion, *Halimeda* bioherms produce and accumulate carbonate sediment at rates comparable to those of coral reefs, but their importance in the global carbon cycles is currently underestimated and requires further study. It would also be useful to quantify the contribution of significant accumulations such as the Miskito Channel (Southwestern Caribbean Sea), K-Bank (Java Sea), and Big Bank Shoals (Timor Sea) to the global carbonate budget (Rees et al., 2007).

1.3 The stratigraphic record of *Halimeda*

Understanding the significance of *Halimeda* bioherms is essential due to their discontinuous distribution in the stratigraphic record, which underscores the need to comprehend the underlying controlling factors. This chapter examines their occurrence within the stratigraphic record, focusing on this critical aspect.

While the presence of *Halimeda* has been documented since the Upper Cretaceous (Conard and Rioult, 1977; Hillis-Colinvaux, 1980) and, possibly, as far back as the late Permian (Poncet, 1989), *Halimeda*-rich beds are scarce in the fossil record until the Holocene. These beds have been described in a few Paleocene and Eocene successions from regions such as Egypt, Morocco, Iraq, and Oman (Elliot, 1959; Dragastan and Soliman, 2002; Dragastan and Herbig, 2007). Additionally, Eocene to early Oligocene *Halimeda*-rich beds have been reported from core wells in the Basho Seamount of the Philippine Sea, though these accumulations do not represent true bioherms (Takayanagi et al., 2007). The largest and oldest known *Halimeda* bioherms, dated to the early Oligocene, have been described from subsurface data in Palawan, offshore of the South China Sea (Fournier et al., 2024) (Fig. 1.12).

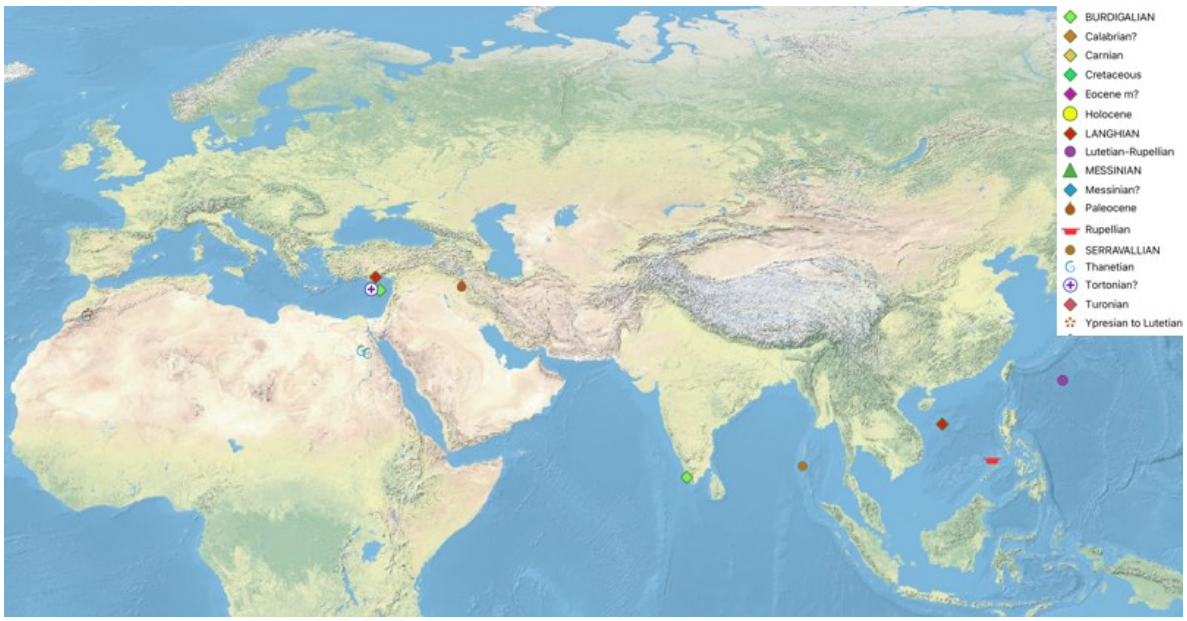

Fig. 1.12. The distribution of *Halimeda* in the sedimentary record, excluding those from the Messinian.

In terms of pre-Holocene *Halimeda* bioherms, the best-documented examples date back to the Late Miocene, particularly during the early Messinian, and are restricted to the Mediterranean Basin (Fig. 1.13). Significant bioherms have been identified in the Sorbas and Níjar basins of southeastern Spain (Mankiewicz, 1988, Franseen and Mankiewicz, 1991; Martín and Braga, 1994; Braga et al., 1996, Braga and Martín, 1996, Martín et al., 1997, Reolid et al., 2014). Other Upper Miocene *Halimeda* deposits are scattered in the Melilla Basin of Morocco (Cornée et al., 1996, Saint Martin and Cornée, 1996; Roger et al., 2000, Münch et al., 2001, Cunningham and Collins, 2002), the Bas-Chelif Basin of Algeria (Saint Martin et al., 1992, Cornée et al., 1996, 2004), the Salento Peninsula in southeastern Italy (Vescogni, 2000; Bosellini F. et al., 2001, 2002), and Crete Island (Brachert et al., 2007).

Fig. 1.13. The lower Messinian *Halimeda* bioherms distribution in the Mediterranean area.

Lower and Middle Miocene *Halimeda*-rich beds have also been identified in India (Xu et al., 2015; Ghosh et al., 2017; Sarkar et al., 2024), as well as in the Neogene Mut Basin in southern Turkey (Vescogni et al., 2014). However, these accumulations are not classified as bioherms (see Fig. 1.12). The *Halimeda* bioherms in the Messinian are considered the most abundant and well-documented, primarily located in the Mediterranean Basin. Despite the relatively rich documentation of *Halimeda* bioherms in the Miocene, the presence of *Halimeda* in Pliocene and Pleistocene deposits remains poorly documented due to incomplete data (Hinde, 1904, Guppy, 1887, Chapman and Mawson, 1906).

Finally, while the genus *Halimeda* comprises 33 extant species today, widely distributed in the tropical belt, its fossil record highlights key evolutionary events. Halimediform genera resembling modern *Halimeda* date back to the Ordovician, but the earliest confirmed fossil of the genus is *Halimeda soltanensis* from the Permian (Elliott, 1982; Poncet, 1989; Bucur, 1994). The genus reached its greatest pre-Cenozoic diversity during the Late Cretaceous and experienced a notable speciation burst in the Holocene (Hillis, 2001).

Halimeda seemingly survived the mass extinction event at the K-Pg boundary, displaying a high diversification in the Paleocene (Bassoullet et al., 1983; Flügel, 1988, 1991) and the production of new species during the Eocene (Fig. 1.12). Scattered evidence of the genus continues through the Oligocene, Miocene, Pliocene, and Pleistocene, although the alga is primarily present in sedimentary form. However, more detailed observations of *Halimeda* fragments within the sediments suggest the genus's continued importance. For instance, descriptions of *Halimeda*-rich layers in Miocene reef complexes of southeastern Spain indicate that they contributed approximately 20% of the slope sediments (Mankiewicz, 1988).

It is also evident that this speciation burst could be confused with intense data collection, as noted by Hillis (2001). According to this Author, a robust paleontological record depends on the quantity and quality of data, thorough research at appropriate sites, and skilled taxonomic analysis. Issues arise when recognizing microscopic features needed for species identification in fossil segments, which are often absent or poorly preserved. Even segment size and shape, typically well-preserved in fossil samples, may create identification problems due to phenotypic variability, resulting in misclassification at the species or genus level. There is also "preferential preservation," which depends on depositional environments and available hydrodynamic energy.

According to Hillis (2001), the phylogeny of *Halimeda* reveals two significant evolutionary events. The first is the division of the genus into two lineages, with the thallus morphology of the three main sections adapted to life in shifting sands (*Rhipsalis*), high-energy fore-reef environments (*Halimeda*), or more protected reef crevices (*Opuntia*). These functional adaptations likely arose early in the genus's history, with subsequent speciation following each lineage. The ability of Halimeda to colonize a wide range of environments compared to most other algae has allowed it to become an important component of tropical reef ecosystems, playing a critical role in reef structure.

The second major event involves the geographic division of the *Rhipsalis* lineage into species groups found in the Atlantic and Indo-Pacific regions. The separation of Atlantic and Pacific populations occurred before the closure of the Isthmus of Panama and is linked to vicariance events likely associated with the blocking of the Tethys Seaway. The *Halimeda* relative distribution and abundance are tied to glacio-eustatic fluctuations, where sea-level drops of about 120 meters reduced shallow-water areas available for reef and *Halimeda* systems, particularly in the Indo-Pacific region, alongside an ocean temperature drop of at least 6°C (Guilderson et al., 1994; Webb et al., 1997; Colinvaux and De Oliveira, 2001).

An alternative hypothesis suggests that the remarkable increase in *Halimeda* species during the Holocene could be linked to vicariance oscillations during Pleistocene glaciations, which may have acted as a "catalyst" for species diversification on Milankovitch time scales. However, Hillis (2001) argues that interglacial periods lasting 10,000 to 20,000 years would be too brief to allow significant speciation in *Halimeda*. Still, it is worth noting that over the last 1-2 million years, habitat availability for *Halimeda* algae differed from current conditions. While these disturbances were too brief to promote vicariant speciation, they were sufficient to encourage local extinctions or migrations, effects still visible in modern *Halimeda* distributions.

2. Materials and methods

The following methods have been integrated to conduct a comprehensive stratigraphic and sedimentological analysis of *Halimeda* bioherms across three Mediterranean regions: Salento Peninsula (southeastern Italy), Sorbas and Níjar (southeastern Spain), and Crete (Greece). This study integrated field measurements, rock sampling, thin section analysis, and advanced photogrammetric techniques to investigate the sedimentary structures and environmental conditions of these bioherms.

All stratigraphic sections were measured using a Jacob staff, which allowed for precise vertical measurements and detailed descriptions of lithological variations. In Salento, two sections were measured, resulting in the collection of a total of 37 rock samples. In southeastern Spain, four sections were measured, also with a Jacob staff, yielding a total of 53 samples. In Crete, during the first campaign, three stratigraphic sections were measured, from which 35 samples were collected. In the second campaign, seven sections were measured, with a total of 65 samples collected. Overall, 190 samples were collected.

Rock samples were reduced into blocks using a REMET TR 80 petrographic cutting saw. Thin sections were prepared in another department, resulting in an equal number of standard-sized thin sections (30 x 45 mm). Once prepared, the thin sections were examined under an optical microscope, integrating field descriptions for the determination of lithofacies. The description of textures and compositional characteristics was based on the classification diagrams of Dunham (1962), Embry and Klovan (1971), and Insalaco (1998). The relative abundance of rock components was estimated from both outcrops and thin sections.

In some areas, photogrammetric surveys were conducted using a DJI Mavic Pro drone equipped with a high-resolution camera capable of capturing images with resolutions up to 12 megapixels. The images were processed using Agisoft Metashape software to generate 3D point clouds, orthomosaics, and digital outcrop models (DOMs).

3. The *Halimeda* bioherms of the Salento Peninsula (Southeastern Italy)

The data presented in this chapter were published in the journal *Sedimentary Geology* (Passaseo and Morsilli, 2025).

The Salento Peninsula constitutes the southernmost margin of the well-known Apulia Carbonate Platform (ACP), one of the peri-Adriatic carbonate banks that developed during Mesozoic and Cenozoic times in the southern portion of the Tethyan Ocean (Bernoulli, 2001; Morsilli et al., 2017, 2021). The ACP represents a major structural element at the northern boundary of the African Plate, characterizing the foreland of thrust belt of opposite vergence (Fig. 3.1): the Dinarides-Albanides-Ellenides and the Appennines (Doglioni et al., 1994). This carbonate bank extends from the Gargano Promontory to the Leuca Cape, cropping out in the Apulia region.

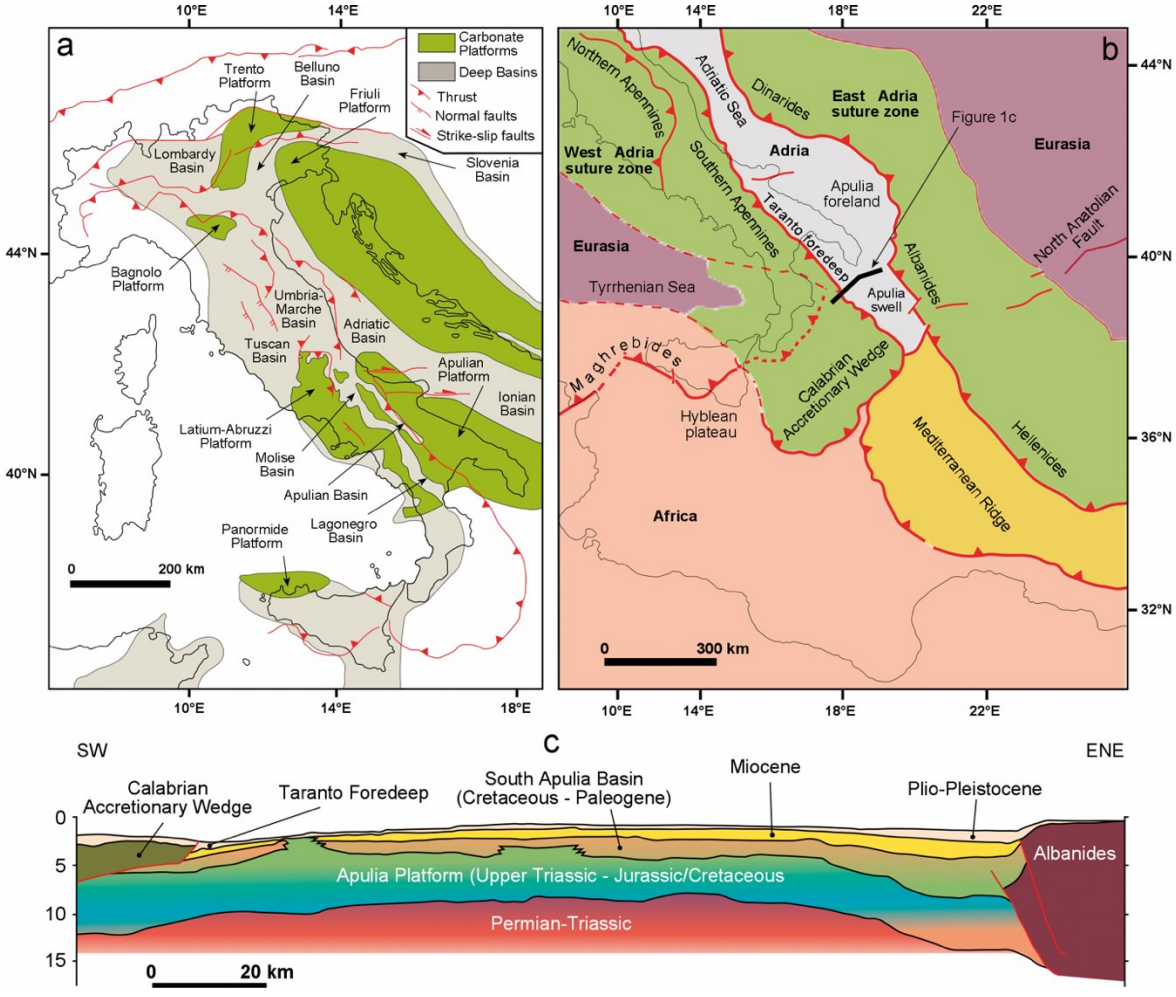

Fig. 3.1. a) Early Jurassic to Early Cretaceous paleogeographic map of the Italian peninsula; b) Simplified geodynamic framework and plate tectonics of the Mediterranean region; c) Crustal-scale geological section across the submerged southernmost sector of the Salento peninsula (Tancredi et al., 2022).

Since the Late Cretaceous, the Salento Peninsula has experienced intensive shallow-water deposition, influenced by moderate sea level oscillations (Bosellini et al., 1999). The

Paleogene and Neogene sediments were deposited in several structural depressions associated with the horst and graben structural setting that characterize the Salento Peninsula (Martinis 1962; Tozzi, 1993). Presently, along the eastern coast of the Salento Peninsula, from Capo d'Otranto to Santa Maria di Leuca, there is a continuous and striking exposure of Upper Cretaceous to Quaternary successions mainly constituted of carbonate rocks and several reef tracts displaying a complex stratigraphic architecture. In fact, the stacking of carbonates occurs with units disposed grafted upon one other and separated by sharp unconformities (Bosellini et al., 1999).

3.1 Geology and Stratigraphy

The paleogeographic evolution of this area began with the rifting phase of the supercontinent Pangea at the end of the Paleozoic, followed by the development of extensive carbonate platforms. It continued with the drifting phase in the Middle Jurassic, marked by the opening of the Ligurian-Piedmont Ocean or Alpine Tethys. From this point, passive margins developed, on which numerous carbonate platforms, such as the Apulian Carbonate Platform, were established, along with adjacent basins resting on continental crust. During the Cenozoic, the subsequent collision between the African and Eurasian plates, accompanied by the subduction of the pre-existing intervening oceanic basin, led to the formation of the Apennine thrust belt and the development of foredeep and foreland areas, of which the Apulian Platform is now part (Bernoulli, 2001; Bosellini, 2004, Bosellini et al., 1999; Morsilli et al., 2017) (Fig. 3.2). From a stratigraphic perspective, at the end of the Paleozoic in the Apulian region, sedimentation began with terrigenous deposits (Verrucano like), and scattered carbonate deposits documented in the Gargano 1 well, followed by carbonate and evaporites represented by the Burano Formation during the Triassic, followed by an extensive and thick shallow-water succession from the Jurassic to the Cretaceous, forming the Apulian Carbonate Platform (ACP).

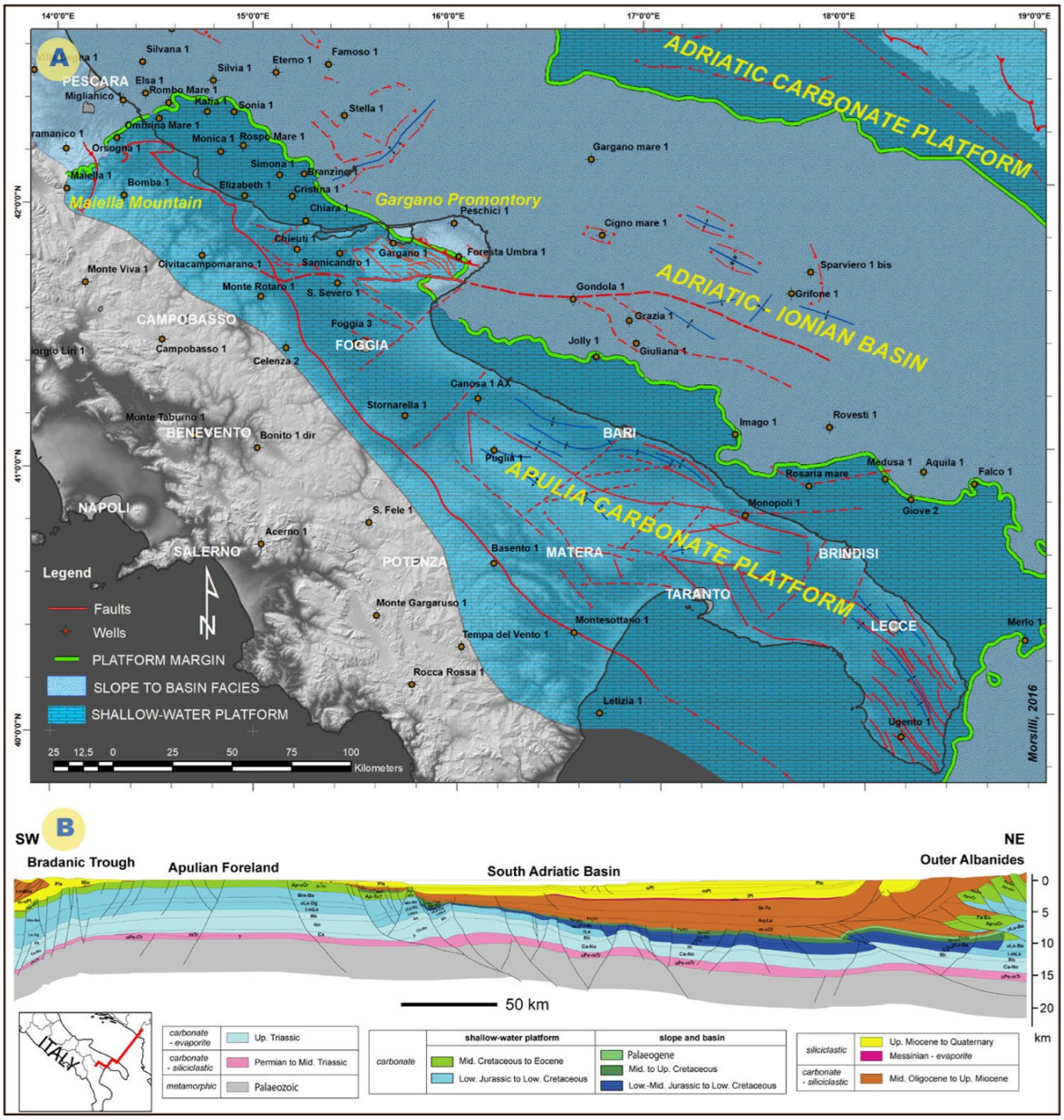

Fig. 3.2. A) Reconstruction of the Apulia Carbonate Platform (ACP) and the adjacent Adriatic Basin passing to the Adriatic Carbonate Platform to the east, including the main structural features and exploration wells, based on the analysis of public seismic lines and exploration wells (Morsilli et al., 2017, 2022). B) Regional cross-section from the Apennines foredeep (Bradanic Trough) to the Outer Albanides (after Fantoni & Franciosi, 2010) showing the poorly deformed ACP margin buried under Cenozoic successions in the offshore domain.

During the Late Cretaceous, at the onset of the collision between the European and African plate margins and the subduction of the Tethyan and Ligurian-Piedmont oceanic crust, the Apulian area experienced a mild folding event, which led to the emergence of the Apulian Carbonate Platform (ACP), lasting throughout the Turonian (Mindszenty et al., 1995; Ciarcia and Vitale, 2025). Subsequently, as the collisional phases between the African and Eurasian plates continued, the ACP underwent further and more intense folding, culminating in its partial emergence at the end of the Miocene and the beginning of the Pliocene (Ciarcia and Vitale, 2025).

As the structural configuration of the ACP was undergoing these modifications, additional carbonate sedimentation occurred along its margins between the Paleocene and the Miocene. This was outlined by the formation of typical coral reefs (documented across the Mediterranean, e.g., Esteban et al., 1996) and is attributed to eustatic fluctuations or paleoenvironmental and evolutionary changes. These additional sedimentary phases persisted until the Middle Miocene, when the ACP became the foreland (Apulian Foreland) of the nascent Apennine and the Dinaric-Hellenic thrust belts (Fig. 3.2B).

The Apulian foreland experienced extensional tectonics related to crustal arching, which can be attributed to the tectonic convergence phases. This resulted in a morphostructural configuration of an asymmetrical tectonic block dipping towards the northeast, later divided into three geological-geographical domains (Fig. 3.2): the Gargano Promontory, the Murge, and the Serre Salentine, separated by the intervening tectonic depressions of the Tavoliere delle Puglie (between the Gargano and Murge), the Bradanic Trough (between the Southern Apennines and Murge), and the Tavoliere di Lecce (between the Murge and Serre Salentine) (Ricchetti et al., 1992).

The stages of this paleogeographic evolution are recorded in the stratigraphic, tectonic, and morphological architecture of the Salento Peninsula, particularly in its southern portion. Throughout the Serre Salentine, sedimentary successions, predominantly carbonate, are exposed, dating from the Late Cretaceous to the present, though with numerous stratigraphic gaps (Bosellini et al., 1999).

The sedimentary complexes, dating from the Cretaceous to the Miocene, generally correspond to carbonate systems, with sequences ranging from lagoon to margin and slope environments. In contrast, the Pliocene-Quaternary systems are represented by toe-of-slope environments (Tropeano et al., 2022).

Structurally, the central Mediterranean region is known for being a mosaic of microplates intertwined through a network of thrust belts, back-arc basins, and transfer zones. The Adria microplate, along with the Ionian and Adriatic seas, lies at the heart of this puzzle. The southernmost part of this plate, characterized by the Salento Peninsula (to the north) and the Apulian Rise (to the south), is part of the foreland attributed to the Neogene-Quaternary period (here referred to as the Apulian Foreland) and bordered by two opposing chains: the Dinaric-Hellenic thrust belt verging southwest, and the southern Apennine chain verging northeast, which merges in the south with the Calabrian Arc trending SSE. The Adria

microplate is primarily characterized by the Apulian Carbonate Platform (ACP), a block of continental crust (Critelli, 2018) that has preserved, in its southwestern portion, the paleo-margin with the Ionian oceanic crust subducted beneath the Calabrian accretionary wedge to the west and the Hellenic arc to the east.

In the Salento Peninsula, the crustal basement is overlain by a thick sequence of autochthonous sediments (Martinis and Pieri, 1964; Ricchetti et al., 1988), predominantly of carbonate origin. These sediments were deposited around the Permian -Triassic boundary, initially with a terrigenous facies likely of fluvial origin. This is followed by a Triassic succession of anhydrite and dolomite, reaching about 1000 meters in thickness, and then by a substantial sequence of platform carbonates laid down during the Jurassic-Cretaceous period.

Several authors have analyzed the structural framework of the Apulian Foreland (Gambini and Tozzi, 1996; Doglioni et al., 1999; Catalano et al., 2000; Argnani et al., 2001; Finetti and Del Ben, 2005; Tondi et al., 2005; Billi et al., 2007; Nicolai and Gambini, 2007; Butler, 2009; Del Ben, 2010; Del Ben et al., 2015; Milia, 2017; Volpi et al., 2011, 2017; Teofilo et al., 2018), all highlighting that the region is affected by E-W strike-slip faults in the northern part (Mattinata Fault – Gondola, MGF) and by NW-SE trending extensional structures towards the Salento Peninsula and the Apulian Rise. The role, age, and origin of these tectonic lineaments remain subject of debate.

The Apulian Foreland is considered a peripheral bulge produced by flexural bending due to the load of the two aforementioned opposing thrust belts (Critelli, 2018; Critelli et al., 2017; Moretti and Royden, 1988). According to several authors, this bending is responsible for the extensional tectonic regime that developed during the Pliocene-Quaternary and thus for the generation of NW-SE normal faults (Argnani et al., 2001; Ciaranfi et al., 1988; Finetti and Del Ben, 2005).

The tectonic framework characterizing the Serre Salentine region corresponds, as previously mentioned, to a structural high elongated in a NW-SE direction, with a more pronounced southwestern flank. This structure breaks the carbonate framework of the ACP into blocks slightly tilted towards the southwest, identifying a series of high-angle, subparallel fault alignments. This arrangement is further intersected by a system of SW-NE transverse faults, causing a progressive lowering of the carbonate strata towards the broad tectonic depression of the Tavoliere di Lecce to the northeast. The structural highs form a series of elongated

ridges converging towards the southeast (Baia di Leuca), consisting of Cretaceous and Paleogene-Miocene carbonate formations, while the fault depressions, covered by Pliocene-Pleistocene terrigenous deposits, correspond to the underlying flat areas. As a result, the morphological landscape is dominated by a system of ridges with nearly flat tops, aligned in a NW-SE direction, reaching a maximum elevation of no more than 200 meters. These ridges are bordered by steep steps on the northeastern side and interspersed with variably extensive levelled depressions.

The study area is located in the southeasternmost part of the Salento Peninsula. The first information on the geology of the Salento Peninsula dates back to the early 1900s, and until the 1950s, studies were mainly aimed at the discovery and characterization of new stratigraphic units. Following the development of the 1:100,000 scale Geological Map of Italy, these studies gained new momentum, and in the last decades of the past century, important contributions were made by Bossio et al. (1989) concerning the Neogene formations within the platform, and by Bosellini and Russo (1992) regarding the Oligocene Castro limestone formation. Finally, in the 1990s, Bosellini (1993) and Bosellini and Parente (1994) were the first to highlight the distinctive architecture characterizing the stratigraphic succession of the Salento Peninsula, a topic further explored in detail by Bosellini et al. (1999).

Bosellini et al. (1999), published a simplified geological map from an original 1:10.000 scale survey of the coastal strip between Otranto and S. M. di Leuca (Fig. 3.3), aiming to provide a more comprehensive illustration of the complex relationships between the various formations than previous studies (sheets "Otranto" and "S. M. di Leuca" of the Geological Map of Italy).

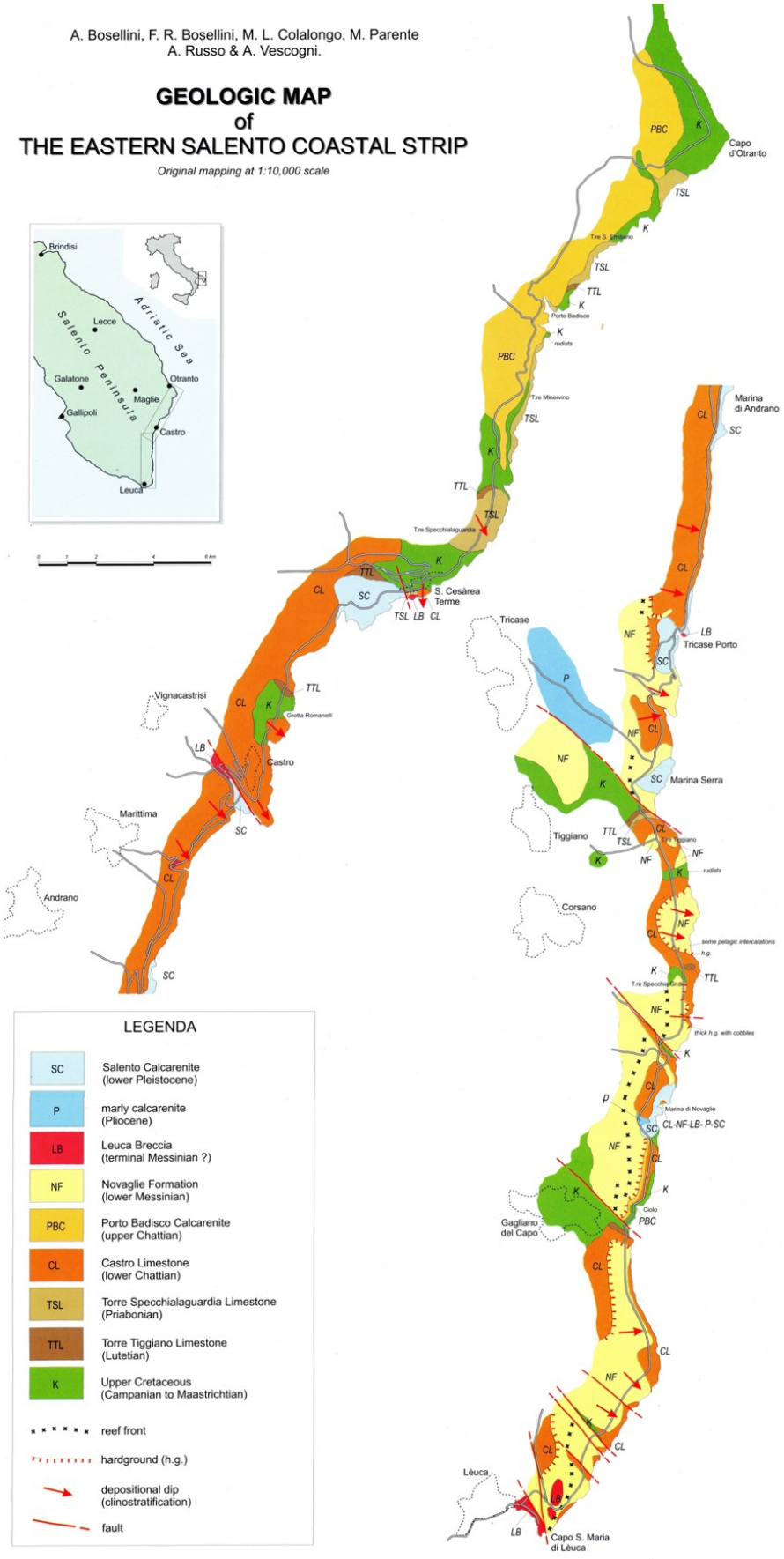

Fig. 3.3. Geological map of the southeastern margin of the Salento Peninsula. The Novaglie formation is highlighted in yellow, showing discontinuous outcrops from Tricase Porto to Santa Maria di Leuca (Bosellini et al., 1999)

The Upper Cretaceous sediments outcropping throughout the Salento Peninsula are predominantly associated with shallow marine environments, representing the inner platform and extending to high-energy settings. Notably, no slope or basin facies are found along the Salento coastline (Bosellini and Parente, 1994; Bosellini et al., 1999). The Cretaceous succession is composed by three formations.

The Melissano limestones, dating up to the early Campanian (Schlüter et al., 2008), consist primarily of meter-scale peritidal cycles, characterized by abundant and thick stromatolitic layers, along with channel deposits and tempestites. A prominent outcrop of this lithology can be seen along the coastal road west of S. M. di Leuca.

The Santa Cesarea limestones, formed during the middle Campanian (Schlüter et al., 2008), have a thickness ranging from 10 to 54 meters. This formation also exhibits peritidal cycles, although the stromatolitic laminations are thinner and less frequent compared to the Melissano Limestones. In contrast, tempestites are more common, often containing accumulations of rudist fragments. The type locality, just north of S. Cesarea, was crucial for dating the formation based on its rudist fauna (Cestari and Sirna, 1987). Additionally, the rocky coastline near Porto Badisco reveals spectacular associations of radiolitids preserved in growth position.

The Ciolo limestones, dating to the upper middle Campanian-Maastrichtian (Schlüter et al., 2008) and measuring around 50 meters in thickness, are composed of bioclastic calcarenites and calcirudites with parallel and oblique laminations. The clasts primarily include fragments of rudists (some found in life position), *Orbitoides*, other large benthic foraminifera, corals, bryozoans, and coralline algae. The formation's age has been determined by a macroforaminiferal assemblage, including *Orbitoides apiculata*, *Omphalocyclus macroporus*, *Siderolites calcitrapoides*, and *Lepidorbitoides socialis*, further confirmed by the presence of rudists such as *Hippurites cornucopiae* (Bosellini et al., 1999). Additionally, the Ciolo limestones feature extensive associations of coralline, peyssonnelid, and dasycladalean algae (Parente 1994, 1997). The type localities for this formation include the Ciolo cove and the coastal road near Torre Tiggiano.

The Eocene successions are represented by two stratigraphic units with relatively limited thicknesses and outcrop areas. The Torre Tiggiano limestones, dating to the Lutetian/Bartonian and with a thickness of 10-15 meters, are characterized by an erosive boundary with the underlying Cretaceous limestone. This formation crops out

discontinuously along the coast, leading to infills and onlaps over the underlying paleomorphologies. It consists of a parallel-laminated grainstone rich in *Alveolina*, *Nummulites*, and other large foraminifera. The presence of *Alveolina callosa*, *Alveolina tenuis*, and *Assilina spira abrardi* allowed the lower portion of the formation to be dated to the early Lutetian, while the occurrence of *Alveolina fusiformis* suggests that the upper part dates to the early Bartonian (Bosellini et al., 1999). The main outcrops are found along the coastal road near Torre Tiggiano, at Torre Specchia Grande, and to the north of the Ciolo cove.

The Torre Specchialaguardia limestones, from the Priabonian and ranging from 14 to 76 meters in thickness, unconformably overlie the Lutetian and Cretaceous deposits. This unit is primarily represented by breccias and bioclastic slope sediments, and in some areas, such as Torre S. Emiliano and Torre Specchialaguardia, abundant fragments of coral colonies can be observed. The age of the formation has been established based on the presence of foraminifera such as *Asterocyclina priabonensis* and *Heterostegina gracilis* (Bosellini et al., 1999).

The first Oligocene formation encountered has been attributed to the much-debated Castro limestone, early Chattian in age (12-80 meters). Specifically, two hypotheses have emerged regarding this formation, each based on different depositional models. According to Bosellini and Russo (1992), the stratigraphic sequence of the Castro limestone represents a fringing reef complex, whose characteristic sigmoidal geometry is simply the result of its progradation. This formation also contains a highly diverse coral fauna with over 50 different species, among the most prominent are *Astrocoenia*, *Astreopora*, *Pavona*, *Siderastrea*, *Goniopora*, *Porites*, *Actinacis*, *Alveopora*, *Favia*, *Montastrea*, *Caulastrea*, and *Tarbellastrea*, thoroughly studied by Bosellini and Perrin (1994). Pomar et al. (2014) argue that the Castro limestone unit no longer represents a fringing reef, instead, they propose that it is a distally steepened ramp with a facies distribution governed by photic zonation. Additionally, they explain that the hydrodynamic energy affecting the meso-oligophotic zone should be attributed to internal waves, rather than storm activity.

The Porto Badisco calcarenites (late Chattian), is represented by poorly cemented sub-horizontal calcarenites, with a thickness of 50-60 meters (Bosellini et al., 1999; Brandano et al., 2010: Pomar et al., 2014). This Formations is notable for its rhodoliths, composed by melobesioids and sporolithaceans, which form a prominent lensoid lithosome at the base of the unit. The accumulation is influenced by the inherited substrate topography, which created

a shallow channel-like depression (firstly recognized by Nardin and Rossi, 1966) that acted as a trap for rhodoliths formed at shallower depths. The age of the Porto Badisco Calcarenites has been confirmed as late Chattian by Parente (1994) based on the foraminiferal association, which includes *Lepidocyclina dilatata, Lepidocyclina morgani, Miogypsina (Miogypsinoides), Neorotalia viennoti, Operculina complanata, Heterostegina assilinoides, Amphistegina sp., and Austrotrillina sp.*

During the middle to late Miocene, the Salento Peninsula experienced a period of intense flooding, resulting in the establishment of pelagic conditions following a long phase of platform emergence and erosion. Along the margin, this phase is documented by the presence of a thin phosphatic hardground surface reaching a maximum thickness of 25 cm (Föllmi et al., 2015; Vescogni et al., 2018). This condensed layer, known as the *Aturia* Level, is characterized by a fossil assemblage including pectinids, gastropods such as *Conus*, brachiopods, cephalopods like *Aturia*, isolated corals, echinoids, and fish teeth and vertebrae. This formation is coeval with the well-known "Pietra Leccese," composed of micrites, biomicrites, and biosparites with predominant calcareous plankton, typical of the more internal areas of the platform, reaching a thickness of 17 m (Bossio et al., 1989). This formation is ascribed to the Serravalian-Tortonian on the base of strontium isotope analyses (Föllmi et al., 2015).

The early Messinian in the Salento Peninsula is represented by two heterotopic stratigraphic units, known as Andrano calcarenites and Novaglie formation; the first is characterized by back-reef deposits rich in bivalves and gastropods, with various intercalations of marly lenses occupying the most internal areas of the carbonate platform, while the second consists of reefal limestone occurring in the coastal area (Fig. 3.3, 3.4). This difference lead Bosellini et al. (1999) to the definition of an informal unit, the Novaglie formation, which includes the reef tract studied in detail by Bosellini et al. (2001, 2002).

The top of this unit is considered the Terminal Carbonate Complex (TTC) before the occurrence of the Messinian Salinity Crisis which affected the whole area (Vescogni et al., 2022). The Novaglie formation is unconformably overlain by the Leuca Breccia formation which features a breccia interval that can reach up to 12 meters in thickness, incorporating clasts from the underlying Novaglie formation. The precise age of the Leuca Breccia remains uncertain due to the absence of reliable biostratigraphic markers. Bosellini et al. (1999) interpret this formation as a consequence of a sea-level drop associated with the late Messinian Salinity Crisis, whereas Bossio et al. (2002) attribute it to an Early Pliocene

marine transgression. Overlying the Leuca Breccia, a discontinuous layer of marls occurs several decimeters thick, dating to the middle Zanclean (Bossio et al., 2002; Bortone et al., 2013). This marl layer is succeeded by the upper Piacentian-Gelasian Uggiano la Chiesa formation, characterized by tens of meters of calcarenite deposits with a basal breccia (Bosellini et al., 1999). This is discordantly overlain by the most recent sedimentary unit, the Salento calcarenites, early Pleistocene in age, characterized by poorly cemented sediments with bioturbation and cross-laminated beds. This formation is rich in bivalves, brachiopods, and coralline algae (Bosellini et al., 1999; Tropeano et al., 2022) (Fig. 3.4).

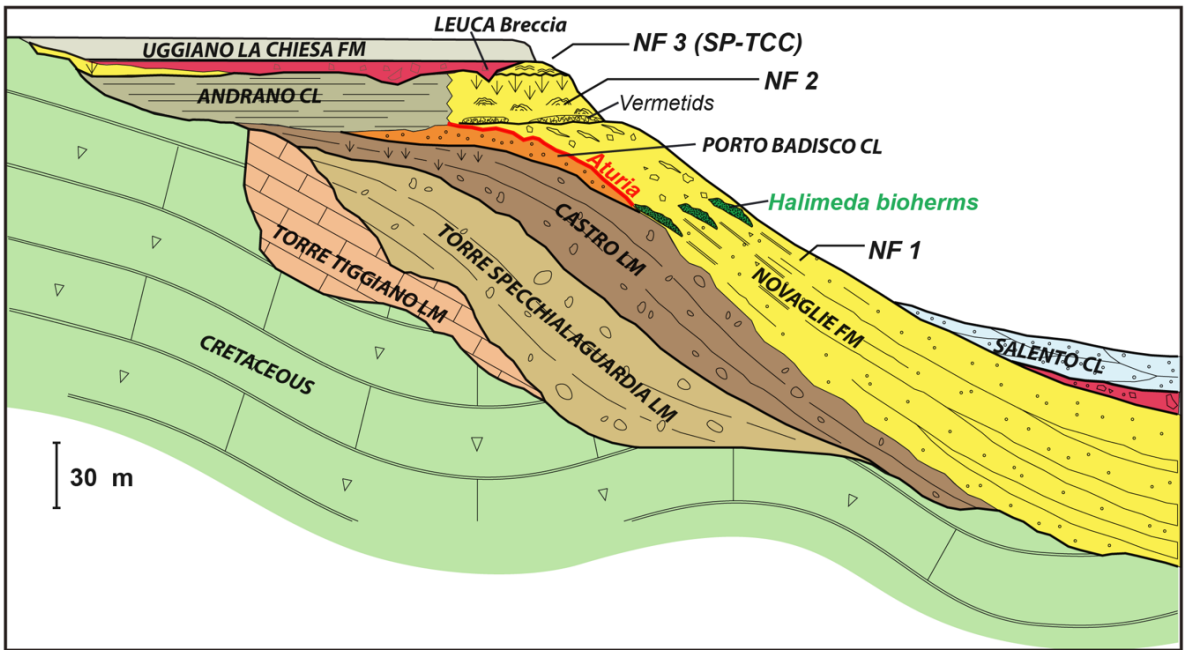

Fig. 3.4. Stratigraphic architecture of the southeastern Salento Peninsula: Upper Cretaceous substrate, Torre Tiggiano limestone (Lutetian/Bartonian), Torre Specchialaguardia limestones (Priabonian), Castro limestones (middle-upper Chattian), Porto Badisco calcarenites (uppermost Chattian), Aturia level (Serravallian/Tortonian), Andrano Calcarenites (lower Messinian), 8. Novaglie formation (lower Messinian), 9. Leuca Breccia (upper Messinian), Uggiano la Chiesa Fm. (Piacenzian/Gelasian), Salento Calcarenites (lower Pleistocene) (modified after Bosellini et al., 1999 and Vescogni et al., 2022).

3.2 The Novaglie formation

This unit crops out discontinuously along the eastern coast of the Salento Peninsula from Tricase Porto to S.M. di Leuca for a total length of 17 km (Fig. 3.3) and was dated to the early Messinian (Bosellini et al. 1999 and Bosellini et al. 2001) on the base of benthic foraminifera and ostracods associations. This unit shows a well-developed reef complex with monogeneric *Porites* coral reefs exhibiting various morphologies, and clinostratified breccia forming prograding slope and distal-slope deposits (Bosellini et al., 2001, 2002; Bosellini, 2006) (Fig. 3.5). This reef complex was generally characterized by heterogeneous reef-

building biota such as *Porites* corals, scattered *Halimeda* bioherms, coralline algae, and vermetid-microbial bioconstructions along with encrusting foraminifera, bryozoans and serpulids (Bosellini et al., 2002; Bosellini, 2006).

A review of the reef architecture was carried out by Vescogni et al. (2022) showing three main superimposed units each separated by erosional surfaces. The first unit, NF1, is 120 m thick and shows a complete margin-to-slope reef tract with reef rubble, m-tick *Halimeda* bioherms and *Halimeda*-rich beds, rhodolith floatstones-rudstones, and bioclastic calcarenites dated as early Messinian (7.3-5.87 Ma). The overlying NF2 unit, 20 m thick, consists of *Porites* coral frameworks which thins out towards the proximal slope. The last unit, NF3, characterized by a 10 m thick oolitic deposits associated with microbialites, colonies of *Porites*, small vermetid and serpulid bioherms (Bosellini et al., 2001, 2002), upper Messinian in age (5.97-5.60 Ma), is interpreted as equivalent to the TCC (Terminal Carbonate Complex) related to the Messinian Salinity Crisis (MSC) (Bosellini et al., 2001; Vescogni et al., 2022). The age of the Novaglie formation was established as early Messinian, consistent with the Andrano Calcarenite, through the identification of the benthic foraminifera *Bulimina echinata*. Additionally, the presence of a characteristic "Sahelian" taxa assemblage, including *Porkyornella italica* among ostracods, further support this data (Bosellini et al., 2001).

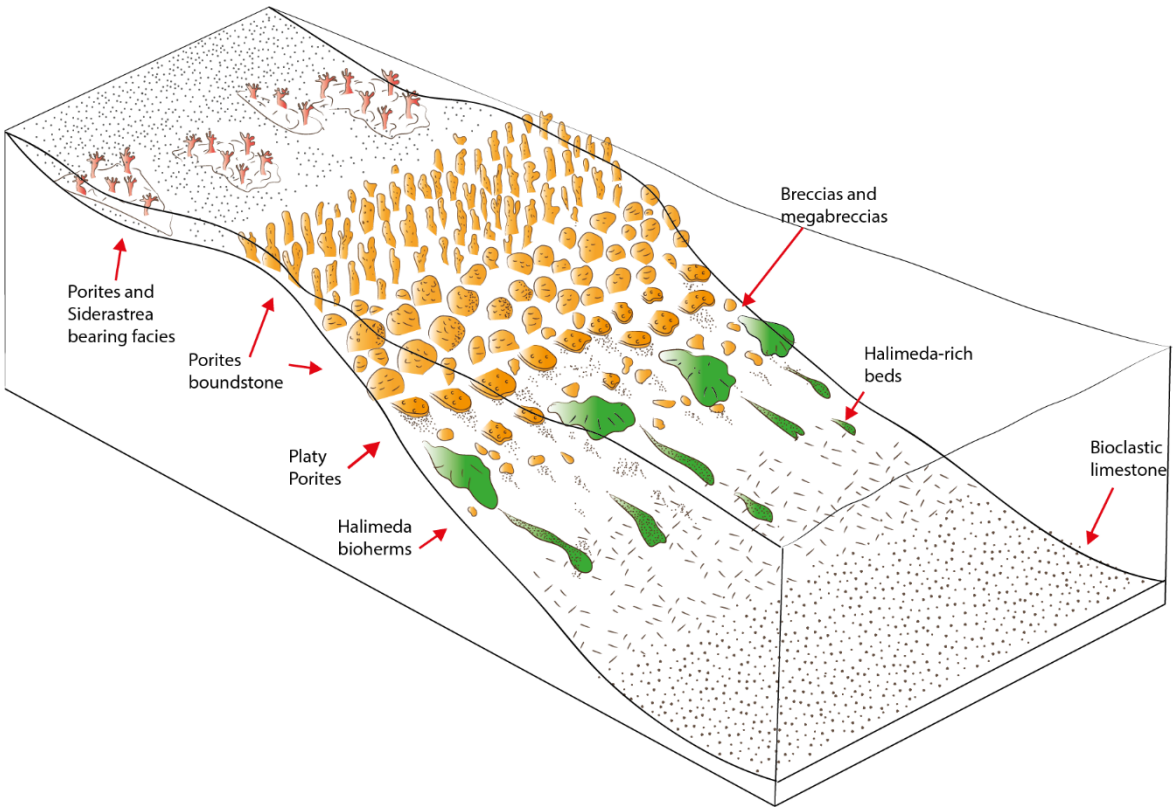

Fig. 3.5. Depositional model of NF1 showing position of *Halimeda* bioherms and *Halimeda* rich-beds on the proximal-to-mid slope and zonation of Porites coral with different morphologies and main facies types (Passaseo and Morsilli, 2025, slightly modified after Bosellini and Russo, 1992).

We measured and analyzed in detail two stratigraphic sections located along the coastal road between the localities of S.M. di Leuca and Ciolo (Fig. 3.6).

The first section called "Tre Fratelli" (39° 49' 03.60" N, 18° 23' 12.51" E) reaches a maximum thickness of about 15 meters, the second section called "Radar" (39° 48' 10.87" N, 18° 22' 31.83" E) is 17 meters thick.

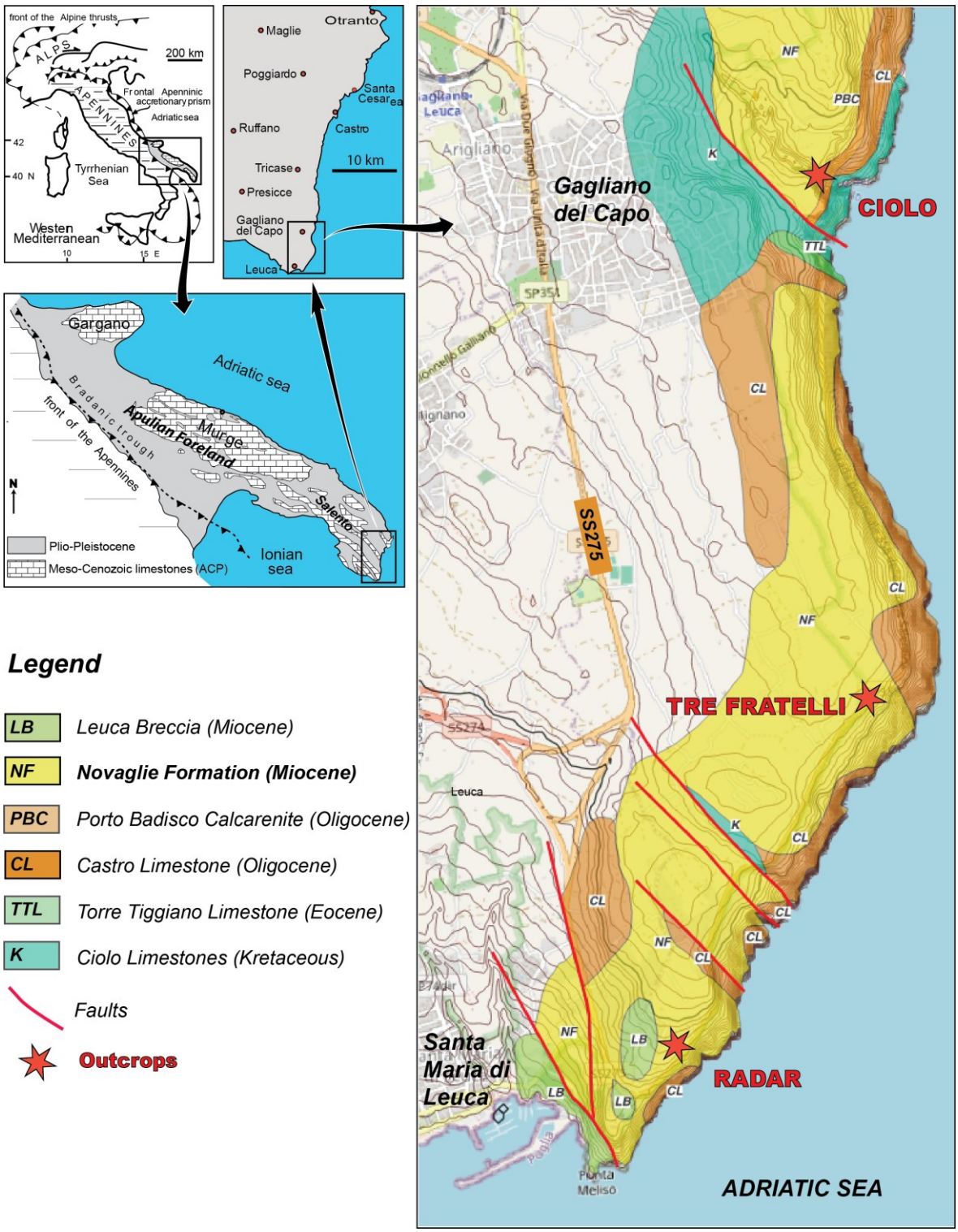

Fig. 3.6. Location map of the Salento Peninsula and of the study sites. A) structural and geological settings; B) map of the outcropping formations along the southeasternmost margin of the Salento Peninsula (Passaseo and Morsilli, 2025, modified after Bosellini et al., 1999).

The *Halimeda*-rich deposits occur in different stratigraphic positions along the Novaglie formation (NF). In the "Radar" section the *Halimeda* bioherms crops out close to the base of NF 1 and overlie disconformably the Castro limestone, instead in the "Tre Fratelli" section *Halimeda* bioherms occurs in an intermediate interval of NF 1 (Fig. 3.6). Both sections were

sampled at a scale ranging from decimeters to meters, and with an accurate taphonomic observations conducted across the *Halimeda* accumulations.

3.3 The Tre Fratelli Section

The stratigraphic section "Tre Fratelli" was measured along road cuts, that intersect at about 30 degree (Fig. 3.7). This intersection permits to observe in 3D the facies relationship and permit a detailed taphonomic description of the *Halimeda* bioherm (Fig. 3.8).

Fig. 3.7. Outcrop aerial view reconstruction through Agisoft metashape software of the "Tre Fratelli" bioherm with a strategic strike cut between two roads, allowing for geometric relationships and detailed description of the internal organization of the *Halimeda* bioherm (Passaseo and Morsilli, 2025).

The "Tre Fratelli" section (Fig. 3.9), located in the proximal-to-mid slope of NF 1 (Bosellini et al., 2002), begins at the ground level, with a thick interval of vermetids reaching a thickness of about 2 meters. This accumulation is characterized by boundstone textures, featuring area of significant primary porosity. Additionally, extensive areas contain reddish geopetal structures, with cavity walls lined with thin isopachous calcite cements (Brachert et al. 2007).

The vermetid accumulation is overlain with a gradational contact, by a 4.85 m thick interval rich in *Halimeda* segments, characterized by a high concentration of densely packed algal segments. This bioherm is organized in centimeter-scale zones or convex lenses consisting

of vertically arranged *Halimeda* segments with a packstone to wackestone matrix (Fig. 3.8). Locally, where the matrix is absent, these small boundstone lenses are characterized by high depositional porosity, filled with abundant early-diagenetic cement. The algal segments encrusted by the cement are well-preserved. The *Halimeda* boundstone laterally transition to rudstone to floatstone textures, identified by a subtle stratification associated with the chaotic or imbricated arrangement of the algal segments. *Halimeda* segments is the predominant component, accounting for almost 80-90% of the bioclasts, followed by other skeletal components such as small benthic epiphytic foraminifera (miliolids and textulariids), fragments of *Porites*, echinoids, bryozoans, and non-articulated red algae.

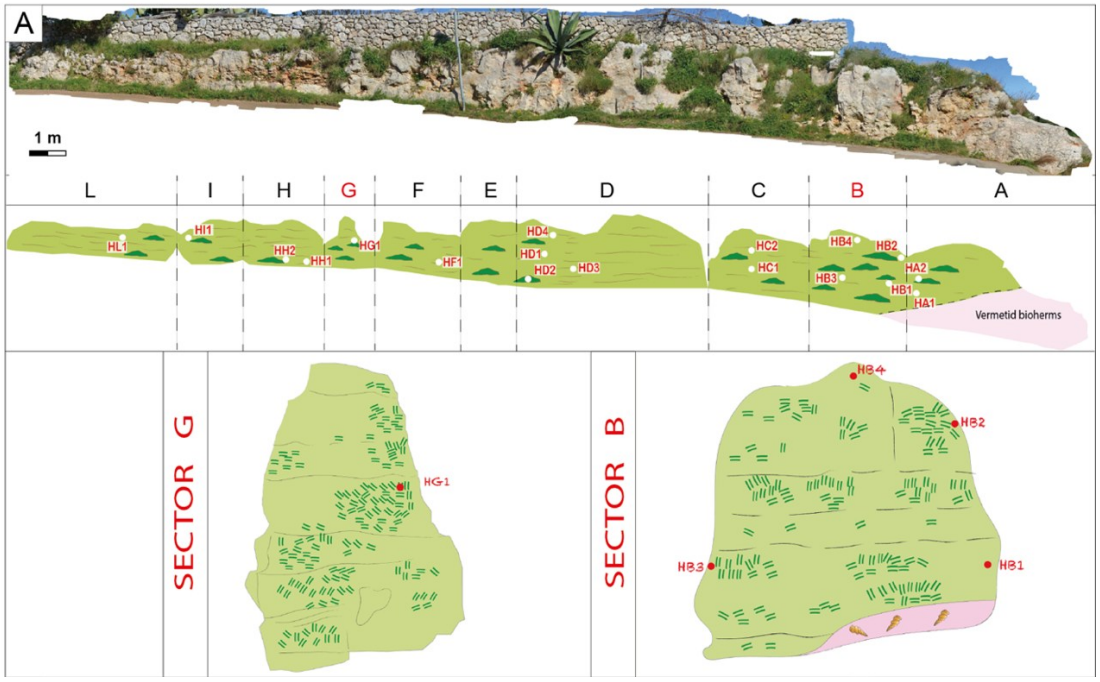

Fig. 3.8 - Reconstruction through Agisoft Metashape software of the two outcrops, highlighting the facies and the location of the samples collected: the dark green areas highlight the occurrence of *Halimeda* thalli in growth position (HB facies) while in light green, areas with rudstones-floatstones textures (HRF facies). A) Draw-line of the outcrop "Tre Fratelli" showing the internal organization of the deposit. In pink, the vermetids bioherm. Below: two enlargements of two sectors of the outcrop (B – G) with the algal segments orientation (Passaseo and Morsilli, 2025).

At the top of the *Halimeda* bioherm, a bivalve rudstone containing few serpulid fragments, crustose and articulate red-algae, *Porites* fragments, and epiphytic benthic foraminifera (miliolids and textulariids) reaches a total thickness of about 4.65 meters (Fig. 3.9). After 1 meter of cover the succession continue with a 1.5 m thick poorly stratified interval of foraminiferal packstone, rich in shallow-water benthic foraminifera, with a reappearance of the *Halimeda* rudstone-floatstone characterized by a 0.5 cm thick layer. The top of the section consists of a thin layer (0.5 cm) of rudstone-floatstone containing crustose red algae interspersed with few scattered *Halimeda* segments.

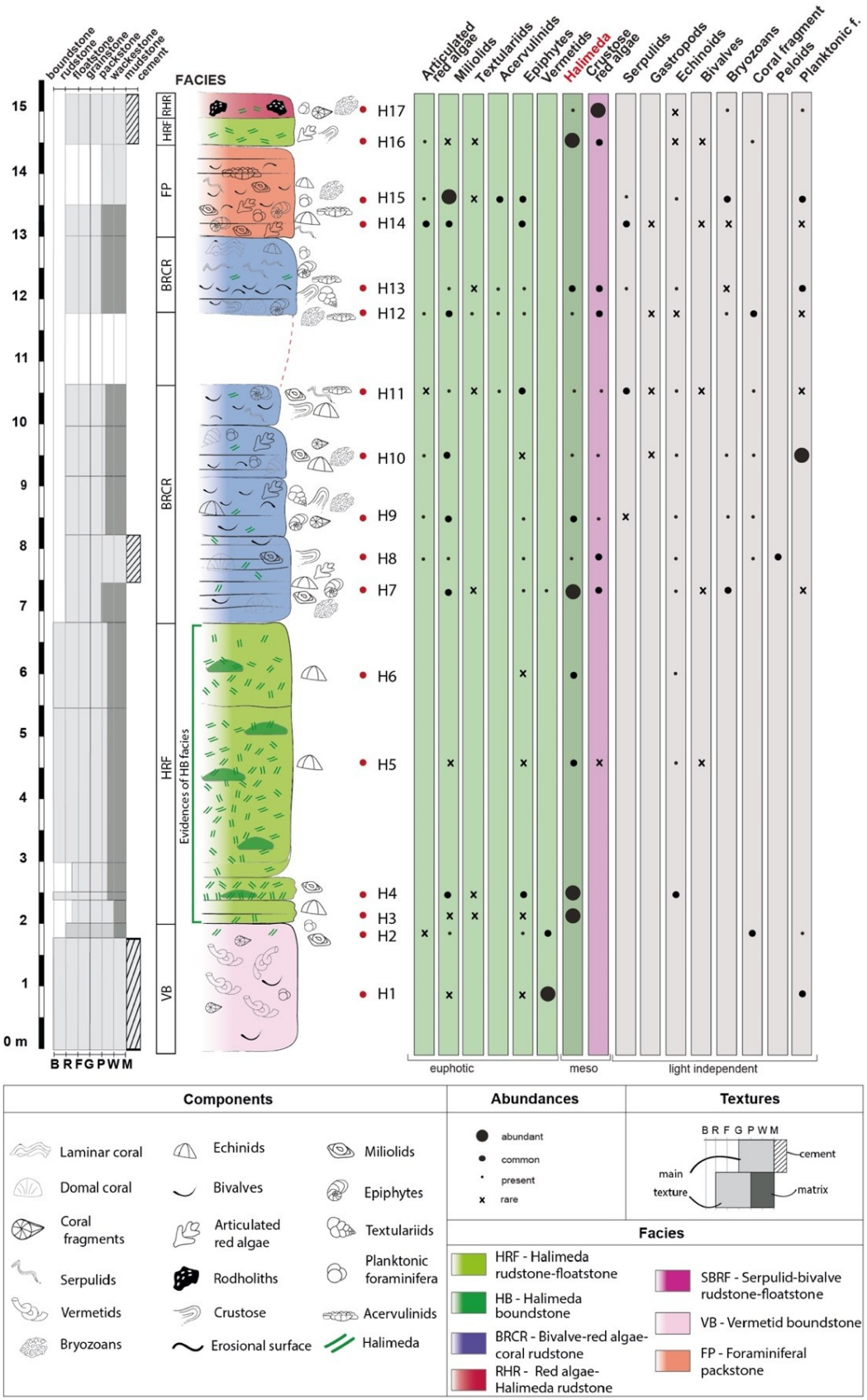

Fig. 3.9. Stratigraphic log of the "Tre Fratelli" section featuring sample locations, textures, facies, and abundances of the respective components. Within the HRF facies (highlighted in bright green), the vertical orientation of *Halimeda* segments indicates autochthonous accumulation, represented by HB facies in dark green (See Table 1 for facies description.

3.4 The Radar section

The 'Radar' stratigraphic section is located close to the Santa Maria di Leuca lighthouse (Figs. 3.6, 3.10). The base of the section (Fig. 3.11) corresponds to the disconformable contact with Castro limestone and begins with layers of *Halimeda* rudstone-floatstone, which are 0.5 meters thick, reaching a total thickness of 5.25 m, within which there are centimeter-scale boundstone lenses containing very well-preserved algal segments and filled with abundant early-diagenetic cements. The edges of these lenses are characterized by rudstone-floatstone textures, with segments chaotically dispersed or imbricated.

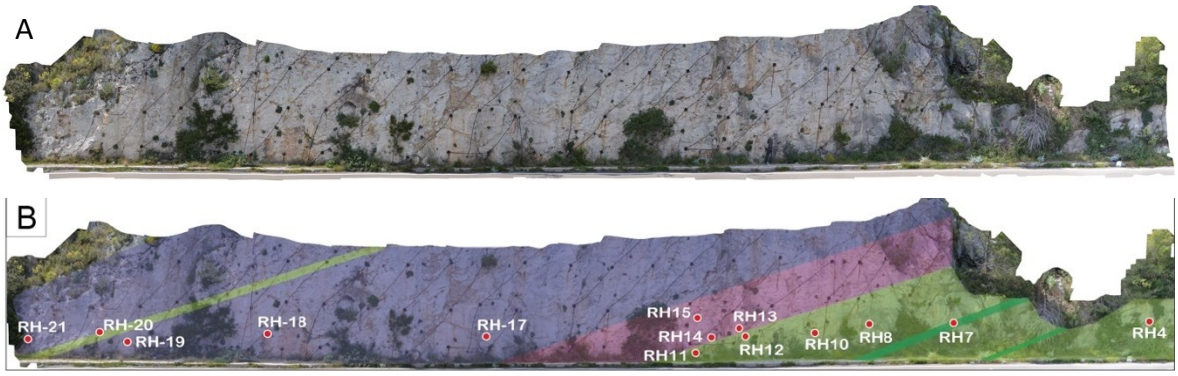

Fig. 3.10 Radar section. In dark-green, levels where the algal thalli are identified in growth position. See Fig. 3.10 for facies legend.

A sharp upper contact marks the transition to a 0.5 m layer of bivalve-rich rudstone with a wackestone matrix, containing a few serpulid fragments, crustose and articulated red algae, fragments of *Porites* corals, and epiphytic benthic foraminifera such as miliolids and textulariids. This layer is capped by a massive layer that is 2.85 meters thick, mainly characterized by an abundance of densely packed serpulids, with scattered bivalve shells. The top of the section consists of 6.7 meters of bivalve-rich rudstone, interrupted by a 0.5 meters layer of *Halimeda* rudstone-floatstone (Fig 3.11).

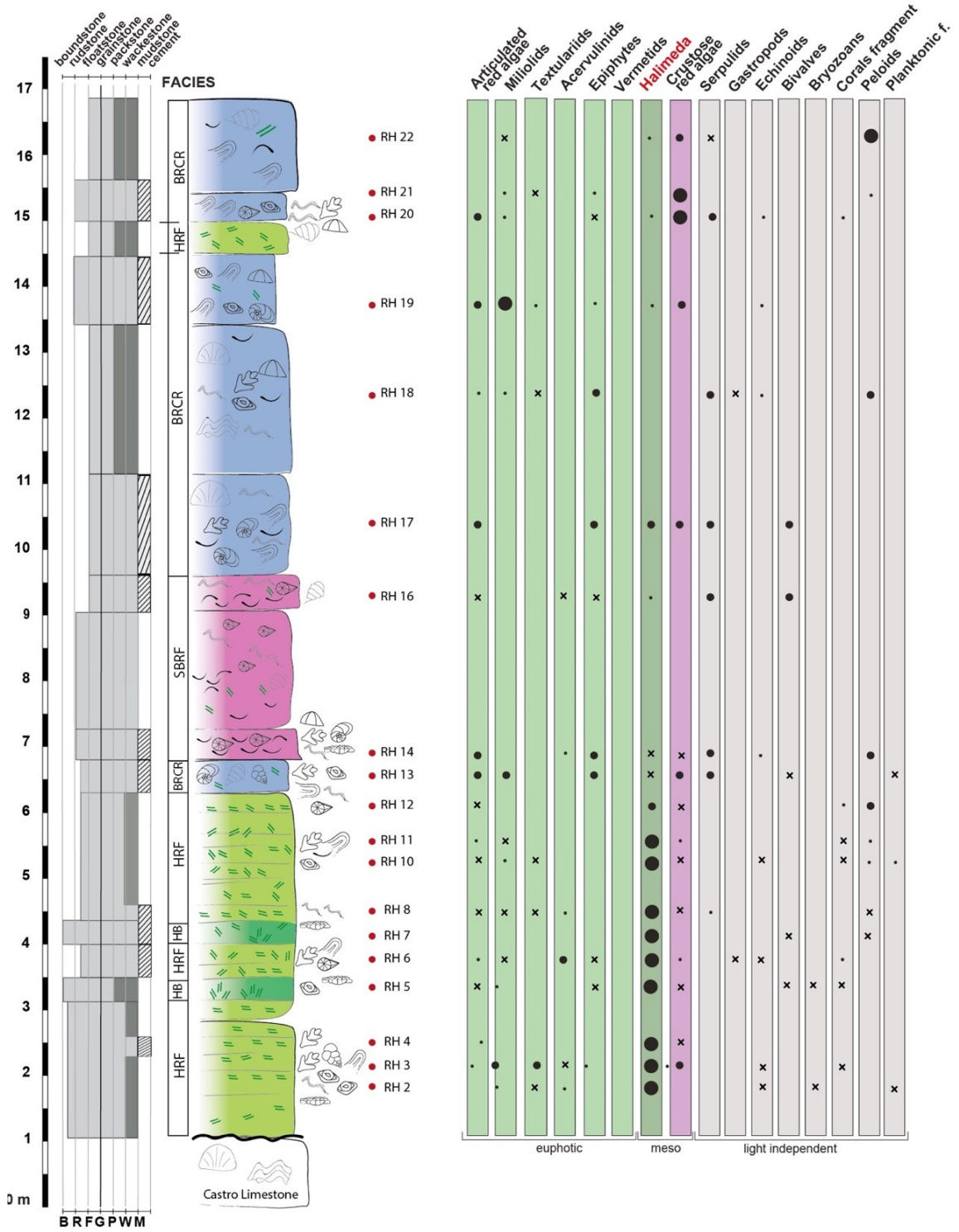

Fig. 3.11 - "Radar" Stratigraphic log featuring sample locations, textures, facies, and abundances of the respective components on the base of the photic zone. The dark green areas identified by the HB sub-facies, where the *Halimeda* segments are vertically oriented, indicate autochthonous sedimentation, while the right green areas identified by the HRF facies, where the algal segments are disorganized or imbricated, reflect areas of allochthonous sedimentation (See Table 1 for facies description and Fig. 3.9 for symbols legend).

3.5 Facies

Field and thin section analysis allowed the identification of six facies (Table 1) with textures spanning from rudstone-floatstone to packstone in which the biota is mainly represented by *Halimeda*, other encrusting organisms like vermetids, serpulids and red algae, including shallow-water benthic foraminifera, bivalve shells and corals sticks.

Table 1. Main facies description. Their relative abundance is expressed as: a-abundant, c-common, p-present, r-rare.

Facies	Matrix	Cement	Skeletal components	Remarks
HRF - *Halimeda* rudstone - floatstone	Packstone to poorly sorted wackestone	Isopachous calcite	*Halimeda* (a); articulated and crustose red algae (c), miliolids (c), acervulinids (c), planktonic foraminifera (p)	Peloidal micrite
HB - Halimeda boundstone	Packstone to poorly sorted wackestone	Fibrous isopachous calcite, thin micritic calcite crust, fibrous aragonite, isopachous calcite	*Halimeda* (a), pectinids (r), planktonic foraminifera (r)	Very well preserved *Halimeda* segments in growth position with high intergranular porosity
RHR - Red algae - *Halimeda* rudstone	Fine wackestone	Fibrous and isopachous calcite layers	Crustose red algae (a); *Halimeda*, bryozoans, planktonic foraminifera (p)	Red algae encrustations
VB - Vermetid boundstone	Wackestone to packstone; mudstone pockets	Botryoidal aragonite; isopachous calcite	Vermetids in growth position (a); coral sticks, planktonic foraminifera (c); epiphytes, miliolids (r)	Geopetal infills; high intergranular porosity
BRCR - Bivalve - red algae - coral rudstone	Packstone to wackestone		Bivalves, crustose red algae (a); laminar and domal corals in growth position, Porites fragments, Halimeda, articulated red algae (c); miliolids, epiphytes, acervulinids, planktonic foraminifera (p); fragments of echinoids and bryozoans (r)	
SBRF - Serpulid - bivalve rudstone - floatstone	Fine reddish wackesto	Isopachous calcite	Serpulids, bivalves (a); coral sticks, gastropods, *Halimeda*, elphidium, acervulinids (c)	
FP - Foraminiferal packstone			Miliolids, textulariids, epiphytes (a); bivalves, fragmented articulated red algae, serpulids, bryozoans, echinoids (c-p); planktonic foraminifera (c)	

Halimeda rudstone-floatstone (HRF)

The HRF facies is the most abundant within the two measured sections. It is predominantly characterized by chaotically to imbricated jumbled *Halimeda* segments within a packstone to poorly sorted wackestone matrix, where a relatively small amount of other skeletal grains can be observed, such as articulated and crustose red algae, echinoids, bryozoans, pectinids, and miliolids and planorbulinids (Fig. 3.12A). A peloidal micrite, probably of microbial origin is visible in thin section (Fig 3.12B).

Halimeda boundstone (HB)

This facies is represented by convex lenses that thin out and is characterized by vertically oriented *Halimeda* segments (Figs. 3.8, 3.12A, 3.12C). The frame cavities are partially filled with wackestone matrix (Fig. 3.12 A-B), while the remaining cavities are filled with two

different generations of syn-depositional cement characterized by an early layer of fibrous isopachous aragonite, followed by an isopachous calcite crust with bladed crystals (Fig. 3.12 D). The preservation quality of the *Halimeda* segments varies significantly, ranging from very high to low. High-quality preservation ensures that the internal structures of the segments remain well-defined, while low-quality preservation results in an indistinct or entirely dissolved structure, leaving molds. Occasionally, these molds are filled with sparry calcite.

Vermetids boundstone (VB)

This facies occurs at the base of the "Tre Fratelli" section where it reaches 2 meters in thickness (Fig. 3.13A). This facies is characterized by recrystallized vermetids and a few *Porites* fragments and contains cavities filled with wackestone-packstone matrix. Other common components include bivalves, bryozoans, echinoids, along with miliolids and textulariids, and few planktonic foraminifera. Notably, some vermetids tubes exhibit geopetal infills characterized by vadose silt and drusy calcite (Fig. 3.14B). Locally, massive early botryoidal aragonite cement fills 40-60% of the remaining cavities (Fig. 3.13C1-C2-D).

Bivalve-red algae-coral rudstone (BRCR)

This facies comprises beds ranging from decimeters to meters in thickness and is characterized by the prevalence of large bivalve molds. Additional biota includes, domal to platy *Porites* coral fragments and crustose and articulated red algae (Fig. 3.14A). Common components include *Halimeda* segments, miliolids, epiphytes such as *Elphydium and Amphistegina*, and planktonic foraminifera. Less abundant occurrences are echinoids, serpulids and bryozoan fragments (Fig. 3.14A). Locally, cavities are filled with a packstone-wackestone matrix, while in other instances, they are filled with sparry calcite (Fig. 3.14A).

Serpulid-bivalve rudstone-floatstone (SBRF)

This facies is exclusively present in the "Radar" section, where it occur as an interval 2.8 meters thick. It is characterized by centimeter-thick layers of serpulid rudstone containing abundant isopachous calcite, interbedded with serpulid floatstone with a fine, reddish wackestone matrix. Common components include bivalves, gastropods, *Porites* coral sticks, articulated red algae, *Halimeda* segments (Fig. 3.14C), and benthic foraminifera such as acervulinids and epiphytes (*Elphidium*) (Fig. 3.14B).

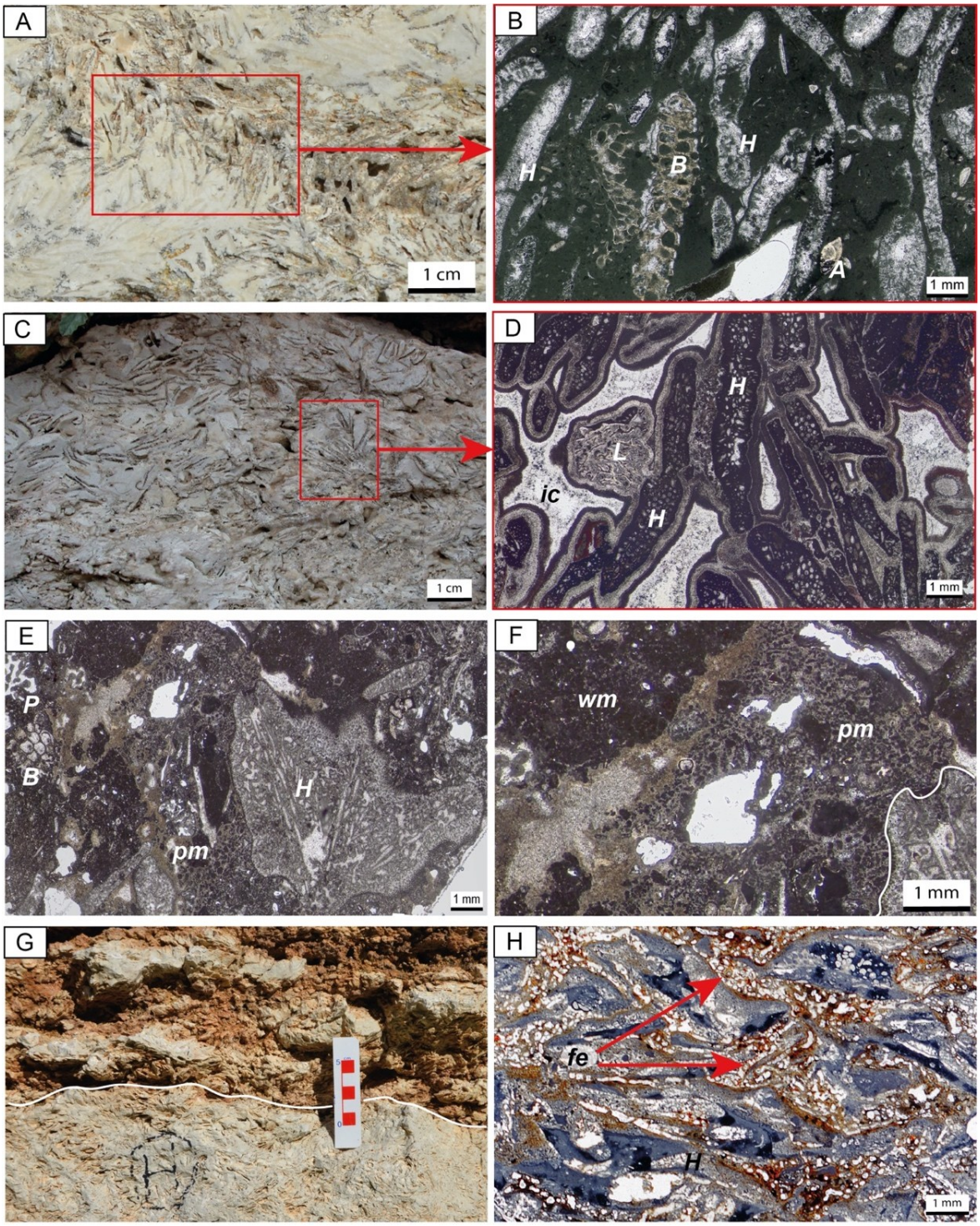

Fig. 3.12. Thin sections of the *Halimeda* facies A-B) HB facies: the vertically oriented algal segments (H) within a fine wackestone to packstone matrix indicate in-situ production of *Halimeda* (red squares). Other components include bryozoan fragments (B) and shallow-water benthic foraminifera like amphisteginids (A). C-D) HB facies: here the vertically oriented very well-preserved *Halimeda* segments (H) occur rimmed by up to four different generation of pre-diagenetic marine cements (red square), including a last stage of isopachous calcite infills. Other components are encrusting foraminifera such as *Laduronia* sp.(L). E) HRF facies: *Halimeda* segments (H) in a packstone to wackestone matrix encrusted by a peloidal micrite crust (pm). Other common components are fragments of bryozoans (B) and *Porites* corals (P). F) HRF facies: close-up on the peloidal micrite encrusting a well-preserved *Halimeda* segment (white line). G) HRF facies: a close-up detail of the terminal (flank) portion of the bioherm in the "Three brothers" section where the deposit appears less massive and more stratified due to the horizontally to imbricated arrangement of *Halimeda* segments. H) HRF facies: *Halimeda* segments in a fine wackestone matrix affected by abundant foraminiferal encrustations (fe) (red arrows).

Foraminiferal packstone (FP)

This grain-supported facies is exclusively present in the upper part of the "Tre Fratelli" section, with a total thickness of 1.5 meters. Its identification is based on the abundance of small shallow-water benthic foraminifera, predominantly miliolids and epiphytes (e.g *Amphistegina* and *Elphidium*) and planktonic foraminifera (e.g., *Globigerinoides*, *Globigerina*). In smaller quantities there are molds of large bivalves, fragments of bryozoans, articulate red-algae, serpulids, and echinoids (Fig. 3.14D).

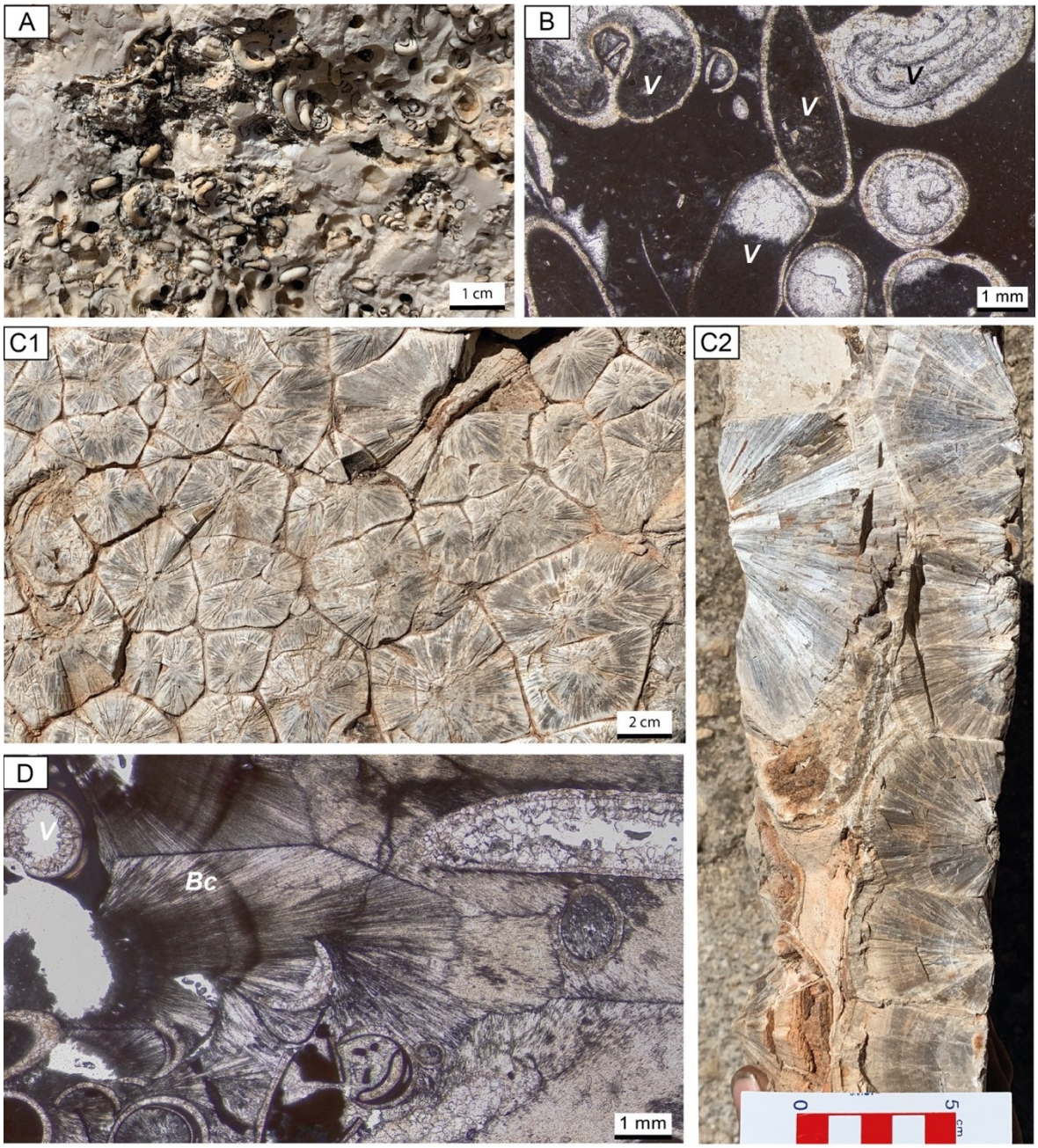

Fig. 3.13. A) VB facies: outcrop close-up of arranged vermetid tubes in a wackestone matrix. B) VB facies: thin sections of arranged vermetid tubes (V) in a wackestone to mudstone matrix with some geopetal infills. C1 and C2) VB facies: the large quantity of aragonitic botryoidal marine cements that fill the porosity up to a maximum of 60 %. D) VB facies: detail of the aragonitic botryoidal cements (Bc) and vermetid tubes (V).

Red algae - *Halimeda* rudstone (RHR)

The RHR facies consists of crustose red algae (*Mesophyllum*) rudstone, containing well-preserved *Halimeda* segments. Additional biota includes planktonic foraminifera, a few benthic foraminifera, including miliolids and textulariids, and rare bryozoans and acervulinids (Fig. 3.15E). Red algae and acervulinids commonly encrust other skeletal fragments. This facies exhibits a high primary intergranular porosity partially filled with fibrous and isopachous cement (Fig. 3.14E).

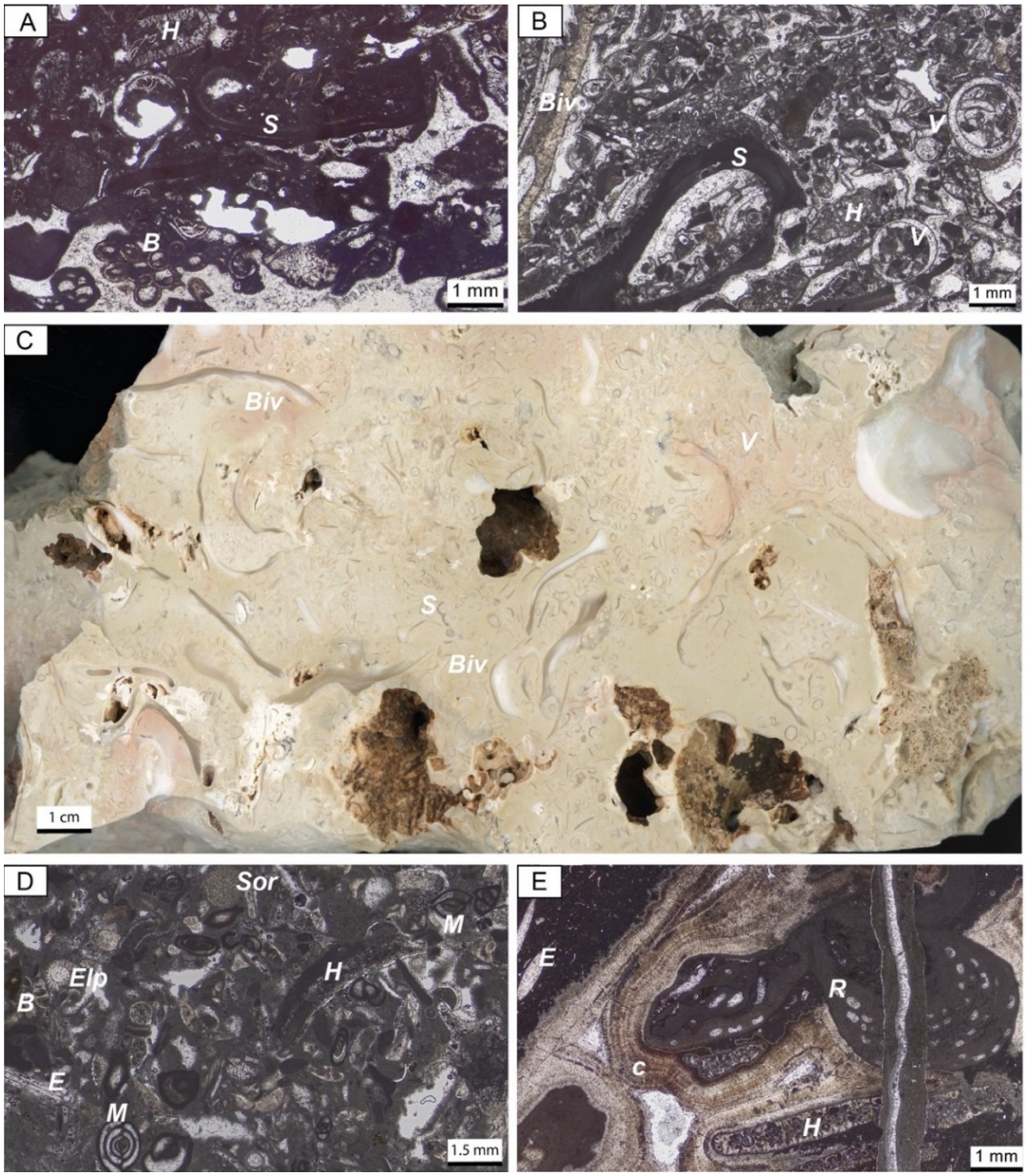

Fig. 3.14. A) BRCR facies: thin section with serpulids (S), bryozoans (B) and *Halimeda* segments (H). B) SBRF facies serpulid fragments (S) along with bivalves (Biv), vermetids and *Halimeda* segments (H) within a peloidal matrix and isopachous cements. C) SBRF facies: polished slab with serpulids (S), vermetids (V) and bivalve fragments (Biv). D) FP facies: arrangement of shallow-water benthic foraminifera like miliolids (M), soritids (Sor), textulariids (T), amphisteginids (A) along with few echinoid spines (E), bryozoans (B), and *Halimeda* segments (H). E) RHR facies: crustose red algae (R) and well-preserved *Halimeda* segments (H) held together by various generations of cements (c)filling the high intergranular porosity, along with a fine wackestone matrix rich in planktonic foraminifera and echinoid spines (E).

3.6 Interpretation and discussion

The *Halimeda* bioherm of the "Tre Fratelli" section was analyzed in detail thanks to the favorable outcrop conditions that permits a partial 3D view (Fig. 3.7). In order to provide a detailed analysis, the bioherm was divided into approximately 1-meter sectors (A–L). Following a thorough taphonomic analysis, it was found that the first seven sectors of the outcrop (A-G) are more massive. These sectors are primarily characterized by rudstone-floatstone textures (HRF facies) with poorly preserved algal segments arranged chaotically or imbricated within a wackestone matrix (Fig. 3.12). Within this interval, boundstone lenses can be identified (dark green spots in Fig. 3.8). The space between the algal segments is either filled with matrix (Fig. 3.12B) or, at times, with cement (Fig. 3.12D). These cements surrounding the segments seems to favor the preservation of their original orientation and their internal structure (Fig. 3.12D). Instead, where the segments are surrounded by wackestone, they have been partially or completely altered. The bioherm laterally gradually thins out and becomes stratified in the terminal part, as observed in the last sectors (H-L) (Fig. 3.8). The stratification is due to presence of a succession of thin layers of floatstone containing largely dissolved imbricated segments, although zones characterized by boundstone textures persist. This stratified area (H-L interval) dominated by HRF facies are interpreted as the flank deposits of the boundstone accumulations (A-G interval) (Fig. 3.7).

The "Tre Fratelli" bioherm exposure allows to observe a variation between the more massive core and the flank, characterized by a reduced thickness and crude bedding. The internal architecture and facies distributions are consistent with a recent study by Reolid et al. (2024), that describe the internal organization of a modern mesophotic *Halimeda* mound in Tregrosse bank (Great Barrier Reef). On the basis of preserved depositional geometries of the Novaglie formation (Bosellini et al., 1999), the *Halimeda* bioherms occur as part of a complex of small bioherms located in the mid-to-proximal slope of the Novaglie formation reef (Fig. 3.15).

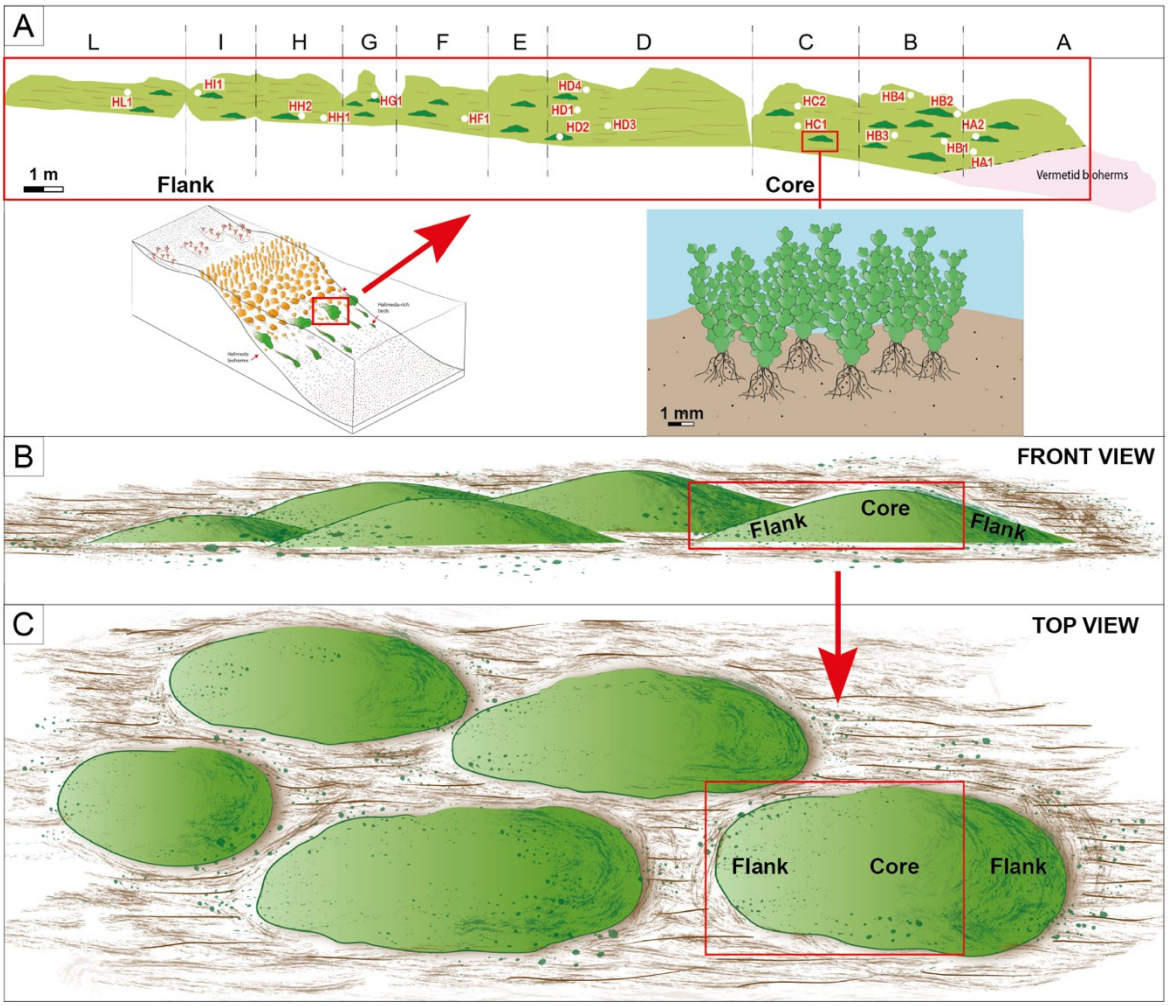

Fig. 3.15. Sketch of the depositional model and internal organization of the "Tre Fratelli" *Halimeda* bioherm subdivided in sectors (A – L) in scale located in the mid-to-proximal slope of the Novaglie formation. A) Distribution of the facies HB (dark green) and HRF (bright green) within the outcrop. Algal thalli orientation in the HB facies. B) Inferred depositional model of the small *Halimeda* bioherm complex (not in scale). C) Top view. The red squares represent the outcropping zones of the bioherm in the Tre Fratelli outcrop (Passaseo and Morsilli, 2025)

3.6.1. Halimeda bioherms in the Messinian reefs of the Mediterranean area

While there are several documented occurrences of *Halimeda* in the Mediterranean during the Messinian, evidence of *in-situ* accumulations forming bioherms is scarce (Esteban, 1979; Brachert et al., 2007). Known examples in the literature are limited to southeastern Spain, southeastern Italy, and Crete where they typically develop along the reef slope area or as isolated mounds on ramp systems (Braga et al., 1996; Martín et al., 1997; Vescogni, 2000; Bosellini et al., 2002; Brachert et al., 2007).

Halimeda deposits in Crete have been interpreted by the authors as small, isolated *in-situ* accumulations (1.8 m wide and 0.6 m thick), associated with resedimented breccia, on the mid-to-proximal ramp (Brachert et al., 2007). These deposits share similar facies with the ones described in this paper, including significant early cementation. Nonetheless, resedimented *Halimeda*-rich beds are also abundant on Crete, indicating extensive *Halimeda* meadows development compared to what is found in the literature (Passaseo and Morsilli, 2024).

In the Sorbas and Níjar basins of southeast Spain, extensive *Halimeda* deposits have been thoroughly documented from Tortonian and Messinian successions (Braga et al., 1996; Braga and Martín, 1996; Martín et al., 1997). According to Braga et al. (1996), the *Halimeda* bioherms of the Sorbas basin reach up to 400 m in length and 40 m in thickness and occur on a mid-to-proximal ramp with a gentle slope of about 5 degrees (Martín et al., 1997). The Salento deposits are smaller (~5 m in thickness) and located on a mid-to-proximal slope with a dip-angle between 15 and 30 degrees (Bosellini et al., 2002). Although, the different size and depositional setting, all these bioherms exhibit similar facies distribution and internal architecture, including the occurrence of syn-depositional marine cementation. However, the bioherms of Salento display more complex cementation with different types of cements, whereas the bioherms in Spain, are characterized by simpler, micritic and peloidal microbial crusts.

The differences in size and morphology of the bioherms may be attributed to the inclination of the slope, which directly affects the development and stabilization of the bioherms, or even to different nutrient availabilities. The high angle slope (up to 30°) was controlled from the morphology of the deep basin located in front of the Salento Peninsula, corresponding to the present Otranto Strait (Bosellini et al., 1999). This is consistent with the fact that the large Holocene bioherms of the GBR (McNeil et al., 2016, 2021, 2022; Reolid et al., 2024) develop on broad, sub-horizontal shelf.

In another area of the Sorbas Basin, a well-preserved fringing reef system near the locality of Cariatiz, features resedimented *Halimeda* deposit along the mid-to-proximal slope (Braga

and Martín, 1996). Although these deposits are resedimented, they occur along the same slope position of the small bioherms of the Salento Peninsula.

3.6.2 Early diagenetic cementation

The succession of two early-marine cements surrounding the *Halimeda* segments in the HB facies (Fig. 3.12D) and large botryoidal cements in the VB facies (Fig. 3.13C1-C2-D), were observed only in the "Tre Fratelli" section. In the HB facies, it was observed that when cement occurs surrounding the algal segments, they are well-preserved. Conversely, when cement is absent and inly mud is present, the *Halimeda* segments are partially or totally dissolved. We infer that aragonitic cement acts as an impermeable film that prevents dissolution. This is because aragonitic cement exhibits greater resistance to dissolution than the algal segments, a resistance attributed its dense crystal fabric (Brachert et al., 2007). In addition, this early cementation preserves the vertical orientation of the segments suggesting an *in-situ* accumulation. This accretion, combined with syn-sedimentary cementation, facilitated the development, accumulation, and stabilization of *Halimeda* bioherms on the steep slopes of the Novaglie formation, as already documented in the bioherms from the Sorbas Basin of Spain (Braga et al., 1996; Martìn et al., 1997).

Early cementation in *Halimeda* bioherms has been documented not only from all three Messinian occurrences in the Mediterranean but also in *Halimeda* facies from offshore deposits of North Palawan – Philippines (Fournier et al., 2024). The specific nature of these cements and their occurrence in these facies remains poorly understood. During the early Messinian, the Mediterranean region began experiencing the initial effects of the salinity crisis (MSC), leading to the effective closure of major exchange routes with the Atlantic Ocean. The presence of marine syn-depositional cements within these facies suggests that specific geochemical conditions, possibly linked to the restricted water exchange during the onset of the (MSC), were critical in their formation. This restricted water exchange, combined with hypersaline bottom waters, and limited nutrient cycling, significantly affected marine biota, including *Halimeda* bioherms and coral reefs (Bosellini et al., 2002; Vertino et al., 2014; Moissette et al., 2018; Vasiliev et al., 2019; Vescogni et al., 2022; Agiadi et al., 2024a; 2024b). The $\delta^{18}O$ compositions of marine cements analyzed in the bioherms of Crete and Salento suggest that sea surface salinity (SSS) peaked at 50–60‰, levels too high for most shallow-water biota, such as zooxanthellate corals (Fig. 3.16). Brachert et al. (2007) note that high salinity events, in both reefs and slope deposits, affected large areas of the Mediterranean but were not coupled with evaporative sea level drawdowns.

This points to the potential existence of refugia for stenohaline organisms like *Halimeda*, allowing them to persist during periods of high salinity.

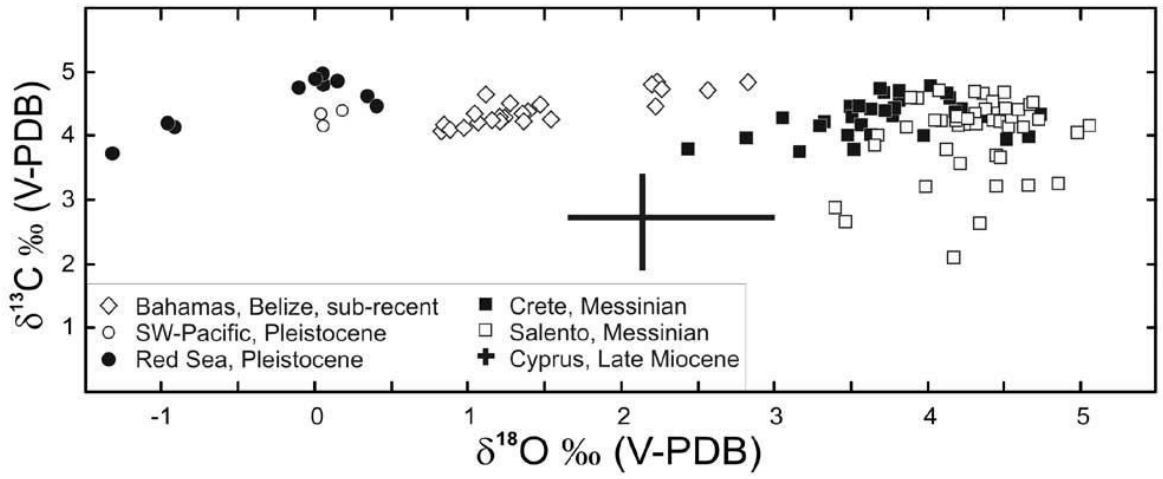

Fig. 3.16. Stable isotope compositions ($\delta^{18}O$, $\delta^{13}C$) of botryoidal and isopachous cements from the Salento Peninsula and Crete Island (Brachert et al., 2007). For comparison, botryoidal aragonites are reported from Belize and the Bahamas (Grammer et al., 1993), the Red Sea (Taviani & Rabbi, 1984; Aïssaoui, 1985), Ouvéa (Aïssaoui, 1985), and Cyprus (Follows, 1992).

Before the Messinian Salinity Crisis (MSC), the Mediterranean region underwent significant environmental stress, severely affecting benthic ecosystems (Bosellini and Perrin, 2008; Vertino et al., 2014; Agiadi et al., 2024a, 2024b). During the late Tortonian and early Messinian, coral reefs, especially in the western Mediterranean, were abundant but exhibited markedly reduced diversity, often dominated by just two genera, *Porites* and *Siderastrea* (Vertino et al., 2014). This environmental degradation near the onset of the MSC triggered a shift from coral frameworks to microbialite-dominated reefs, with *Halimeda* and vermetid gastropods becoming more prevalent (Brachert et al., 1996; Braga et al., 1996; Martín et al., 1997; Bosellini et al., 2002; Vescogni et al., 2008; Vertino et al., 2014). Stress on *Halimeda* and associated coral reefs intensified due to escalating changes in salinity, temperature, and nutrient availability. Reduced water exchange led to hypersaline conditions, with recorded SSS ranging from 48 to 58‰, well above the tolerance limits for most reef-associated organisms (Vasiliev et al., 2019). As the influx of Atlantic waters waned, oxygen-poor, hypersaline bottom waters developed, limiting vertical mixing, nutrient recycling, and biodiversity (Moissette et al., 2018; Agiadi et al., 2024a, 2024b). Nutrient dynamics also shifted: reduced Atlantic inflow initially promoted productivity, but intensified water stratification limited nutrient cycling within the photic zone, diminishing primary productivity over time (Kontakiotis et al., 2022). Geochemical data from the Sorbas Basin, including $\delta^{13}C$ and δ^{1} O isotopes, further suggest that reduced freshwater input and increased aridity restricted nutrient availability (Reghizzi et al., 2017). Given this context, we believe

internal waves (IWs) may have facilitated nutrient delivery to *Halimeda* bioherms, aiding their proliferation but also creating unfavorable conditions for coral reefs.

Temperature fluctuations further destabilized these ecosystems, with alternating cooling and warming phases, particularly from 6.4 to 6.1 million years ago (Kontakiotis et al., 2022). These adverse conditions contributed to episodic shifts within reef communities, with less tolerant corals being replaced by microbialites and *Halimeda* (Vertino et al., 2014). In areas such as Salento, Spain, and Crete, *Halimeda* bioherms exhibited thick aragonitic cements, potentially indicating high salinity stress (Brachert et al., 2007). Additionally, Vasiliev et al. (2019) noted Mediterranean SSS and SST oscillations, with a cooling phase around 6.4 million years ago followed by rapid warming near 6.15 million years ago, temporarily reducing salinity due to freshwater influxes, before returning to hypersaline conditions, which further stressed marine life.

The cumulative effects of tectonic isolation, nutrient limitations, salinity stress, and temperature fluctuations contributed to the decline of *Halimeda* bioherms and coral reefs, thereby preconditioning the Mediterranean for the extreme evaporitic phase of the MSC (Roveri et al., 2020; Bulian et al., 2023; Agiadi et al., 2024a, 2024b). The presence of early cementation observed in *Halimeda* bioherms provides valuable insights into the interactions between biological activity, sedimentation, and environmental change during the Messinian.

3.6.3 Nutrients as the key factor on the blooming of Halimeda bioherms

The *Halimeda* bioherms of the Australian GBR have been extensively studied since the 1980s (Drew, 1983; Davies and Marshall, 1985; Drew and Abel, 1985; Orme,1985; Drew and Abel, 1988; Roberts et al., 1987, 1988; Hine et al., 1988; Marshall and Davies, 1988; Orme and Salama, 1988; Phipps and Roberts, 1988; Searle and Flood, 1988; Mc Neil et al., 2016; 2022).

Wolanski et al. (1988) outlined a direct relationship between the extensive distribution of *Halimeda* bioherms behind the GBR Ribbon Reefs and a stable supply of nutrients, that supports their persistence over time. McNeil et al. (2021) further investigated this aspect by using the $^{15}N/^{14}N$ ratio ($\delta^{15}N$ skeletal organic material – SOM) on algal tissue. Although nutrients can originate from sources like terrestrial runoff, sewage input, or groundwater intrusion, the authors identified upwelling of cold water generated at great depths as a source of nutrient supply, specifically originating from thermocline waters (Mc Neil et al., 2021).

The laterally and stratigraphically localized development of the Salento bioherms, suggests a periodic external nutrient input. As discussed earlier in the paragraph 3.6.2, we propose

that this input gradually diminished due to the onset of the MSC, ultimately leading to the isolation of the Mediterranean Sea. According to Bosellini et al. (1999), the Salento carbonate system was part of an open, isolated platform, away from continental areas, characterized by a very limited freshwater influx and minimal terrigenous inputs. In contrast, the depositional setting of the Western Mediterranean localities, received significant amounts of freshwater and siliciclastic sediment, and were influenced by Atlantic waters (Esteban, 1979; Riding et al., 1991; Rouchy and Saint Martin, 1992; Martin and Braga, 1994; Franseen et al., 1998; Bourillot et al., 2009; Roveri et al., 2009, 2020; Pérez-Asensio et al., 2014). These differences suggest that the Salento carbonate system accounts for the smaller size of the *Halimeda* bioherms in Salento compared to those in Spain.

The availability of large quantities of nutrients is also attributed to specific climatic conditions, such as those found in tropical areas. Meteorological phenomena influenced the flourishing growth of *Halimeda*, as demonstrated by the large-scale bioherms of the Australian Great Barrier Reef (McNeil et al., 2021), where local upwelling intrusions at the shelf-break likely intensified during peak El Niño periods, delivering more thermocline NO_3- toward *Halimeda* bioherms. This process is similarly inferred for the Oligocene bioherms present offshore of North Palawan – Philippines (Fournier et al., 2024), where upwelling currents associated with the onset of coastal jet in the Proto-South China Sea, established by a modern-like East Asian Monsoon summer circulation as early as the late Eocene, supplied essential nutrients for bioherm development. There is no evidence of meteorological phenomena of this kind, however, affecting the Mediterranean basin during the Messinian, and perhaps for this reason, the nutrients supplied to the bioherms in Salento were not sufficient for their development into large-size sedimentary bodies or their persistence.

3.6.3 Upwelling history in the central Mediterranean Basin

The upwelling of cold nutrient-rich waters is not unusual in the stratigraphic record of the central-eastern Mediterranean. Deposits associated with upwelling have been documented in various areas throughout the Tortonian (Fig. 3.17), including Malta (Föllmi et al., 2008), southeast Sicily (Föllmi et al., 2008), the Matese area in the central Appennines, the Maiella Mountain (Mutti and Bernoulli, 2003), the Latium-Abruzzi carbonate platform in the Apennines (Brandano et al., 2009), the Menorca Island and the Salento Peninsula (Föllmi et al., 2015).

Specifically, the Salento Peninsula experienced a flooding during the Serravalian-Tortonian, which impacted the entire area. This event was responsible of the deposition of pelagic

sediments of the Pietra Leccese inland and the Aturia Level hardground in coastal areas (Vescogni et al., 2018).

This Aturia Level is characterized by glauconitic and phosphoritic micrite, and rests between two thick, shallow-water formations: the Porto Badisco Calcarenites (upper Oligocene) and the Novaglie formation (early Messinian), as can be observed in the Ciolo locality a few km north of the described sections, at the Ciolo locality (Fig. 3.4) (Föllmi et al., 2015). In this location, a small cave permit to observe a thin, brownish layer a few tens of centimeters thick (Fig. 3.18). Moving southward, before the Tre Fratelli area, the Aturia Level reaching its maximum thickness of about 50 cm.

This regionally extensive condensed level, rich in macrofossils, has been related to a system of upwelling currents originating from the deepest areas of the Mediterranean Basin and reaching the eastern parts of the shelf (Föllmi et al., 2015). Changes in the direction and intensity of these bottom currents created a complex and variable depositional environment, where low sedimentation rates vertically alternate with areas of prevalent erosion (Vescogni et al., 2018).

Based on the occurrence of this hardground layer in the Salento Peninsula and other Mediterranean areas previously mentioned, which is interpreted as recording nutrient-rich upwelling currents throughout the Tortonian period, we infer that upwelling phenomena persisted into the early Messinian. Although these phenomena were of lower intensity, they continued to supply the necessary nutrients for the development of the small *Halimeda* bioherms in the Salento Peninsula.

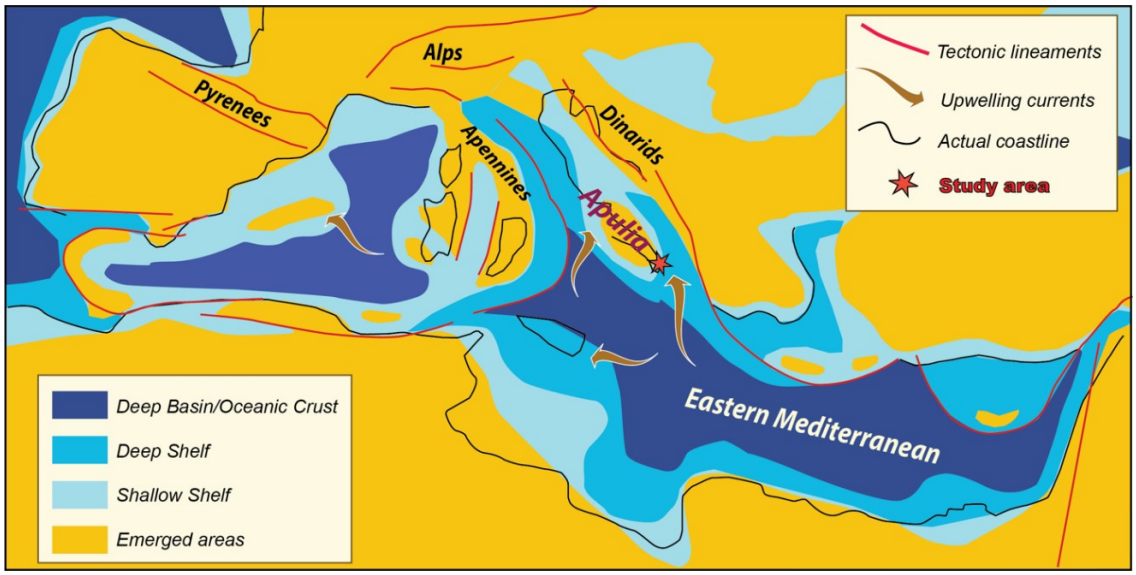

Fig. 3.17. Paleogeographic map of the Mediterranean area during the Tortonian - early Messinian with upwelling currents system that have promoted the formation of phosphatic condensed layers (modified after Popov et al., 2004). Considering

the position of the Salento area and the proximity to the adjacent deep-water basin, we infer that weak upwelling currents were still active during the early Messinian.

Fig. 3.18. The condensed phosphatic hardground known as Aturia level (red line) located between the top of the Porto Badisco calcarenites and the base of the Novaglie formation at the Ciolo locality with its characteristic brownish color. In the white box: specimen of *Aturia aturii*.

3.6.4 *Internal waves and their impact on nutrients dynamics*

An additional hydrodynamic mechanism to consider for the delivery of nutrients to the small bioherms of Salento is the potential action of internal waves (IWs) and tides. Internal waves and tides are gravity waves oscillations that occur within stratified ocean waters, propagating along the interfaces between layers of water with different densities (pycnocline) due to changes in temperature and salinity. These waves are generated by various forces, including tides, wind stress, storms etc. (Lamb, 2014; Boegman and Stastna, 2019; Woodsoon, 2018 and reference therein). Internal waves can travel over long distances and play a critical role in ocean mixing processes, transporting heat, nutrients, and larvae vertically through the water column (Leichter et al., 2005), as well as in sediment resuspension and transport, at various depth, along the continental slopes and platform where they break (Cacchione et al., 2002; Pomar et al., 2012; Lamb, 2014). IWs and internal tides can have significant impacts on the distribution of nutrients and the structure of marine ecosystems (Leichter et al., 2005; Pomar et al., 2012; Reid et al., 2019; Johnston et al., 2022).

It is not unusual for IWs to play a role in transporting nutrients to euphotic and mesophotic communities like corals and calcareous algae. It is known that in coastal regions, vertical mixing associated with IWs may result in a significant input of deep-water nutrients and particulate organic matter into shallow environments (Sandstrom and Elliot, 1984). Leichter et al. (1996) also documented that in modern Florida Keys, high excursions in temperature, salinity, current velocities, and concentration of chlorophyll-a are caused by the breaking of internal waves. Furthermore, Leichter et al. (1998, 2003, 2005) and Smith et al. (2004) reported enhanced growth rates of *Halimeda* specimen to be associated with enhanced fluxes of nutrients and suspended particles carried by internal waves. In addition, recent studies based on the nitrogen isotopic signature in the organic tissue of *Halimeda* segments in the GBR have confirmed a deep-water origin of the nutrients delivered to the *Halimeda* bioherms coming from the thermocline zone (McNeil et al., 2021), where usually IWs are common.

While the essential role of nutrients in the development of many *Halimeda* species and bioherms in modern oceans is well-established (McNeil et al., 2021), a recent study by Reolid et al. (2024) on *Halimeda* bioherms identified at Teagross Bank (Queensland Plateau – GBR) revealed a new type of bioherms. These bioherms, which are associated with mesophotic corals, are thought to have developed in an oligotrophic environment, and thus not related to upwelling currents. However, this work does not discuss the significance of the nutricline position (70-80 m), just below and near the depth of the bioherms (40-70 mbsl), where internal tides have been documented (Bendinger et al., 2023). In this context, without documented upwelling currents, internal tides can serve as a mechanism for transporting nutrients to this *Halimeda* communities. Moreover, their chlorophyll-a rate measurements are point-specific (<12 h) and therefore not representative of the significant seasonal variability, including phenomena such as tropical monsoons and storms that appear to favor the remixing of oceanic waters (Rao et al., 2018; McNeil et al., 2021; Fournier et al., 2024).

In summary, internal waves (IWs) provide an additional mechanism for nutrient delivery to the small *Halimeda* bioherms examined in this study. This nutrient transport may be particularly significant in oligotrophic regions, where the absence or weakness of upwelling currents necessitates alternative nutrient enrichment mechanisms to support the growth of *Halimeda* bioherms in the mesophotic zone along the slope of the Novaglie formation.

3.7 Conclusions

The detailed analysis and comparison of *Halimeda* bioherms in the "Tre Fratelli" and “Radar” sections, highlights their internal organization and depositional features. In the "Tre Fratelli" outcrop, the bioherm core is distinguished by *in situ Halimeda* segments alternating with rudstone and floatstone layers, while the upslope flank is characterized by thin to medium beds of rudstone and floatstone.

The small bioherms occur along the proximal-to-mid slope part of the Novaglie formation. The internal organization and facies distribution of the "Tre Fratelli" bioherm are consistent with recent studies describing the internal structure of Holocene *Halimeda* mounds. Additionally, the presence of marine syn-depositional cements within the algal segments plays a critical role in preserving the internal structure of the algae and ensuring the stability of the deposits. These cements provide valuable insight into the fluctuations in salinity within the Mediterranean basin during the Messinian.

Comparison of lower Messinian *Halimeda* deposits in the Mediterranean area revealed that *Halimeda* bioherms development is limited to a few examples in Spain, southeastern Italy, and Crete Island. In contrast, *Halimeda*-rich beds have been reported across the Mediterranean region, including Morocco, Tunisia, and Egypt.

Nutrient supply is a crucial factor for the development of *Halimeda* bioherms. As observed in modern oceans, a stable supply of nutrients is essential for the persistence of these bioherms over time. Similarly, in the Salento area, sporadic and weak nutrient supply events could explain the development of these bioherms in a specific depositional setting along the mid slope, within a defined stratigraphic interval, just before the onset of Messinian Salinity Crisis. Hydrodynamic mechanisms such as the upwelling of nutrient-rich waters and internal waves may have facilitated the transport of nutrients to the bioherms.

Although the *Halimeda* bioherms in Salento are not as large as some modern analogs, they offer valuable insights into the sedimentary and paleoenvironmental dynamics of the central Mediterranean during the early Messinian. Recognizing *Halimeda* as a significant carbonate producer, particularly in mesophotic environments where other calcifying organisms are less productive, is crucial. In the context of global warming, *Halimeda* bioherms become increasingly important for their potential role in CO_2 sequestration. Further studies of both past and present bioherms are essential to understand their capacity to mitigate climate change impacts and possibly serve as refugia for other marine organisms, particularly in the mesophotic zone.

4. The *Halimeda* bioherms of the Sorbas and Níjar-Carboneras Basins (southeastern Spain)

Sorbas and Níjar-Carboneras Basins represent the largest areas and exhibit the highest number of outcrops from the Upper Miocene, which have been extensively studied by Esteban (1979), Dabrio et al. (1981), Mankiewicz (1988), Franseen and Mankiewicz (1991), Jiménez and Braga (1993), Martín and Braga (1994), Esteban et al. (1996), Braga & Martín (1996), Braga et al. (1996), Martín et al. (1997), Sánchez-Almazo et al. (2001), Martín et al. (2003), Cornée et al. (2004), Braga et al. (2009), Bourillot et al. (2009), Martín et al. (2014), Pérez-Asenzio et al. (2014), and Reolid et al. (2014). Therefore, our fieldwork was not focused on acquiring new data but on comparing the different geometric characteristics of the outcrops and the depositional systems.

The primary goal was to compare these systems with those from the Salento Peninsula, while also understanding the distribution of the deposits and identifying potential factors within the successions, such as sedimentary structures that could be correlated with upwelling or internal waves phenomena. Additionally, a key focus was on investigating the depositional environment of *Halimeda*, both in terms of resedimented layers and isolated bodies with autochthonous or allochthonous deposition.

Another important objective was to conduct taphonomic observations on *Halimeda* algal segments and the sedimentary matrix in which they are embedded. These investigations aimed to enhance the understanding of the transport, preservation, and deposition processes of the algal segments, allowing for the differentiation between resedimented bodies and those deposited in situ.

4.1 The Sorbas Basin

The Sorbas Basin, situated in the internal zones of the Betic Cordillera in southern Spain, represents an intermontane Neogene basin that extends from east to west and is bounded by two of these metamorphic domes (Martínez-Martínez and Azañon, 1997, 2002; Augier et al., 2005a, 2005b) the Sierra de Los Filabres to the North and the Sierra Ahlamilla to the South and is part of a mosaic of other Neogene basins that shape the Iberian landscape, including the Tabernas, Vera, and Níjar-Carboneras basins (Fig. 4.1).

During the Eocene, the geodynamics of the Mediterranean region were characterized by the development of back-arc basins, extending from the Alboran Sea in the west to the Aegean Sea in the east. This phase followed a major shift in the subduction regime during the

Oligocene (Rehault et al., 1984; Faccenna et al., 1997; Jolivet and Faccenna, 2000). The formation of these basins—such as the Pannonian Basin, Aegean Sea, Liguro-Provençal Basin, Tyrrhenian Sea, and Alboran Sea—occurred above retreating slabs.

The current complex geometry of the subduction zones and back-arc basins reflects the initial configuration of the African margin (Frizon de Lamotte et al., 2011), combined with progressive slab tearing and detachments (Wortel and Spakman, 2000), and is influenced by a complex 3D mantle convection pattern (Faccenna and Becker, 2010). At the western end of the Mediterranean, the Alboran Domain documented this regional episode of back-arc extension and slab retreat (Faccenna et al., 2004; Spakman and Wortel, 2004). This extensional regime continued until approximately 7-8 Ma, when it was succeeded by a compressional regime due to renewed convergence between Africa and Eurasia (Jolivet et al., 2008).

The Sorbas Basin serves as a crucial peripheral basin that captures sedimentary records from the upper Serravallian to the Pliocene. These sediments document the interactions between tectonic activity and eustatic changes in the southwestern Mediterranean region. Various interpretations of the Neogene evolution of the Alboran region have relied on the stratigraphy and structure of this basin (Weijermars et al., 1985). Initially, the basin's formation during the Serravallian to early Tortonian has been attributed to different tectonic mechanisms, ranging from strike-slip to pure extension. Since the upper Tortonian, the Sorbas Basin has undergone NW-SE shortening, which has significantly influenced its current geometry (Weijermars et al., 1985) (Fig. 4.2).

The basin remained connected to the Atlantic Ocean to the west until the early Messinian. After the closure of the Guadalhorce corridor (Fig. 4.2), which is generally considered to have occurred during the early Messinian (Martin et al., 2001), marine connections were maintained only with the Mediterranean, through narrow and shallow sills to the south and east.

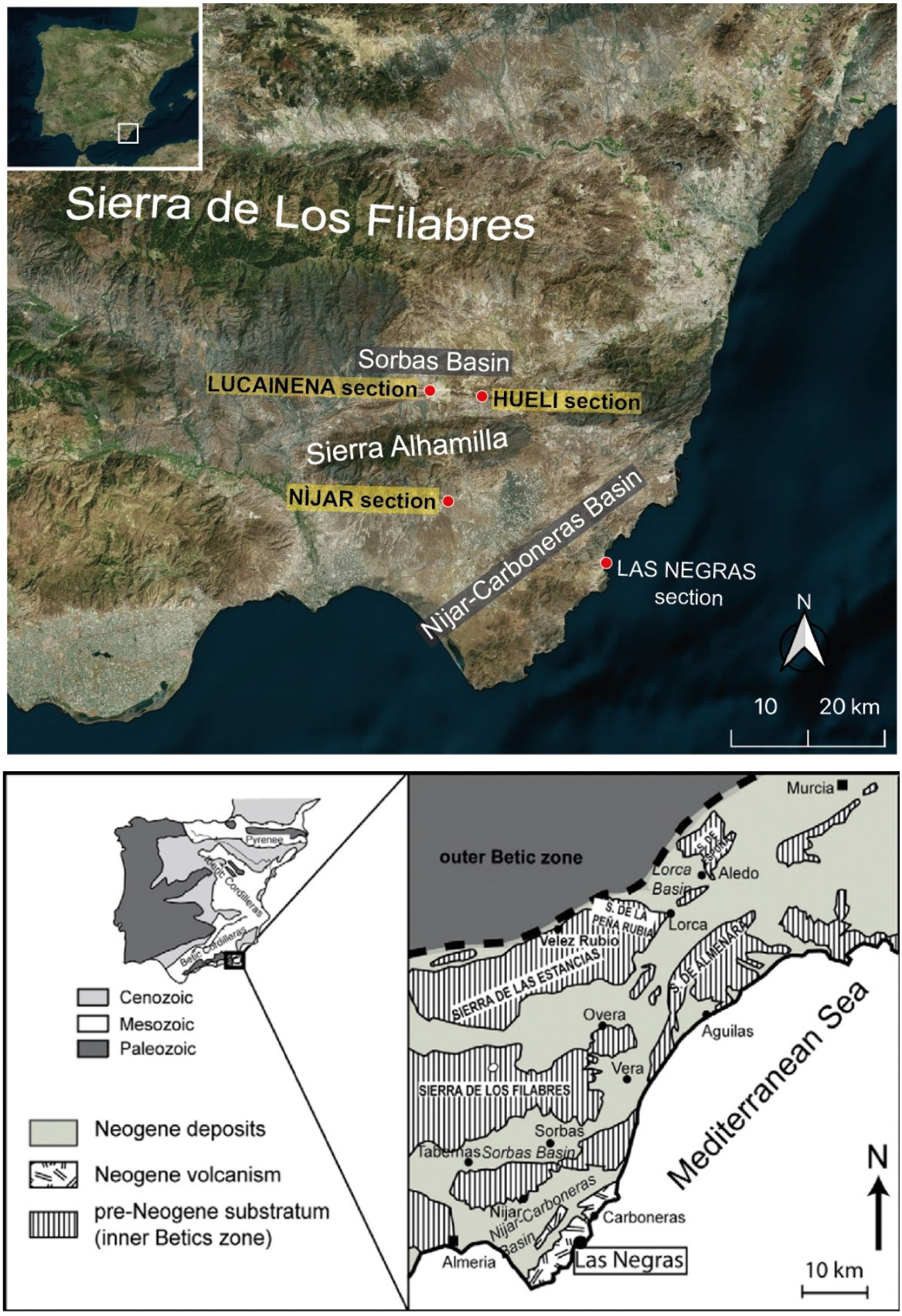

Fig. 4.1. Geographic and geological maps of southeastern Spain (Almeria) highlighting the locations of the measured stratigraphic sections (Bourillot et al., 2009).

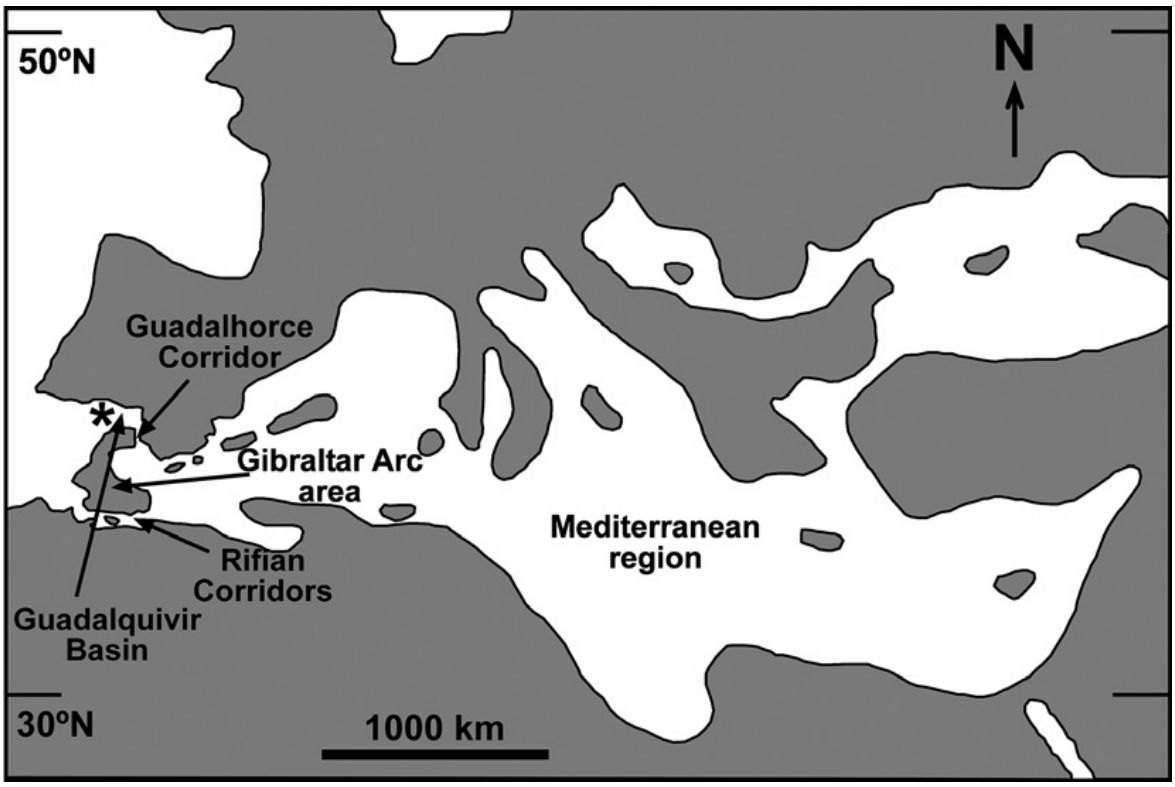

Fig. 4.2. Palaeogeography of the Guadalquivir Basin, Gibraltar Arc area, with the location of the Guadalhorce corridor, and the Mediterranean region during the early Messinian (Pérez-Asensio et al., 2014).

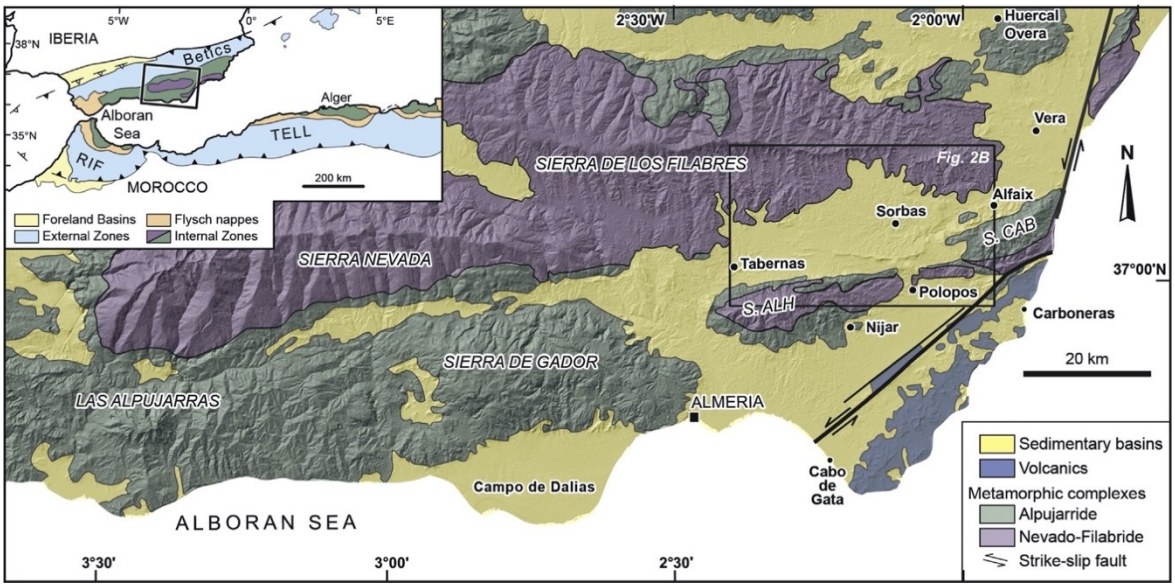

Fig. 4.3. Simplified structural map of Southeastern Spain. Located are the main metamorphic domes of the Sierra de los Filabres-Nevada and the Sierra Alhamilla-Cabrera and the main sedimentary basins (Do Couto et al., 2015).

4.1.1 Geology and Stratigraphy

The sedimentary history of the Sorbas Basin begins with sparse Serravallian conglomerates (Ott d'Estevou and Montenat, 1990), which are subsequently overlain by Tortonian sediments ranging from shallow to deep marine environments. The deposition of these

sediments in the southern region of the basin was predominantly influenced by tectonic erosion of the Sierra Alhamilla (Do Couto et al., 2014) (Fig. 4.4).

The succession from the upper Tortonian to the Lower Pliocene includes the Turre and Caños Formations (Voelk and Rondeel, 1964; Ruegg, 1964; Martín and Braga, 1994). The Turre Formation is comprised of three members (Fig. 4.4) that document a general transgressive trend following a significant phase of transpressive deformation during the late Tortonian.

The basal Azagador Member consists of fossiliferous shallow marine calcarenites with a notable basal conglomerate that transition upwards and basinwards into epibathyal marls, sapropels, and diatomites of the Upper Abad Member (Ott d'Estevou, 1980). The Azagador Mb is dated to the Tortonian/Messinain boundary (Sierro et al., 1993; Gautier et al., 1994; Krijgsman et al., 2001). The Lower Abad Member then transitions upslope into carbonate platform deposits of the Canteras Member, which includes bioclastic units with isolated coral and *Halimeda* bioherms (the "Bioherm unit" sensu Martín and Braga, 1994) and the Porites fringing reef exhibiting striking progradational geometries (e. g. Caritiz reef, Martín and Braga, 1994).

At the center of the basin, the Abad marls are overlain by primary selenitic gypsum deposits, which form the Yesares Member of the Caños Formation and are generally correlated with other primary gypsum bodies known as the Lower Gypsum. The Yesares Member is conformably overlain by shallow-water clastic deposits of the Sorbas Member, which in turn are covered by upper Messinian to lower Pliocene fluvial deposits of the Zorreras Member. These fluvial deposits contain two prominent basin-wide lacustrine limestone horizons (Roep et al., 1998; Krijgsman et al., 2001), or four according to Mather et al. (2001).

The Sorbas Member, thoroughly studied by Roep et al. (1998), transitions towards the basin margins into mixed coarse-grained siliciclastic and reefal carbonate deposits, characterized by oolites, *Porites*, and stromatolites (Fig. 4.4). These deposits evolve upwards and laterally into lower Messinian fringing reefs, collectively referred to as the Terminal Carbonate Complex (TCC).

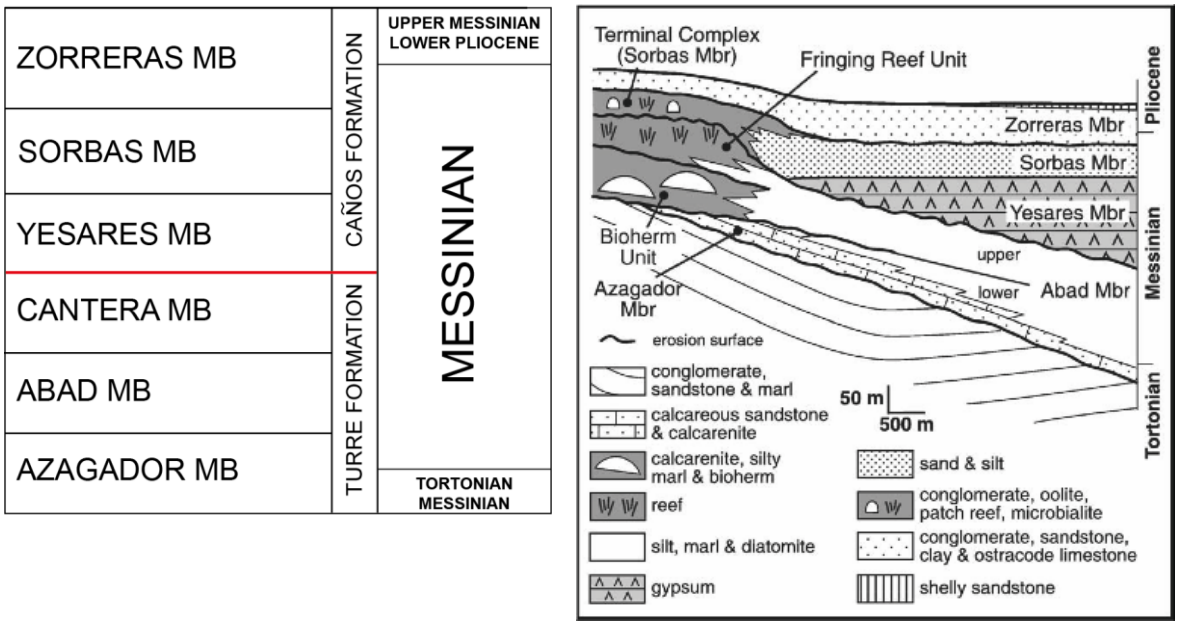

Upper Miocene stratigraphic units in the Sorbas Basin featuring the Bioherm unit with *Halimeda* reefs, dates to the early Messinian (Braga et al., 1996)

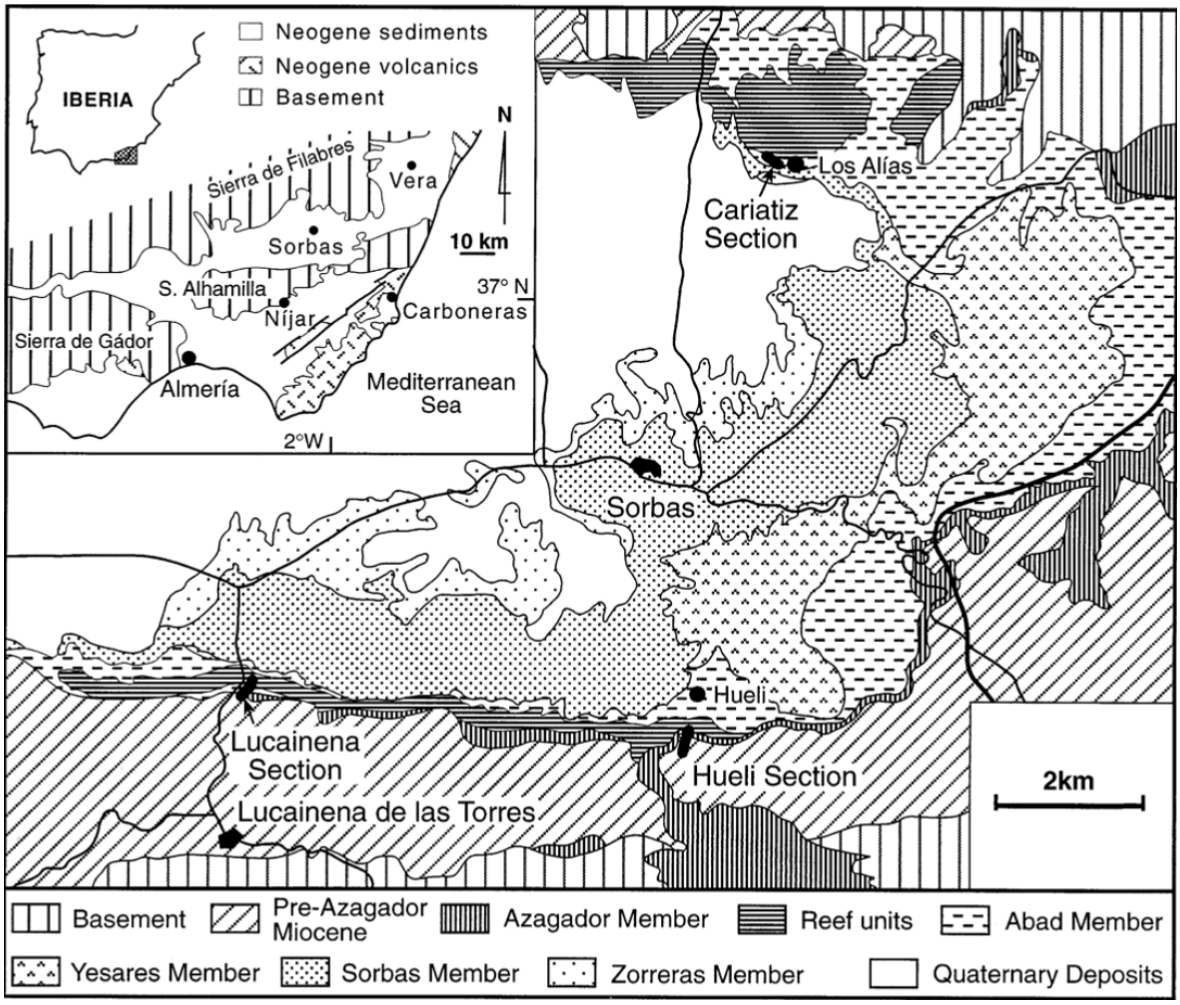

Fig. 4.4. Geological map of the Sorbas Basin in southeastern Spain (Sanchez-Almazo et al., 2001).

The distinct basal contact of the Terminal Carbonate Complex (TCC) over the lower Messinian fringing reef has traditionally been interpreted as a recovery of carbonate

platforms following the main Messinian Salinity Crisis (MSC) desiccation phase. This contact has often been regarded as a subaerial unconformity correlated with the Messinian erosional surface (MES) (Riding et al., 1999, 2000; Braga et al., 2006). However, an alternative interpretation proposed by Fortuin et al. (2000) suggests a less dramatic sea-level drop (around 100 m) associated with this boundary. Cornée et al. (1996, 2004) and Conesa et al. (1999) argue that this sharp boundary represents a marine planation surface, not necessarily linked to a sea-level fall.

The Messinian stratigraphy of the Sorbas Basin remains debated because, unlike its Mediterranean counterparts, it does not clearly exhibit the MES. This has led to conflicting stratigraphic scenarios, summarized by Krijgsman et al. (2001). The Yesares Member gypsum has been interpreted in two ways: 1) as overlying the MES, thus postdating the primary deep basin desiccation stage (Riding et al., 1998, 1999; Martín and Braga, 1994; Braga et al., 2006), or 2) as coeval with other primary Lower Gypsum units of Sicily and the Northern Apennines, predating the main desiccation phase (Fortuin et al., 2000; Cornée et al., 1996, 2004, 2006; Conesa et al., 1999), with the MES placed at the base of the Zorreras Member (Fortuin et al., 2000; Krijgsman et al., 2001).

Typically, the Sorbas Member and its lateral equivalent, the TCC, are considered to overlie the Yesares Member, based on the conformable contact observed in the basin center. However, at the basin margins, especially along the northern edge, the transition from gypsum deposits is not clearly exposed. To the south, gypsum beds show an onlap contact against the upper Abad Member and the Bioherm unit in the Hueli area (Riding et al., 1998, 1999, 2000). This observation has been used to argue for a significant (subaerial) unconformity at the base of the gypsum and to estimate a minimum sea-level fall of 240 m from the basin margin (top of the Fringing Reef unit) to the basin center, assuming primary gypsum was deposited at sea level. However, Fortuin et al. (2000) question this interpretation, noting that gypsum deposits are definitely subaqueous (Lugli et al., 2008), forming in a maximum water depth of 150-200 m.

4.1.2 The Hueli section

The Hueli stratigraphic section (37° 03’ 32.88’’ N – 2° 06’41.02’’ W; Figs. 4.5, 4.6) is located within the Bioherm unit of the Cantera Member. Specifically, the mound studied in this unit is situated in a small area around Hueli, close to an abandoned farm, in the southern margin of the Sorbas Basin. In Fig. 4.5A, the interdigitations between the Abad Member silty marls (in green) and the Bioherm unit (in brown) can be clearly seen. Fig. 4.6 features

two distinct mounds, mound 1 and mound 2, which are part of 35 other mounds (Braga et al., 1996). The mounds, which are variably distributed along the ramp, are not only dominated by *Halimeda* facies, but also include, for instance, *Porites* coral patch reefs, and others characterized by the dominance of bivalves, bryozoans, and serpulids (Braga et al., 1996). According to Braga et al. (1996), based on their composition, these mounds occupy different positions along the ramp. For example, *Porites* coral patch reefs are located in the upper-ramp, while *Halimeda* mounds occupy a mid-ramp position. Bivalve-bryozoan-serpulid reefs, on the other hand, are found in more distal part of the ramp.

Fig. 4.5. Aerial view map of the Hueli section with a particular focus on the two mounds of *Halimeda*.

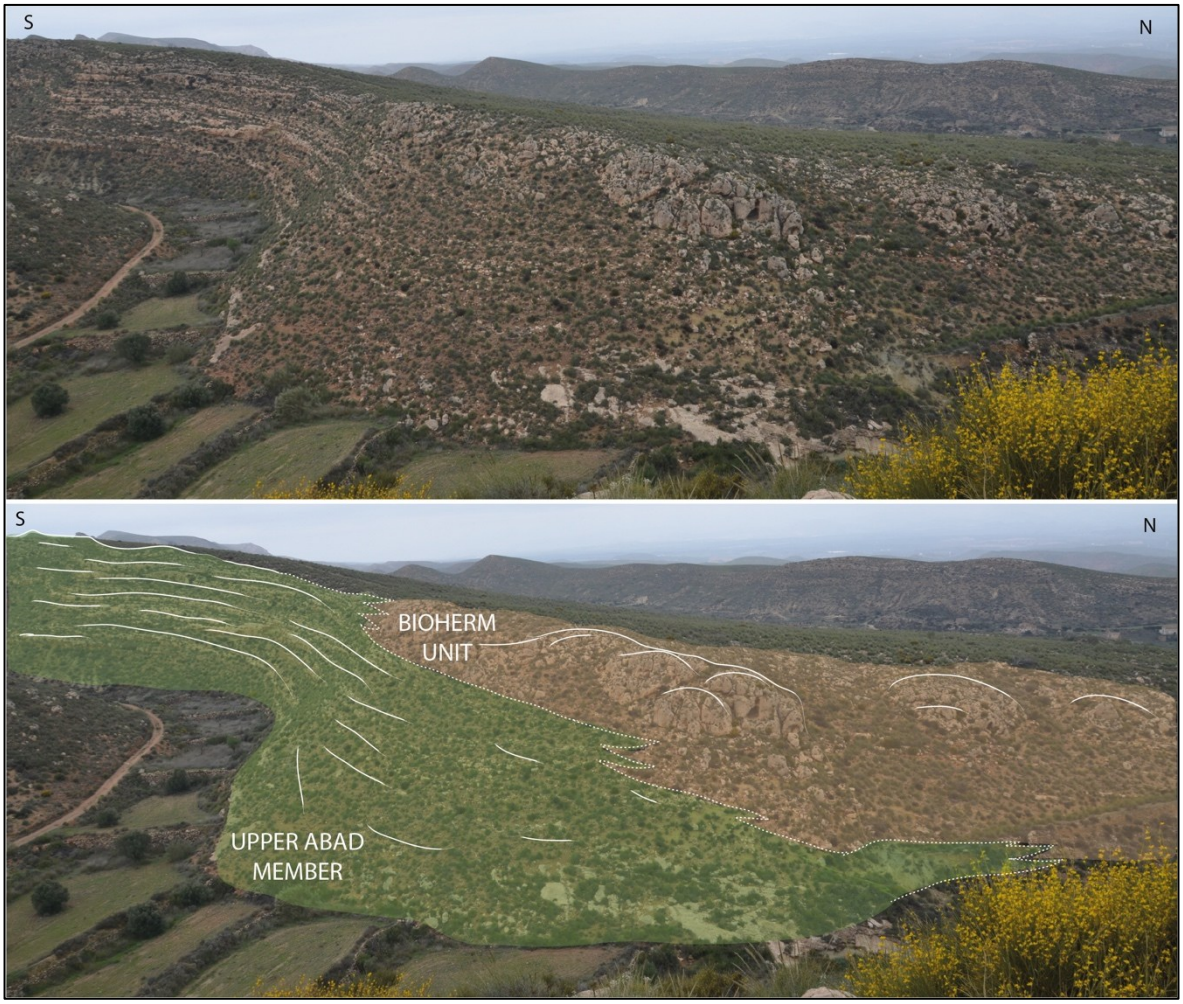

Fig. 4.6. Overview of the outcrop viewed from the east, showing the interdigitation of the clays of the Abad Member (in green) with the *Porites* coral mound of the Bioherm unit (in brown).

On the basis of the outcrop conditions and visible geometries, mound 2 was selected for detailed taphonomic observations and sampling (Fig. 4.7). A stratigraphic section approximately 17 meters thick was measured, starting from the contact between the silty marls of the Abad Member and the base of mound 2. In the lower-middle part (Mound 1) few scattered samples were collected. In the uppermost part (La Cueva - Mound 2), where the outcrop exhibited significant and clear taphonomic characteristics, including evidence of early cementation, a more detailed observation and sampling was carried out (Figs. 4.7, 4.8).

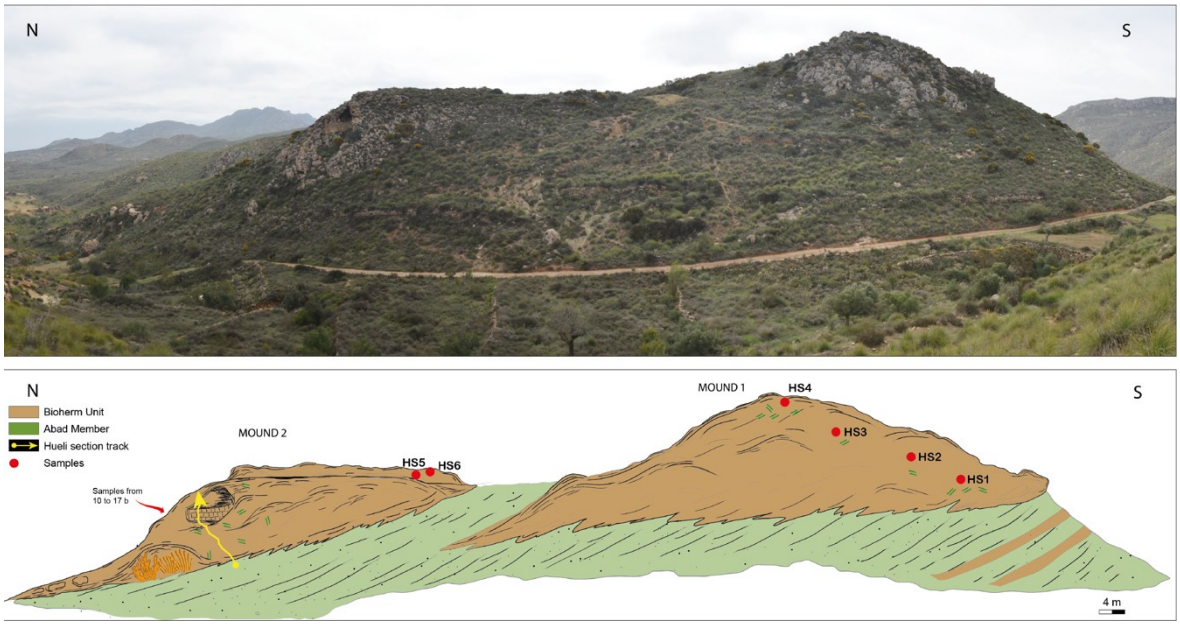

Fig. 4.7. Overview of the Hueli outcrop, viewed from the west, showing mound 1 e mound 2 belonging to the Bioherm unit (in brown) and the clays of the Abad Member (in green). The sample location (red dots) and the track of the measured section (in yellow) are indicated.

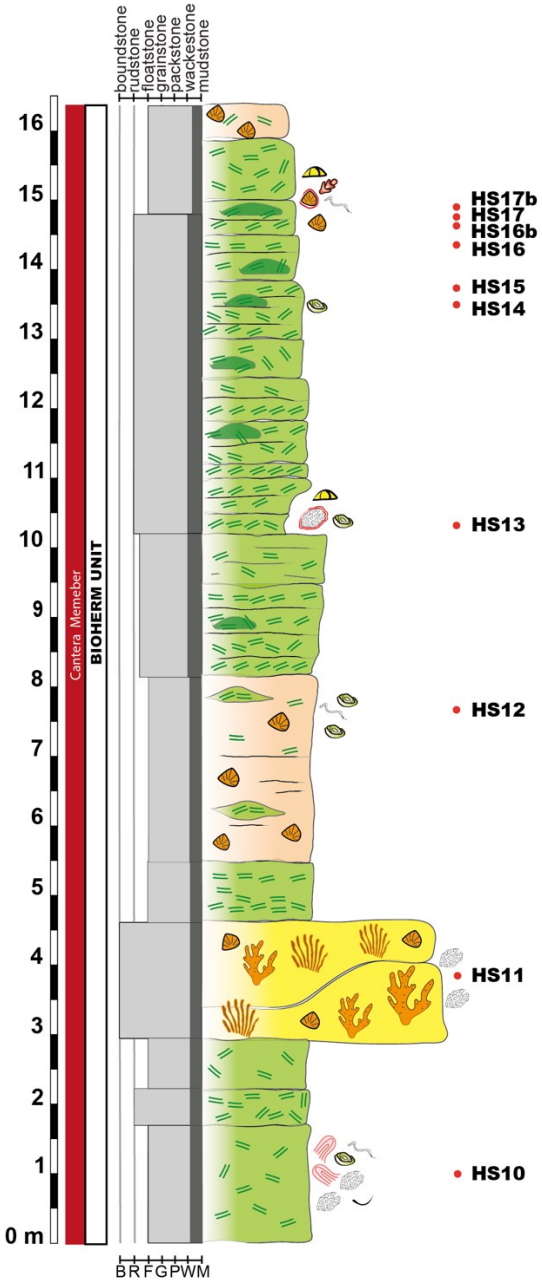

Fig. 4.8. Stratigraphic log of the Hueli section featuring samples, textures, and facies. Within the HRF facies (bright green), the vertical orientation of *Halimeda* segments indicates autochthonous accumulation, represented by HB facies (dark green spots).

The Hueli section (Fig. 4.8) is characterized, in the first three meters, by the presence of a *Halimeda* floatstone with a micritic matrix. In association with *Halimeda*, there are some miliolids, crustose red algae, bryozoans, bivalve shells, and a few fragments of serpulid. Interspersed within these three meters of floatstone is a 0.5m level where the algal segments are more densely and chaotically packed, forming rudstone textures, with a very fine wackestone matrix. In the subsequent 1.5m, *Porites* patches colonies dominate the interval, along with their fragments embedded in a fine wackestone matrix that contains bryozoan fragments. With a gradual transition, the section shifts back to an about 1m interval of *Halimeda* rudstone/floatstone, along with some boundstone lenses with a fine matrix.

From 8.2 to 10.2 m, well-stratified intervals of *Halimeda* rudstones are present, along with *Halimeda* boundstone lenses. In the final meter, the concentration of segments decreases, transitioning towards floatstone textures. Subsequently, there are levels of calcarenite with grain sizes ranging from coarse to medium, rich in *Halimeda* boundstone lenses.

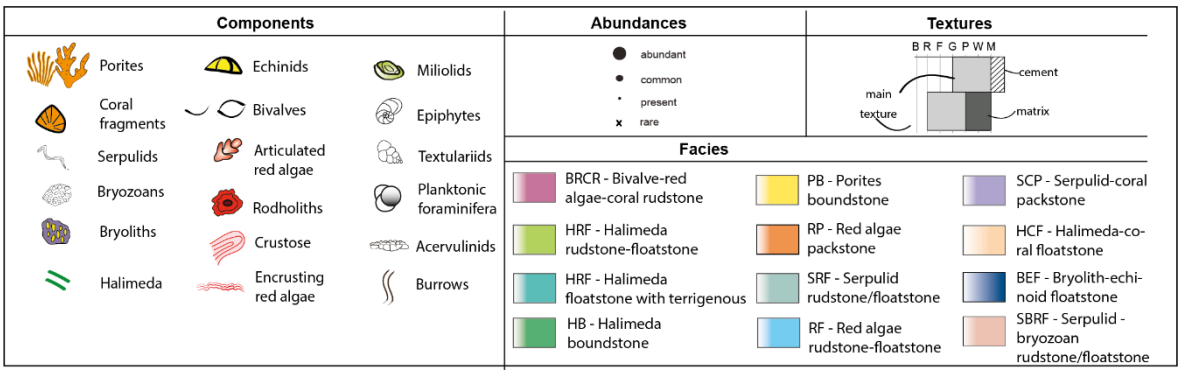

In association, there are a few other components, including bryozoans encrusted with red algae, miliolids, and fragments of echinoids.

From meter 10.2 onwards, we refer to this part of the section as the 'Cueva' (a former cave used for sheltering grazing animals). The outcrop condition inside the small cave permits a more detailed description. This last 3.35 m, characterized by a single interval of biocalcarenite, starts with a first interval with *Halimeda* rudstone with segments imbricated creating an apparent stratification. The fine matrix content is very low. Approximately halfway through this interval, there is a thin layer with *Halimeda* boundstone lenses, with a low internal preservation.

Moving upward, there is a significant increase in the matrix percentage, leading to a more compact and massive appearance. In this section, the *Halimeda* segments become drastically reduced and are chaotically dispersed, forming floatstone textures, while in others, they create small concentrations of boundstone lenses. The presence of cavities filled with sparry cement highlights the areas where the segments are better preserved (Fig. 4.9).

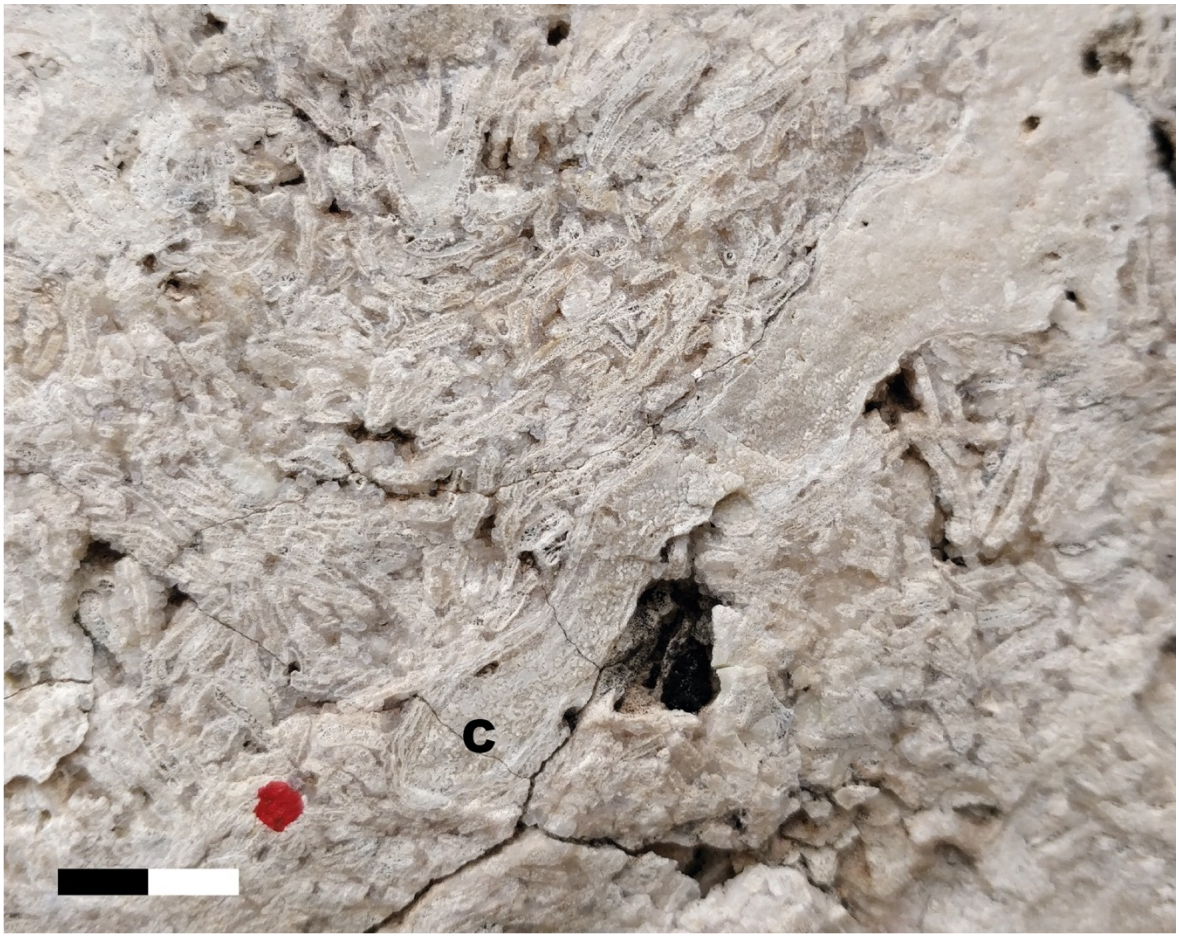

Fig. 4.9. *Halimeda* boundstone lens with a coral stick (c) and sparry cements surrounding the algal segments (scale bar = 1,5 cm).

In the above interval, the overall appearance remains massive and compact due to a higher matrix content. Small zones still contain *Halimeda* segments, along with few echinoid fragments, fragments of branching red algae and, serpulid, particularly in the basal part, forming boundstone texture. The number of cavities filled with sparry cement increases toward the top, and some *Porites* sticks can be found near the ceiling of this interval, with a consistently high rate of preservation of the algal articles.

The top interval maintains a massive and compact appearance, with localized areas of less compact fine calcarenite that provide a hint of stratification. The lower part features lenses of *Halimeda* boundstones, while higher up, there is a marked increase in cavities filled with sparry cement, with the segments exhibiting excellent preservation throughout the interval.

4.1.3 The Lucainena de Las Torres section

The stratigraphic section of Lucainena de Las Torres (37° 3’ 51.89’’ N – 2° 11’ 42.91’’ W, (Figs. 4.10, 4.11) is exposed near the road to Lucainena and Níjar, which branches off from road N-340 near the locality of Tabernas towards Sorbas. The succession starts with the Azagador Member at the base and extending up to the Fringing Reef unit. In particular, Fig. 4.11 highlights the stratigraphic relationships between the members and units. At the base the Azagador Member consists of calcirudites and calcarenites, followed by the yellowish silty marls and grey marls of the Lower Abad Member. An unconformity separates this unit from the overlying silty marls and fine-grained calcarenites containing coral blocks of the Upper Abad Member. These fine-grained materials laterally transition into calcarenites and conglomerates that include *Halimeda* bioherms and *Porites* patch reefs and their blocks (Bioherm unit). At the top of the section, *Porites* reefs from the Fringing Reef unit unconformably overlay the Bioherm unit (Braga and Martín, 1992). The boundaries between the members that are not crossed by the section are based on Sanchez-Almazo et al. (2001).

Fig. 4.10. Location map of the Lucainena outcrop (in red).

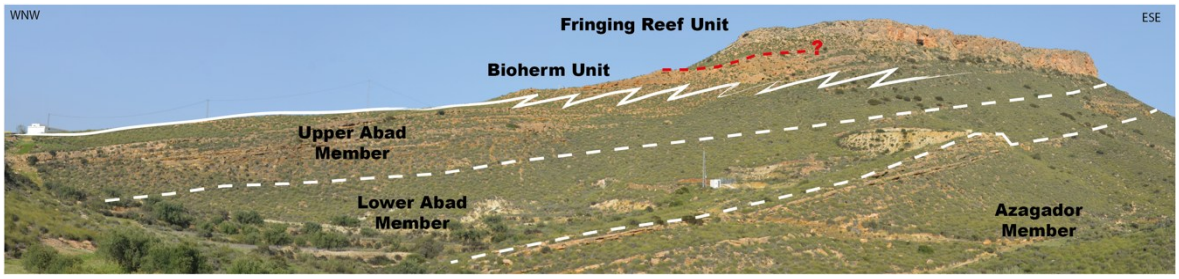

Fig. 4.11. Overview of the Lucainena de Las Torres outcrop reconstructed using Agisoft Metashape software displaying the succession from Tortonian to lower Messinian. The attribution of the Members is based on Sanchez Almazo et al. (2001).

At Lucainena de Las Torres, we measured a section of about 47. The most prevalent facies are *Halimeda* rudstone-floatstone, *Halimeda* floatstone rich in terrigenous inclusions, and *Porites* boundstone. The matrices are predominantly composed of fine wackestone, and throughout the section, especially in the lower to middle parts of the Bioherm unit, there are abundant layers of brown clays and marls. Detailed observations in the *Halimeda* zones documented the presence of lenses with boundstone textures, particularly in the early part of the Bioherm unit. A total of 13 samples were collected along the entire section, from which thin sections were prepared for the determination of micro components and facies.

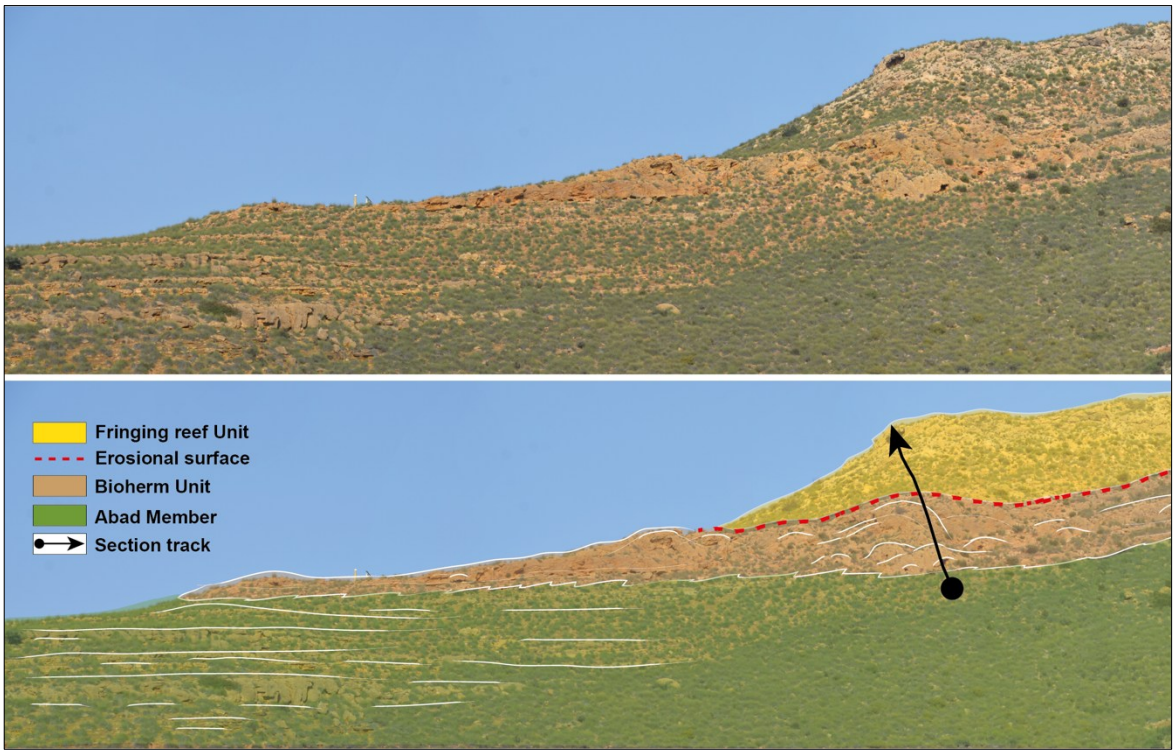

Fig.4.12. The stratigraphic section of Lucainena de Las Torres featuring the clayey marls of the Abad Member (in green), laterally shifting in the Bioherm unit (in light brown). The latter is unconformably overlain by the Fringing Reef unit (in yellow). The erosional surface between the units is marked by a red dashed line. In black the track of the measured section.

The stratigraphic section starts with a polymictic paraconglomerate with a coarse, friable calcarenite matrix (Fig. 4.14) which also contains a Porites block (Fig. 4.14). There is a sharp contact transitioning to a meter of yellowish-red clays, followed by a centimeter-thick layer characterized by grayish-yellow marls. At 2 m from the base, the first carbonate facies occur, characterized by fine wackestone matrix containing scattered segments of *Halimeda* and some crustose red algae, along with coral fragments and small bivalves, forming floatstone textures (Fig. 4.13). The occurrence of *Halimeda* marks the onset of the Bioherm unit.

Between 2.5 to 5.5 beds characterized by *Halimeda* floatstone with crustose algae, in a matrix of packstone to wackestone, alternate with thin layers of yellowish-grey marl. This facies is also characterized by the presence of small terrigenous inclusions. The algal segments appear completely dissolved. Subsequently, there are layers 0.5 meters thick, rich in serpulid encrustations along with small fragments of coralline red algae, that form rudstone textures with a packstone matrix, which extend for 2 meters and alternate with yellowish-grey marly layers approximately 20 cm thick (Fig. 4.13).

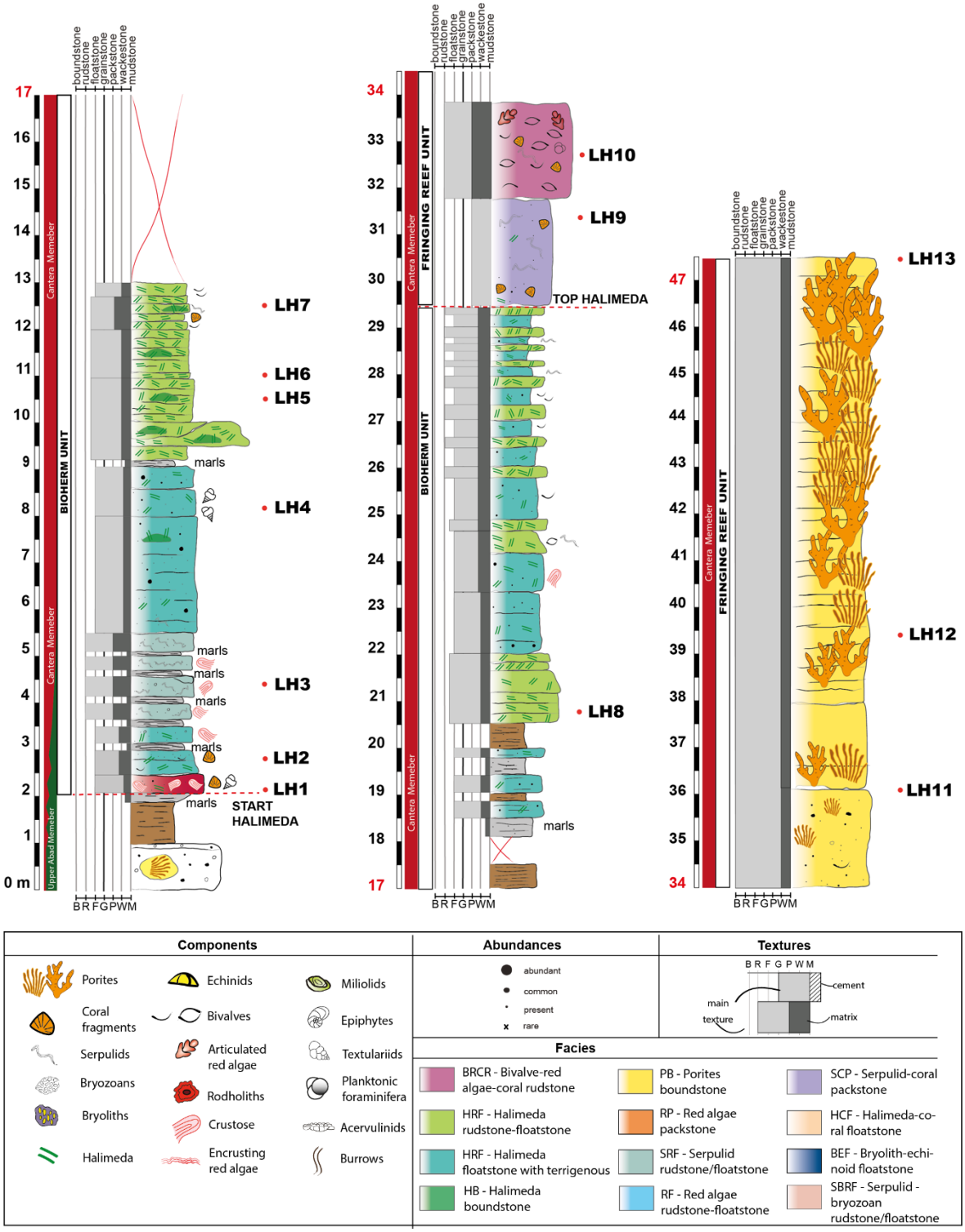

Fig. 4.13. Stratigraphic log of the Lucainena de Las Torres section featuring sample locations, textures, and facies distributions. The transition between the Upper Abad Member and the Cantera Member is highlighted, with a red column indicating the Cantera Member and a green column for the Upper Abad Member. Adjacent to these, a white section delineates the Bioherm unit and the Fringing Reef unit.

At around 9 m, with a sharp contact, the succession passes to thick beds of calcarenite with a total thickness of 3.5 meters, characterized by the presence of *Halimeda*, whose segments are arranged in floatstone to rudstone textures with a fine wackestone matrix (Fig. 4.15). Additionally, abundant terrigenous inclusions are scattered in this facies. This is the first

level where lenses of *Halimeda* bounstone are present. At the top, there is a thin clayey layer. Laterally, in the lower part of this interval, with a gradual contact, a lenticular body about 12 meters thick is established, extending 20 meters in length, predominantly composed of *Porites* colonies (Fig. 4.16). In most cases, it is clearly observed that the arrangement of *Porites* sticks is strongly oriented. The inter-reef sediments with sub-parallel stratification interdigitate with the flanks of the *Porites* patch reef body (Fig. 4.16). From the figure, it can be observed that similar bodies are scattered within the Bioherm unit.

Through a sharp contact (at 12 m), the succession passes to a more or less stratified beds characterized by the presence of *Halimeda*. Here, the content of terrigenous inclusions decreases drastically, resulting in predominantly carbonate facies dominated by *Halimeda* rudstone to floatstone with a wackestone to packstone matrix. There are often areas with lenses of boundstone (Fig. 4.13, 4.17). Above this (at 13 m), there are 5 meters of cover, where only a layer of 0.5 meters thick brown laminated clays is exposed. Continuing upward, a ~ 0.5 m of greenish marls containing small terrigenous inclusions level occur, occasional *Halimeda* segments, and small gastropods. From 18.5 to 20.5 m, there is an alternation of *Halimeda* floatstones with some terrigenous inclusions and a fine wackestone matrix, interspersed with centimeter-thick layers of brown clays and marls. Between 20.5 and 29.5 meters, the sequence consists of alternating decimetric layers of *Halimeda* rudstone-floatstone and *Halimeda* floatstone with terrigenous inclusions. At 29.5 meters, a sharp facies change occurs, marked by a drastic reduction in algal segments, which marks the end of the Bioherm unit. From this point and until approximately 32 m, the succession is characterized by a serpulid-rich and coral fragments packstone. The remaining 2 m of this transitional interval between the Bioherm unit and the Fringing Reef unit is characterized by dense accumulations of large bivalve shells, many of which are still articulated, along with fragments of *Porites*, vermetids, and lateral pockets of branching coralline algae (Fig. 4.13).

From 34 m from the base of the section to the top of at 47 m (about 11 m in thickness), the succession belongs to the Fringing Reef unit. This unit is characterized by substantial *Porites* bioconstructions with big branching colonies (Fig. 4.18). The spaces between the reef framework are filled with a fine-grained wackestone matrix.

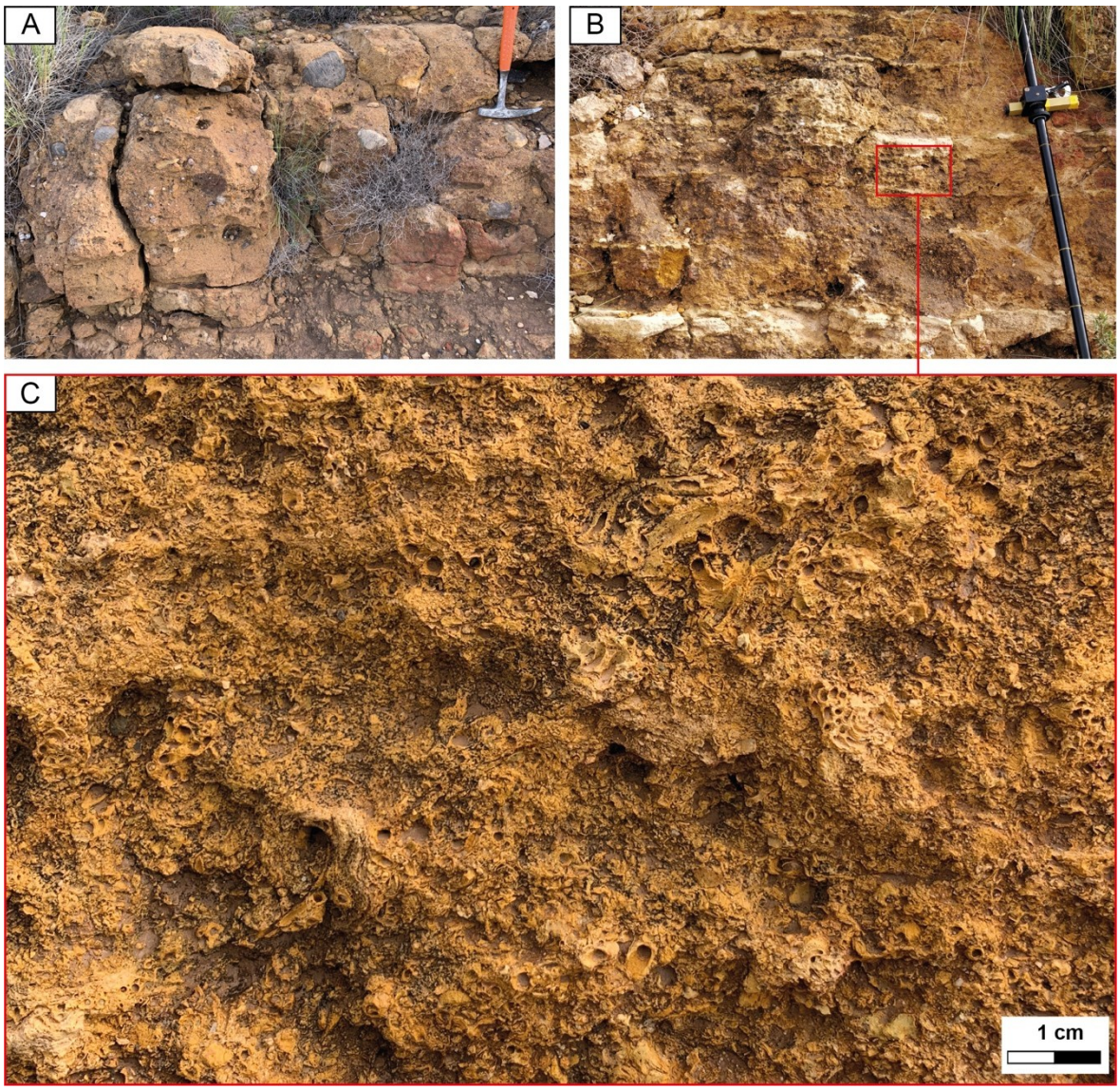

Fig 4.14. A) Base of the section: the 1-meter thick polymictic para-conglomerate; B) the coarse calcarenite with serpulid rudstone interbedded with 20 cm thick yellowish-grey marly layers; C) a close-up of the serpulids accumulation with their characteristic tubes.

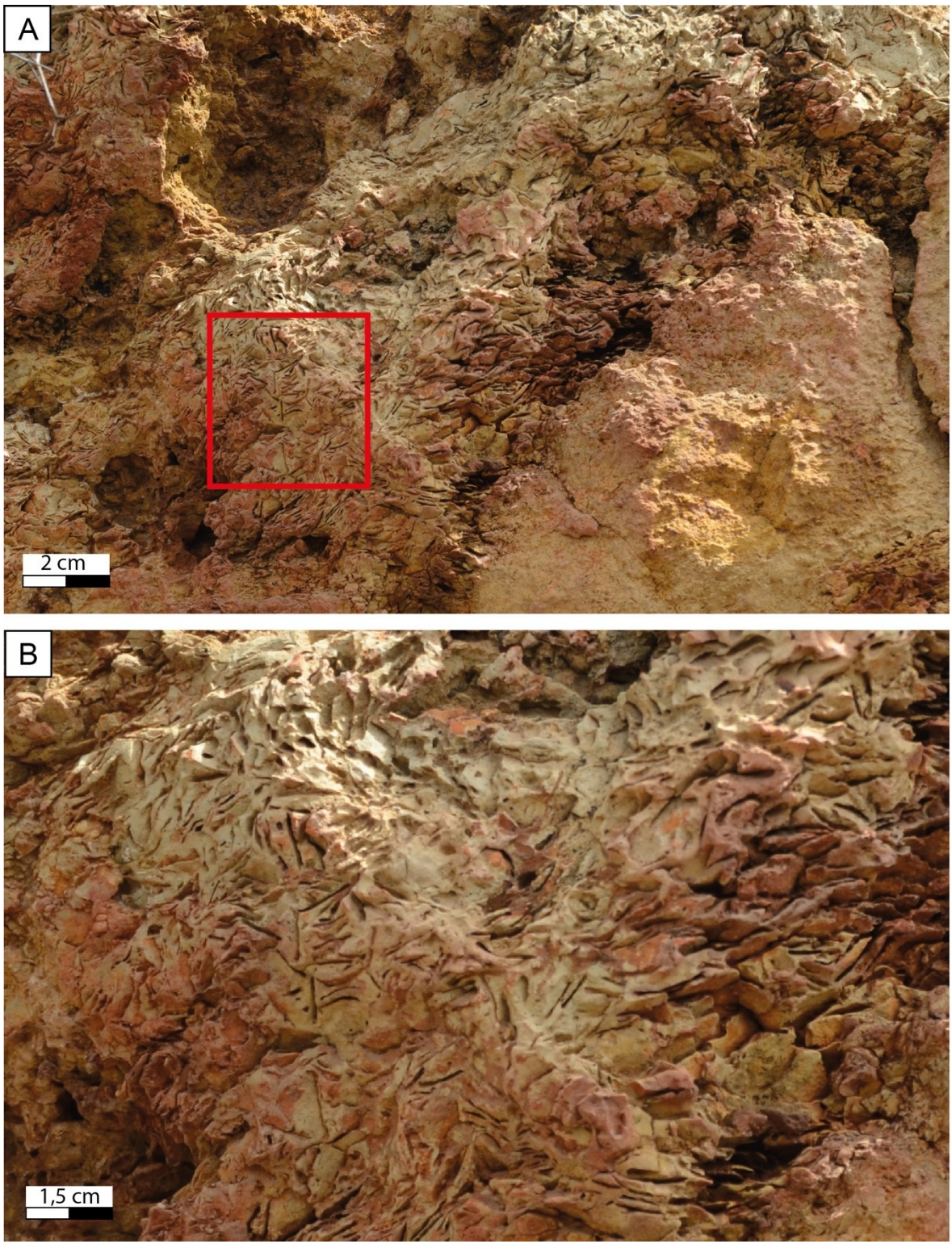

Fig. 4.15. A close-up to the *Halimeda* rudstone facies. A) Level of *Halimeda* rudstone facies with boundstone lenses (red square); B) *Halimeda* segments vertically oriented.

-

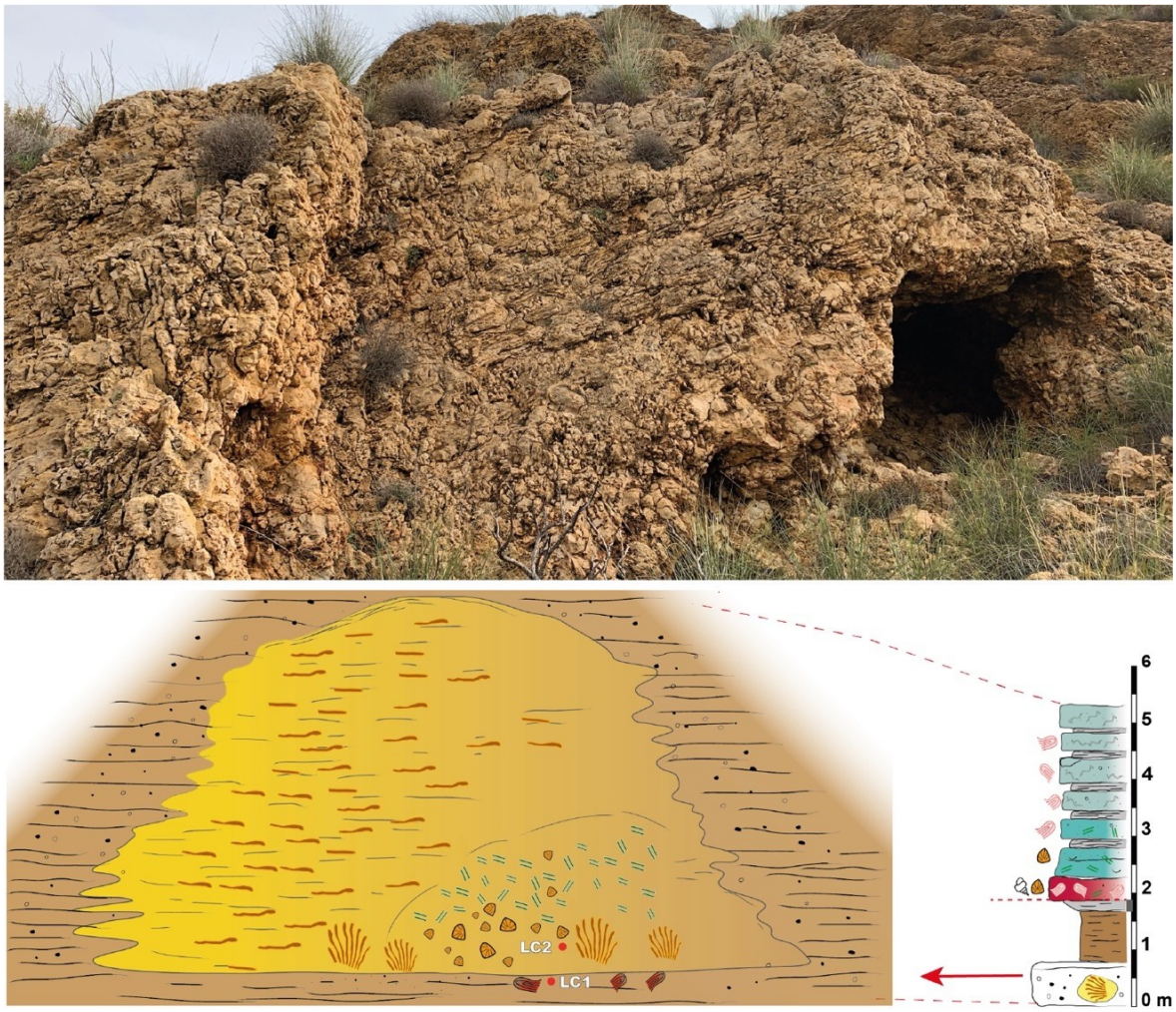

Fig. 4.16. Sketch of the *Porites* patch reef located within the Bioherm unit, highlighting the iso-oriented *Porites* sticks. The inter-reef sediments (in brown) interdigitate with this lenticular body. At the base (on the walls of the small entrance to the right), lenses of *Halimeda* rudstone-floatstone are present, with some segments documented in growth position. Two samples were taken here for matrix analysis, which revealed a very fine wackestone.

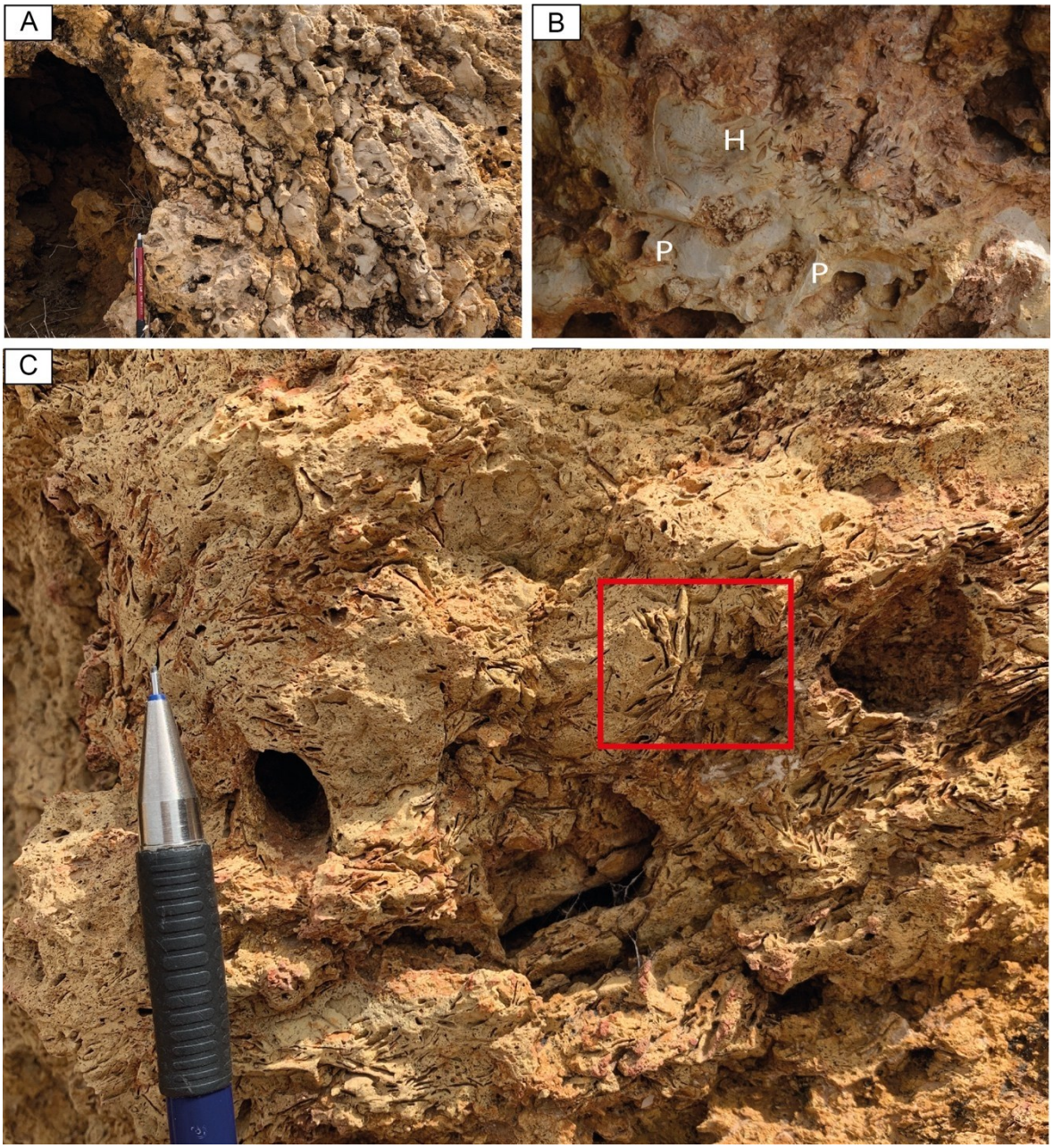

Fig. 4.17. A close-up to the facies of the Porites patch reef. A) Porites sticks; B) The *Halimeda*-coral floatstone facies with wackestone matrix; C) *Halimeda* rudstone with segments in growth position interspersed with coral sticks.

Fig. 4.18. *Porites* bioconstructions with large branching colonies in the Fringing Reef unit, characterizing the section from meter 34 to the top at meter 47.

4.2 The Níjar-Carboneras Basin (Southeastern Spain)

4.2.1 Geology and stratigraphy: the Cabo de Gata region

The Níjar–Carboneras Basin is part of a series of Neogene basins (e.g., Tabernas, Sorbas, etc.) that opened during the Serravallian, associated with regional extension linked to the exhumation of the Betic Paleozoic and Mesozoic metamorphic cores (Augier et al., 2005). Back-arc calcalkaline volcanism developed in the southeastern part of the basin during the Neogene (15–8 Ma, Montenat et al., 1990), leading to the formation of the Cabo de Gata Mountain range (Fig. 4.19). Volcanic hills and valleys formed a complex archipelago, where widespread carbonate sediments accumulated during the Tortonian and Messinian over a period of more than 3 million years (Franseen et al., 1998; Montgomery et al., 2001).

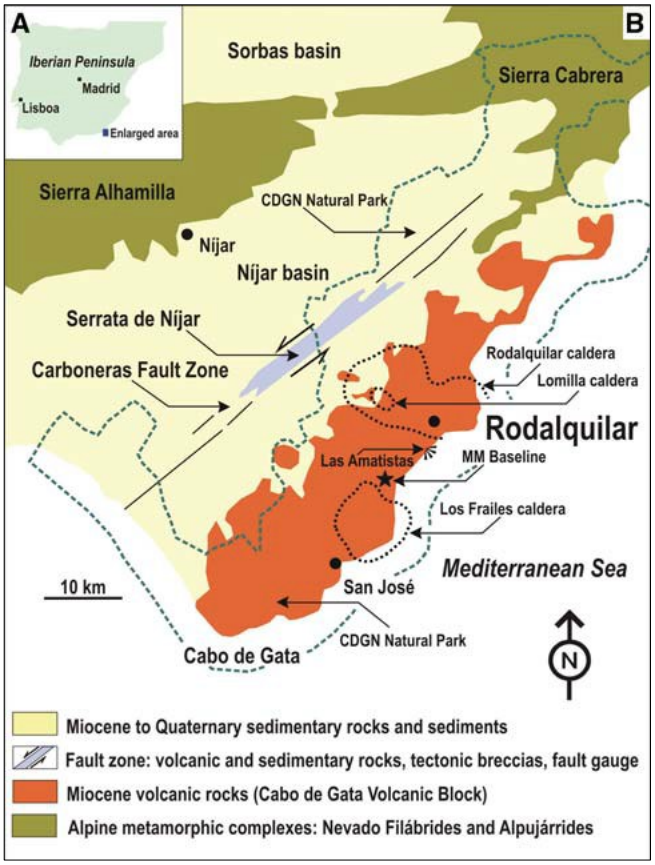

Fig. 4.19. Geology of the Cabo de Gata region (Oyarzun et al., 2009).

The Cabo de Gata volcanic province is situated within the Betic Cordillera, the westernmost part of the European Alpine orogenic belt. Separated from the rest of the Betic Cordillera by the Carboneras strike-slip fault system, this area is predominantly composed of Miocene volcanic rocks (Fig. 4.19). These rocks formed as a result of extensional processes linked to the development of the Alboran Basin following the Alpine collision (Platt and Vissers, 1989; Fernández-Soler, 2001). The volcanic sequences are interbedded with, and overlain by, Neogene sedimentary rocks that were deposited in small marine basins connected to the Mediterranean.

The volcanic rocks in the area belong to two main phases, separated by a period of sedimentation. The earliest volcanic activity occurred between 14 and 10 Ma (Fernández-Soler, 1992), producing a typical calc-alkaline suite ranging from basaltic andesites to rhyolites. These volcanic deposits are primarily dome complexes with significant associated pyroclastic flows. In some locations, these volcanic rocks are overlain by bioclastic

carbonates that contain early Tortonian planktonic foraminiferal assemblages (Braga et al., 1994). In the Agua Amarga area, these carbonates are represented by calcirudites and calcarenites composed of bryozoan, bivalve, echinoid, and large benthic foraminifera fragments, along with minor solitary corals, brachiopods, barnacles, and coralline red algae (Figs. 4.20, 4.21). These temperate carbonates were deposited in coastal environments adjacent to the emergent volcanic topography (Betzler et al., 1997). Bioclastic calcarenites rich in large benthic foraminifera can also be found in small outcrops in other areas, such as Los Frailes and Los Escullos, and likely correlate with the lower Tortonian carbonates of Agua Amarga (Braga et al., 1996; Betzler et al., 1997).

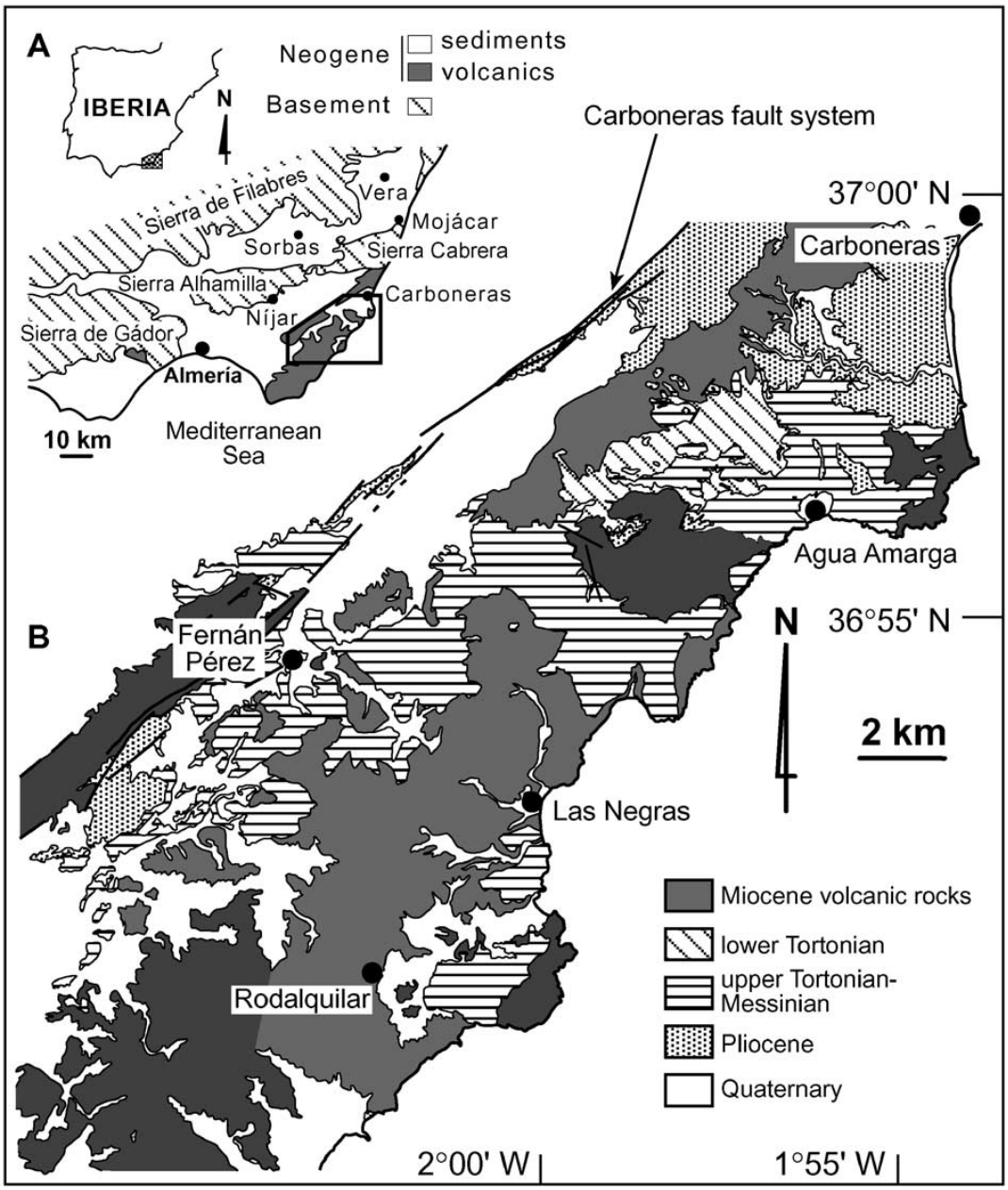

Fig. 4.20. (A) Geographic location and schematic map of the Neogene basins in SE Spain. (B) Simplified geological map of the study area in the Cabo de Gata volcanic province (Martín et al., 2003).

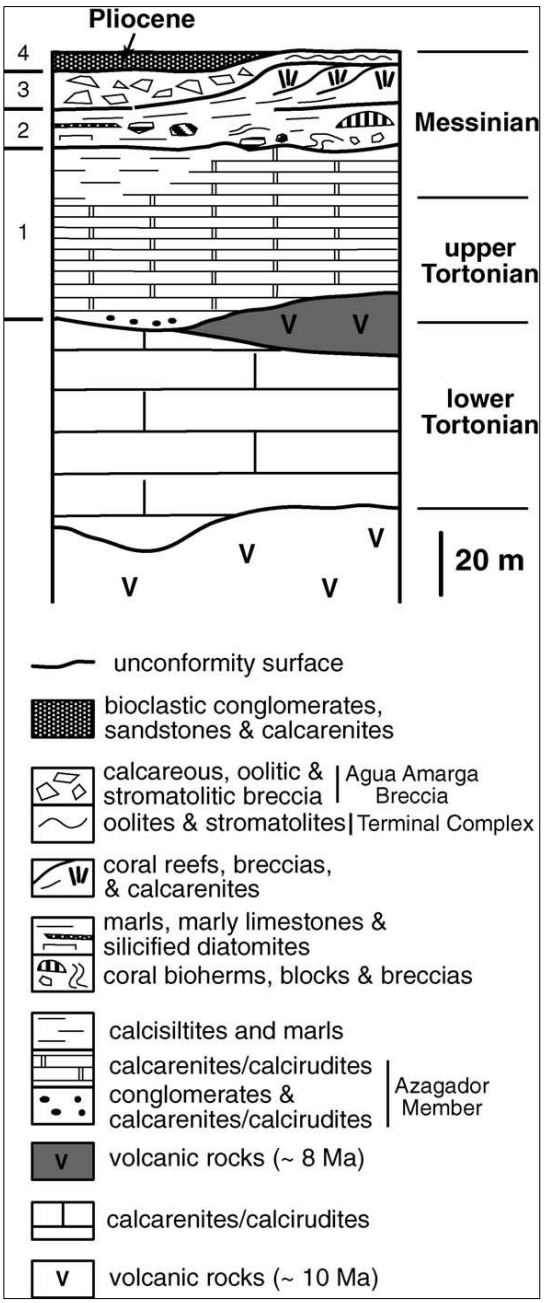

Fig. 4.21. Neogene stratigraphy of the Agua Amarga Basin in the northern Cabo de Gata (Martín et al., 2003)

The second and final phase of volcanic activity occurred between 8.7 and 7.5 Ma (late Tortonian). This phase produced volcanic rocks similar in composition and emplacement style to those of the earlier episode (Fernández-Soler, 1992). Both the volcanic rocks and the lower Tortonian bioclastic carbonates are overlain by a second sequence of temperate bioclastic carbonates, similar in composition to the underlying unit. These deposits consist of calcirudites and calcarenites that grade vertically and laterally into finer-grained calcarenites and silty marls. Planktonic foraminiferal assemblages mark the Tortonian–Messinian boundary at the base of the marls in the Agua Amarga area (Braga et al., 1994).

Messinian reefs unconformably overlie these earlier volcanic and sedimentary units. The lower Messinian unit consists of coral bioherms, reef blocks, and coral breccias interspersed with silty marls and turbiditic calcarenites. At the end, prior to the Messinian Salinity Crisis (MSC) we have the occurrence of *Halimeda*-rich deposits (Bourillot et al., 2009). In areas like La Molata de Las Negras, the lower reef unit is overlain by prograding Messinian reefs (Franseen and Mankiewicz, 1991; Brachert et al., 1996; Bourillot et al., 2009). The late Messinian is marked by oolitic and stromatolitic limestones, which, in some areas, are brecciated and cap an erosion surface on top of the reefs (Esteban and Giner, 1980; Braga et al., 1996; Franseen et al., 1998). In the Mesa Roldán, the oolitic limestones contain small *Porites* patch reefs (Riding et al., 1991). Finally, Pliocene bioclastic carbonates, sandstones, and conglomerates complete the Neogene sequence in the Cabo de Gata area (Montenat et al., 1990; Aguirre, 1998).

4.2.1.1 The early Messinian in Cabo de Gata

The early Messinian in the Cabo de Gata area is characterized by two distinct reef units. The reef carbonates transition laterally into silty marls and marls belonging to the Upper Abad Member (Fig. 4.22), as firstly described by Volk and Rondeel (1964). The presence of *Globorotalia mediterranea* within the marls indicates an early Messinian age for the reefs (Sanchez-Almazo, 1999). The lower unit (Bioherm unit) is primarily composed of coral bioherms (*Porites*, *Tarbellastrea*, and *Siderastrea*) as well as bioherms and deposits rich in *Halimeda* (Martín et al., 2003).

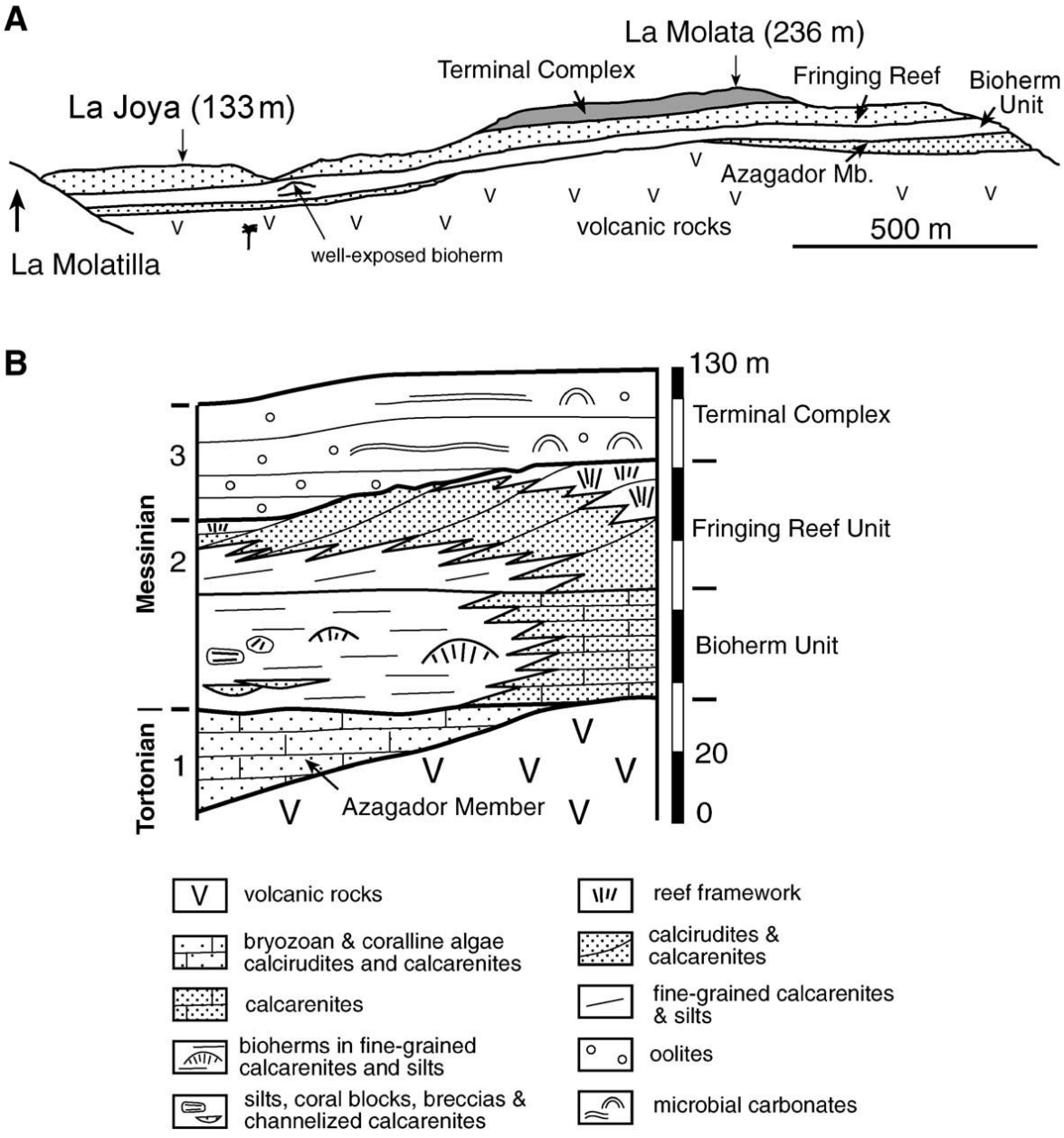

Fig. 4.22. Cross-section (A) and stratigraphic column of La Molata de Las Negras (see Fig. 4.23) in the eastern Cabo de Gata. (B) Post-volcanic units (Martín et al., 2003).

On the other hand, the upper unit (Fringing Reef unit) consists of fringing *Porites* reefs that prograded basinwards. The reef framework consists of *Porites* colonies encrusted by microbial micrite, coralline red algae, and foraminifers. Down-slope, the framework facies pass to coral blocks and breccias, which further grade into calcirudites, calcarenites, and distally into basinal silty marls and marls intercalated with diatomitic marls and turbiditic calcarenites. The distribution of the fringing reefs indicates that the N45°E-aligned topographic high, which was emergent in the late Tortonian, expanded during the early Messinian (Martín et al., 2003). At its western margin, in the La Tórtola area, fringing reefs developed around a volcanic dome, forming an isolated, atoll-like elliptical reef structure. The narrow strait at the eastern margin of the main island, which was present during the deposition of the underlying Azagador carbonates, closed at its southern end, creating a bay opening to the northeast.

Fig. 4.23. Map of the main locations in the Cabo de Gata region.

According to Martín et al. (2003), significant paleogeographic changes in the Cabo de Gata area occurred during the early Messinian. The previously emergent northern area subsided and was inundated by the sea, with the volcanic rocks and shallow-water Azagador deposits being covered by deep-water marls equivalent to the reef deposits. At the same time,

proximal facies of the reef units suggest the presence of submarine highs or emerged reliefs east of the present-day coast, from Punta Javana to Agua Amarga (Fig. 4.23). The volcanic dome of Mesa Roldán evolved into a shallow high or emerged relief, now covered by reefs. This tectonic reorganization of the basin topography is evidenced by the angular, erosional unconformity that separates the Azagador Member from the overlying reef units, with the best exposure of this unconformity found at La Molata de Las Negras.

4.2.2 The Las Negras section

The stratigraphic section measured is located near the small village of Las Negras, on the southern margin of the Níjar-Carboneras Basin, in the Cabo de Gata region (Figs. 4.23, 4.24). The sequence stratigraphy has been established by Franseen and Mankiewicz (1991) and Bourillot et al. (2009).

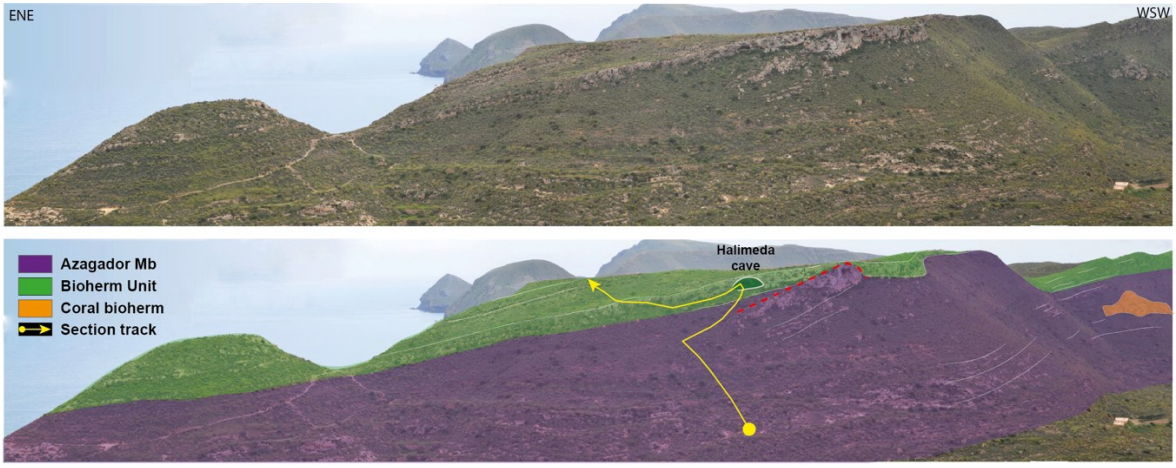

Fig. 4.24. Overview of the Las Negras outcrop reconstructed using Agisoft metashape software. The attribution of the Tortonian coral-photozoan platform (Azagador MB in violet) and lower Messinian heterozoan ramp deposits (Bioherm unit in green) is based on based on Bourillot et al. (2009). The track of the section measured is shown in yellow, and the red dashed line highlights the onlap termination against the beds containing *Halimeda*. In dark green the *Halimeda* cave.

The section measured at Las Negras (36° 52' 11.76" N - 2° 00' 22.30" W) is 88.5 meters thick and includes the Tortonian-Messinian boundary succession (Fig. 4.25). Starting from the base, different facies are observed, including coralline algae packstone to rudstone-floatstone textures, *Porites* coral rudstone-floatstone, and *Halimeda*-rich facies.

The section begins with approximately six meters of fine calcarenite of bioturbated packstone, rich in coralline algae fragments, bivalve shells, and terrigenous inclusions. This facies is interbedded with a two meters of coralline algae rudstone-floatstone with a packstone matrix, still marked by vertical bioturbation, along with abundant bivalve shells. At 5.8 m, a corse-grained calcarenite body occur with a sharp contact, characterized by the presence of rhodoliths and coralline algae, bivalve shells, arranged in rudstone to floatstone textures with a wackestone matrix. In the bioturbated lower part, fragments of bryozoans, some serpulids, and a few echinoids are present. With a gradual transition, this facies shifts to a coralline algae floatstone, containing some rhodoliths and a few coral fragments with a wackestone matrix. For approximately five meters, up to meter 13, there is vegetation cover from which thin layers of calcarenite with red algae facies emerge, exhibiting bioturbation. Between meters 13.1 and 15.8, there is a mound, predominantly characterized by the

presence of *Porites* corals in a growth position, along with their fragments. The fine matrix contains fragments of coralline algae. After approximately two meters of cover and a few poorly exposed levels of red algae, the stratified calcarenites of red algae packstone onlap the second coral mound, exhibiting the same features as the previous one. A 12 meters thick interval with yellowish coralline algae packstone, intensely bioturbated, starts at 21.5 m, with some small bivalves and terrigenous clasts, occasionally interrupted by thin laminated clay levels. At the top of this facies (33.5 m), there are laminated clay beds with some traces of bioturbation, with a total thickness of 2.5 meters. A clear facies change, at about 38 m, is marked by serpulid rudstone along with some echinoids, with a fine wackestone matrix, interrupted by a decimeter-thick clay interval in the lower part (Fig. 4.25).

Moving laterally to meter 44.75, a further facies change is marked by clinostratified calcarenite intervals of *Halimeda* rudstone and boundstone lenses, inclined at about 30° (Fig. 4.26). Within this interval, a decimeter-thick coral-rich lens is present. At approximately meter 48.0, above the clinoforms, a lenticular body of *Halimeda* rudstone is present, where the percentage of well-preserved *Halimeda* segments reaches about 95% of the total sediment. There is no matrix, but the voids are filled with sparry calcite (Fig. 4.27). Within this mound, which reaches a thickness of several meters, another coral-rich lens is present.

At the top of this first interval, between 50 and 52 m, the presence of *Halimeda* gradually decreases, giving way to facies dominated by significant encrustations of serpulids and bryozoans. *Halimeda* rudstones then reappears in a 1.5 m thick bed at 54 m.

At meter 67, where the clinoforms ends, beds of *Halimeda* rudstone-flotastone and boundstone lenses reappear. These facies are occasionally associated with other organisms such as serpulids, coralline algae, small bivalves, and miliolids. The matrix of fine wackestone tends to transition into fine packstone toward the top. These *Halimeda* beds are interspersed with a 0.5 meters breccia layer containing clasts of the same composition. At the top of these beds (77.5 m), a drastic decrease in *Halimeda* segments is observed, and a thin *lumachella* layer marks the end of the fossiliferous facies. From meter 80 to the top of the section, the following sequences are observed: marly calcarenites, micritic intervals coarsening upward, a marly level that thickens upward, grayish, finely laminated turbidite deposits, and at the top, at meter 88.5 a final micritic interval. No *Halimeda* segments are present in this last interval.

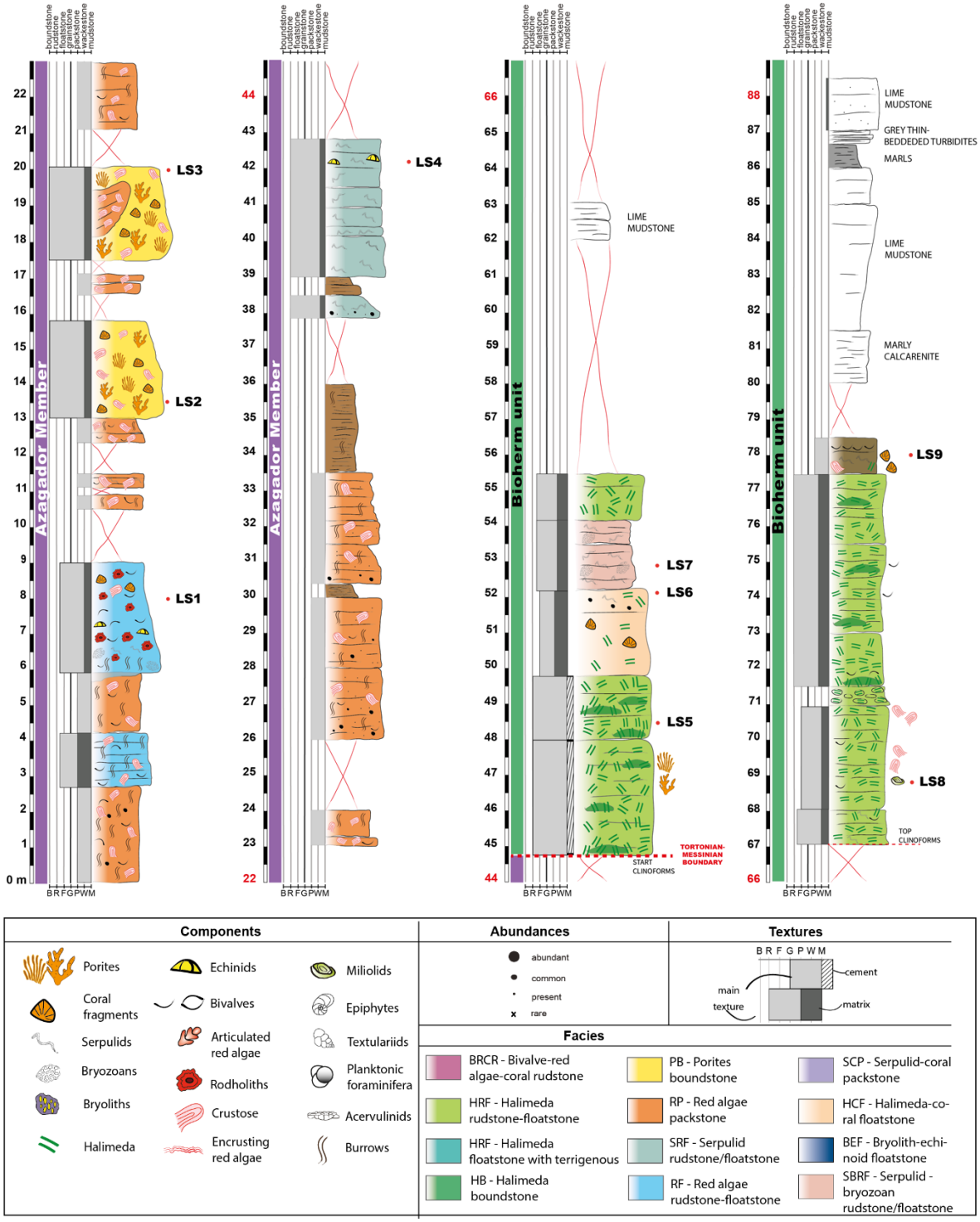

Fig. 4.25. Stratigraphic log of the Las Negras section featuring sample locations, textures, and facies distributions.

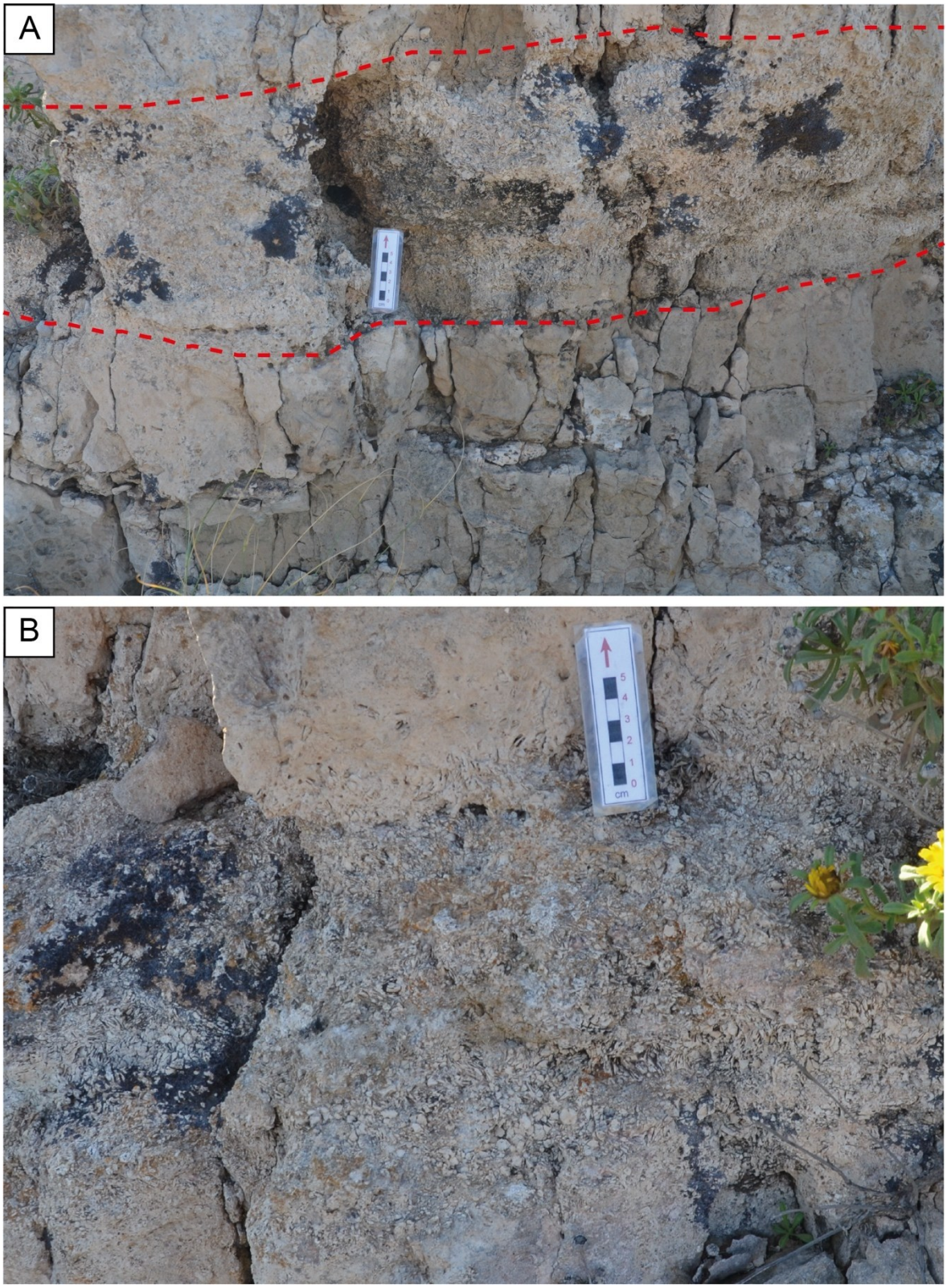

Fig. 4.26. A close-up to the *Halimeda*-rich beds in the Las Negras section. A) A decimeter-thick level rich in *Halimeda* separated (dashed red lines) from floatstone facies rich in terrigenous sediments; B) A detailed zoom on the contact between the *Halimeda*-rich level and the overlying facies, showing how this contact is not sharp but rather characterized by a gradual decrease in segments.

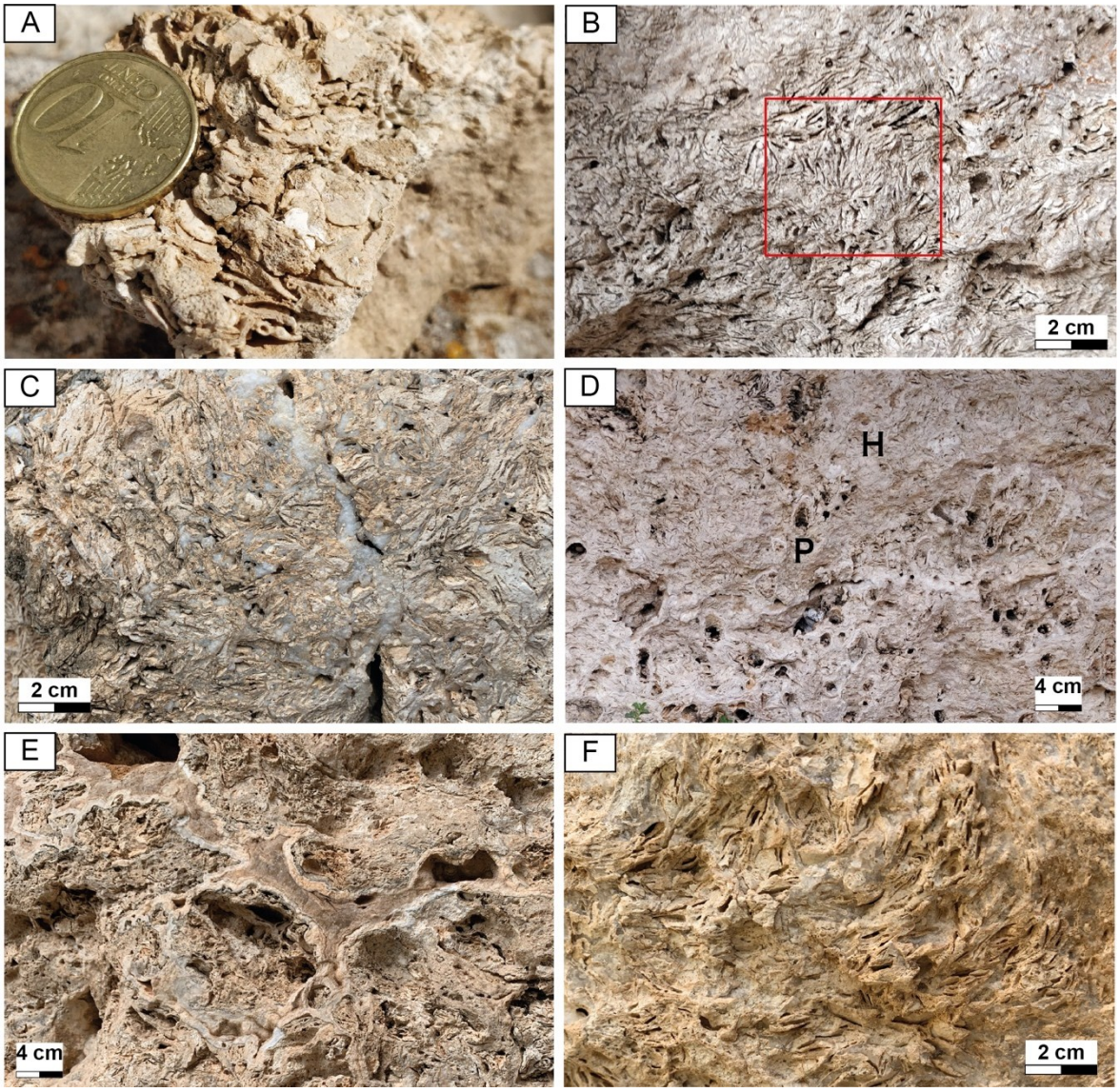

Fig. 4.27. The *Halimeda* facies. A) Example of *Halimeda* rudstone with characteristic segments (10 cents for scale); B) HB facies showing the vertically oriented algal segments C) a close-up to the sparry calcite filling the fractures in the *Halimeda* rudstone; D) HCF facies with *Porites* sticks (P) and *Halimeda* segments (H); E) internal cavities in the HRF facies rimmed with sparry calcite and filled with fine sediments; F) a close-up of a HB lens with *Halimeda* segments vertically oriented.

Fig. 4.28. Location of the Níjar section.

4.2.3 The Níjar section

We measured this stratigraphic section because previous literature reported the presence of *Halimeda* bioherms in this area. However, we did not encounter this interval during our measurements. Therefore, this data is included as part of our work, but it does not provide results directly comparable to other studies.The stratigraphic section of Níjar is located about 1.5 km southeast of the town of Níjar (Fig. 4.28), where it is well-exposed in a cross-sectional view (36° 57’ 43.23” N – 2° 11’ 31.51” W). The measured section reaches a thickness of approximately 50 meters (Fig. 4.29). The predominant facies are red algae and rhodoliths packstone to floatstone.

The stratigraphic section begins with a 0.5 m of brecciated layer, followed by an interval of calcarenite of predominantly coralline algae packstone and terrigenous inclusions, along with bivalve shells. At approximately 1.8 meters, the calcarenite transitions to a finer texture and shifts to clays in the central part, the latter are marked by intense bioturbation in the upper 50 cm, with small burrows present.

Starting from 3 meters, alternating layers of coarse calcarenite with terrigenous inclusions and finer-grained levels rich in coralline algae appear. From 4.2 to 6 meters, there is a notable alternation of coarse calcarenitic layers highlighted by floatstone with red algae and terrigenous clasts, though these clasts become less abundant than in previous intervals.

Between 7 and 10 meters, a decrease in red algae is observed in the floatstone, followed by a resurgence of abundant algae fragments and encrusting forms between 10 and 11.3 meters. From 11.5 to 16.1 meters, coarse floatstone rich in rhodoliths and red algae becomes thinner upward, with an increase in terrigenous inclusions. Rhodolith levels are clearly visible, especially in the lower part of this interval.

Moving upward, the section features a sequence of fine to coarse calcarenites rich in red algae and occasional rhodoliths. Around 32 to 34 meters, layers of stratified floatstone appear, containing encrusting bryozoans (bryoliths) (Fig. 4.30), bivalves, and echinids. This

portion is characterized by significant bioturbation, evidenced by burrows, and microbial lamination, with serpulid encrustations at the top.

Between 34 and 46 meters, the stratigraphic section displays a transition from sterile clays to a marly level devoid of macrofossils. This is overlain by stratified coarse calcarenites with some terrigenous inclusions. The unit consists of stratified red algae floatstone with notable bioturbation. A unit of calcarenite with crossbedding emerges, decreasing in intensity towards the top, where large, recrystallized burrows are present.

The section then shows heavily bioturbated calcarenites, followed by massive layers of red algae floatstone along with rare bivalves, and abundant terrigenous inclusions.

The uppermost layers consist of a rudstone - floatstone facies rich in serpulids with terrigenous inclusions, coralline algae fragments, and rare bivalves. This layer is intensively bioturbated, especially near the top, where serpulid encrustations are prominently displayed.

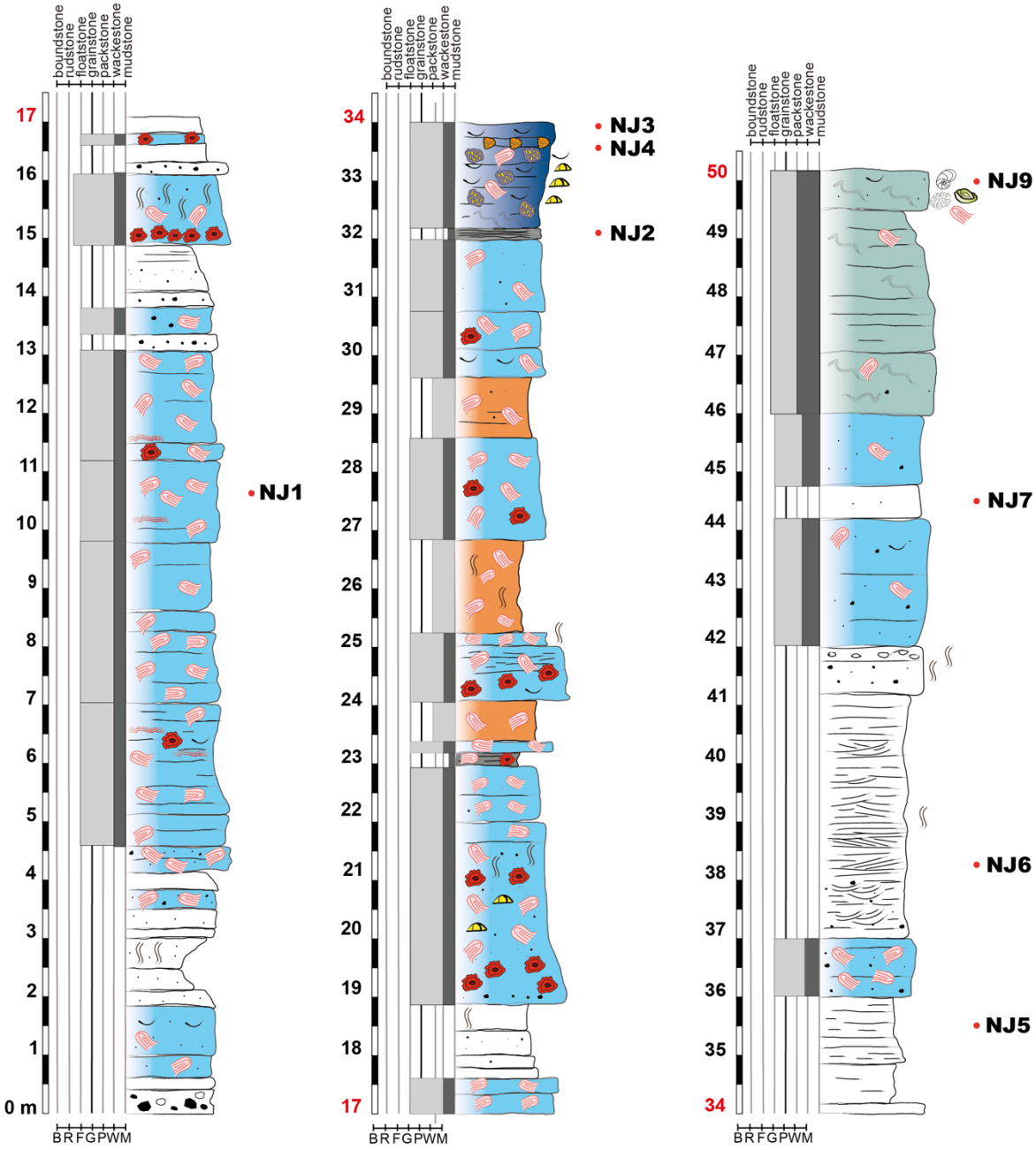

Fig. 4.29. Stratigraphic log of the Níjar section featuring sample locations, textures, and facies distribution.

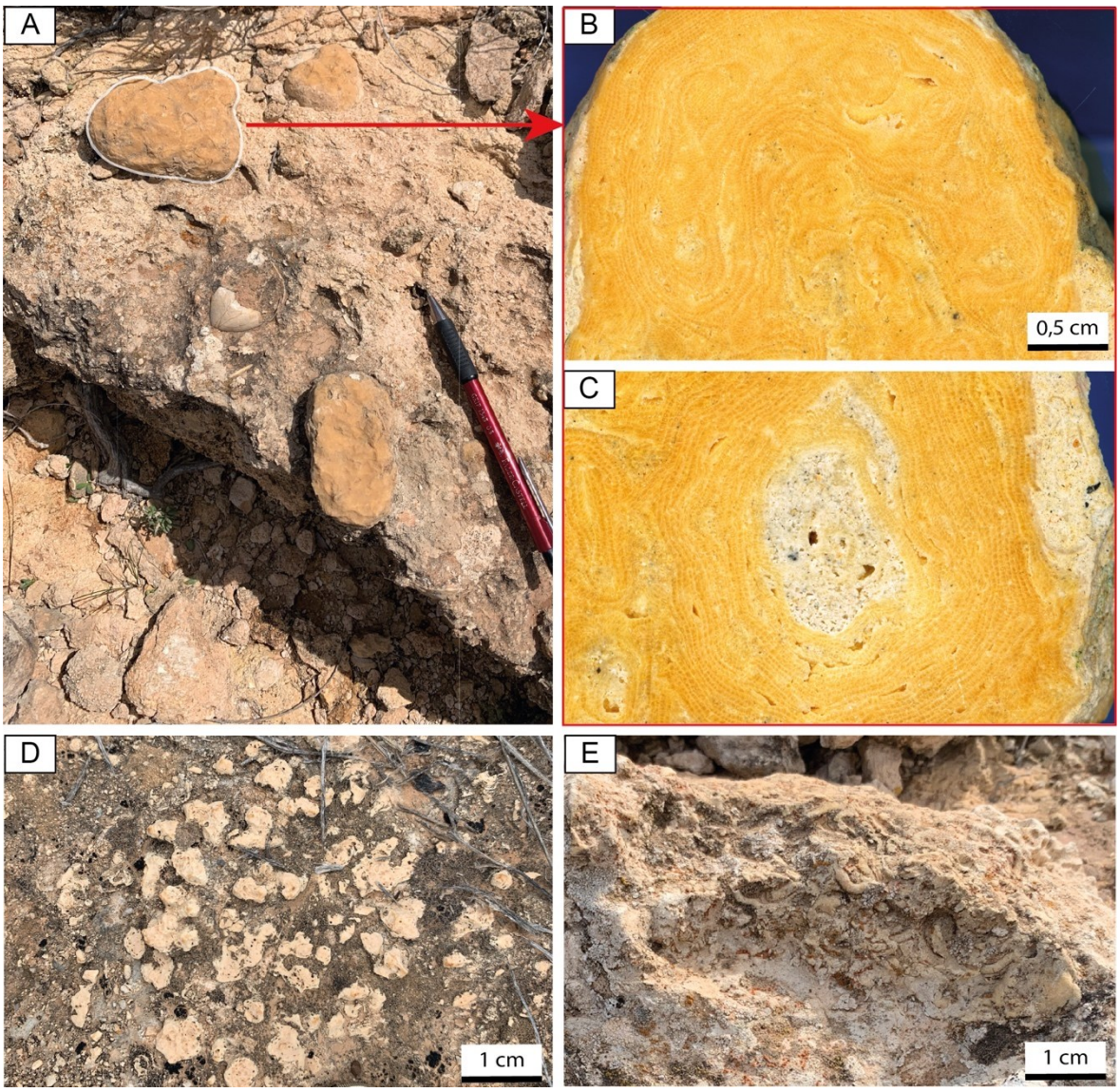

Fig. 4.30. The encrusting facies of the Níjar section. A) Layer of stratified floatstone of large bryoliths; B-C) Polished slab in longitudinal section of one of the characteristic bryoliths occurring in the encrusting facies of the section, the peculiar internal structure with the cells (zooecia) can be observed, but the origin of the central core is not distinguishable. D) example of a rhodolite belonging to the red algae floatstone facies, predominant in the section; E) the serpulid encrustations at the top of the section.

4.3 Discussion

Preliminary observations indicate that, in some sections, *Halimeda* occurs in thick beds, whereas in other sections, it is found as isolated mounds. The analyzed sections also revealed a significant terrigenous input, evidenced by the presence of numerous clayey layers and terrigenous inclusions within the carbonate facies, as documented in the stratigraphic logs. This influx of siliciclastic components may have influenced both the distribution and preservation of the *Halimeda* segments, contributing to greater variability in the depositional environment.

From the detailed analysis of the stratigraphic sections and the taphonomic investigations conducted on the *Halimeda* accumulations, it has emerged that *Halimeda* is present within the Messinian successions of the Almeria and Sorbas region both as isolated mounds (associated with coral mounds of *Porites*) as is the case in the Hueli section (Sorbas Basin), which interdigitates with the clays of the Upper Abad Member, and as decimeter-to-meter beds, as observed in the sections of Lucainena de Las Torres (Sorbas Basin) and Las Negras (Níjar-Carboneras Basin). Moreover, the eastern part of the Las Negras outcrop has been investigated for the first time, leading to a complete documentation of the *Halimeda* deposit in this area, since the western portion had already been analyzed and studied by Franseen and Mankiewicz (1991) and later by Bourillot et al. (2009).

Although no *Halimeda* levels were directly encountered in the measured section at Níjar, the data collected contribute significantly to understanding the paleoenvironmental and stratigraphic variability in the area. By documenting the depositional environment dominated by coralline algae floatstone and packstone, this section offers a valuable comparison to the other settings where *Halimeda* bioherms developed. This comparison helps to contextualize the spatial and environmental constraints influencing the distribution of *Halimeda* bioherms in the basin and supports the findings of Mankiewicz (1988) by further delimiting the stratigraphic and depositional intervals in which *Halimeda*-rich beds are expected.

4.3.1 Differences and similarities in bioherms across stratigraphic sections

The *Halimeda* bioherms from the stratigraphic sections of Spain, specifically from Hueli, Lucainena, and Las Negras, exhibit distinct similarities and differences in their composition, texture, matrix types, taphonomy, and associated features. Below is a comparison of these bioherms based on the data provided and summarized in Table 4.1.

In the **Hueli section**, the thickness of the bioherm is approximately 7.25 meters. The dominant facies is characterized by *Halimeda* rudstone-floatstone, which has a fine wackestone matrix. The secondary facies, represented by *Halimeda* boundstone, lacks matrix, and its voids are filled with cements. The preservation of the *Halimeda* segments is excellent. The bioherm has a mound-like morphology, and like Mound 2, it is positioned within a ramp system. There is no terrigenous input in this bioherm.

In the **Lucainena section**, the bioherm thickness is approximately 9 meters. The *Halimeda* accumulations primarily consist of rudstone-floatstone textures (dominant facies), with the secondary facies being rudstone-floatstone containing terrigenous material. The matrix here is mostly fine wackestone in the dominant texture but packstone in the *Halimeda* boundstone. The preservation rate is low compared to Hueli. These algal accumulations are located in a ramp depositional environment, with terrigenous input, especially in the secondary facies. *Halimeda* accumulations occur both as isolated mounds and beds, and sometimes lenses of algal segments are found in a growth position.

In the **Las Negras section**, the bioherm thickness is approximately 6.5 meters. The dominant facies consists of rudstone-floatstone, similar to the facies found in Hueli, but the matrix here is more coarse compared to the fine wackestone matrix in Hueli. The secondary facies consists of boundstone lenses, which also shows significant cementation. The preservation rate is very good, with well-preserved segments. The morphology is mixed, with both mounds and *Halimeda*-rich beds. There is no terrigenous input within the *Halimeda* accumulations, although terrigenous material is present elsewhere in the section.

Taphonomic evidence shows well-preserved material with minor diagenetic cements.

When comparing these sections, the following distinctions can be made:

- The bioherm of Hueli stands out with its excellent preservation, mound morphology, and the presence of cements. The matrix is mainly fine wackestone, and no terrigenous input is noted.
- Lucainena shows a lower preservation rate, with the presence of terrigenous material in the secondary occurrence of *Halimeda* rudstone-floatstone. The matrix is typically fine wackestone but also includes packstone in the boundstone.
- The Las Negras section shares similarities with the Hueli one in terms of dominant texture but differs in the matrix composition with a wackestone-fine packstone matrix. The preservation rate is very good, and the morphology is continuous. This section also lacks terrigenous input.

The maximum *Halimeda* accumulation is slightly thicker at Lucainena (approximately 9 meters), followed by Hueli (7.25 meters), and Las Negras, with the thinnest occurrence at around 6.5 meters. All the algal accumulations have a ramp depositional environment. However, taphonomic evidence varies greatly, with Hueli showing the best-preserved material, Lucainena showing low preservation, and Las Negras showing very good preservation.

Although vertical segments of *Halimeda* in growth position have been documented in all three sections, this evidence was less prominent at Lucainena.

Table 4.1. Features of the *Halimeda* bioherms from the different stratigraphic sections of Spain, including the maximum thickness measured, the dominant and secondary facies, textures and matrix types, occurrence morphology, preservation rates, taphonomic evidence, associated fauna, and depositional environments. The "dominant" facies represent the most frequent facies within the bioherm, while the "secondary" facies refer to less frequent textures that still contribute to the overall composition. The table also compares the occurrence of cementation, preservation rates, and associated fauna across the different sections.

		SECTIONS		
FACIES	**FEATURES**	**Hueli**	**Lucainena**	**Las Negras**
Dominant	**Texture**	Rudstone-floatstone	Rudstone-floatstone	Rudstone
	Matrix	Fine wackestone	Fine wackestone	Wackestone-fine packstone
	Taphonomic evidence	Cahotic/imbricated	Few growth positioned/ cahotic	Cahotic/imbricated
Secondary	**Texture**	Boundstone	Rudstone-floatstone with terrigenous	Boundstone
	Matrix	No	Packstone	No
	Taphonomic evidence	Growth positioned	Cahotic	Growth positioned
	Max. thickness of the bioherm (m)	~ 7.25	~ 9	~ 6.5
	Cementation	✓	×	✓
	Preservation rate	Excellent	Very low	Very well preserved
	Associated fauna	Echinoid, coralline algae, serpulid	Few serpulids, crustose	Serpulids, coralline algae, small bivalves, miliolids
	Depositional environment	Ramp	Ramp	Ramp
	Terrigenous input	×	✓	×
	Type of Occurrence	Isolated mounds	Beds	Beds + mounds

4.3.2 The role of terrigenous inputs in the development of Halimeda bioherms

Although the abundant presence of *Halimeda* within the successions of the Sorbas and Níjar-Carboneras Basins has been widely discussed (Mankiewicz, 1988; Martín and Braga, 1994; Braga et al., 1996; Martín et al., 1997; Sánchez-Almazo et al., 2001, 2007; Brachert et al., 2007; Braga et al., 2009; Reolid et al., 2014), especially in relation to their larger extent

compared to those of the Salento region, there is still no comprehensive understanding of the factors that determined their proliferation. Specifically, Martín et al. (1997) attributes the mound shape and the lack of horizontal extension of *Halimeda* deposits to the higher input of siliciclastic sediments present in these basins. This sediment influx likely inhibited their lateral development, limiting the extent of the deposits. Although the authors acknowledge nutrient-rich upwelling currents as a factor initially proposed by Mankiewicz (1988) to explain the presence of *Halimeda*-rich beds in the Níjar successions, they ultimately contest its role in the development of *Halimeda* bioherms in the Messinian successions of the Sorbas Basins. This disagreement stems from the absence of supporting sedimentary evidence, such as structures or deposits typically associated with upwelling activity, in the studied sections.

However, these interpretations have never been further explored or developed. Therefore, this chapter aims to clarify these aspects, considering the palaeogeographical context and other variables. Similarly, to the research conducted on the *Halimeda* bioherms in the Salento Peninsula, the nutrient dynamics in Spanish bioherms, such as those found in the Sorbas and Níjar-Carboneras Basins, are crucial for their growth and persistence.

While factors like upwelling and freshwater runoff have been identified in various studies (such as in the GBR – e.g., Furnas et al., 2001 and in the Salento Peninsula – Passaseo and Morsilli, 2025), a clearer understanding of the nutrient sources driving the proliferation of *Halimeda* bioherms in Spain is still needed. In this context, stable nutrient supply, potentially from sources like upwelling or terrestrial runoff, may explain the presence and persistence of these bioherms.

Unlike the Salento Peninsula, characterized by predominantly carbonate sedimentation and lacking significant terrigenous input, the Sorbas and Níjar-Carboneras basins were surrounded by prominent mountain systems that played a key role in sedimentation. Specifically, the Sorbas Basin is bordered to the north by the Sierra de Baza, to the southeast by the Sierra Alhamilla, and to the west by the imposing Sierra Nevada (Fig. 4.23) The Níjar-Carboneras Basin, although closer to the coast, is influenced by the Sierra Alhamilla to the north and the volcanic complex of Cabo de Gata to the southeast. These mountain ranges contributed to considerable terrigenous input, through river runoff and precipitation.

In the Sorbas Basin, the presence of terrigenous contributions within the *Halimeda* bioherms has been highlighted as a key factor supporting their development. This observation is particularly evident in the Lucainena section (Fig. 4.13) where a significant amount of terrigenous material has been identified, potentially originating from runoff and riverine discharge (Weijermars et al., 1985). These sediments, likely rich in essential nutrients like

nitrogen and phosphorus, would have contributed to the enhancement of primary productivity in the region, fostering the growth of *Halimeda* bioherms.

This increased input of terrigenous sediments and thus nutrients to the *Halimeda* bioherms in the Sorbas Basin is supported by studies that confirm a higher concentration of precipitation recorded during the Late Miocene (Gladstone et al., 2007).

In fact, the Late Miocene period was characterized by a shift in the position of the Intertropical Convergence Zone (ITCZ), which led to a significant increase in rainfall in regions of North Africa. This climatic change could have influenced the hydrological regime in southern Spain as well. Gladstone et al. (2007) highlighted that during this period, the region received much more freshwater through precipitation and river discharge, thus affecting the availability of nutrients in the region, supporting enhanced productivity of benthic organisms, including *Halimeda*.

4.3.3. Hydrodynamic interplay as a control factor in the development of Halimeda bioherms

Another possible interpretation for the occurrence of bioherms and *Halimeda*-rich layers within the Spanish successions of the Níjar-Carboneras Basin could be attributed to the influence of nutrient-rich upwelling currents.

The upwelling of cold, nutrient-rich waters is a well-documented phenomenon in the stratigraphic record of the central-eastern Mediterranean. Evidence of such upwelling deposits has been identified in several locations throughout the Tortonian period (Fig. 3.17), including Malta (Föllmi et al., 2008), southeast Sicily (Föllmi et al., 2008), the Matese region in the central Apennines, the Maiella Mountains (Mutti and Bernoulli, 2003), the Latium-Abruzzi carbonate platform in the Apennines (Brandano et al., 2009), the Salento Peninsula and Menorca Island (Föllmi et al., 2015).

Particularly, De la Vara et al. (2015) focus on understanding the hydrodynamic conditions that influenced the Mediterranean-Atlantic water exchange through the Betic and Rifian corridors during the Tortonian-Messinian transition (Fig. 4.32), specifically during the early Messinian, around 7.2 million years ago (Ma), providing valuable insights into how these currents behaved prior to the Messinian Salinity Crisis (MSC).

During this period, the Betic and Rifian corridors acted as key marine gateways between the Mediterranean and the Atlantic, and the hydrodynamics of these regions were influenced by changes in water depths and the relative positioning of the corridors. According to De la Vara et al. (2015), the depth of these corridors played a crucial role in determining the nature of the water exchange. Specifically, the deeper corridor controlled the behavior of the entire

system, and the flow patterns depended on the relative depth of the shallower corridor compared to the deeper one.

The study demonstrates that the flow through these corridors was predominantly anti-estuarine, driven by evaporation in the Mediterranean, which increased water salinity and density. This created a pressure gradient, with dense Mediterranean water flowing out over the sill, compensating for surface inflow from the Atlantic (similar to the modern conditions of the Strait of Gibraltar). This dynamic led to a characteristic pattern of inflow and outflow that depended on the configuration of the corridors.

Fig. 4.32. . Earliest Messinian paleogeography showing the two marine gateways (the Rifian and the Betic corridors) connecting the Atlantic and the Mediterranean water masses (modified after De la Vara et al., 2015).

At 7.2 Ma, significant geological changes occurred that likely affected these dynamics. The Taza-Guercif basin in the Rifian corridor, for example, experienced rapid shoaling, while the Betic corridor saw the opening of the Guadalhorce connection, changing the relative depths of the two corridors. As a result, the Betic corridor could have accommodated two-way flow, while the Rifian corridor likely saw predominantly inflow from the Atlantic. These changes suggest that Atlantic-derived water began to dominate the Rifian corridor during this time,

potentially altering the flow regime and contributing to changes in the Mediterranean water mass.

The siphon theory proposed by Benson et al. (1991) initially suggested a unidirectional flow through the Rifian corridor during this period, with Atlantic waters flowing into the Mediterranean and Mediterranean outflow restricted to the Betic corridor. However, recent modeling by De la Vara et al. (2015) challenges this simplistic view, showing that the exchange between the Mediterranean and Atlantic was more complex, involving a two-way flow dynamic under specific conditions, particularly influenced by the relative depth and configuration of the corridors.

Thus, the De la Vara et al. (2015) model underscores the importance of understanding the relative depth and configuration of the Betic and Rifian corridors when reconstructing past hydrodynamic conditions and their influence on the Mediterranean-Atlantic exchange during the late Miocene.

Given the conditions outlined, it is likely that upwelling currents bringing cold, nutrient-rich waters from the Rifian corridor were a key factor. These waters, originating from the Atlantic Ocean, would have been carried through the Rifian corridor, supplying the Mediterranean with essential nutrients. This influx of cold waters likely contributed to the conditions necessary for the growth of *Halimeda* bioherms during the early Messinian in southeastern Spain.

Although there is no direct evidence of phosphatic hardgrounds in the Betic successions to confirm the action of upwelling currents, as seen in other regions, the possibility of upwelling activity in this interval should not be completely excluded.

4.3.4. Early-marine cementation

As already observed the early-marine cements surrounding the *Halimeda* segments (Fig. 4.33) in the rudstone and boundstone textures were only documented in Hueli and Las Negras sections. In these facies, it was noted that when cement surrounds the algal segments, they are well-preserved. In contrast, when cement is absent and only the matrix is present, the *Halimeda* segments are partially dissolved, as observed in the Lucainena section. We infer that these cements act as an impermeable film that prevents dissolution, as it is more resistant to dissolution than the algal segments, owing to its dense crystal structure (Brachert et al., 2007; Passaseo and Morsilli, 2025). Moreover, this early cementation preserves the vertical orientation of the segments, suggesting an *in-situ* accumulation. This process, along with syn-sedimentary cementation, facilitated the accumulation, accretion, and stabilization

of *Halimeda* bioherms on the ramp substrate, as already stated for Hueli by other authors (Braga et al., 1996; Martín et al., 1997).

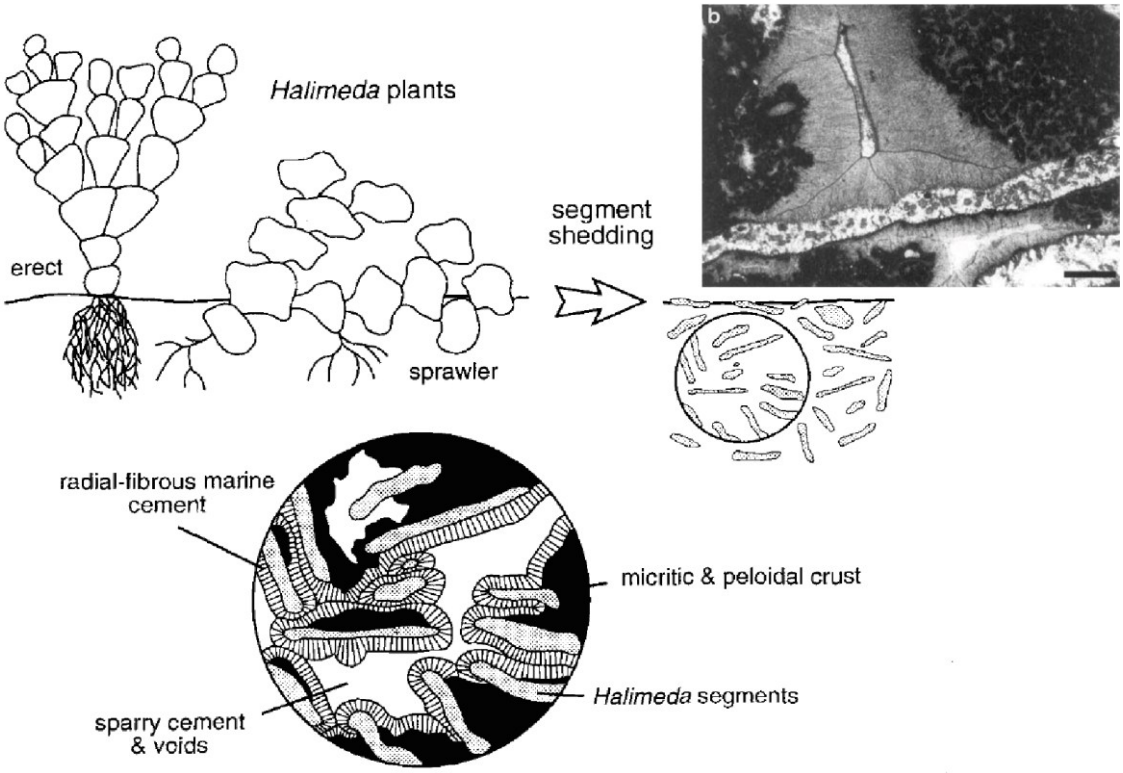

Fig. 4.33. Development of *Halimeda* segment reef fabric (*sensu* Braga et al., 1996), from living *Halimeda* to segment shedding during life and after death, followed by lithification into rigid segment rock with micritic and peloidal microbial crusts and marine cement. Individual segments are approximately 1 cm across. In the top-right corner, a thin section of *Halimeda* rudstone facies showing shelter cavities, which were nearly entirely occluded by radial-fibrous marine cement. Scale bar = 0.5 mm (From Martín et al., 1997).

Early-marine cementation in *Halimeda* bioherms has been documented in all the three Messinian occurrences but also in *Halimeda* facies from offshore deposits of North Palawan, Philippines (Fournier al., 2024). However, the specific nature of these cements and their occurrence within these facies remains poorly understood.

During the early Messinian, the Mediterranean basin began to experience the initial effects of the salinity crisis (MSC), leading to the effective closure of major exchange routes with the Atlantic Ocean. The presence of marine syn-depositional cements suggests that specific geochemical conditions, potentially related to restricted water exchange during the onset of the MSC, played a crucial role in their formation.

The discussion of this interplay has already been addressed for the Salento region in paragraph 3.6.2.

4.4 Conclusions

The fieldwork conducted in the Sorbas and Níjar basins aimed not only to verify and directly observe what has been published in the literature but also to make detailed observations on the *Halimeda*-rich levels. Careful taphonomic observations on *Halimeda* algal segments and their sedimentary matrix were performed to enhance the understanding of transport, preservation, and depositional processes. This analysis focused on understanding the distribution of deposits and identifying sedimentary factors relevant to the studied areas.

The analysis of the lower Messinian successions in southeastern Spain has enabled a detailed characterization of *Halimeda*-rich deposits, focusing on their spatial and stratigraphic distribution. Key sections from Hueli and Lucainena de Las Torres areas (Sorbas Basin) and Las Negras and Níjar (Níjar-Carboneras Basin) were studied, revealing distinct facies and depositional features that reflect varying environmental conditions and degrees of terrigenous input.

The Hueli section is particularly notable for the presence of well-preserved *Halimeda* bioherms, which predominantly form rudstone-floatstone textures with boundstone lenses embedded in a fine wackestone matrix. In contrast, the Lucainena section presents a more complex stratigraphic architecture, where *Halimeda*-rich beds of rudstone-floatstone are interbedded with silicate-rich packstone layers. The significant terrigenous component observed in this section indicates episodic influx of siliciclastic material, which likely played a role in modifying the original depositional environment and influencing bioherm development and preservation.

The Las Negras section presents an intermediate setting between Hueli and Lucainena, with *Halimeda*-rich deposits occurring both as bioherms and as bedded accumulations. This variability could suggest fluctuations in environmental conditions, possibly controlled by hydrodynamic variations and periodic input of fine-grained sediments. The lateral facies transitions observed within this section highlight the dynamic nature of the carbonate platform, where localized conditions could favor either bioherm growth or the accumulation of bioclastic material in more dispersed deposits.

While *Halimeda*-rich deposits were absent in the Níjar section analyzed here, previous studies have documented their presence in other parts of the basin. These deposits are often associated with upwelling currents, which may have influenced their development and distribution. These observations underscore the importance of local environmental factors—

such as water depth, substrate stability, and sediment supply—in shaping the depositional framework of these carbonate successions.

The findings from this study contribute to a broader understanding of the paleoenvironmental conditions that shaped the formation of *Halimeda* bioherms in the Mediterranean during the pre-evaporitic Messinian. The observed differences between sections emphasize the complexity of carbonate platform dynamics and the interactions between carbonate production and siliciclastic input in marine settings. These results provide a valuable foundation for future comparative studies of fossil *Halimeda* bioherms and their modern analogs in tropical carbonate systems, shedding light on the factors that control their formation, distribution, and evolution.

5. The *Halimeda* bioherms of the Crete Island (Greece)

5.1 Geological Setting of the Heraklion Basin (Central Crete Island)

The island of Crete is located within the tectonically active Hellenic Arc, which results from the long-term subduction of the African plate beneath the Eurasian plate. This subduction has been active since the pre-Neogene and played a significant role in shaping the geological architecture of the Eastern Mediterranean. During the Late Oligocene–Early Miocene, the rollback of the subduction zone toward the south triggered extension and subsidence across the Aegean region, leading to the formation of several Neogene sedimentary basins across Crete (Meulenkamp et al., 1979; Keupp et al., 1994; Frydas et al., 1999; ten Veen & Postma, 1999; Pomoni-Papaioannou et al., 2002; Rahl, 2004).

The Heraklion Basin, located in central Crete, developed as a result of this extensional tectonic regime. Initially, during the Middle Miocene, the region underwent subsidence, forming a series of E–W-trending grabens (Fassoulas, 2001). This was followed by a phase of maximum extensional stress rotation during the Messinian, which reoriented deformation patterns and influenced sedimentary processes (Fig. 5.1). From the Pliocene to the present, a multi-directional extension system has continued to shape the basin's structural evolution (Fassoulas, 2001).

The Heraklion Basin is structurally constrained by:

- West: The Psiloritis Mountains, composed primarily of Mesozoic carbonate sequences and overlying flysch deposits.
- East: The Lasithi Mountains, reaching elevations of up to 2500 m.
- South: The Messara Plain, which marks the southern boundary of the basin.
- North: A gradual dip into the Cretan Sea, indicating continued subsidence.

The basin's bedrock is composed of Mesozoic limestones from the Tripolitza and Plattenkalk units, overlain by Paleogene flysch, which consists of sandstones, shales, and blocks of Mesozoic limestone (Meulenkamp et al., 1979; ten Veen & Postma, 1999; van Hinsbergen & Meulenkamp, 2006). The contact between these units is often structurally controlled, with major normal faults influencing deposition.

The structural evolution of the Heraklion Basin strongly influenced facies distribution and the location of carbonate system development. The Heraklion Basin

experienced a dynamic evolution throughout the Middle to Late Miocene, transitioning from non-marine and marginally marine environments to a fully marine system by the early Tortonian. During the Middle Miocene, sedimentation was dominated by brackish lagoons, marginal marine settings, and offshore marine conditions (ten Veen & Postma, 1999; Moisette et al., 1993). By the late Serravallian and early Tortonian, the basin evolved into an open marine environment characterized by the deposition of coarse clastic sediments along its coastlines.

With the onset of Late Tortonian extensional tectonics, rotational uplift of blocks at the basin margins led to the formation of isolated carbonate platforms (Fig. 5.4). These environments supported coral reefs, which developed along steep cliffs and gentle carbonate ramps, often associated with level-bottom coral communities in open marine settings (Brachert et al., 2007).

During the Tortonian-Messinian transition, increased subsidence and hinterland uplift resulted in the drowning of shallow-water environments, restricting coral growth to narrow platforms near the Ida Mountains (Reuter et al., 2006; Reuter & Brachert, 2007).

In the Eastern Mediterranean, the subduction of the African plate beneath the Eurasian plate has been active since the pre-Neogene. During the late Oligocene and Early Miocene, the rollback of the subduction zone to the south caused rapid extension and subsidence of the Aegean landmass (Rahl, 2004). In this area, the Neogene basins related to this process are found throughout the Island of Crete, showing notable similarities in sedimentary architectures and lithofacies (Meulenkamp et al., 1979; Keupp et al., 1994; Frydas et al., 1999; ten Veen & Postma, 1999; Pomoni-Papaioannou et al., 2002). During the Middle Miocene, an initial phase of subsidence led to the formation of east-west oriented grabens (Fassoulas, 2001), with a maximum extensional stress rotated in an east-west direction in the Late Miocene (Messinian) (Fig. 5.1). From the Mid-Pliocene to the present, a multidirectional extension system has been established (Fassoulas, 2001).

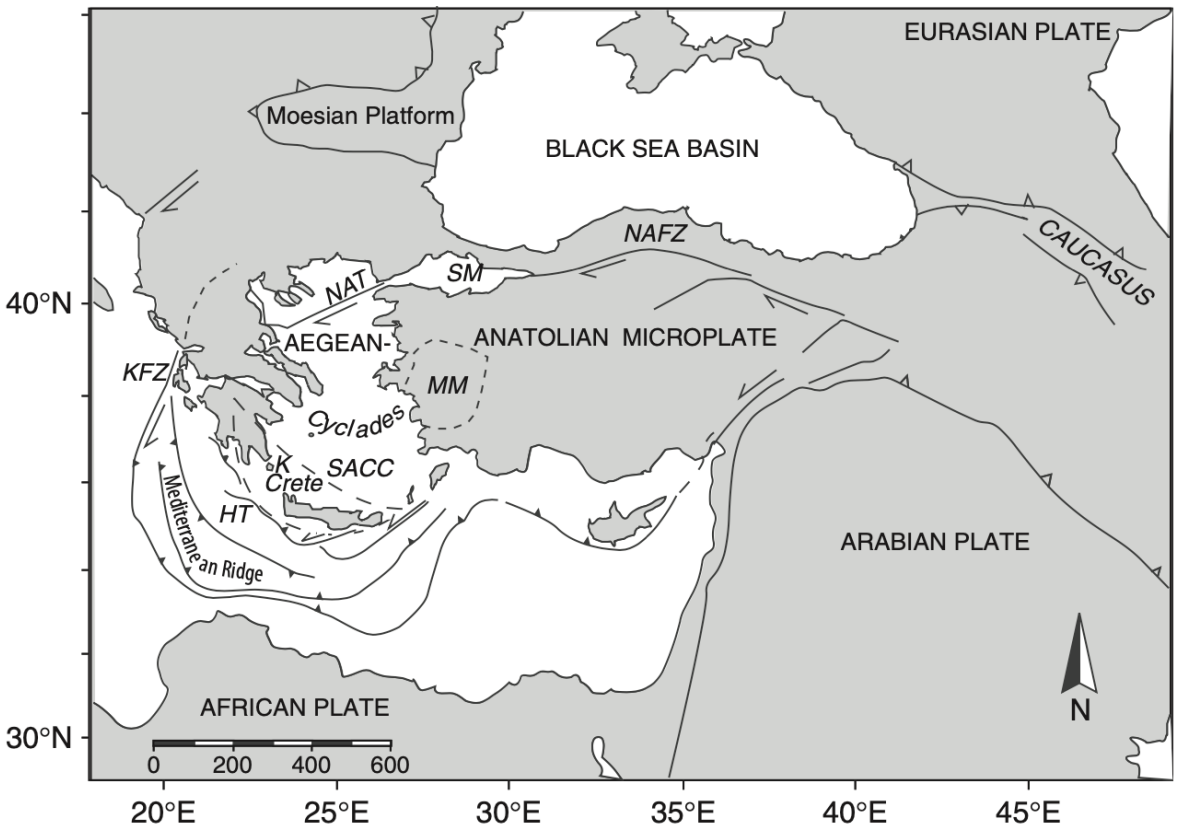

Figure 5.1. Map of the Aegean region. HT, Hellenic Trench; NAFZ, North Anatolian Fault Zone; NAT, North Anatolian Trough; KFZ, Kephalonia Fault Zone; SACC, South Aegean Crystalline Complex; K, Kythira; MM, Menderes Massif; SM, Sea of Marmara (Zachariasse et al., 2011).

The Heraklion Basin, located in central Crete, is bordered to the west by the Psiloritis Mountains, to the east by the Lasithi Mountains (with a maximum elevation of 2500 m), and to the south by the Messara plain (Fig. 5.2). This basin is tilted to the north, dipping into the Cretan Sea. The substrate of the basin consists of Mesozoic limestones from the Tripolitza and Plattenkalk units, overlaid by Paleogene flysch composed of sandstones and shales containing blocks of Mesozoic limestone (Meulenkamp et al., 1979; ten Veen and Postma, 1999; van Hinsbergen and Meulenkamp, 2006).

Fig. 5.2. Geographical settings of the Heraklion basin and location of the stratigraphic sections measured.

The Heraklion Basin covers an area of approximately 900 km². The Neogene deposits in the basin and in the Psiloritis Mountains rest upon the bedrock of the Upper Nappes (UN), which include the Tripolitza and Pindos units, predominantly non-metamorphic or of low-grade metamorphism (Rahl et al., 2005; Klein et al., 2008), and an upper heterogeneous unit composed of units related to ophiolites, some of which are metamorphic (Seidel et al., 1981; Bonneau, 1984). The UN rocks in the Psiloritis and Lasithi Mountains are separated from the metamorphic rocks of the Lower Nappes (LN) by the Cretan detachment fault (Kilias et al., 1994; Fassoulas, 1999; Papanikolaou and Vassilakis, 2010), which exhibits movement both to the south and to the north (Jolivet et al., 1996). The LN includes the Phyllite-Quartzite and Plattenkalk units, with the latter easily identifiable due to its lead-gray crystalline carbonates and the frequent presence of chert beds (Bonneau, 1984). This distinguishes it from the more blue-azure Tripolitza unit, dominated by mudstones and wackestones with occasional dark crystalline dolomites (Fig. 5.3).

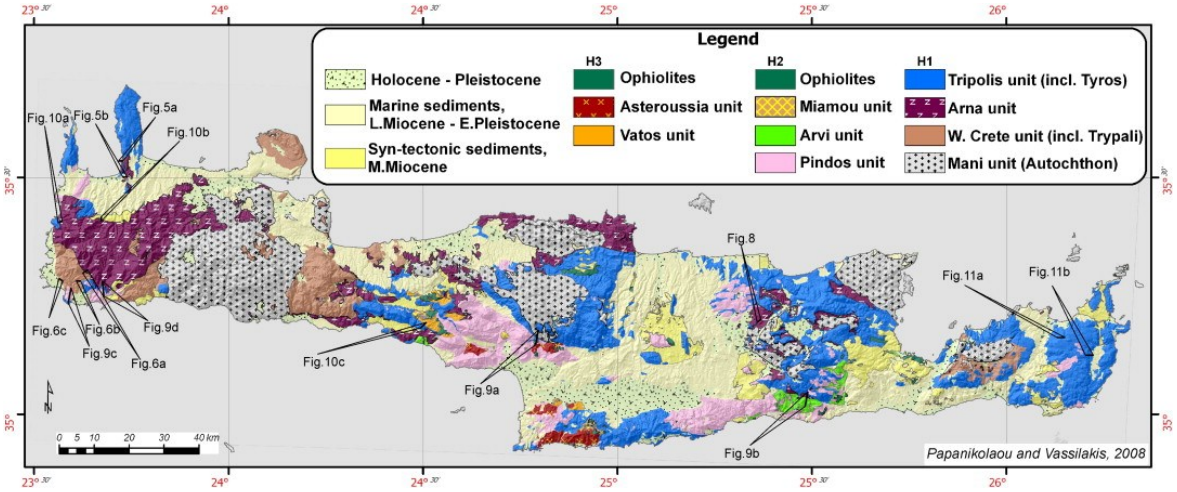

Fig. 5.3. Geological map of Crete indicating the main tectono-stratigraphic units – Heraklion Basin in the central part (Papanikolaou and Vassilakis, 2010; modified after Papanikolaou and Vassilakis, 2008).

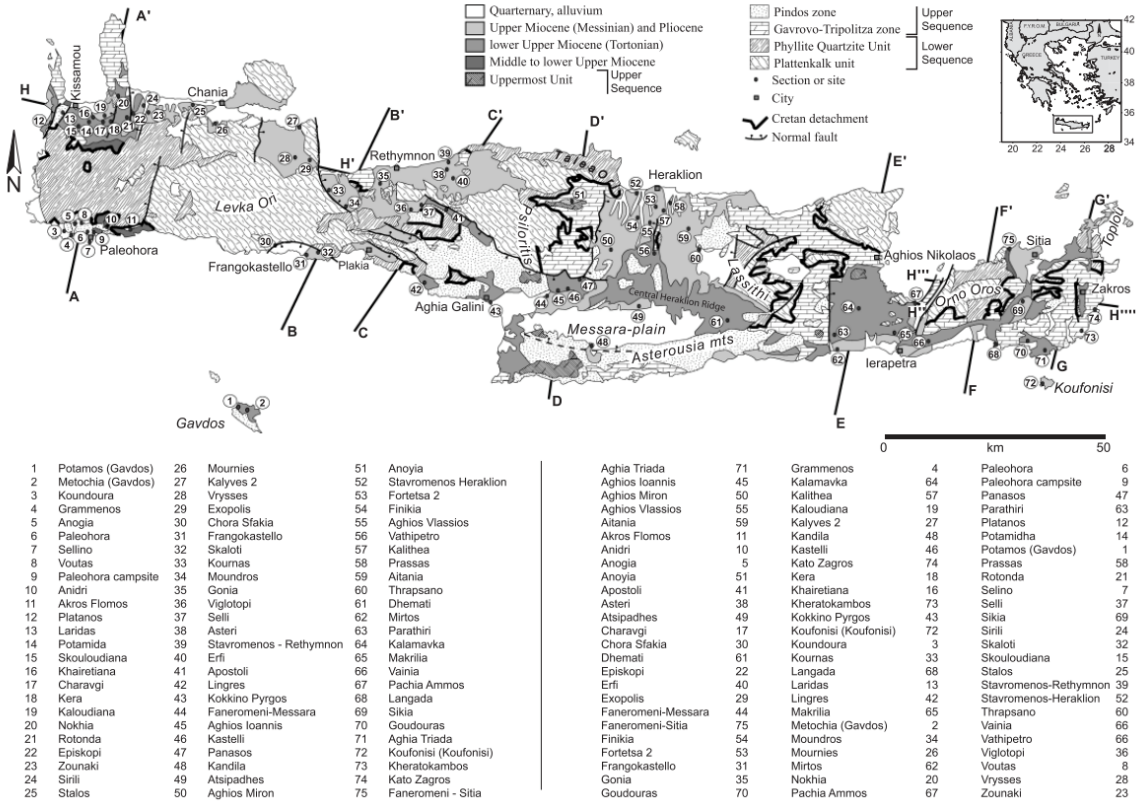

1	Potamos (Gavdos)	26	Mournies	51	Anoyia	Aghia Triada	71	Grammenos	4	Paleohora	6
2	Metochia (Gavdos)	27	Kalyves 2	52	Stavromenos Heraklion	Aghios Ioannis	45	Kalamavka	64	Paleohora campsite	9
3	Koundoura	28	Vrysses	53	Fortetsa 2	Aghios Miron	50	Kalithea	57	Panasos	47
4	Grammenos	29	Exopolis	54	Finikia	Aghios Vlassios	55	Kaloudiana	19	Parathiri	63
5	Anogia	30	Chora Sfakia	55	Aghios Vlassios	Aitania	59	Kalyves 2	27	Platanos	12
6	Paleohora	31	Frangokastello	56	Vathipetro	Akros Flomos	11	Kandila	48	Potamidha	14
7	Sellino	32	Skaloti	57	Kalithea	Anidri	10	Kastelli	46	Potamos (Gavdos)	1
8	Voutas	33	Kournas	58	Prassas	Anogia	5	Kato Zagros	74	Prassas	58
9	Paleohora campsite	34	Moundros	59	Aitania	Anoyia	51	Kera	18	Rotonda	21
10	Anidri	35	Gonia	60	Thrapsano	Apostoli	41	Khairetiana	16	Selino	7
11	Akros Flomos	36	Viglotopi	61	Dhemati	Asteri	38	Kheratokambos	73	Selli	37
12	Platanos	37	Selli	62	Mirtos	Atsipadhes	49	Kokkino Pyrgos	43	Sikia	69
13	Laridas	38	Asteri	63	Parathiri	Charavgi	17	Koufonisi (Koufonisi)	72	Sirili	24
14	Potamida	39	Stavromenos - Rethymnon	64	Kalamavka	Chora Sfakia	30	Koundoura	3	Skaloti	32
15	Skouloudiana	40	Erfi	65	Makrilia	Dhemati	61	Kournas	33	Skouloudiana	15
16	Khairetiana	41	Apostoli	66	Vainia	Episkopi	22	Langada	68	Stalos	25
17	Charavgi	42	Lingres	67	Pachia Ammos	Erfi	40	Laridas	13	Stavromenos-Rethymnon	39
18	Kera	43	Kokkino Pyrgos	68	Langada	Exopolis	29	Lingres	42	Stavromenos-Heraklion	52
19	Kaloudiana	44	Faneromeni-Messara	69	Sikia	Faneromeni-Messara	44	Makrilia	65	Thrapsano	60
20	Nokhia	45	Aghios Ioannis	70	Goudouras	Faneromeni-Sitia	75	Metochia (Gavdos)	2	Vainia	66
21	Rotonda	46	Kastelli	71	Aghia Triada	Finikia	54	Moundros	34	Vathipetro	66
22	Episkopi	47	Panasos	72	Koufonisi (Koufonisi)	Fortetsa 2	53	Mournies	26	Viglotopi	36
23	Zounaki	48	Kandila	73	Kheratokambos	Frangokastello	31	Mirtos	62	Voutas	8
24	Sirili	49	Atsipadhes	74	Kato Zagros	Gonia	35	Nokhia	20	Vrysses	28
25	Stalos	50	Aghios Miron	75	Faneromeni - Sitia	Goudouras	70	Pachia Ammos	67	Zounaki	23

Figure 5.4. Geological map of Crete Island. The Heraklion basin is located in the central part (van Hinsbergen and Meulenkamp, 2006).

5.2. Stratigraphy

The Neogene deposits were formed in terrestrial to deep marine environments, indicating significant changes in depositional depths due to a combination of vertical movements and substantial climatic changes (Panagopoulos et al., 2022). These deposits include a sequence of conglomerates, sands, marls, clays, and coals, with abrupt lateral and vertical lithological

changes. Plant fossil assemblages are recorded in late Serravalian-early Tortonian and Middle Tortonian sediments.

Meulenkamp et al. (1979) subdivided the Neogene sedimentary sequence of Crete into six lithostratigraphic groups: the Prina, Tefelion, Vrysses, Hellenikon, Finikia, and Agia Gallini groups (Fig. 5.5).

The Tefelion and Vrysses Groups consist of four lithostratigraphic formations. The Viannos Formation includes a wide range of depositional environments, such as channel-belt, overbank, lake deposits. The Skinias Formation conformably overlies the Viannos Formation and consists of marine clays interbedded with sandstones and occasionally gravels. The Ambelouzos Formation, equivalent to the Kasteliana Formation (Zachariasse et al., 2011), was deposited in fluvio-lacustrine, lagoonal, and inner-neritic environments. Lastly, the Varvara Formation is notable for including Messinian evaporites. The end of the Messinian Salinity Crisis (MSC) was marked by the "Lago Mare" phase, a period of fluvio-lacustrine conditions that preceded the marine Pliocene reflooding (Panagopoulos et al., 2022).

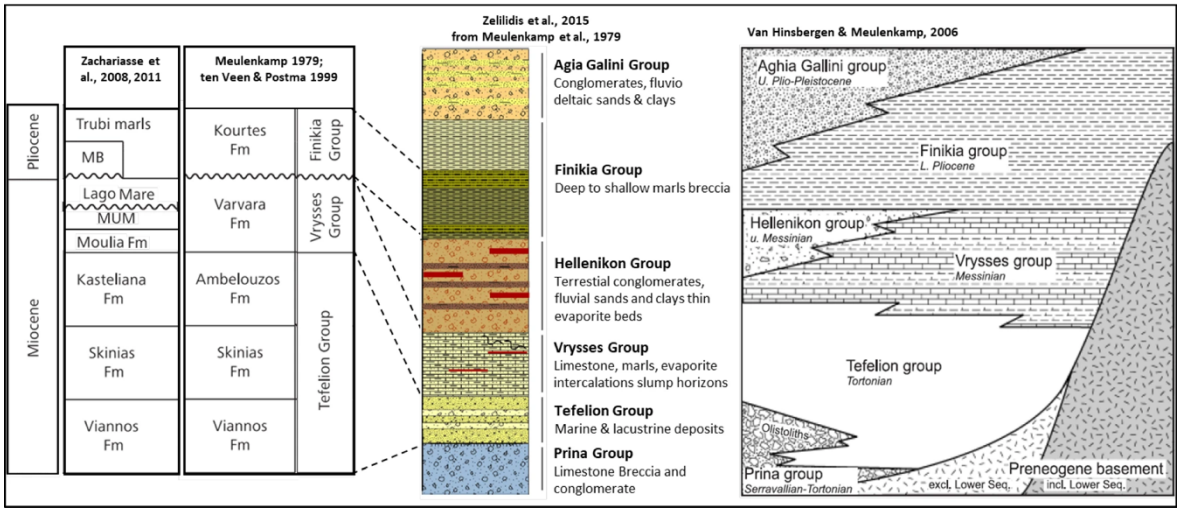

Fig. 5.5. From left to right: the two proposed classification schemes of the Miocene to Pliocene deposits according to Zachariasse et al. (2008; 2011) and Meluenkamp (1979), ten Veen and Postma (1999); general lithostratigraphic column of the Neogene deposits of Crete; schematic lithostratigraphy of Crete, with the main Groups and their architecture (Panagopoulos et al., 2022).

5.3. The structural context

The structural context of the Heraklion Basin reflects its position within the tectonically active Hellenic Arc system (Caputo et al., 2010). The basin's evolution has been profoundly influenced by extensional tectonics (Fig. 5.6) and the dynamic interplay between crustal subsidence, block faulting, and hinterland uplift (Fassoulas, 2001). These processes,

particularly active during the Late Miocene, shaped a complex depositional environment with diverse sedimentary settings ranging from steep slope systems to isolated carbonate platforms.

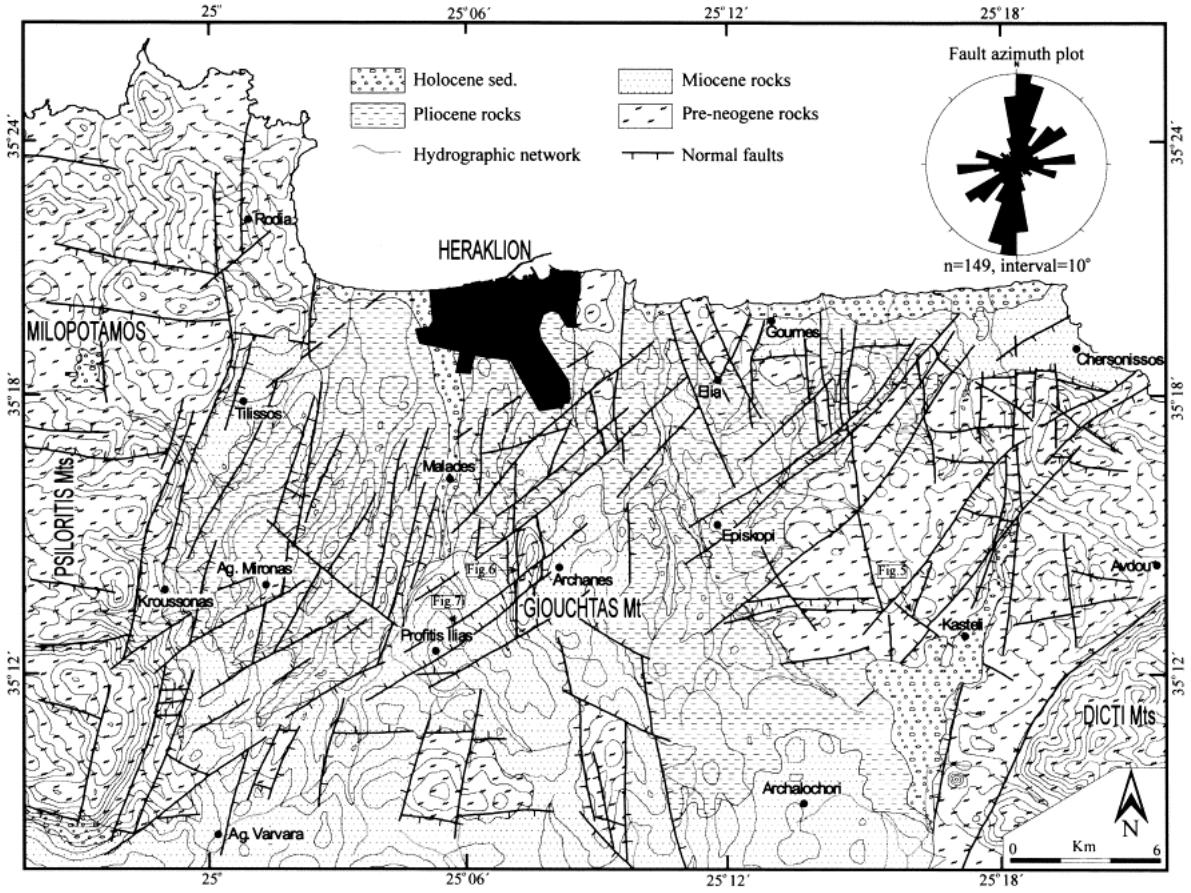

Fig. 5.6. Structural map of the Heraklion Basin showing the fault azimuths (Fassoulas, 2001).

The Heraklion Basin experienced a dynamic evolution throughout the Middle to Late Miocene, transitioning from non-marine and marginally marine sedimentary environments to a fully marine system by the early Tortonian. During the Middle Miocene, sedimentation was dominated by brackish lagoons, marginal marine zones, and offshore marine settings (ten Veen & Postma, 1999; Moisette et al., 1993). By the late Serravallian and early Tortonian, the basin evolved into an open marine environment characterized by the deposition of coarse clastic sediments along its coastlines. These sediments were intermittently colonized by colonial corals (*Porites*, *Tarbellastrea*, with minor contributions from *Acanthastraea* and *Siderastraea*), which formed laterally extensive coral biostromes. The onset of extensional tectonics in the late Tortonian resulted in rotational uplift of blocks distal to the basin margins, creating isolated carbonate platform. These environments supported the development of coral reefs along steep cliffs and gentle ramps, often associated with level-bottom coral communities in open marine conditions (Brachert et al., 2007).

During the transition from the Tortonian to the Messinian, relative basin subsidence coupled with hinterland uplift caused the drowning of most shallow-water environments. As a result, early Messinian coral growth was confined to narrow zones fringing the Lasithi Mountains (Reuter et al., 2006; Reuter and Brachert, 2007).

Kinematic studies of the faults conducted by various authors (Angelier, 1975; Meulenkamp et al., 1988; ten Veen & Postma, 1999; Fassoulas, 2001) have identified two main phases of normal faulting, followed by a transpressive phase that activated an oblique fault system (ten Veen & Kleinspehn, 2003). Vertical studies based on foraminifera have helped define the uplift and subsidence history of the basin (Meulenkamp et al., 1994; ten Veen and Postma, 1999; van Hinsbergen and Meulenkamp, 2006; Zachariasse et al., 2008).

Stratal geometries in the superficial marine sediments indicate the presence of three main stratigraphic sequences. The coral reef has been dated at 10 Ma (Kroeger, 2004), and the basal deposits of the escarpment, at the contact between the Ambelouzos and Varvara formations, mark the Tortonian/Messinian boundary (ten Veen & Postma, 1999). These events have been correlated with global third-order sequence boundaries (Haq et al., 1988; Hardenbol et al., 1998), reflecting high-frequency climatic oscillations documented in both deep and shallow marine sediments (Santarelli et al., 1998; Kroeger, 2004).

According to Reuter et al. (2006), the Varvara Formation consists of fine-grained sediments characterized by distinct bipartite cycles of homogeneous and laminated marl or fissile limestone. Near the top of the formation, a unit of sedimentary gypsum is intercalated, potentially linked to the Messinian Salinity Crisis. In more proximal settings, the fine-grained sediments of the Varvara Formation transition laterally into calciturbidites and debrites, which, in turn, grade into bioclastic limestones and coral buildups. This interval represents the focus of the present chapter.

5.1.2 The Moni Gorgolaini section

The stratigraphic section of Moni Gorgolaini is located close to the western flank of the Heraklion Basin, probably along a tilted fault block where a mixed siliciclastic-carbonate systems developed during the Late Miocene (Reuter et al., 2006) (Fig. 5.2).

The total thickness of the section is about 14 meters and mainly consists of marl intervals alternating with bioclastic calcarenite with various skeletal components (Fig. 5.7, 5.8A).

The section begins with a one-meter-thick layer of brownish laminated marls interspersed with a centimeter-thick layer of floatstone with coralline red algae. Between 1 and 2 m lenses of polymictic conglomerates or vermetid-rich floatstone, with a channel-like shape, are intercalated to the marly layers (Fig. 5.9).

At around 2 m, a 3 m thick interval of bioclastic calcarenite is characterized by abundant vermetids accumulation with rudstone to floatstone texture in a fine wackestone matrix,

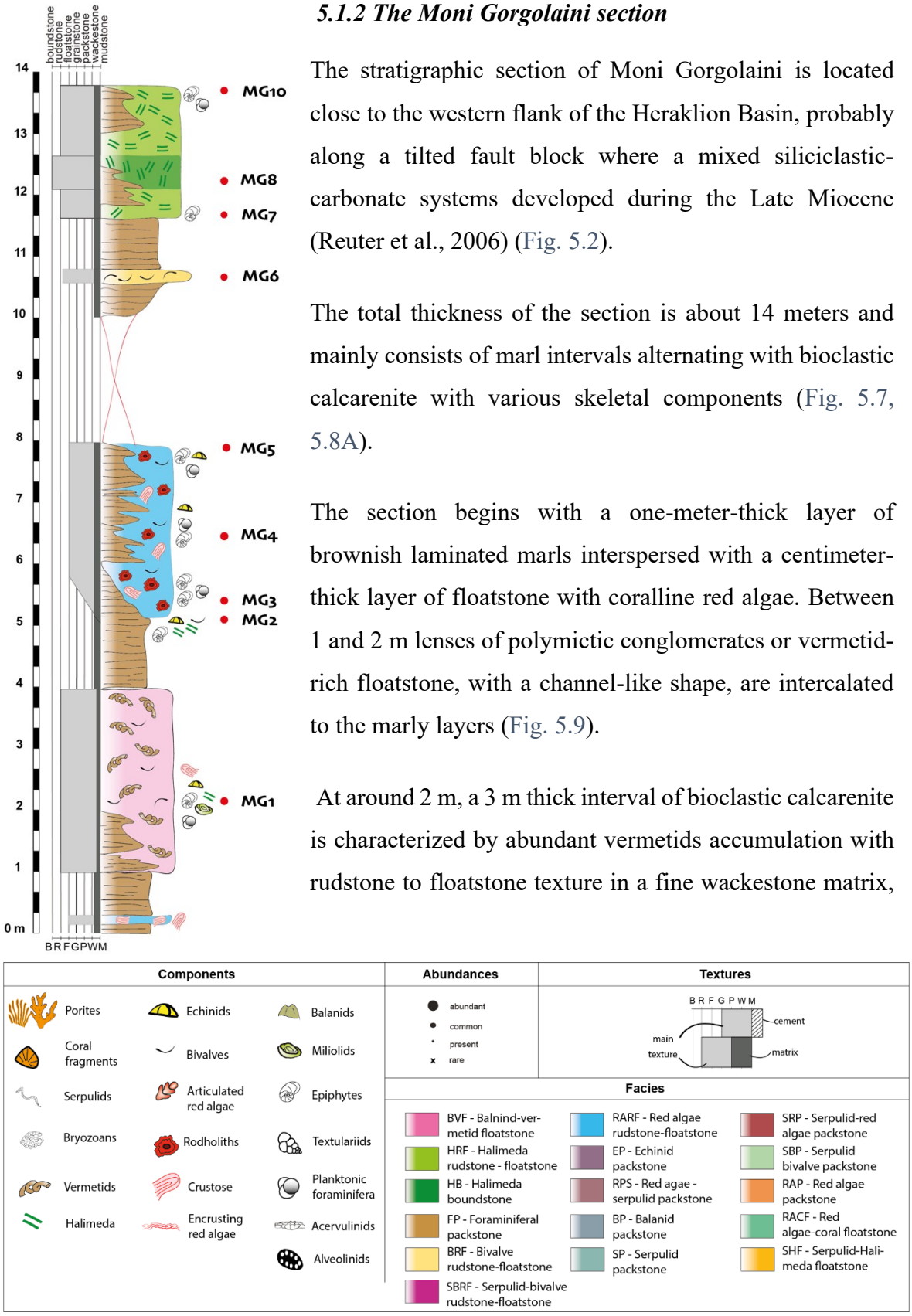

Fig. 5.7. Stratigraphic log of the Moni Gorgolaini section with sample locations, textures, facies and legend.

which includes miliolids, epiphytes, fragments of coralline algae, echinoderm fragments, and rare segments of *Halimeda* (Fig. 5.8B). The base of this interval is erosive and pass

laterally to marly deposits. The geometrical features suggest a channel-like geometry with mass-flow deposits.

At the base of this surface, thin, elongated polymictic breccia lenses composed of coral fragments and terrigenous clasts are documented (Fig. 5.9). For about another meter, between 4 and 5 m, another marly interval is present. At 5 meters, another deposit approximately three meters thick that interdigitates laterally with the marls. This body represents an accumulation of coralline algae and rhodoliths along with bivalve shells arranged in textures ranging from rudstone to floatstone and is characterized by a fine wackestone matrix containing miliolids, planktonic foraminifera, epiphytes, echinoderm fragments, and rare segments of *Halimeda*. This interval has a mound-like geometry with a lateral extension of less than 10 m and a marked interfingering with background marly sediments.

Between 8 and 10 m from the base occasionally marl levels intercalated with a centimeter-thick layer with abundant bivalve shells crops out.

At 11.70 meters, with a sharp contact, a mound-like body approximately two meters thick and 6 m in lenght is visible. This small bioherm is entirely dominated by *Halimeda* segments. The algal segments are predominantly arranged in rudstone/floatstone textures (Fig. 5.10), with scattered layers of boundstones where the algal segments are in growth position. The matrix of these facies is represented by a very fine packstone containing some epiphytes and planktonic foraminifera. Furthermore, in this accumulation, botryoidal aragonitic cements are present (Fig. 5.11). Moving laterally southward, outside the *Halimeda* mound, coral breccia beds are visible.

Fig. 5.8. Panoramic view of the Moni Gorgolaini section track measured in the central-western flank of the Heraklion Basin (in yellow). (A) and the small *Halimeda* bioherm (B).

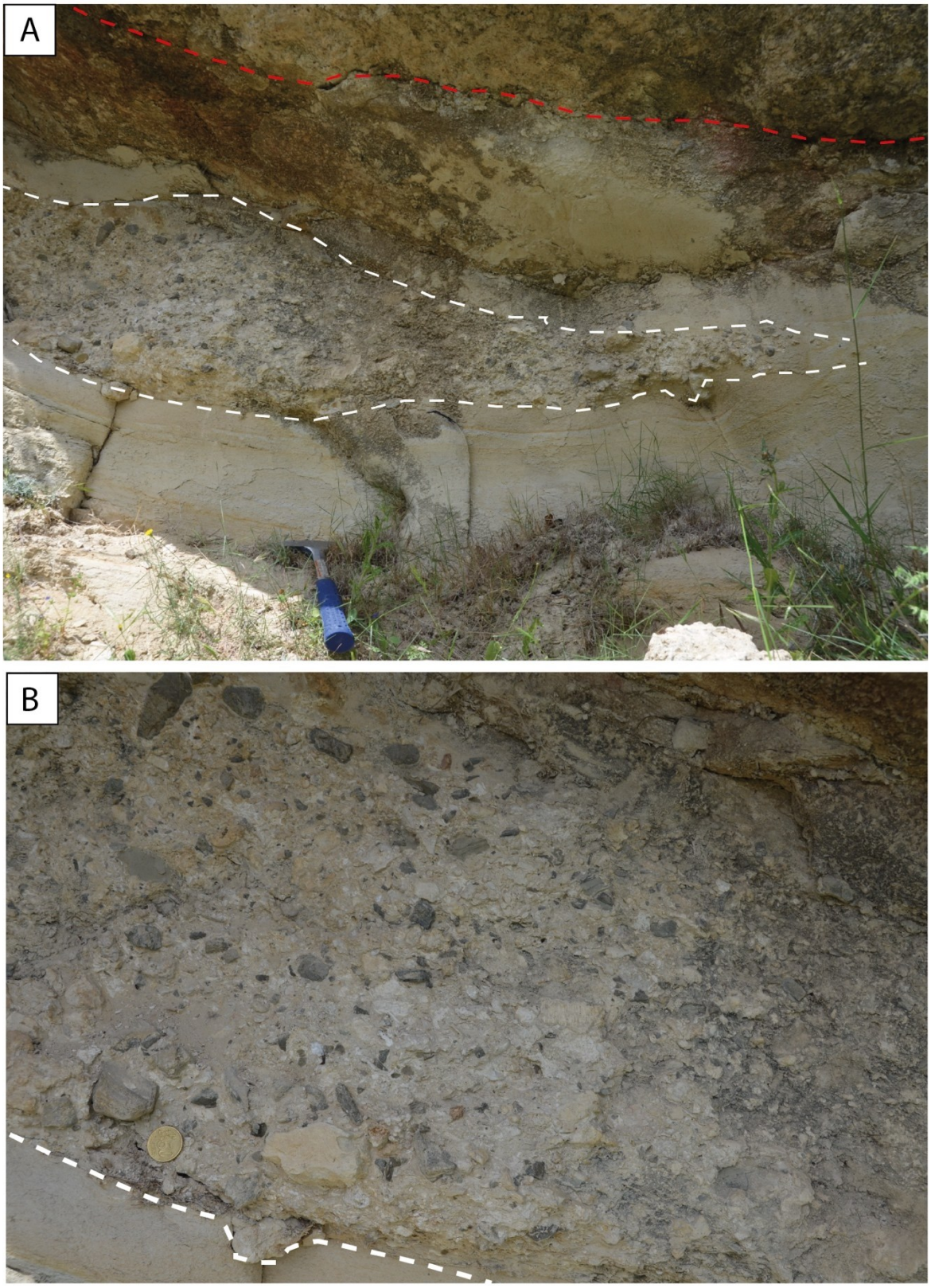

Fig. 5.9. Close-up on the channelized surface: A) one of the elongated breccia lenses within the marls (dashed white line). The dashed red line separates the marls from the vermetid deposit; B) a close-up of the polymictic breccia with its angular to sub-rounded clasts.

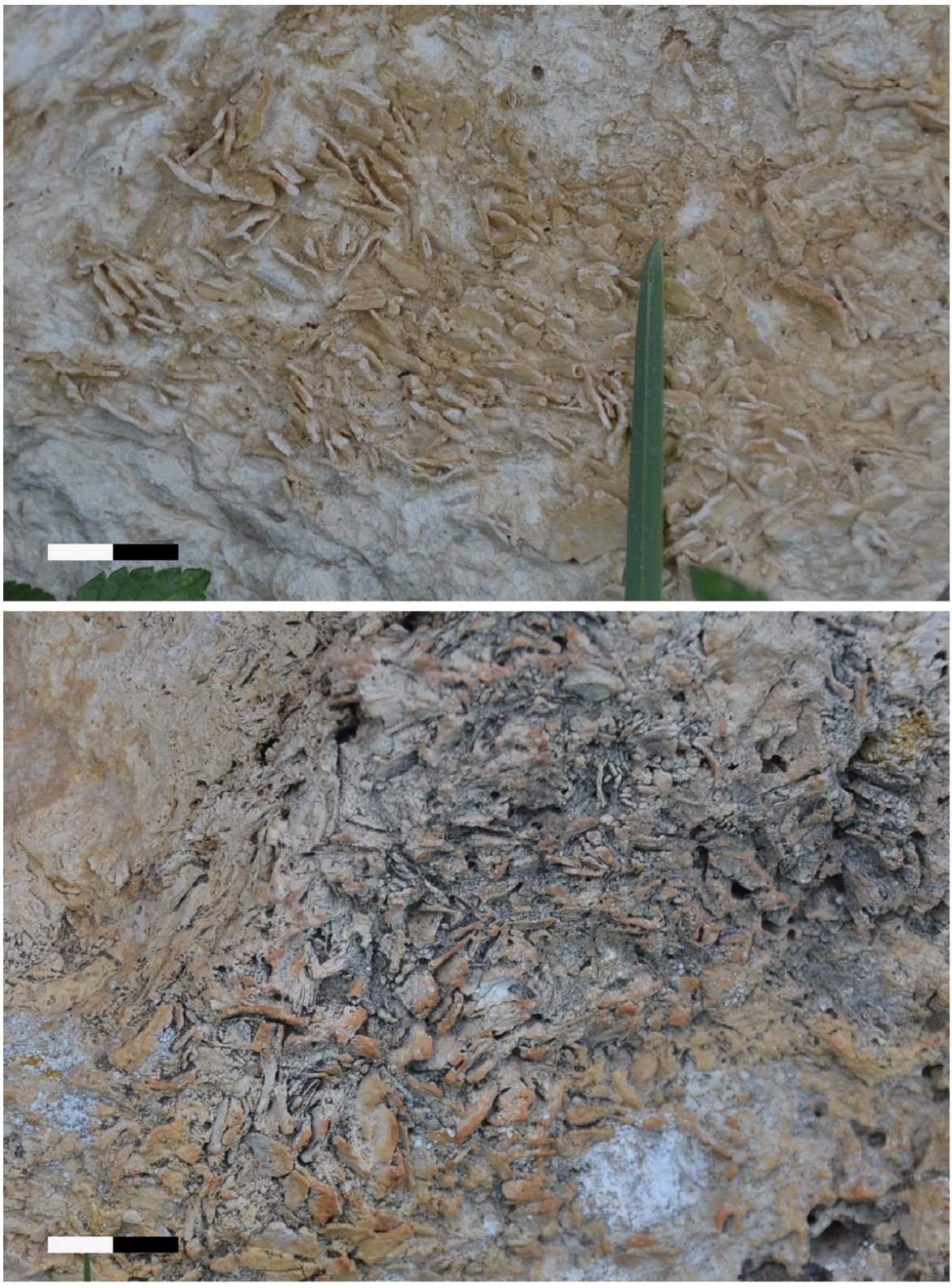

Fig. 5.10. A close-up to the *Halimeda* rudstone-floatstone facies in the Moni Gorgolaini section (scale is 2 cm).

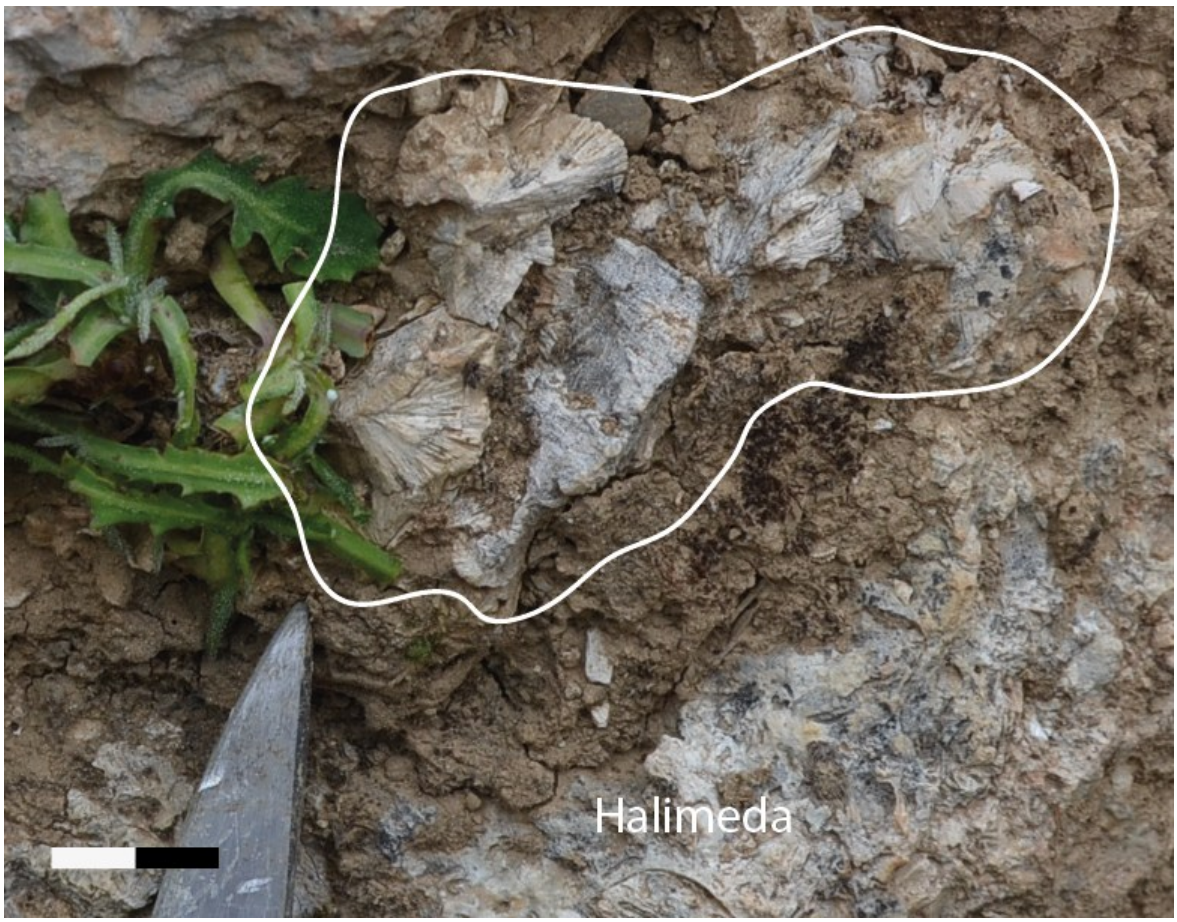

Fig. 5.11. Field aspect of the botryoidal aragonitic cements in *Halimeda* rudstone-floastone facies at Moni Gorgolaini (scale is 2.5 cm).

5.1.3 The Souvlaki section

The Souvlaki section is near to the eastern flank of the Heraklion graben (35° 13’ 05.93’’N, 25° 10’ 26.22” E), (Fig. 5.2). The section has been measured along a new road trench with a very fresh exposure and is approximately 22 meters thick (Figs. 5.12, 5.13). The succession is very well stratified with medium to thick beds composed of bioclastic calcarenite, predominantly rudstone-floatstone textures in a medium to coarse wackestone matrix, with abundant accumulations of *Halimeda*. These are interbedded with serpulid facies and beds of floatstone containing coralline algae and rhodoliths.

Fig. 5.12. Souvlaki outcrop features along the main road.

The section (Fig. 5.13) begins with 1.8 meters of rudstone-floatstone with serpulids, associated with fragments of coralline algae and some rhodoliths, in a coarse wackestone matrix containing small fragments of echinoids, red algae, epiphytes, and miliolids. A decimeter-thick interval of bivalve shell concentrations is present at top. Between 1.8 and 2.5 m the first well-stratified *Halimeda*-rich interval, organized in thin to medium beds, occurs. The algal segments, along with some bivalve shells, are oriented horizontally (Fig. 5.14B-C). The matrix of the *Halimeda* is represented by a medium-coarse wackestone containing few fragments of coralline algae, echinoids, miliolids, and epiphytes. At 2.5 there is a 0.6-meter-thick layer of packstone with bivalves and another 0.6-meter-thick layer of packstone with scattered serpulids. At 3.8 m, a second stratified 1.4 thick interval with *Halimeda* is visible, exhibiting almost the same characteristics as the underlying first interval.

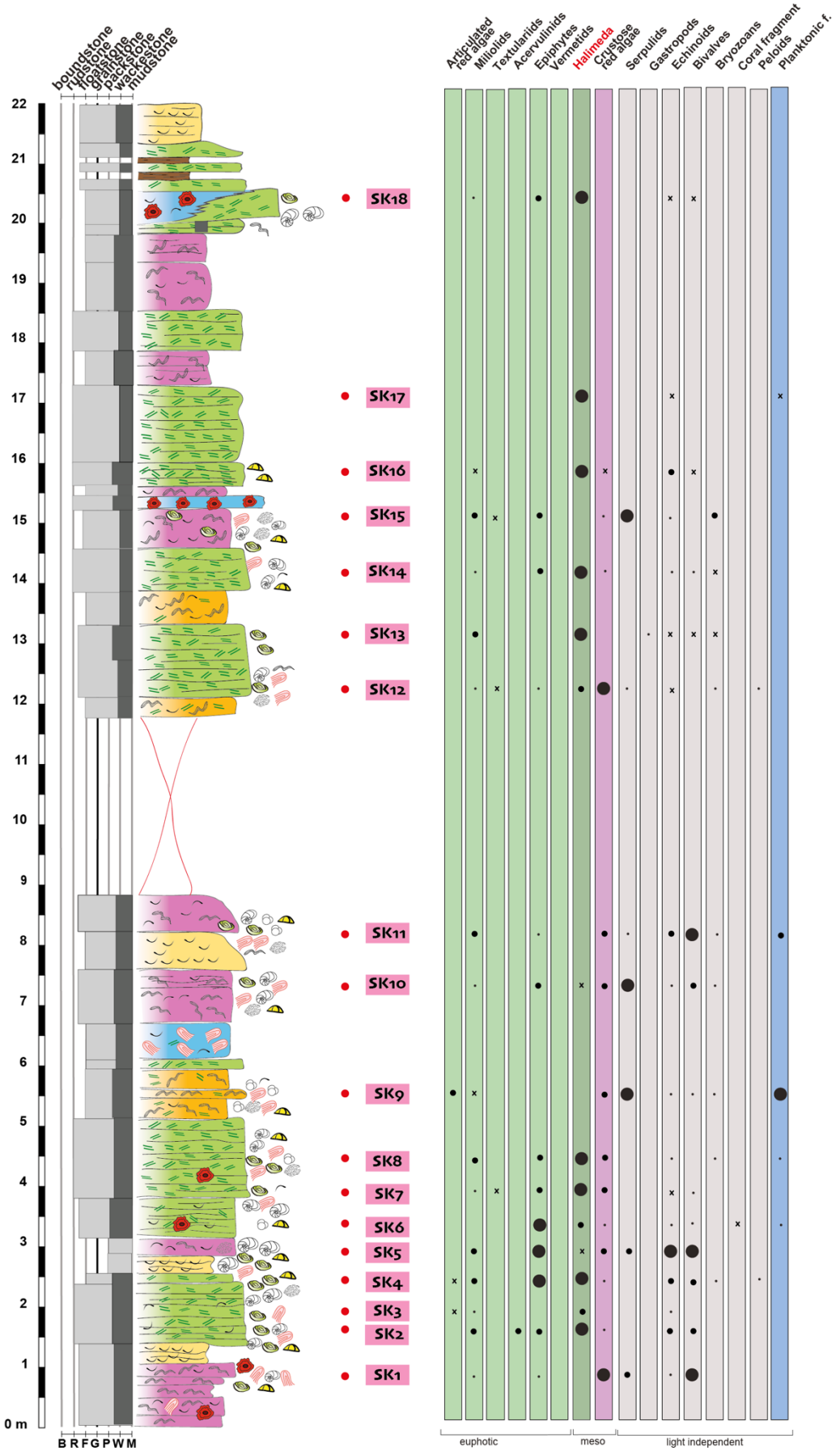

Fig. 5.13. Stratigraphic log of the Souvlaki section featuring sample locations, textures, facies, and abundances of the respective components on the base of the photic zone.

Between 5.2 and 6.1 m, there are alternating intervals of serpulid facies and floatstone with red algae, as well as bivalve levels, and a 40 cm bed rich in *Halimeda* (Fig. 5.14A). The serpulid facies is characterized by a coarse wackestone matrix.

At 6.1 m, a 60 cm bed of red algae floatstone and rare bivalves and *Halimeda* consists of serpulid and bivalve floatstone with rare red algae and *Halimeda,* followed by 90 cm of floatstone to coarse rudstone rich in serpulids and some bivalves. At 7.6 m a normally graded bed, 70 cm thick, whit coarse bivalve's floatstone occurs. Followed by another normally graded bed of floatstone with serpulids, bivalve and some gastropods.

After a covered interval at 11.70 m a thin bed of floatstone-rudstone with serpulids and *Halimeda* is present, exhibiting similar characteristics to the previous layers. Followed by 1.4 m of rudstone dominated by *Halimeda*, with a coarse wackestone matrix with some red algae fragments, miliolids and epiphytes. At 13.3, there are 0.6 meters of floatstone with bivalve and serpulid in a packstone matrix. At 13.9 m a second stratified interval with *Halimeda*, about 60 cm thick, have similar characteristics to the first interval. In all the *Halimeda*-rich intervals, the algal segments are almost always horizontally oriented.

The interval between 14.60 and 15.7 m consists of serpulid and bivalve floatstone with rare red algae, interrupted by a 10 cm thick rhodolithic rudstone and followed by another *Halimeda* rudstone bed of 30 cm in thickness.

At 15.7 m another *Halimeda*-rich bed of 30 cm, interrupted by 30 cm of serpulids floatstone mark the base of an interval of 70 cm of *Halimeda* rudstone. At 17.30 m a 50 cm layer of marly limestone and floatstone with serpulids and scattered bivalves occur. On top another well-bedded *Halimeda* rudstone of about 70 cm reappears. Between 18.5 and 19.9 m serpulid floatstone and bivalves characterize this interval with more abundant serpulids in the lower part. The last occurrence of *Halimeda*, between 19.9 and 21.10 m, is characterized by thin levels intercalated with laminated clays and by a lenticular bed of *Halimeda* floatstone passing laterally to a rhodolithic floatstone. The section ends at meter 22 with a bivalve rudstone.

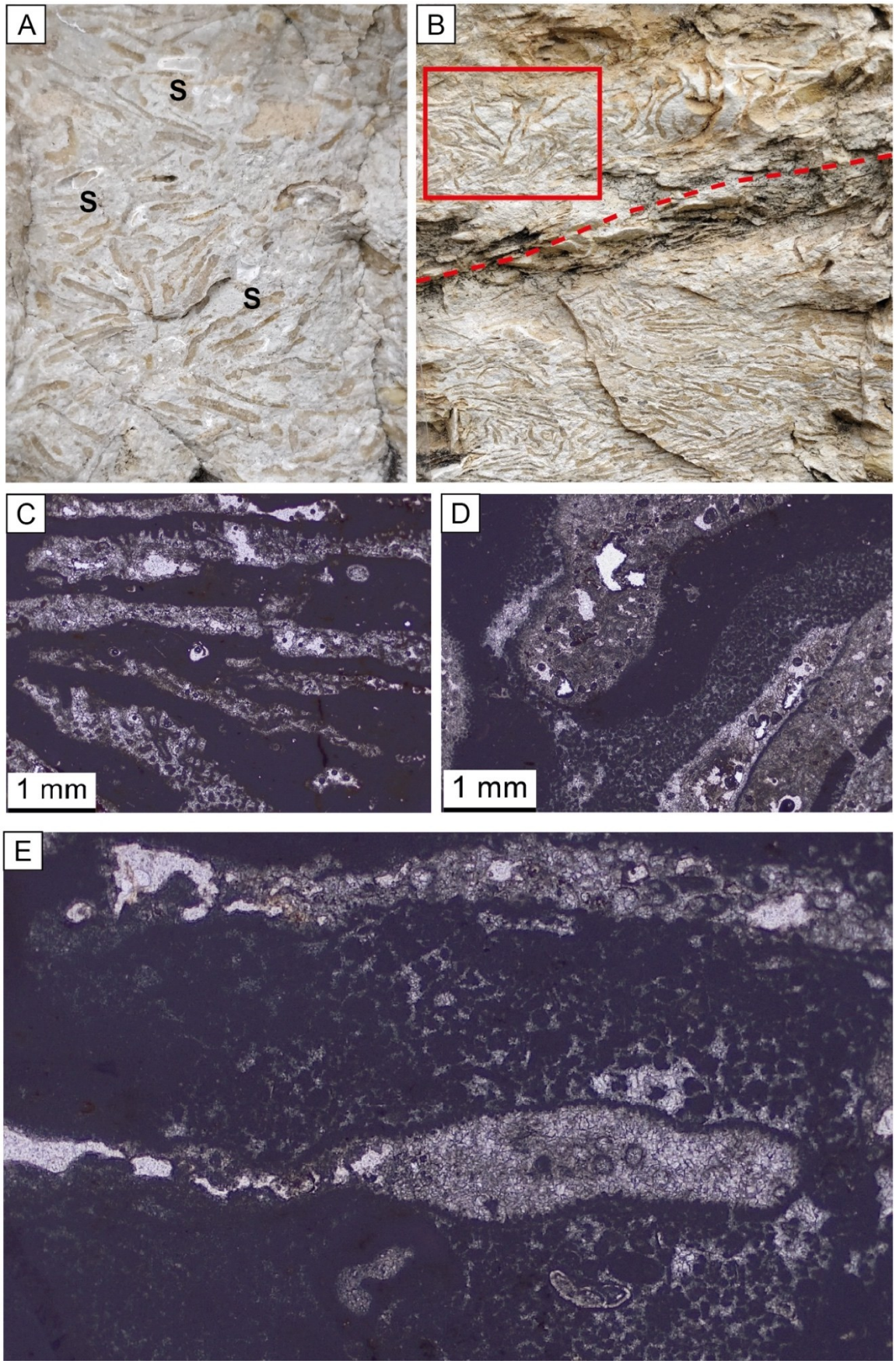

Fig. 5.14. The *Halimeda* facies in the Souvlaki stratigraphic section. A) *Halimeda*-serpulid floatstone with well-preserved algal segments; B) *Halimeda* rudstone with isoriented segments and segments in growth position (red square); C) Thin section showing *Halimeda* segments horizontally-oriented in the fine wackestone matrix; D – E) thin sections of *Halimeda* segments and peloidal matrix.

5.1.4 The Knossos sections

This notable outcrop (Fig. 5.15), located near the city of Heraklion directly opposite the well-known Palace of Knossos, extends north to south for approximately 2.8 km. Its exceptional state of preservation, due to both its long exposure and the absence of tectonic disturbances affecting its geometries, has made it possible to reconstruct the complete features of this extensive and continuous outcrop from a proximal to a distal setting.

Fig. 5.15. Aerial view of extensive outcrop (red line) where the sections of Knossos are measured and sampled.

The visible geometries in Fig. 5.16 are characteristic of a carbonate ramp system (Burchette & Wright, 1992), with most of the succession displaying typical depositional features of a gently dipping carbonate ramp. However, certain portions of the outcrop show geometries that can be ascribed to a distally steepened ramp (*sensu* Read, 1985), characterized by clinoforms with increased angles. The excellent exposure of these geometries allows for a detailed reconstruction of depositional environments and lateral facies transitions, making this outcrop a possible key reference for understanding ramp-type carbonate depositional systems. Despite its scientific significance, this outcrop has never been studied before, making this the first detailed investigation of its stratigraphic architecture and facies distribution.

To systematically document facies variations along a proximal-to-distal transect, multiple stratigraphic logs were measured, and facies distributions were mapped across different stratigraphic layers. From the five measured sections, it emerged that Knossos 1, Knossos 2, and Knossos 3 are characterized by banks dominated by encrusting facies with rudstone and floatstone textures, primarily composed of red algae and serpulids, with variable terrigenous input, quite abundant in the covered intervals. Notably, *Halimeda* was absent in these sections. Moving stratigraphically upward and toward the distal part of this ramp profile, significant levels rich in *Halimeda* accumulations begin to appear. These accumulations, displaying rudstone textures, are particularly well documented in the two quarries where the Minosse and Nikita sections were measured.

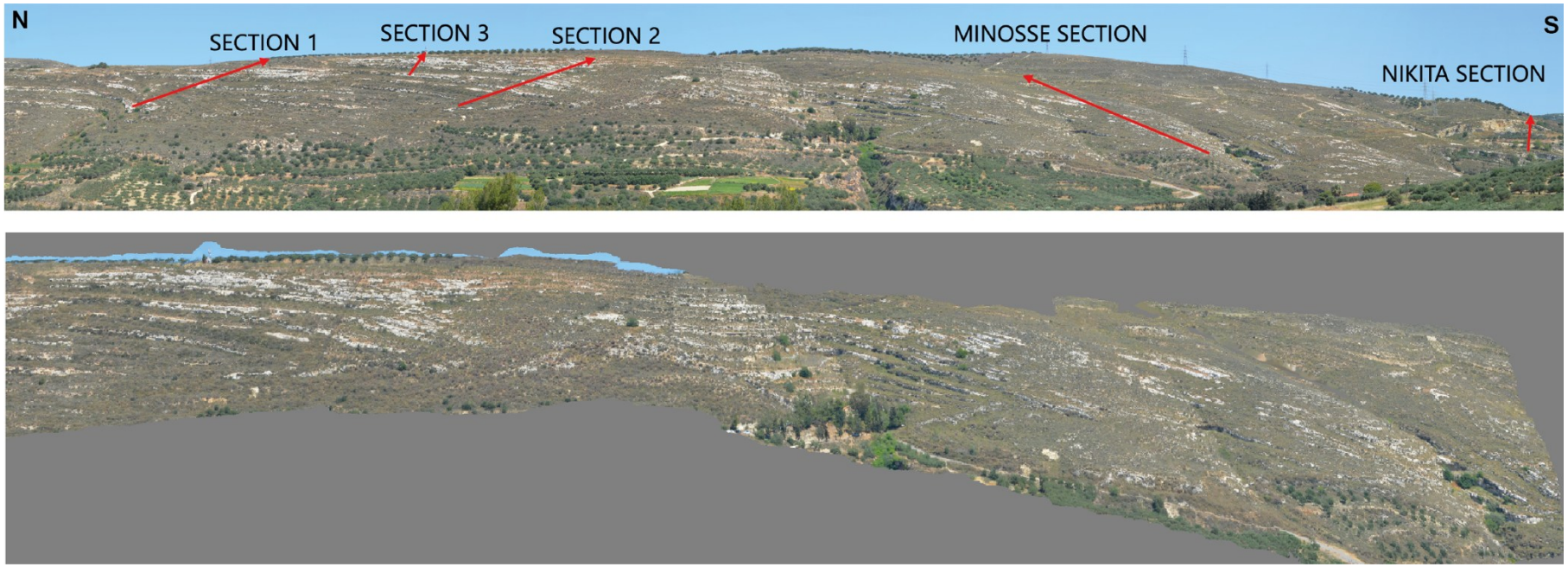

Fig. 5.16. the north-south sections with the location and tracks of the stratigraphic sections and a model created with Agisoft Metashape that highlights the geometries of the clinoforms.

Fig. 5.17. The prominent Knossos outcrop, running from north to south, showcases its depositional geometries. Different levels (numbers in the white spots) along the outcrop are represented by color coding. Also marked are the locations of the measured and sampled stratigraphic sections: Knossos 1, Knossos 2, Knossos 3, Minosse and Nikita.

The Knossos section 1

The first section measured in this area (Fig. 5.17, 5.18) is characterized by metric beds of bioclastic calcarenite alternating with covered intervals. The predominant facies are rich in coralline algae, mainly displaying floatstone textures with coarse wackestone to packstone matrices. Few clay and marly levels are present. This section reaches a thickness of approximately 55 meters and has been subdivided into levels for ease of description, due to both the size of the outcrop and the presence of significant clinoforms and numerous non-exposed intervals. The section intersects 10 levels represented in Fig. 5.17.

The levels represented in this log and in the other sections are those that exhibited good exposure, allowing us to trace their continuity along the entire outcrop, and these were effectively described. Seventeen samples were collected from this section, and no *Halimeda* was detected.

Due to the poor condition of level 1, which was poorly exposed laterally, the section starts with level 2 (Fig. 5.19A) characterized by coralline algae floatstone with a fine wackestone matrix that becomes coarser towards the top. Level 3 starts (at 4 m) with a metric bed consisting of encrusting red algae rudstone at the base, transitioning to coralline algae fragments towards the top (Fig. 5.19D). This is followed by a metric interval of coralline algae facies with coral fragments and bivalves (Fig. 5.19C). In the central part, the texture tends to become a coralline algae packstone with occasional bivalves, and towards the top, there is a metric marly level containing rare bioclasts. A covered interval separates level 4 (at around 10 m), which shares similar characteristics with the preceding level. Level 5 8at around 17 m) is characterized by alternating coralline algae floatstone and clay intervals, ending with a metric marly level at the top. A one-meter concentration of bivalve shells separates level 5. Level 6 (at 22 m) begins with a two-meter interval composed of monogenic breccias, dominated by floatstone facies with coralline algae in a coarse wackestone matrix. These facies extend to about halfway up the level, where the same breccias reappear. At the top, there is a thin packstone layer with coralline algae and poorly exposed echinoids, followed by a 2.5-meter-thick cover. The base of level 7 (at 35 m) is characterized by the alternation of coralline algae packstone beds and thin marly layers, extending to about halfway through the level. From this point to the top, the level is dominated by floatstone rich in coralline algae and rhodoliths within a coarse wackestone matrix.

A marly level, about 50 cm thick, separates level 7 from level 7A. The latter, which is just over 1 meter thick, is characterized by a fine red algae packstone.

At 42. 5, level 8 consists of about 3 meters of red algae packstone, which gradually becomes finer towards the top and enriched in serpulids.

An additional layer of marl separates level 9 (at 45.5 m), which exhibits characteristics similar to those of level 7A. Subsequently, the section begins to be disturbed by vegetation, with occasional exposures of thin layers of packstone containing echinoids and serpulids. The section ends with level 10 (at 48 m), consisting of one meter of packstone with serpulids.

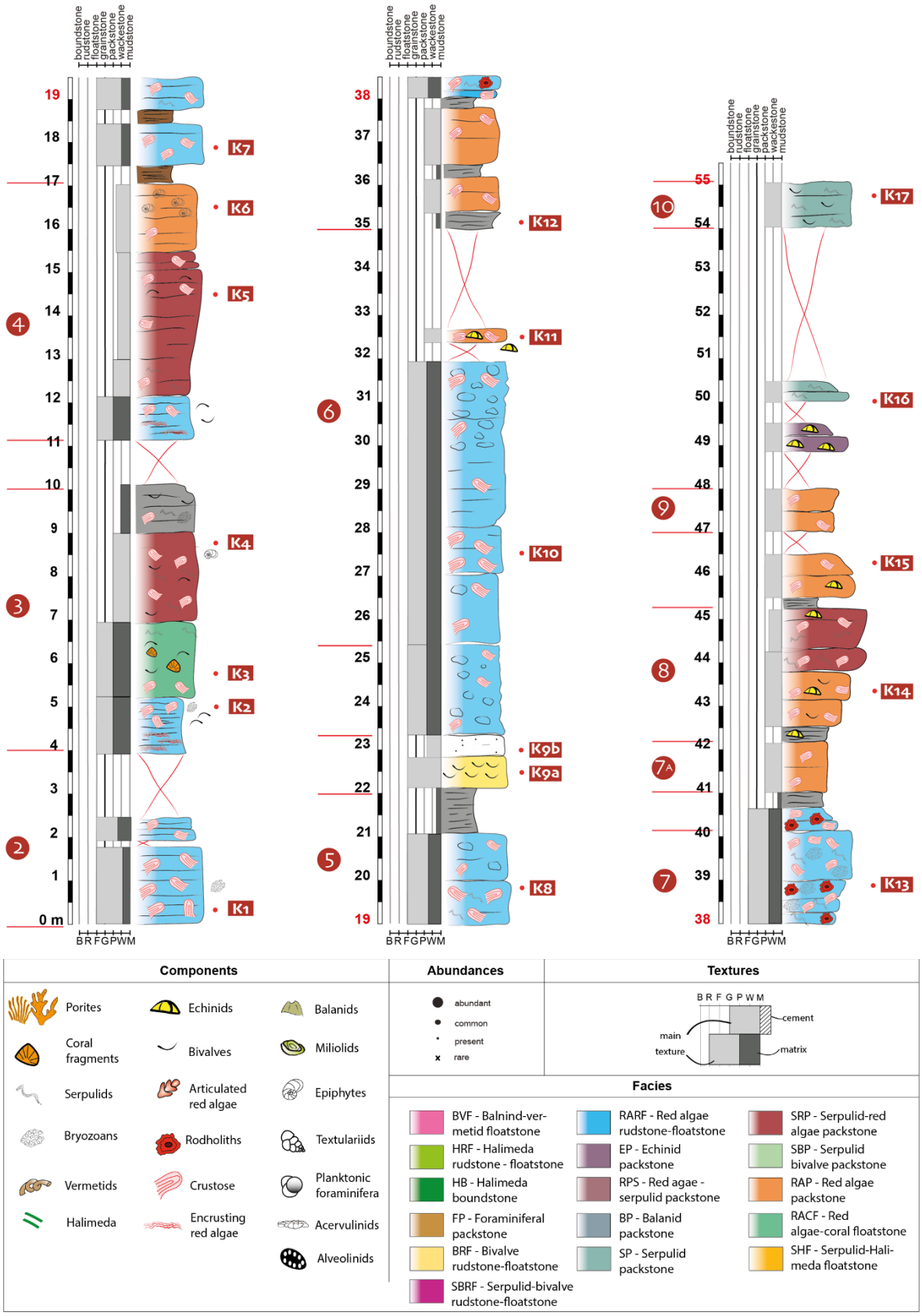

Fig. 5.18. Stratigraphic log of **Knossos section 1** featuring facies, textures, and sample locations. The red dots with numbers next to the scale indicate the levels intersected by the section, corresponding to those in Fig. 5.17.

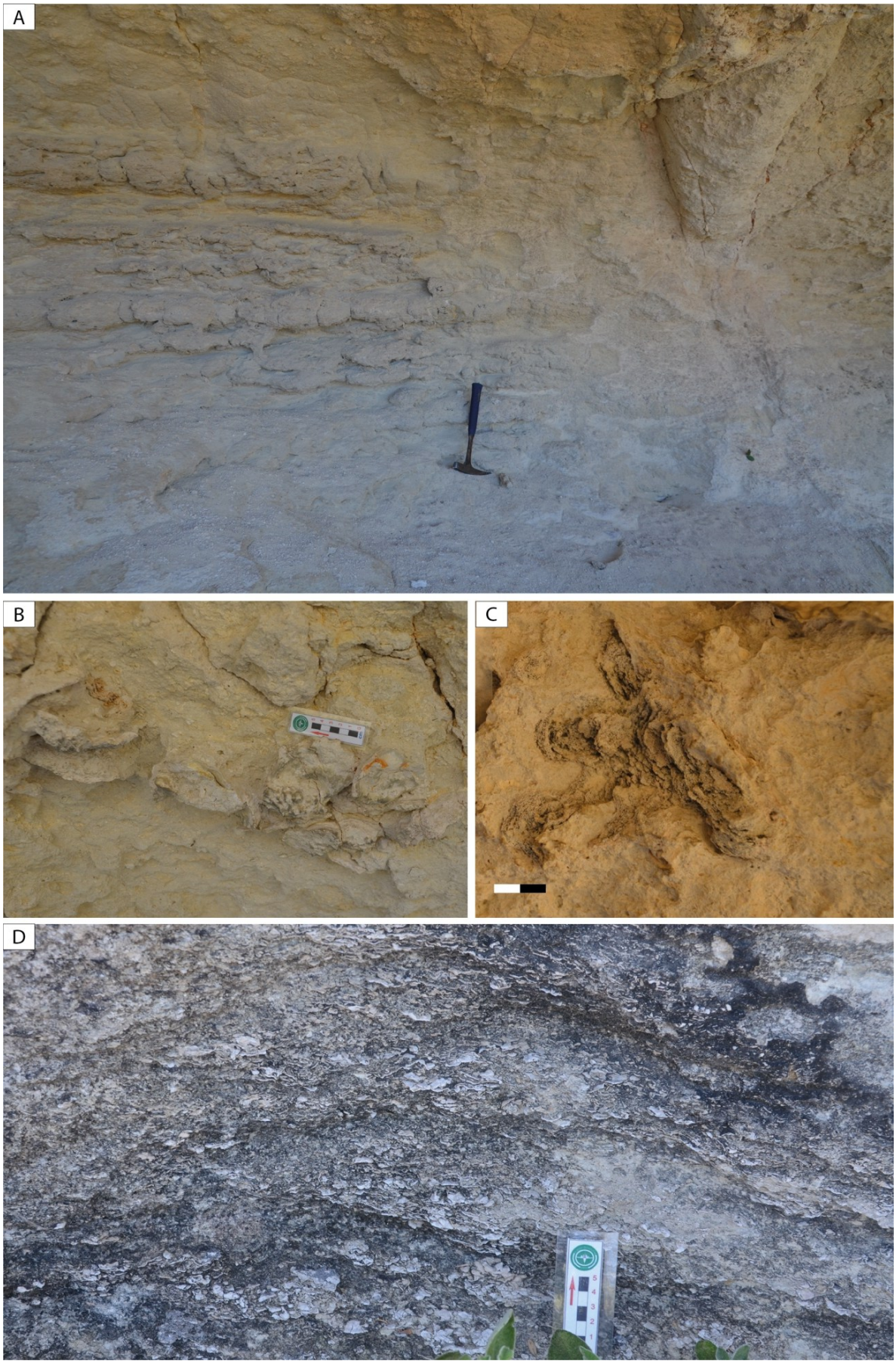

Fig. 5.19 – Field view of the rhodalgal facies characterizing the Knossos 1 section. A) Marl levels rich in encrusting red algae (red algae rudstone-floatstone); B) Oyster accumulations; (C) Close-up of a coral fragment within the red algae-coral floatstone facies; (D) Encrusting red algae rudstone.

The Knossos section 2

The Knossos 2 section was measured beginning at level 7 and continuing upward through the stratigraphic succession. As highlighted in Fig. 5.20, the log of this section shows facies similar to those found in section 1, with an increase in serpulid facies and a sudden decrease in terrigenous input. This section also exhibits numerous interruptions due to cover. It has been divided into levels, from 7 to 16, with level 16 representing not only the top of the section but also the final level of the outcrop. Levels 15 and 16 will be described in greater detail in section 3, as they are more prominently exposed. A total of 22 samples were collected along the section.

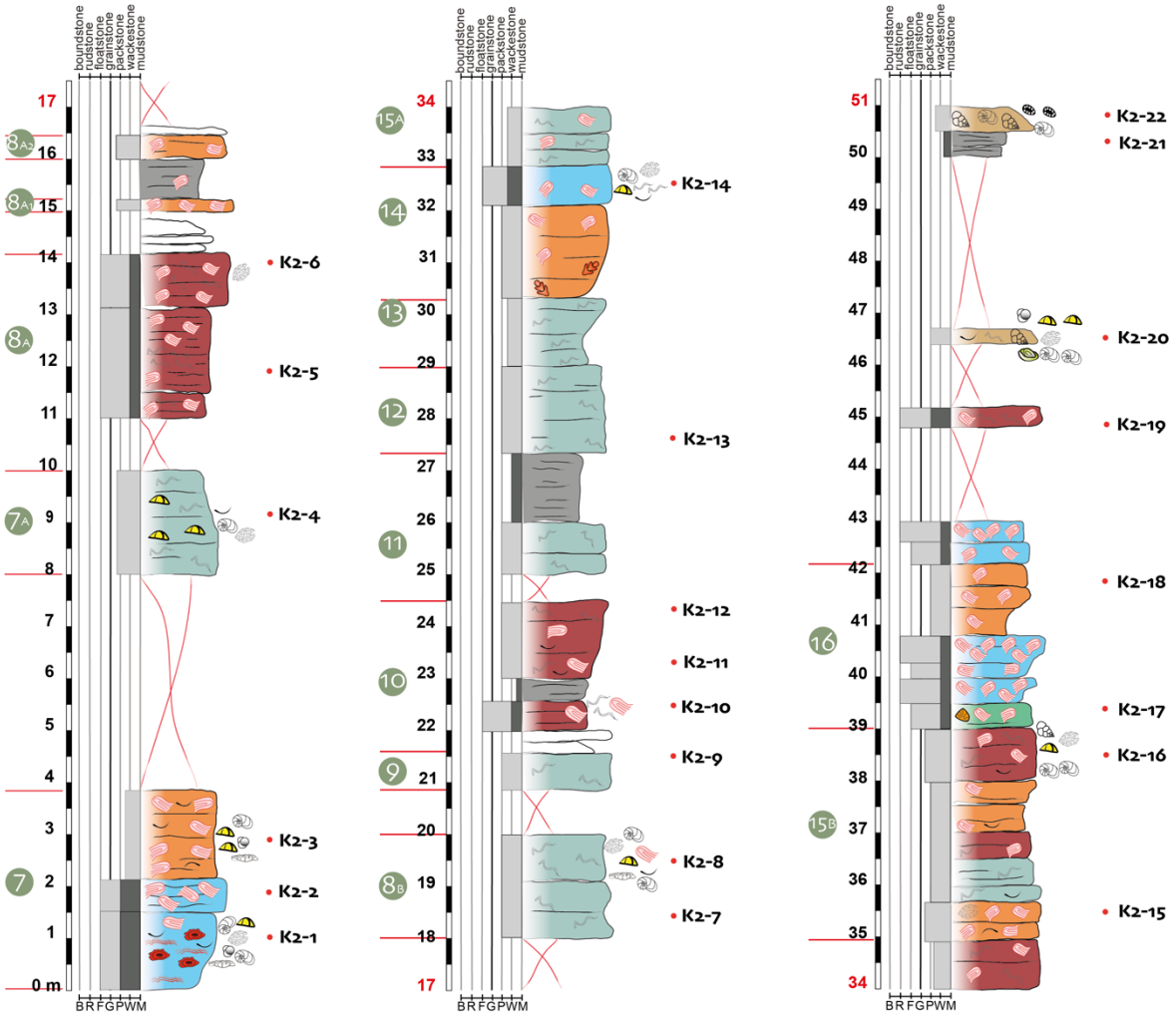

Fig. 5.20. Stratigraphic log of **Knossos section 2** featuring facies, textures, and sample locations. The green dots with numbers next to the scale indicate the levels intersected by the section, corresponding to those in Fig.5.17. See Fig. 5.18 for facies legend.

Level 7 exhibits the same characteristics as that of section 2 (Fig. 5.21A-B), while level 7A (at 8m) consists of medium to coarse packstone with a great abundance of serpulids. Level 8 (at 11m) about eight meters thick has been divided into multiple sub-levels, referred to 8A1, 8A2, and 8B (Fig. 5.20). This subdivision corresponds to the onset of distally steepened

profile of the ramp, as visible in Figs. 5.16, 5.17. These levels are also characterized by facies rich in serpulids and coralline algae, exhibiting floatstone textures with wackestone to packstone matrix. Levels 9 and 10, between 21 and 24.5 m, retain the same characteristics described for section 2. Levels 11, 12, and 13 are dominated by serpulid packstone facies interspersed with a thick marl layer. Level 14 (at 30.5 m) displays a greater enrichment in coralline algae, with floatstone textures toward the top.

Level 15A, approximately 2 meters thick, is divided into two parts: the first part 1 meter thick, consists of coarse packstone layers with serpulids, while the second part is made up of packstone with serpulids and red algae.

Level 15B is characterized by an alternation of more or less coarse packstone layers rich in red algae, which become enriched in serpulids in the central part. At the top, small benthic foraminifera such as miliolids, epiphytes, textulariids, and fragments of bryozoans and echinoids are found in associations.

At approximately meter 39, a change in texture occurs, transitioning from packstone to floatstone, rich in crustose red algae, with fine wackestone matrix. These facies characterize the last well-visible level, which is level 16.

From meter 42 to the top of the section at meter 51, a thick vegetal cover persists, with thin slightly exposed layers that show a drastic decrease in red algae, giving way to packstone facies rich in small benthic foraminifera (Fig. 5.20).

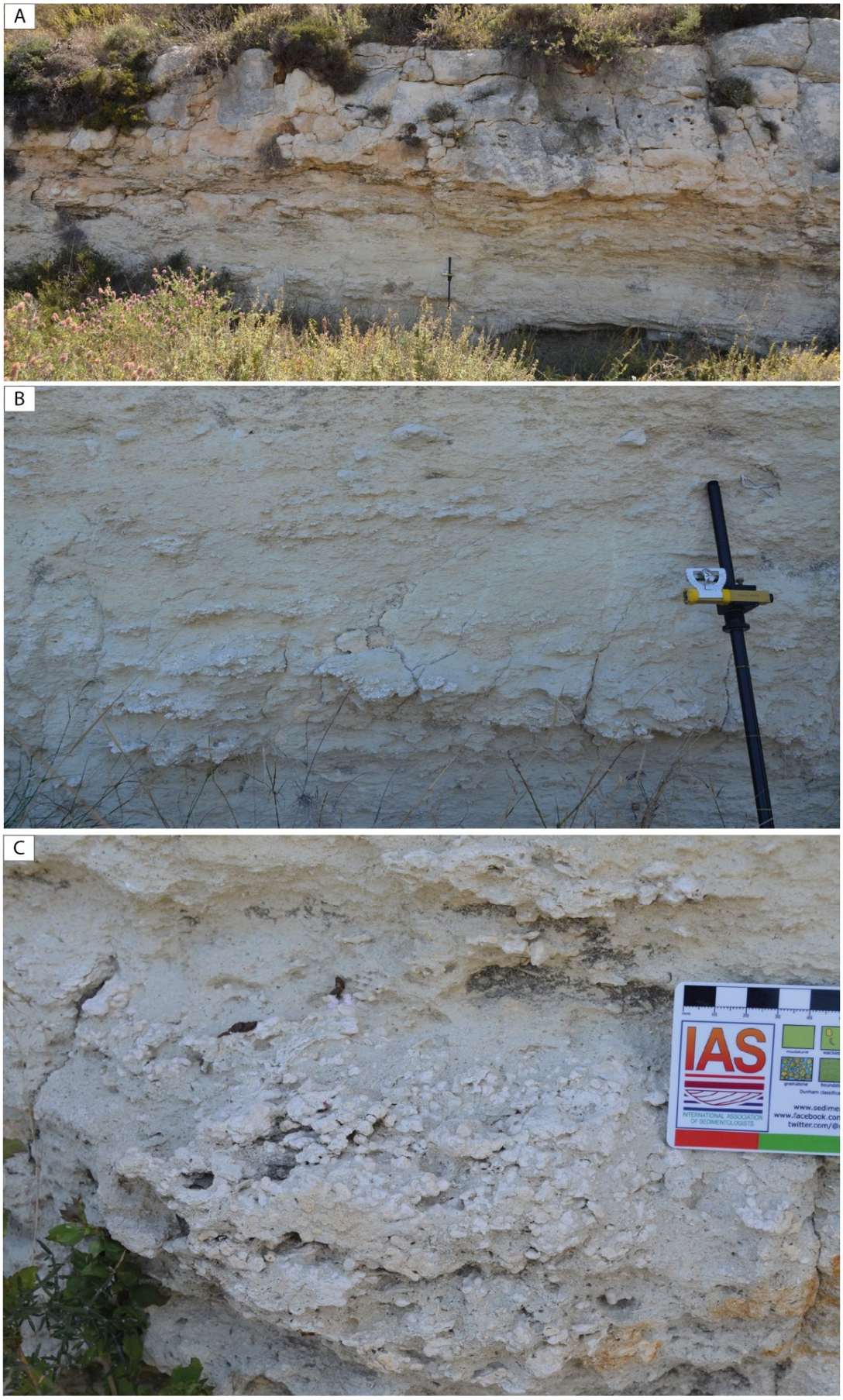

Fig. 5.21. Field aspect of the rhodalgal facies characterizing the Knossos 2 section. (A-B) Marl levels rich in encrusting red algae (red algae rudstone-floatstone); (C) Close-up of a large rhodolith specimen.

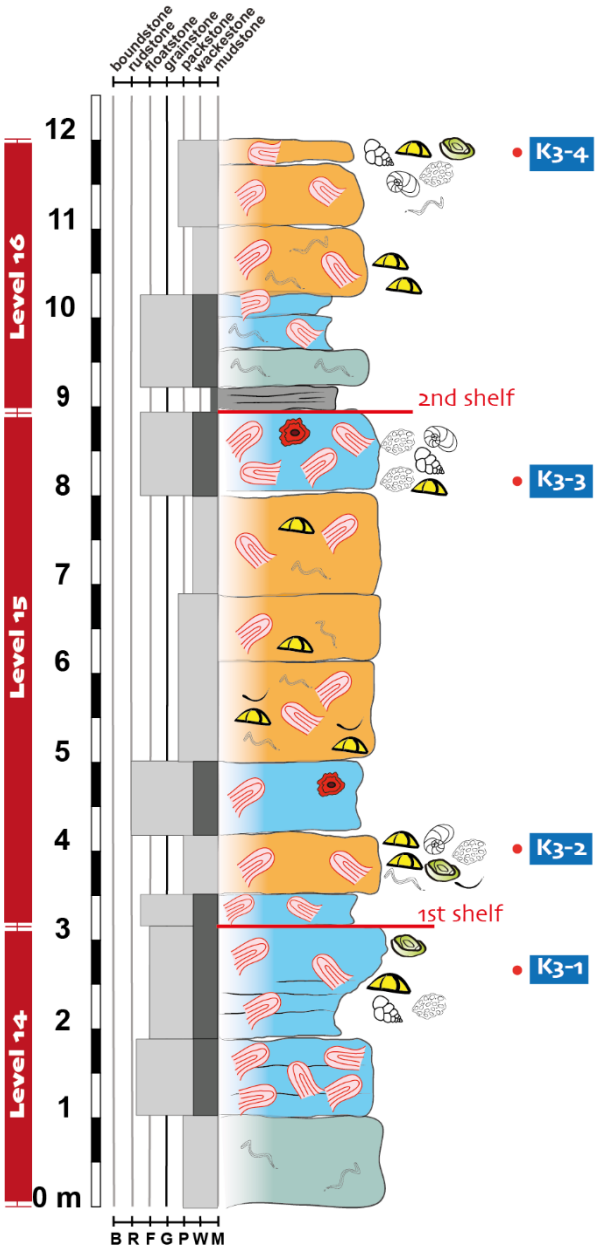

Fig. 5.22. The stratigraphic log of **Knossos section 3** featuring sample locations, textures, and facies. For facies legend see Fig. 5.18

The Knossos section 3

This section (Knossos section 3 – Figs. 5.16; 5.22), measuring 12 meters in thickness and is positioned in an intermediate area between section 1 and 2. It includes the thick banks representing levels 14, 15, and 16. Level 14 exhibits a greater thickness here compared to what was measured in section 2. The base is characterized by a 1-meter-thick layer rich in packstone with serpulids. A distinct contact separates this facies from two additional levels of 2 meters, dominated by coralline algae with predominantly floatstone textures. The top of this bank is marked by a well-defined sharp surface.

This surface separates it from level 15, which is amalgamated in this location and reaches a thickness of 6 meters (while in section 2, it is fragmented into sub-levels 15A and 15B, although the total thickness remains the same). Here too, the dominant facies are floatstone and packstone, but they display a higher content of red algae compared to serpulids.

A well-defined surface characterized by gray marls separates Level 16, which consists of a single bank with a thickness equal to that measured in Section 2, exhibiting the same facies.

The Minosse quarry section

The Minosse quarry stratigraphic section (35° 17’ 32.75” N, 25° 10’ 12.61” E) reaches a thickness of approximately 72 meters and is characterized by red algae facies, barnacle and vermetid facies, and *Halimeda* facies (Figs. 5.16, 5.23, 5.24). A total of 10 samples were collected.

Fig. 5.23. Location of the two ancient quarries (Minosse and Nikita).

The section begins with decimetric levels of bioclastic calcarenite, predominantly composed of fragments of various organisms, including serpulids, bivalves, some barnacles, bryozoans, and echinoids (Fig. 5.26B). From 2.5 meters onwards, the first red algae facies appear, with textures ranging from packstone to floatstone, containing abundant rhodoliths (Fig. 5.26A). These facies are interspersed with levels of red algae packstone and packstone with serpulids and bivalves, featuring coarse packstone matrices.

Further up the section, at 13 meters, the first barnacle facies appear, alternating with metric levels of vegetative cover and facies with serpulids and red algae. Their abundance increases significantly between 21.5 and 25 meters, with rudstone textures associated with vermetids. From this point to 30.5 meters, the section is characterized by poorly exposed levels of packstone-wackestone with vermetids, brecciated levels, and marly layers.

From 30.5 meters, the first decimetric *Halimeda* levels appear, characterized by floatstone to rudstone textures, with a wackestone matrix (Fig. 5.24). The *Halimeda* segments are often well-preserved (Fig. 5.27). These levels are not continuous, as they are often interrupted by vegetative cover or intercalated with floatstone-rudstone layers containing vermetids. This alternation persists up to the top of the section at 72 meters.

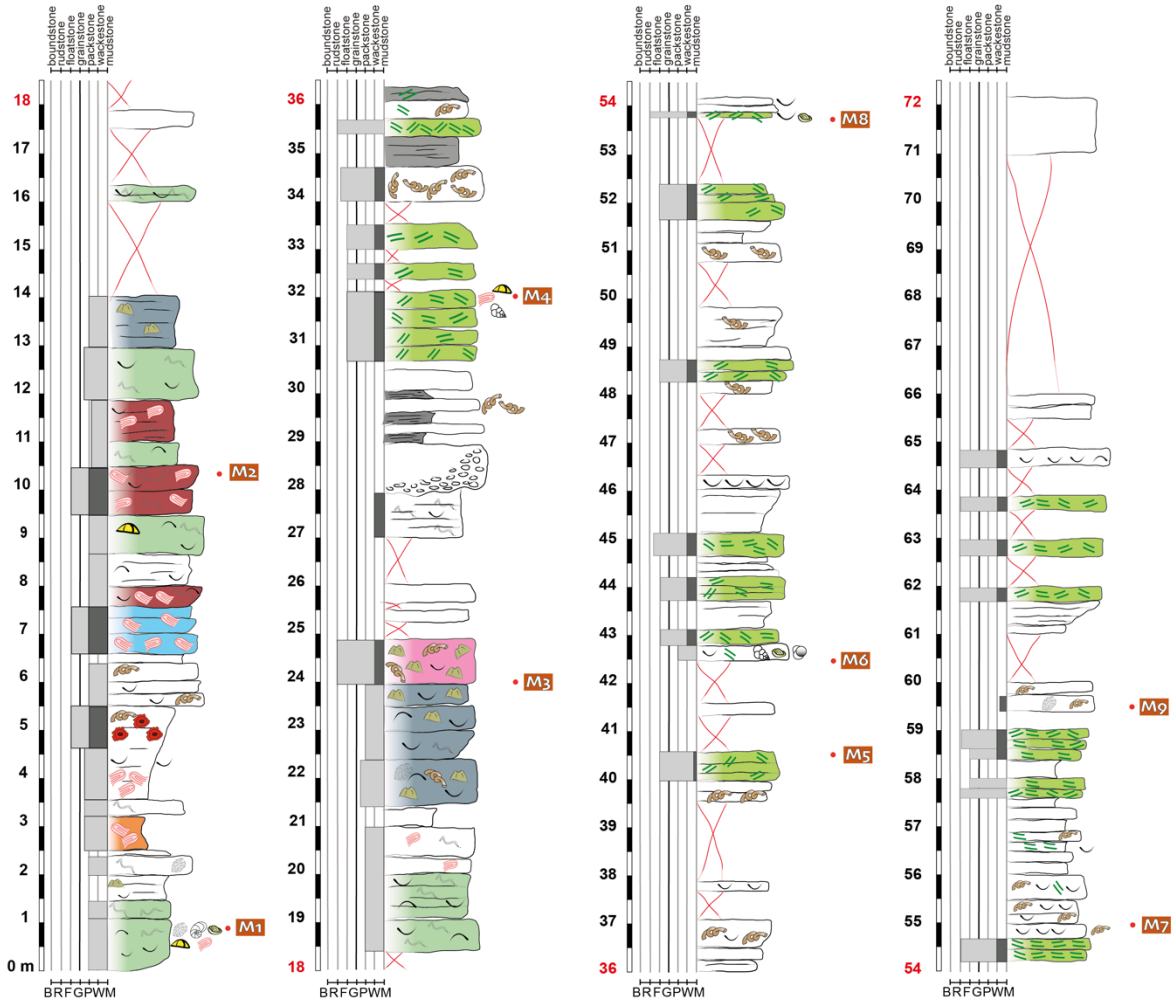

Fig. 5.24. Stratigraphic log of the "Minosse" section featuring sample locations, textures, and facies. For facies legend see Fig. 5.18.

Fig. 5.25. Overview of the ancient "Minosse" quarry, featuring *Halimeda*-rich levels. In the image, inclined geometries can be clearly distinguished, characteristic of a mound structure.

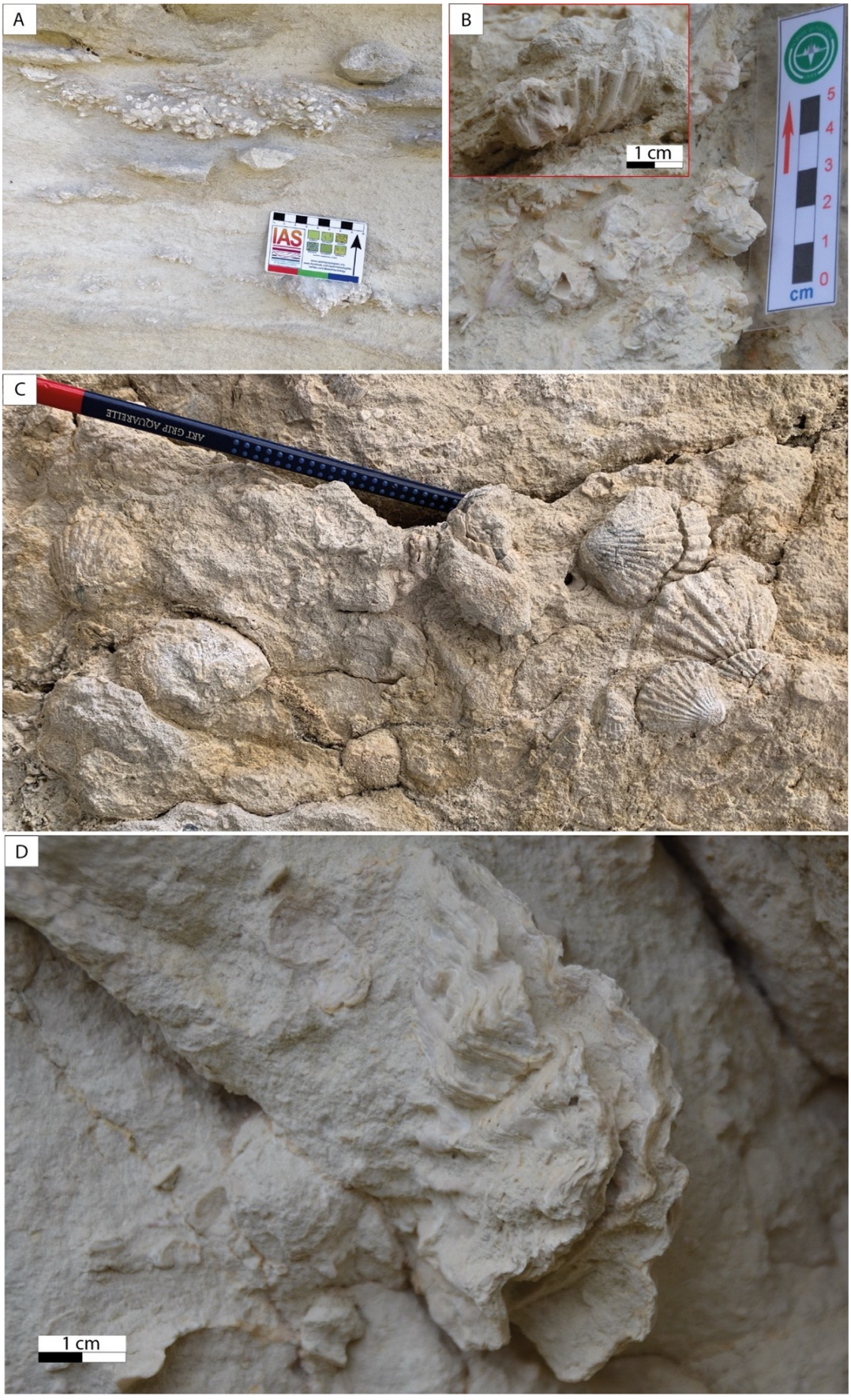

Fig. 5.26. Field aspect of the facies of the "Minosse" section. A) Encrusting red algae floatstone; B) Close up to the balanid rudstone-floatstone, with balanids encrusting a bivalve shell; C) Bivalve rudstone featuring small bivalves; D) Close-up of the large oysters.

Fig. 5.27. Field aspect of the *Halimeda* layers with rudstone textures characterizing the “Minosse” quarry (Fig. 5.20) within the corresponding section.

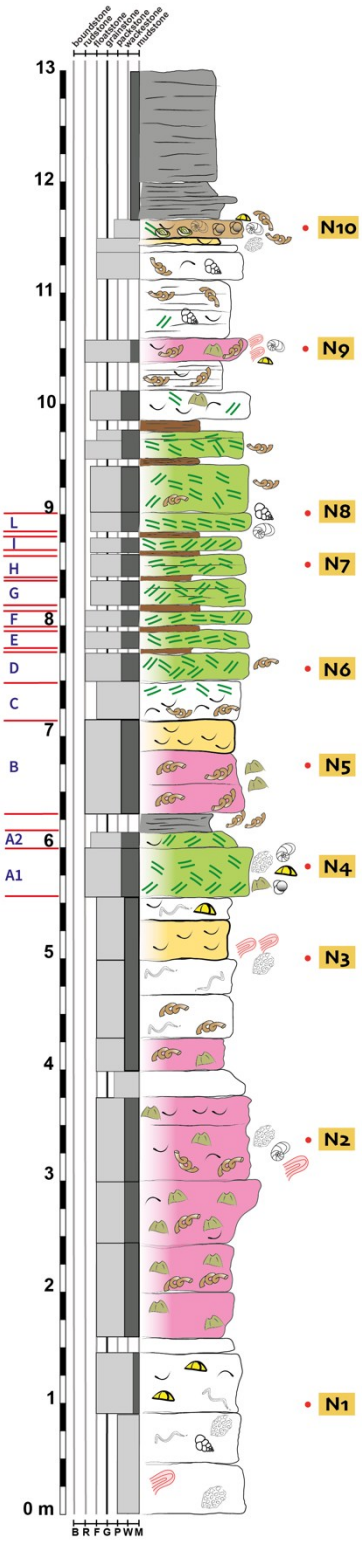

Fig. 5.28. Stratigraphic log of the Nikita section measured in an ancient quarry. This log features textures, facies, and sample location and is located in the southernmost portion of the Knossos outcrop. See Fig. 5.18 for facies legend.

The Nikita section

The Nikita stratigraphic section was measured within an abandoned quarry (35° 171 15.84" N, 25° 10' 07.25" E) and reaches a thickness of approximately 13 meters (Figs. 5.23, 5.28). This section corresponds to the more distal part of the ramp systems that is visible along the whole outcrop (see Fig. 5.16). The section is characterized by the presence of yellowish bioclastic calcarenite. Similar to the Minosse section, it begins with a metric level of packstone that transitions into floatstone upwards, containing echinoids, bivalves, fragments of coralline algae, bryozoans, and serpulids, with a fine wackestone matrix.

From 1.5 meters onward, levels rich in barnacle and vermetid facies appear, with floatstone textures and a coarse wackestone matrix. These levels are interrupted at 5 meters by an interval characterized by an accumulation of bivalve shells. Starting from 5.5 meters, the first *Halimeda* levels appear. The segments are immediately arranged in rudstone textures within a coarse wackestone matrix. Alongside the algal segments, there are fragments of barnacles, echinoids, bryozoans, epiphytic foraminifera, and some planktonic foraminifera. This level transitions into floatstone upwards.

A centimeter-thick marly layer separates this *Halimeda* facies from the reappearance of rudstone levels with barnacles and vermetids, up to 6.80 meters, where another small accumulation of bivalve shells is found. From approximately 7.5 meters to 9.8 meters, decimetric levels of *Halimeda* rudstone with a coarse wackestone matrix alternate, transitioning to floatstone upwards. These levels are interspersed with intervals of clay layers (Fig 5.29).

Starting at 9.8 meters, rudstone and floatstone layers with barnacles and vermetids reappear (Fig. 5.30), containing sparse *Halimeda* segments, bivalve shells, and textulariids.

At 11.5 meters, a thin packstone layer is observed, dominated by foraminifera, including alveolinids, miliolids, epiphytes, along with minor echinoid fragments, vermetids, bryozoans, *Halimeda*, and bivalves. Above this interval, marly layers persist up to the top of the section.

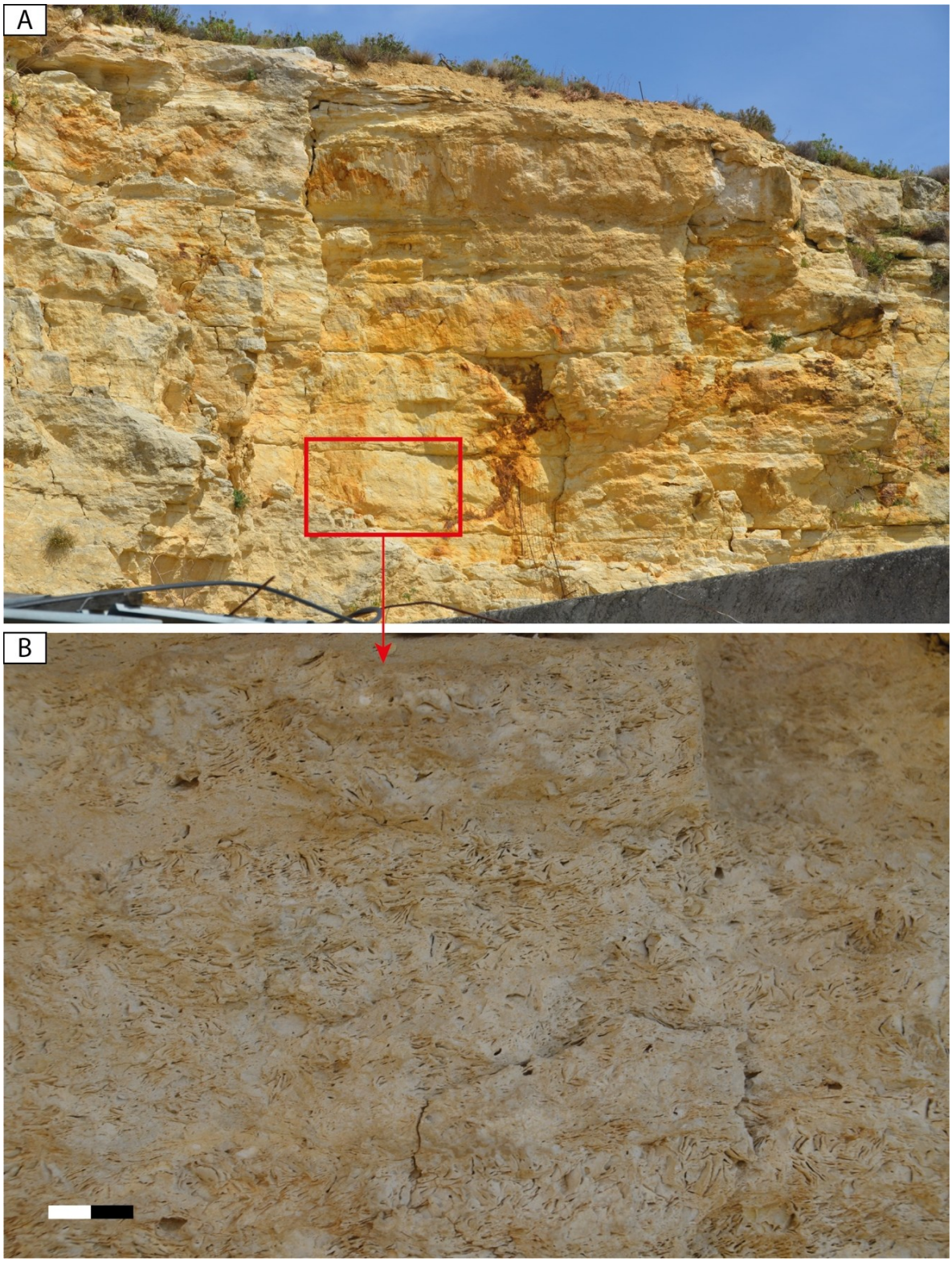

Fig. 5.29. The Nikita Quarry. (A) The *Halimeda*-rich beds characterizing the Nikita Quarry, distinguished by their striking ochre color. (B) Close-up view of the *Halimeda* rudstone-floatstone facies that define these beds.

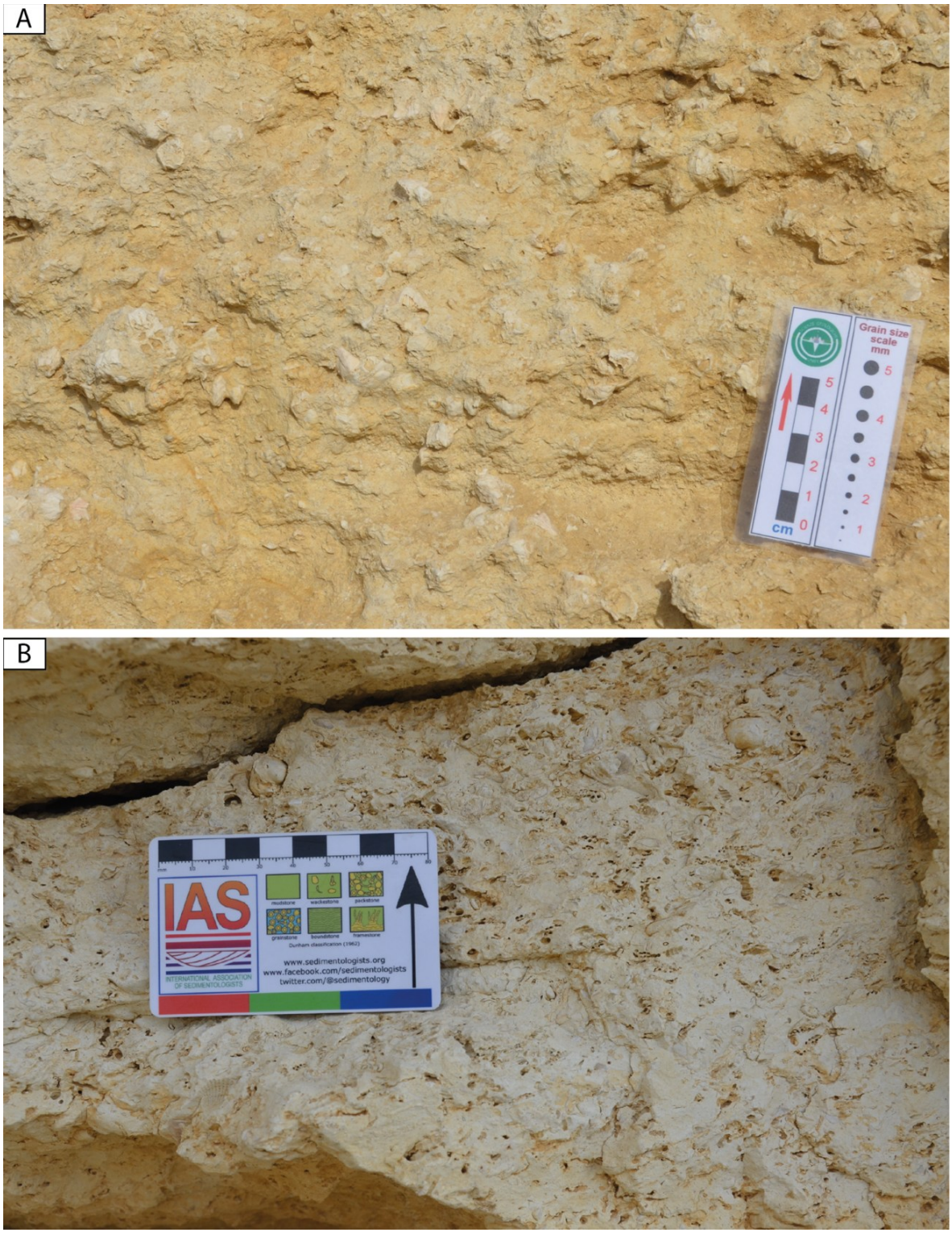

Fig. 5.30. The balanid-vermetid floatstone facies observed in the Nikita Quarry. (A) Close-up view of barnacles (balanids); (B) Close-up view of vermetids.

5.2 Discussions

5.2.1 Depositional Environment and Facies Distribution

The outcrop in front of the Knossos Palace represents an exceptionally well-preserved example of a distally steepened carbonate ramp (Fig. 5.31), with depositional geometries comparable to those documented in the Tortonian throughout the Mediterranean, particularly in Menorca (Esteban, 1979; Esteban et al., 1996; Mateu-Vicens et al., 2008). Distally steepened ramps tend to evolve under fluctuating sea levels, resulting from a combination of moderate-amplitude, high-frequency changes (Tella et al., 2022).

The continous exposure at the site has enabled detailed observations of lateral and vertical facies variability, allowing for a comprehensive reconstruction of the architecture of this ramp system. The first three measured sections (Knossos 1, Knossos 2, and Knossos 3) are characterized by rudstone-floatstone banks with coralline algae and rhodoliths, alternating with rudstone-floatstone facies rich in serpulids. Significant terrigenous input is evident throughout these sections, influencing depositional conditions (Figs. 5.18, 5.20, 5.22).

The Knossos outcrop exhibits a strongly prograding system with clinoforms, where occurrences of *Halimeda* bioherms are documented in two distinct stratigraphic positions. Specifically:

- A distal and stratigraphically highest bioherm occurs in the Minosse quarry.
- A slightly more proximal setting in the Nikita quarry, where *Halimeda* accumulations appear as extensive beds (Fig. 5.31).

The depositional environment is interpreted as a mid-ramp system. Given the lack of biostratigraphic data and the fact that *Halimeda* in the Mediterranean is typically confined to pre-evaporitic Messinian successions, we infer that the distal portion of the Knossos ramp represents the lower Messinian interval. However, further development of these accumulations was likely hindered by strong siliciclastic input, which affected all Knossos sections. These *Halimeda* accumulations may represent a mesophotic environment with limited light and some turbidity.

In the Minosse section, *Halimeda* accumulations exhibit mound-shaped geometries, suggesting in situ development (Fig. 5.25). In contrast, in the Nikita section, *Halimeda* occurs as well-defined beds (Fig. 5.29A), suggesting a moderate transport toward basin through gravity flow processes.

Furthermore, the new survey conducted as part of this study (Souvlaki, Minosse and Nikita stratigraphic sections) has shown that *Halimeda*-rich beds are much more widespread than mound-shaped bioherms, such as the one documented at Moni Gorgolaini (Figs. 5.7, 5.8). These *Halimeda*-rich beds are typically extensive and thick, often associated with significant terrigenous input. This contrast underscores the greater prevalence of *Halimeda*-rich beds compared to the less frequent mound-shaped bioherms, reflecting different depositional conditions across the basin. The reasons of these different occurrences have not yet fully investigated. However, Braga et al. (1996) attributed the limited lateral development of the *Halimeda* bioherms at Heuli (Spain) to the type of substrate or to an excess of terrigenous sediments. In this study, we argue that terrigenous input, providing greater nutrient availability, is the predominant factor influencing the development and extent of *Halimeda* bioherms in the Heraklion Basin, as well as in the Sorbas and Níjar-Carboneras Basins.

The outcrop in front of the Knossos Palace, representing an example of a distally steepened ramp (Fig. 5.31), stands out due to its impressive size and spectacular depositional geometries (Fig. 5.17) and comparable to the more well-known ones documented in the Tortonian throughout the Mediterranean especially in Menorca island as a result of high rates of sediment production and accumulation, distally, in the oligophotic zone (Esteban, 1979; Esteban et al., 1996; Mateu-Vicens et al., 2008). The distally steepened ramp tended to evolve during sea level fluctuations resulting in a combination of moderate amplitude and high frequency sea-level fluctuations (Tella et al., 2022).

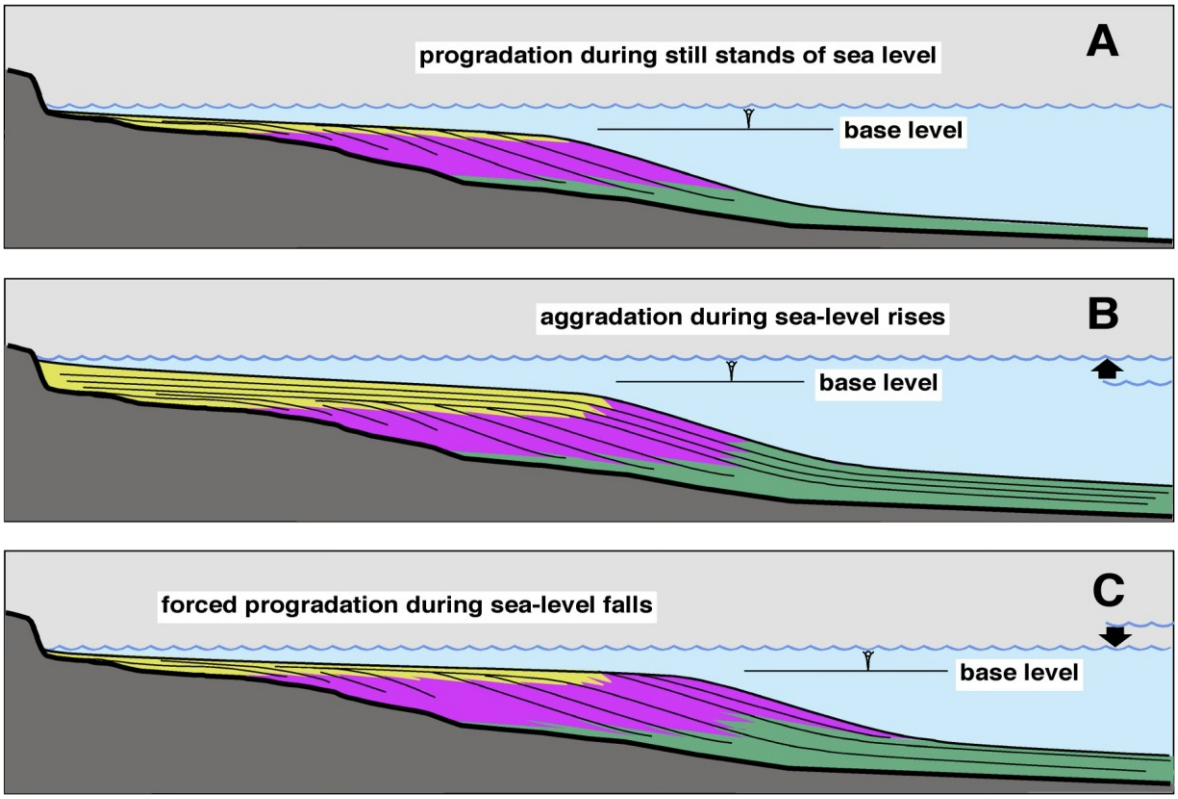

Fig. 5.31. Example of accretional processes in the lower Tortonian distally steepened ramp. (A) Progradation occurred during sea-level stillstands due to the basinward transport of sediment derived from the inner and middle ramp settings, primarily composed of loose grains from foramol-rhodalgal associations. (B) During sea-level rises, aggradation took place in response to the elevation of the base level. (C) High-frequency sea-level falls enhanced progradation through a basinward shift of carbonate production areas, increased erosion, and intensified sediment transport toward the basin, driven by the lowering of the base level (modified after Pomar, 2001).

Coupled with the sparse vegetation cover, this has enabled to measure and observe the facies variability in detail, allowing for a thorough understanding of the history of this ramp depositional system. The first three measured sections (Knossos 1, Knossos 2, and Knossos 3) at the Knossos outcrop are characterized by banks of rudstone-floatstone with coralline algae and rhodoliths, alternating with rudstone-floatstone facies rich in serpulids. As shown in the logs (Figs. 5.18, 5.20, 5.22), a significant terrigenous input is evident in these sections, affecting the whole depositional system.

The Knossos outcrop represents a strongly prograding system characterized by clinoforms, in which occurrences of *Halimeda* bioherms have been documented in two distinct stratigraphic positions. Specifically, an *Halimeda* bioherm is found in the distal and stratigraphically highest part of the succession, referred as Minosse quarry while in the slightly more proximal part referred as Nikita quarry, *Halimeda* occurr as beds (Fig. 5.23).

Based on the lithofacies present in these zones, the depositional environment can be attributed to a mid-ramp system. Due to the lack of biostratigraphic data and considering

that the presence of *Halimeda* in the Mediterranean is only documented in pre-evaporitic Messinian successions, as well as the higher stratigraphic position of *Halimeda* relative to the entire ramp system, we can infer that the distal part of the system represents the lower Messinian interval, which does not further develop due to strong siliciclastic inputs, documented in all Knossos sections. These *Halimeda* accumulations may therefore reflect a mesophotic environment with limited light and some turbidity.

Furthermore, from Fig. 5.25, it is clear that the interval containing *Halimeda*-rich levels in the Minosse section is characterized by mound-shaped geometries, and the occurrences of several lenses of boundstone suggests that these accumulations are in situ. As for the rich beds in Nikita, being composed of well-defined beds (Fig. 5.29A).

5.2.1 Influence of Terrigenous Input and Nutrient Supply

The structural context of the Heraklion Basin influenced nutrient supply, which is a key factor in the size, persistence, and spatial distribution of both fossil and modern *Halimeda* bioherms (Wolanski et al., 1988; McNeil et al., 2021). In the Heraklion Basin, *Halimeda* accumulations developed within a mixed ramp system, influenced by terrigenous input from the eroding flanks of the Heraklion graben (Fig. 5.32). The Psiloritis and Lasithi Mountains supplied significant siliciclastic material through erosion and runoff, which in turn enriched the water column with nutrients.

Unlike the *Halimeda* bioherms of the Salento Peninsula (Bosellini et al., 1999), which formed in predominantly carbonate-dominated environments with upwelling-driven nutrient input (Passaseo and Morsilli, 2025), those in the Heraklion Basin appear closely linked to the terrestrial nutrient supply—similar to the Sorbas and Níjar-Carboneras Basins in southeastern Spain.

This process, where riverine discharge and terrestrial runoff act as primary nutrient sources, has been documented in modern systems such as the Great Barrier Reef (Furnas, 2003; Furnas et al., 2011). However, in those cases, fluvial input was less significant due to greater distances between bioherms and terrigenous sources (McNeil et al., 2021). In contrast, the close proximity of the Heraklion Basin's uplifted margins to the depositional environments likely provided a sustained and direct nutrient influx for *Halimeda* growth.

Furthermore, unlike the Salento Peninsula, where phosphoritic hardgrounds confirm the action of upwelling currents during the Tortonian (Föllmi et al., 2015), no phosphoritic

layers have been identified in the Heraklion Basin. This suggests that local siliciclastic input, rather than upwelling, was the dominant nutrient source for *Halimeda* bioherms in this setting.

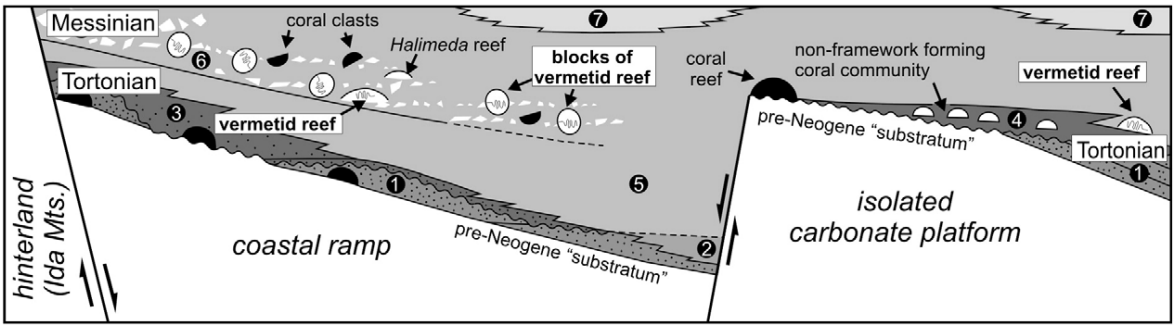

Fig. 5.32. Upper Miocene stratigraphy of central Crete includes: 1) sandstone and conglomerate deposits interfingering with coral reefs, forming coastal sediment wedges; 2) mudstone representing deeper basin environments; 3) sandy skeletal limestone associated with coastal sediment wedges; 4) skeletal limestone corresponding to an isolated carbonate platform; 5) calcareous mudstone indicative of deeper basin settings; 6) calcareous mudstone interbedded with debrites and calciturbidites, interpreted as a submarine debris cone; 7) gypsum deposits (from Vescogni et al., 2008).

5.2.2 Early Diagenesis and Cementation of *Halimeda* Bioherms

As observed in other Mediterranean *Halimeda* accumulations, early marine cementation played a crucial role in preserving bioherms in the Heraklion Basin. At Moni Gorgolaini, the isolated *Halimeda* mound is predominantly composed of rudstone-floatstone textures with a fine packstone-to-wackestone matrix. However, localized centimeter-scale boundstone lenses preserve *Halimeda* segments in near-vertical orientation, indicating in situ growth.

In these areas, botryoidal aragonitic cements occur around *Halimeda* segments, acting as an impermeable barrier against dissolution (Figs. 5.11, 5.33). These cements, described in detail by Brachert et al. (2007), are interpreted as syn-depositional, forming under early marine diagenetic conditions.

During the Messinian, the Mediterranean began experiencing early salinity crisis effects, leading to restricted water exchange and hypersaline conditions (Vertino et al., 2014; Moissette et al., 2018; Vasiliev et al., 2019; Vescogni et al., 2022; Agiadi et al., 2024a; 2024b). The presence of syn-depositional aragonitic cements suggests that the geochemical conditions of the early MSC promoted marine cementation, enhancing the preservation potential of *Halimeda* bioherms in the Heraklion Basin.

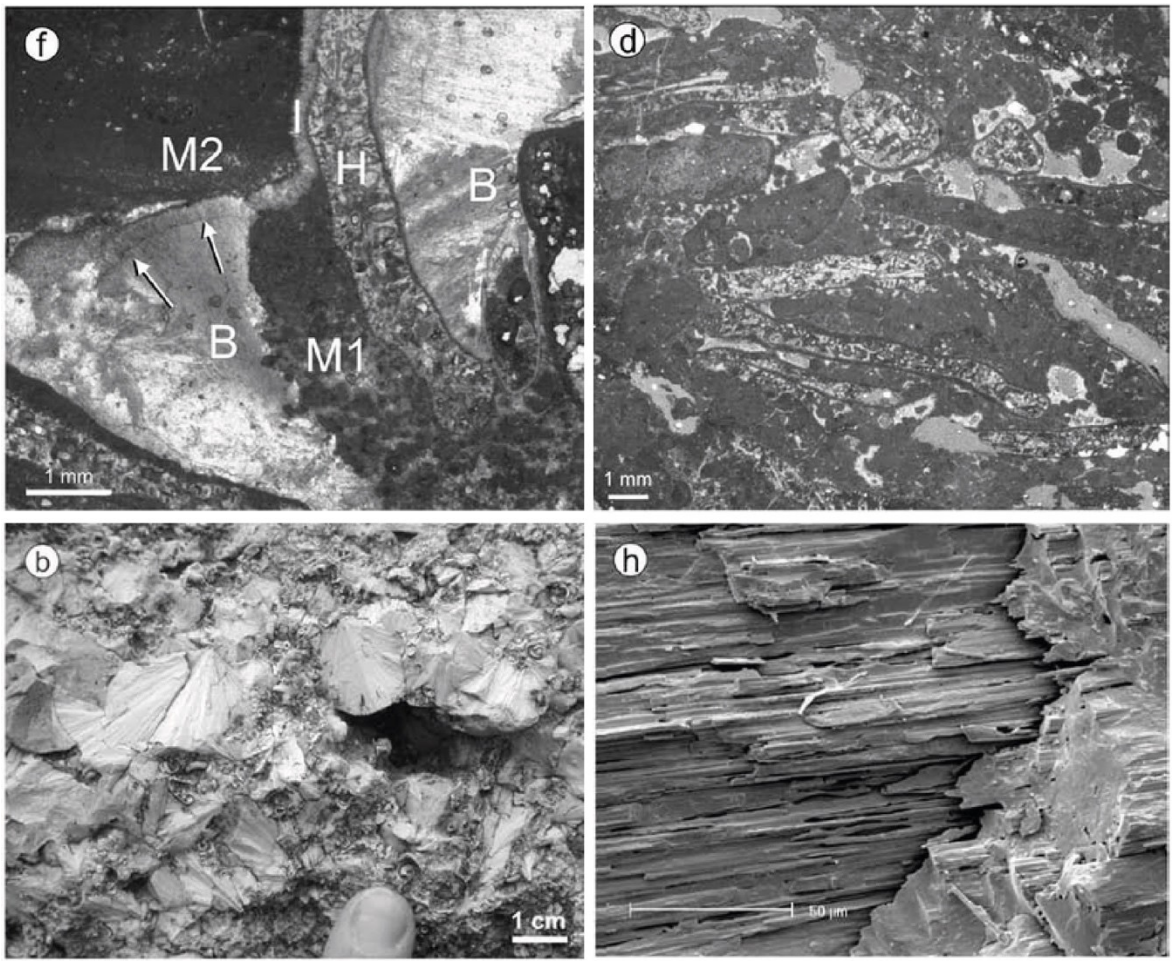

Fig. 5.33. The botryoidal aragonitic cements in the *Halimeda* bioherm at Moni Gorgolaini - Varvara Formation. f) Thin-section micrograph of HB. *Halimeda* segment (H) covered by botryoidal (B) and isopachous (I) linings of fibrous cement and peloidal micrite (M1). Isopachous linings have a cover of micrite (M2). Arrows denote "dust line" of peloids incorporated into botryoid; d) Thin section micrographs showing well-preserved *Halimeda* segments; b) Field aspect of early diagenetic aragonite cements; h) SEM photographs of sections of aragonite fibres showing well-developed crystal faces and longitudinal grooves. Minor dissolution may be inferred from rounded grooves in H. (Brachert et al., 2007).

5.3 Conclusions

The results of this study significantly expand our understanding of the distribution and depositional significance of *Halimeda*-rich deposits in the pre-evaporitic Messinian successions of Crete. Previous research had documented only two primary occurrences of *Halimeda* accumulations on the island, at Faneromeni and Moni Gorgolaini. However, new field investigations and stratigraphic analyses reveal that *Halimeda*-rich deposits are far more extensive than previously recognized, occurring in multiple locations within the Heraklion Basin, including the Souvlaki, Minosse, and Nikita sections. This broader distribution suggests that *Halimeda* played a more prominent role as carbonate producer in this basin than previously thought.

A key finding of this study is the distinction between two primary modes of *Halimeda* deposition: mound-shaped bioherms, such as those observed at Moni Gorgolaini and the Minosse quarry, and more extensive *Halimeda*-rich beds, such as those documented in the Nikita quarry and Souvlaki section area. The latter are well bedded and typically associated with significant terrigenous input, indicating that variations in depositional environments and sediment supply were critical in shaping the development and spatial distribution of these deposits. The interplay between carbonate production and siliciclastic influx appears to have been a major control on bioherm morphology and development, a pattern also observed in other Mediterranean basins, such as the Sorbas and Níjar-Carboneras Basins in Spain.

The structural setting of the Heraklion Basin played a fundamental role in the development of *Halimeda* accumulations. The presence of high-relief topographic features, such as the Psiloritis and Lasithi Mountains, provided a significant source of terrestrial runoff and nutrient supply. This contrasts with other Messinian *Halimeda* bioherms, such as those in the Salento Peninsula, which developed in a predominantly carbonate environment with limited terrigenous influence. The nutrient availability from run off input likely enhanced *Halimeda* productivity, facilitating bioherm formation despite potential challenges posed by higher sedimentation rates.

In addition to its implications for the distribution of *Halimeda* accumulations, this study provides new insights into the evolution of depositional systems in the Heraklion Basin during the pre-evaporitic Messinian. The Knossos outcrop, in particular, represents an excellent example of a distally steepened ramp system, characterized by alternating rudstone-floatstone facies with coralline algae and serpulids, extensive clinoform

geometries, and prograding stratigraphic patterns. The presence of *Halimeda* accumulations at different stratigraphic positions within this system suggests a complex interaction between sea-level fluctuations, sediment transport, and nutrient dynamics. High-frequency sea-level changes, as documented in other Mediterranean distally steepened ramps, may have played a role in modulating the development of these carbonate accumulations.

Another key observation from this study is the absence of phosphoritic hardgrounds in the Heraklion Basin successions. This stands in contrast to the Salento Peninsula, where phosphoritic layers (such as the Aturia level) provide clear evidence of upwelling activity during the Tortonian. The lack of similar hardgrounds in the Cretan successions suggests that upwelling or internal wave activity was not a dominant control on nutrient supply in this region. Instead, the primary source of nutrients appears to have been terrestrial runoff, a conclusion supported by the association of *Halimeda*-rich deposits with significant siliciclastic input. This finding further differentiates the Heraklion Basin from other Mediterranean carbonate systems and underscores the importance of local environmental controls in shaping the distribution of *Halimeda* bioherms and related resedimented deposits.

Overall, this study provides a more comprehensive view of the development of *Halimeda* bioherms or rich-beds during the Messinian of Crete, highlighting the need for further research to fully understand the factors controlling their formation and redistribution within the basin. Future investigations should focus on refining the biostratigraphic framework of these deposits, assessing potential diagenetic modifications, and integrating sedimentological, geochemical, and paleoecological approaches. This will help clarify the role of *Halimeda* in Late Miocene carbonate systems and its response to environmental and climatic changes during the Messinian.

6. Final remarks

The study of *Halimeda* bioherms across three distinct Mediterranean regions—the Salento Peninsula in southeastern Italy, the Sorbas and Níjar-Carboneras basins in southeastern Spain, and central Crete Island—provides a comprehensive understanding of the depositional and paleoenvironmental dynamics that shaped these important carbonate-producing organisms during the late Miocene, particularly in the pre-evaporitic Messinian. By examining the internal structure, distribution, and facies of *Halimeda* deposits, this research highlights the complex interplay of factors that controlled their development and persistence, including nutrient supply, hydrodynamic processes, and restricted marine conditions. The integration of the data from these diverse locations not only expands our understanding of *Halimeda* bioherms but also provides valuable insights into the broader context of Mediterranean carbonate systems during this period of significant environmental changes, especially in light of the impending Messinian Salinity Crisis (MSC).

Salento Peninsula: the internal organization and the role of syn-depositional cementation

In the Salento Peninsula, the two observed *Halimeda* bioherms present a well-defined internal organization that allows for a deeper understanding of *Halimeda* bioherm development in mesophotic environments. These bioherms were likely located in areas with reduced light availability, possibly due to their depth. The alternating layers of *Halimeda* segments and rudstone-floatstone facies mirror the internal structure of these modern bioherms, providing important insights into their spatial arrangement and growth dynamics. The preservation of *Halimeda* segments, facilitated by marine syn-depositional cements, played a crucial role in stabilizing the bioherms and preserving their intricate structures. These cements, primarily composed of aragonite, provide valuable insights into fluctuations in salinity within the Mediterranean Basin, particularly during the Messinian.

The development of these bioherms was likely influenced by weak and sporadic nutrient supply events, potentially driven by hydrodynamic mechanisms such as upwelling of nutrient-rich waters and internal waves. Despite the relatively small size of the bioherms in Salento compared to modern analogs, these findings underscore the significant role of *Halimeda* as a carbonate producer, particularly in mesophotic environments where other calcifying organisms are less abundant.

Spain: taphonomy and variability in *Halimeda* deposits

The research conducted in the Sorbas and Í basins in Spain allowed for a comparative analysis of *Halimeda* deposits and associated facies, focusing on taphonomic aspects and sedimentary characteristics. Taphonomic observations of *Halimeda* segments and their associated sedimentary matrices revealed important differences between resedimented and in situ bodies, providing insights into the transport, preservation, and deposition of these organisms. The sedimentary context of these basins was influenced by significant terrigenous input, including clay layers and the presence of siliciclastic sediments, which played a key role in the distribution and preservation of *Halimeda* accumulations. This variability may account for the differences in the development of *Halimeda* mounds and beds within the Almeria region, with factors such as higher inputs of siliciclastic material potentially inhibiting the lateral growth of bioherms.

Despite the absence of direct evidence supporting the role of upwelling currents in the development of *Halimeda* bioherms in Almeria, the nutrient dynamics of the region are believed to be influenced by runoff from the surrounding mountain ranges, which likely provided the necessary nutrients for *Halimeda* growth. The study of *Halimeda* in the Sorbas and Í basins, although preliminary, contributes valuable information about the sedimentary processes and paleoecological conditions in Messinian basins, underscoring the need for further investigations into the role of terrigenous input and other factors in the development of these bioherms. The findings also highlight the importance of understanding the broader geological context, particularly in regions where tectonic processes and volcanic activity may have influenced the sedimentary history and nutrient supply.

Crete island: a complex and dynamic depositional setting

Along with Spain, Crete represents one of the areas with the greatest presence of *Halimeda* bioherms in the Mediterranean, providing significant new insights into the distribution and depositional settings of these organisms in the pre-evaporitic Messinian successions. While previous studies had documented few occurrences of *Halimeda* bioherms or *Halimeda*-rich deposits in isolated sections, this research reveals a much more widespread distribution, particularly within the Heraklion Basin, where new stratigraphic sections—such as Souvlaki, Minosse, and Nikita—demonstrate the presence of *Halimeda* both in mound-shaped bioherms and extensive beds. The new documented widespread occurrence of these deposits suggests a more complex depositional environment, shaped by a combination of factors,

including nutrient availability, water depth, and terrigenous input from the surrounding mountain ranges.

The study of the Knossos outcrop offers further insights into the evolution of *Halimeda* accumulations within a distally steepened ramp depositional system, where varying facies and depositional geometries reflect a prograding system influenced by climatic shifts. The presence of *Halimeda* in the distal, deeper parts of the ramp system suggests that these bioherms thrived in environments characterized by limited light and some turbidity—conditions that were less favorable for other carbonate-producing organisms. This mesophotic environment, dominated by *Halimeda*, illustrates the organism's adaptability and its ability to persist in conditions that were suboptimal for other reef-building organisms.

The presence of terrigenous material, including clay and silt, within the *Halimeda*-rich beds provides evidence of the dynamic interaction between marine and terrestrial processes in shaping the Mediterranean carbonate factory. In contrast to the Salento Peninsula, where upwelling currents may have played a larger role, Crete's proximity to mountainous regions likely influenced the nutrient dynamics, facilitating the development of *Halimeda* in a range of depositional settings, from deeper, mesophotic environments to shallower, more nutrient-rich zones.

Moreover, early diagenetic processes, including the aragonitic cementation of *Halimeda* segments, played a crucial role in preserving the bioherms and stabilizing the deposits. This cementation, which occurred *in situ*, is indicative of favorable geochemical conditions during the Messinian, a period marked by significant environmental stress due to the onset of the Mediterranean Salinity Crisis (MSC). The cementation processes observed in Crete, as well as in Spain and the Salento Peninsula, suggest that *Halimeda* bioherms were able to withstand environmental fluctuations, preserving their structure and contributing to the carbonate budget of the region.

Shaping Our Understanding of *Halimeda* Bioherms in the Mediterranean

The comparative study of *Halimeda* bioherms and deposits from the Salento Peninsula, Spain, and Crete offers crucial insights into the paleoenvironmental conditions that shaped the development of these remarkable carbonate-producing organisms during the Messinian in the Mediterranean region. The analysis highlights the importance of nutrient dynamics, early diagenetic processes, and tectonic settings in controlling the distribution and preservation of *Halimeda* deposits across the Mediterranean region. Although the factors

influencing *Halimeda* growth varied between regions, the widespread presence of these bioherms, particularly in Spain and Crete underscores their significance as key components of the Mediterranean carbonate factory.

Moreover, this research contributes to the broader understanding of the response of marine ecosystems to climatic and environmental stress during the Messinian, particularly in the context of the onset of the Mediterranean Salinity Crisis. The findings suggest that *Halimeda* bioherms were not only resilient to environmental changes but also played a crucial role in maintaining carbonate production in a variety of depositional settings. As modern climate change continues to affect marine ecosystems, the role of *Halimeda* bioherms in CO_2 sequestration and becomes increasingly important. The lessons learned from these ancient bioherms will inform future studies of modern coral reefs and carbonate ecosystems, helping to improve our understanding of how marine organisms will adapt to the challenges posed by global warming.

The lessons learned from these ancient bioherms will inform future studies of modern coral reefs and carbonate ecosystems, helping to improve our understanding of how marine organisms will adapt to the challenges posed by global warming.

In conclusion, the study of *Halimeda* bioherms in the Mediterranean offers a window into the past, revealing the intricate interactions between marine organisms, sedimentary processes, and environmental conditions. This research provides a comprehensive understanding of the paleoecology of *Halimeda* and its role in shaping the Mediterranean carbonate systems during the Messinian. As the important contribution of *Halimeda* in the production of $CaCO_2$ sediments, future investigations into the factors that controlled *Halimeda* development will be essential for improving our understanding of past and present climate variability and its impact on marine ecosystems.

References

Agiadi, K., Hohmann, N., Gliozzi, E., Thivaiou, D., Bosellini, F.R., Taviani, M., Bianucci, G., Collareta, A., Londeix, L., Faranda, C., Bulian, F., Koskeridou, E., Lozar, F., Mancini, A.M., Dominici, S., Moissette, P., Campos, I.B., Borghi, E., Iliopoulos, G., Antonarakou, A., Kontakiotis, G., Besiou, E., Zarkogiannis, S.D., Harzhauser, M., Sierro, F.J., Coll, M., Vasiliev, I., Camerlenghi, A., García-Castellanos, D., 2024. The marine biodiversity impact of the Late Miocene Mediterranean salinity crisis. Science 385, 986–991.

Agiadi, K., Hohmann, N., Gliozzi, E., Thivaiou, D., Bosellini, F.R., Taviani, M., Bianucci, G., Collareta, A., Londeix, L., Faranda, C., Bulian, F., Koskeridou, E., Lozar, F., Mancini, A.M., Dominici, S., Moissette, P., Campos, I.B., Borghi, E., Iliopoulos, G., Antonarakou, A., Kontakiotis, G., Besiou, E., Zarkogiannis, S.D., Harzhauser, M., Sierro, F.J., Coll, M., Vasiliev, I., Camerlenghi, A., García-Castellanos, D., 2024. Late Miocene transformation of Mediterranean Sea biodiversity. Sci. Adv. 10, 1–12.

Aguirre, J., 1998. El Plioceno del SE de la Península Ibérica (provincia de Almería). Síntesis estratigráfica, sedimentaria, bioestratigráfica y paleogeográfica. Rev. Soc. Geol. Espana 11, 297-315.

Angelier, J., 1975. Sur les plates-formes marines Quaternaires et leurs deforamtions: les rivages meridionaux de la Crete orientale (Grece), C. R. Acad. Sci. Paris, 281, 1149–1152.

Argnani A., Ricci Lucchi F., 2001. Tertiary silicoclastic turbidite systems of the Northern Apennines. In: Vai G.B., Martini I.P. (Eds.), Anatomy of an Orogen: the Apennines and Adjacent Mediterranean Basins. Kluwer Academic Publishers, 327- 350.

Augier, R., Jolivet, L., Robin, C., 2005. Late orogenic doming in the eastern Betic Cordilleras: final exhumation of the Nevado–Filabride complex and its relation to basin genesis. Tectonics 24, TC4003.

Bassoullet, J.P., Bernier, P., Genot, P., Poncet, J., Roux, A., 1983. Les algues Udoteacées du Paléeozoique au Cénozoique. Bull. Cent. Rech. Explor. Prod. Elf-Aquitaine 7, 449-621.

Bendinger A., Cravatte S., Gourdeau L., Brodeau L., Albert A., Tchilibou M., Lyard F., Vic C., 2023. Regional modeling of internal-tide dynamics around New Caledonia-Part 1: Coherent internal-tide characteristics and sea surface height signature. Ocean Sci. 19,

1315–1338.

Bernoulli, D., 2001. Mesozoic–tertiary carbonate platforms, slopes and basins ofthe external Apennines and Sicily. In: Vai, G.B., Martini, I.P. (Eds.), Anatomy of an Orogen: the Apennines and adjacent Mediterranean basins. Kluwer Acad. Publishers 307–325.

Betzler, C., Brachert, T.C., Nebelsick, J., 1997. The warm temperate carbonate province. A review of the facies, zonations, and delimitations. Cour. Forsch.—Inst. Senckenberg 201, 83–99.

Billi, A., Gambini, R., Nicolai, C., Storti, F., 2007. Neogene-Quaternary intraforeland transpression along a Mesozoic platform-basin margin: The Gargano fault system, Adria, Italy. Geosphere, 3, 1–15.

Blakeway, D., Hamblin, M.G., 2015. Self-generated morphology in lagoon reefs. PeerJ, 3, e935.

Boegman, L., Stastna, M., 2019. Sediment Resuspension and Transport by Internal Solitary Waves. Annu. Rev. Fluid. Mech. 51, 129–154.

Bonneau, M., 1984. Correlation of the Hellenides nappes in the south-east Aegean and their tectonic reconstruction. Geol. Soc. London (Sp. publ) 17, 517-527.

Bortone, U., De Santis, V., Margiotta, S., Reina, A., Spalluto, L., Cartografico, O., Stato, D., 2013. NOTE ILLUSTRATIVE della CARTA GEOLOGICA D'ITALIA alla scala 1:50.000 CAPO SANTA MARIA DI LÈUCA a cura di Ricchetti, G., Ciaranfi N., (aree marine) con la collaborazione di: SERVIZIO GEOLOGICO D'ITALIA.

Bosellini, A., Bosellini, F.R., Colalongo, M.L., Parente, M., Russo, A., Vescogni, A., 1999. Stratigraphic architecture of the salento coast from capo d'otranto to S. Maria Di Leuca (Apulia, Southern Italy). Riv. Ital. di Paleontol. e Stratigr. 105, 397–416.

Bosellini, F.R., 2006. Biotic changes and their control on Oligocene-Miocene reefs: A case study from the Apulia Platform margin (southern Italy). Palaeogeogr. Palaeoclimatol. Palaeoecol. 241, 393–409.

Bosellini, F.R., Russo, A., 1992. Stratigraphy and facies of an oligocene fringing reef (Castro Limestone, Salento Peninsula, Southern Italy). Facies 26, 145–165.

Bosellini, F.R., Russo, A., Vescogni, A., 2001. Messinian reef-building assemblages of the Salento Peninsula (southern Italy): Palaeobathymetric and palaeoclimatic significance. Palaeogeogr. Palaeoclimatol. Palaeoecol. 175, 7–26.

Bosellini, F.R., Russo, A., Vescogni, A., 2002. The Messinian reef complex of the Salento Peninsula (southern Italy): Stratigraphy, facies and Paleoenvironmental interpretation. Facies 47, 91–112.

Bossio, A., Guelfi, F., Mazzei, R., Monteforti, B., Salvatorini, G., 1989. Studi sul Neogene e Quaternario della Penisola Salentina. III— Stratigrafia del Pozzo Poggiardo (N. 54, PS 1490/3). Atti Conv. Conosc. Geol. Territ. Sal., Lecce 1987—Quad Centro Studi Geo- tecn D'Ing 11, 55-88.

Bossio, A., Mazzei, R., Monteforti, B., Salvatorini, G., 1994. La successione miocenica nell'area tipo delle Calcareniti di Andrano (Puglia, Italia meridionale). Boll. Soc. Paleontol. It. 33, 249-255.

Bossio, A., Mazzei, R., Monteforti, B., Salvatorini, G., 2002. Note illustrative alla carta geologica della zona di S. Maria di Leuca. Atti della Società Toscana di Scienze Naturali, Memorie 107, 97-163.

Bourillot, R., Vennin, E., Rouchy, J.M., Durlet, C., Rommevaux, V., Kolodka, C., Knap, F., 2009. Structure and evolution of a Messinian mixed carbonate-siliciclastic platform: the role of evaporites (Sorbas Basin, South-east Spain). Sedimentology 57, 477–512.

Bourillot, R., Vennin, E., Kolodka, C., Rouchy, J.M., Caruso, A., Durlet, C., Chaix, C., Rommevaux, V., 2009. The role of topography and erosion in the development and architecture of shallow-water coral bioherms (Tortonian-Messinian, Cabo de Gata, SE Spain). Palaeogeogr. Palaeoclimatol. Palaeoecol. 281, 92–114.

Brachert, T.C., Betzler, C., Braga, J.C., Martín, J.M. 1996. Record of climatic change in neritic carbonates: Turnovers in biogenic associations and depositional modes (Upper Miocene, southern Spain). Geologische Rundschau, 85, 327-337.

Brachert, T.C., Vescogni, A., Bosellini, F.R., Reuter, M., Mertz-Kraus, R., 2007. High salinity variability during the early Messinian revealed by stable isotope signatures from vermetid and *Halimeda* reefs of the Mediterranean region. Geologica Romana 40, 51–66.

Braga, J.C., Martin, J.M., 1992. Messinian carbonates of the Sorbas basin: sequence stratigraphy, cyclicity and facies. In: Late Miocene Carbonate Sequences of Southern Spain: A Guidebook for the Las Negras and Sorbas Areas, in conjunction with the SEPM/IAS Research Conference on Carbonate Stratigraphic Sequences: Sequence Boundaries and Associated Facies, August 30-September 3, La Seu, Spain, pp. 78-108.

Braga, J.C., Martín, J.M., 1996. Geometries of reef advance in response to relative sea-level changes in a Messinian (uppermost Miocene) fringing reef (Cariatiz reef, Sorbas Basin, SE Spain). Sedimentary Geology 107, 61–81.

Braga, J.C., Martín, J.M., Riding, R., 1996. Internal structure of segment reefs: *Halimeda* algal mounds in the Mediterranean Miocene. Geology 24, 35–38.

Braga, J.C., Bassi, D., Martín, J.M., Riding, R., Aguirre, J., Sánchez-Almazo, I.M., Dinarès-Turell, J., 2006. Testing models for the Messinian salinity crisis: the Messinian record in Almería, SE Spain. Sediment. Geol. 188-189, 131-154.

Braga, J.C., Vescogni, A., Bosellini, F.R., Aguirre, J., 2009. Coralline algae (Corallinales, Rhodophyta) in western and central Mediterranean Messinian reefs. Palaeogeography, Palaeoclimatology, Palaeoecology 275, 113–128.

Brandano, M., Mateu-Vicens, G., Gianfagna, A., Corda, L., Billi, A., Quaresima, S., Simonetti, A., 2009. Hardground development and drowning of a Miocene carbonate ramp (Latium-Abruzzi): from tectonic to paleoclimate. J. of Mediterranean Earth Science 1, 47–56.

Brandano, M., Westphal, H., Mateu-Vicens, G., Preto, N., Obrador, A, 2016. Ancient upwelling record in a phosphate hardground (Tortonian of Menorca, Balearic Islands, Spain). Mar. Pet. Geol. 78, 593–605.

Bucur, I.I., 1994. Lower Cretaceous Halimedaceae and Gymnoco- diaceae from southern Carpathians and Apuseni Mountains (Romania) and the systematic position of the Gymnocodiaceae. Beitr. Palaeontol. 19, 13-37.

Bulian, F., Jiménez-Espejo, F.J., Andersen, N., Larrasoaña, J.C., Sierro, F.J., 2023. Mediterranean water in the Atlantic Iberian margin reveals early isolation events during the Messinian Salinity Crisis. Glob. Planet. Change 231, 104297.

Burchette, T.P. and Wright, V.P., 1992. Carbonate Ramp Depositional Systems. Sedimentary Geology, 79, 3-57.

Butler, R.W.H., 2009. Relationships between the Apennine thrust belt, foredeep and foreland revealed by marine seismic data, offshore Calabria. Bollettino della Società Geologica Italiana 128, 269-278.

Cacchione, D. A., Pratson, L. F., & Ogston, A. S., 2002. The shaping of continental slopes by internal tides. Science*, 296*(5568), 724-727.

Capella, W., Barhoun, N., Flecker, R., Hilgen, F.J., Kouwenhoven, T., Matenco, L.C., Sierro, F.J., Tulbure, M.A., Yousfi, M.Z., Krijgsman, W., 2018. Palaeogeographic evolution of the late Miocene Rifian Corridor (Morocco): Reconstructions from surface and subsurface data. Earth-Science Rev. 180, 37–59.

Caputo, R., Catalano, S., Monaco, C., Romagnoli, G., Tortorici, G., Tortorici, L. 2010. Active faulting on the island of Crete (Greece). *Geophysical Journal International*, Volume 183, 1, 111–126.

Castro-Sanguino, C., Bozec, Y., Mumby, P.**,** 2020. Dynamics of carbonate sediment production by *Halimeda*: implications for reef carbonate budgets. Mar. Ecol. Prog. Ser. 639, 91–106.

Catalano R., Doglioni C., Merlini S., 2001. On the Mesozoic Ionian Basin. Geophysical Journal International 144, 49-64.

Cestari, R., Sirna, G., 1987. Rudist fauna in the Maastrichtian deposits of southern Salento (Southern Italy). Mem. Soc. Geol. It. 40, 133-147.

Chapman, F., Mawson, D., 1906. On the importance of Halimeda as reef-forming organisms with description of the Halimeda limestones of the New Hebrides. Quarterly Journal ofthe Geological Society London, 62, 702-711.

Ciaranfi N., Pieri P., Ricchetti G., 1988. Note illustrative alla carta geologica delle Murge e del Salento (Puglia centromeridionale). Memorie della Società Geologica Italiana 41, 449-460.

Ciarcia, S., Vitale, S., 2025. Orogenic evolution of the northern Calabria–southern Apennines system in the framework of the Alpine chains in the central-western Mediterranean area. Geol. Soc. Am. Bull. 137, 1143–1176.

Conard, M., Rioult, M., 1977. *Halimeda elliotti* nov. sp., Algue calcaire (Chlorophyceae) du Turonien des Alpes-Maritimes (SE France). Géologie Méditerranéenne 4, 83–97.

Conesa, G., Saint Martin, J.P., Cornée, J.J., Muller, J., 1999 Nouvelles contraintes sur la crise de salinité messinienne par l'étude d'une plateforme carbonatée marginale (bassin de Sorbas, Espagne). Comptes Rendus 'Acad. Sci. Paris. 328, 81–87.

Cornée, J.J., Saint Martin, J.P., Conesa, G., André, J.P., Muller, J., Benmoussa, A., 1996. Anatomie de quelques platesformes carbonatées progradantes messiniennes de Méditerranée occidentale. Bull. de la Soc. Geolog. de France 167, 495–507.

Cornée, J.J., Saint Martin, J.P., Conesa, G., Münch, P., André, J.P., Saint Martin, S., Roger, S., 2004. Correlations and sequence stratigraphic model for Messinian carbonate platforms of the western and central Mediterranean. Intern. J. of Earth Sciences 93, 621–633.

Critelli, S., Muto, F., Perri, F., Tripodi, V., 2017. Interpreting provenance relations from sandstone detrital modes, southern Italy foreland region: Stratigraphic record of the Miocene tectonic evolution. Marine and Petroleum Geology 87, 47-59.

Critelli, S., 2018. Provenance of Mesozoic to Cenozoic circum-Mediterranean sandstones in relation to tectonic setting. Earth-Science Reviews v. 185, 624-648.

Cunningham, K.J., Collins, L.S., 2002. Controls on facies and sequence stratigraphy of an upper Miocene carbonate ramp and platform, Melilla basin, NE Morocco. Sedimentary Geology 146, 285–304.

Dabrio, C.J., Esteban, M., Martin, J.M., 1981. The coral reef of Í, Messinian (uppermost Miocene), Almeria Province, SE Spain. J. Sediment. Petrol. 51, 521–540.

Davies, P., Hopley, D., 1983. Growth fabrics and growth-rates of holocene reefs in the great barrier-reef. BMR J. Aust. Geol. Geophys. 8, 237-251.

Davies, P.J., Marshall, J.F., 1985. *Halimeda* bioherms – low energy reefs, northern Great Barrier Reef. Proc. 5th Int. Coral Reef Symp. 5, 1-7.

De La Vara, A., Topper, R.P.M., Meijer, P.T., Kouwenhoven, T.J., 2015. Water exchange through the Betic and Rifian corridors prior to the Messinian Salinity Crisis: A model

study. Paleoceanography 30, 548–557.

Del Ben A., Geletti R., Mocnik A., 2010. Relation between recent tectonics and inherited Mesozoic structures of the central-southern Adria plate. Bollettino di Geofisica Teorica e Applicata 51, 99-115.

Del Ben A., Mocnik A., Volpi V., Karvelis P., 2015. Old domains in the South Adria plate and their relationship with the West Hellenic front. Journal of Geodynamics 89, 15-28.

Doglioni C., Merlini S., Cantarella G., 1999. Foredeep geometries at the front of the Apennines in the Ionian Sea (central Mediterranean). Earth and Planetary Science Letters 168, 243-254.

Dragastan, O.N., Herbig, H.G., 2007. *Halimeda* (green siphonous algae) from the Paleogene of (Morocco) - Taxonomy, phylogeny and paleoenvironment. Micropaleontology 53, 1–72.

Dragastan, O.N., Soliman, H.A, 2002. Paleogene calcareous algae from Egypt: Micropaleontology 48, 1–30.

Drew, E.A., 1983. *Halimeda* biomass, growth rates and sediment generation on reefs in the central Great Barrier Reef Province. Coral Reefs 2, 101-110.

Drew, E. A., Abel, K. M., 1985. Biology, sedimentology, and geography of the vast inter-reefal *Halimeda* meadows within the Great Barrier Reef province. Proc. 5th Int. Coral Reef Symp. 5, 15-20.

Drew, E.A., Abel, K.M., 1988. Studies on *Halimeda* - I. The distribution and species composition of *Halimeda* meadows throughout the Great Barrier Reef Province. Coral Reefs 6, 195–205.

Drew, E.A., 1993. Production of geological structures by the green alga *Halimeda.* South Pacific Underwater Medicine Society J. 23, 93-102.

Do Couto, D., Gumiaux, C., Augier, R., Lebret, N., Folcher, N., Jouannic, G., Jolivet, L., Suc, J.P., Gorini, C., 2014. Tectonic inversion of an asymmetric graben: Insights from a combined field and gravity survey in the sorbas basin. Tectonics 33, 1360– 1385.

Do Couto, D., Gumiaux, C., Jolivet, L., Augier, R., Lebret, N., Folcher, N., Jouannic, G., Suc, J.P., Gorini, C., 2015. 3D modelling of the Sorbas Basin (Spain): New constraints on the Messinian Erosional Surface morphology. Mar. Pet. Geol. 66, 101–116.

Doglioni, C., Mongelli, F., Pieri P., 1994. The Puglia uplift (SE-Italy): an anomaly in the foreland of the Apenninic subduction due to buckling of a thick continental litosphere. Tectonics 13, 1309-1321.

Dunham, R.J., 1962. Classification of Carbonate Rocks According to Depositional Textures. In: Ham WE (ed) Classification of Carbonate Rocks, a Symposium. AAPG Memoir n. 1, 108-121.

Elliott, G.F., 1959. Fossil calcareous algal floras of the Middle East with a note on a cretaceous problematicum, gen. et sp. Nov. Quarterly Jour. of the Geol. Soc. of London 115, 217–232.

Elliott, G.F., 1965. The interrelationships of some Cretaceous Codiaceae (calcareous algae): Palaeontology 8, 199–203.

Embry, A.F., Klovan, J.E., 1971. A Late Devonian reef tract on northeastern Banks Island, NWT. Bull. Can. Pet. Geol. 19, 730–781.

Esteban, M., 1979. Significance of the upper Miocene coral reefs of the Western Mediterranean. Palaeogeogr. Palaeoclimatol. Palaeoecol. 29, 169–188.

Esteban, M., Giner, J., 1980. Messinian coral reefs and erosion surfaces in Cabo de Gata (Almería, S.E. Spain). Acta Geol. Hisp. 15, 97–104.

Esteban, M., 1996. "An Overview of Miocene Reefs from Mediterranean Areas: General Trends and Facies Models", Models for Carbonate Stratigraphy from Miocene Reef Complexes of Mediterranean Regions, Evan K. Franseen, Mateu Esteban, William C. Ward, Jean-Marie Rouchy

Faccenna, C., Mattei, M., Funiciello R., Jolivet, L., 1997. Styles of back-arc extension in the central Mediterranean. Terra Nova 9, 126–130.

Faccenna, C., Piromallo, C., Crespo-Blanc A., Jolivet, L., Rossetti, F., 2004. Lateral slab deformation and the origin of the western Mediterranean arcs. Tectonics 23, TC1012.

Faccenna, C., Becker, T.W., 2010. Shaping mobile belts by small-scale convection. Nature 465, 602–605.

Fassoulas, C., 1999. The structural evolution of Central Crete: insight into the tectonic evolution of the South Aegean (Greece), J. Geodynam., 27, 23-43.

Fassoulas, C., 2001. The tectonic development of a Neogene basin at the leading edge of the active European margin: The Heraklion basin, Crete, Greece. J. Geodyn. 31, 49–70.

Fernández-Soler, J.M. (1992): El volcanismo calco-alcalino de Cabo de Gata (Almería). Estudio volcanológico y petrológico. Ph. D. Thesis Universidad de Granada. 243 p. Granada.

Fernández-Soler, J. M., 2001. Volcanics of the Almería Province. In: Mather, A., Martín, J.M., Harvey, J.C., Braga, J.C. (eds) A field guide to the Neogene Sedimentary Basins of the Almería Province, south-east Spain. Blackwell, Oxford, pp 58–88.

Finetti I.R., Del Ben A., 2005. Crustal tectono-stratigraphic setting of the Adriatic Sea from new CROP seismic data. In: Finetti I.R. (Ed.), CROP PROJECT: Deep seismic exploration of the Central Mediterranean and Italy). Amsterdam, Elsevier Science, 519-547.

Flügel, E., 1988. Halimeda: paleontological record and palaeoenvir- onmental significance. Coral Reefs 6 (3-4), 123-130.

Flügel, E., 1991. Triassic and Jurassic marine calcareous algae: a critical review. In: Riding, R. (Ed.), Calcareous Algae and Stromatolites. Springer, Berlin, pp. 167-188.

Föllmi, K.B., Gertsch B., Renevey J.P., de Kaenel E., Stille P., 2008. Stratigraphy and sedimentology of phosphate-rich sediments in Malta and southeastern Sicily (latest Oligocene to early Late Miocene). Sedimentology 55, 1029–1051.

Föllmi, K.B., Hofmann, H., Chiaradia, M., de Kaenel, E., Frijia, G., Parente, M., 2015. Miocene phosphate-rich sediments in Salento (southern Italy). Sedimentary Geology 327, 55–71.

Fornos, J.J., Forteza, V., Jaume, C., Martinez-Taberner, A., 1992. Present-day *Halimeda* carbonate sediments in temperate mediterranean embayments: Fornells, Balearic Islands. Sedimentary Geology 75, 283–293.

Fortuin, A.R., Krijgsman, W., Hilgen, F.J., Sierro, F.J., 2000. Late Miocene Mediterranean desiccation: topography and significance of the 'Salinity Crisis' erosion surface on-land in southeast Spain: comment. Sediment. Geol. 133, 167-174.

Fournier, F., Teillet, T., Licht, A., Borgomano, J., Montaggioni, L., 2024. Eocene-Oligocene large-scale circulation of the East Asian summer monsoon recorded in neritic carbonates of the proto-South China Sea. Palaeogeogr. Palaeoclimatol. Palaeoecol. 633, doi:111883. 10.1016/j.palaeo.2023.111883

Franseen, E.K., Mankiewicz, C., 1991. Depositional sequences and correlation of middle(?) to late Miocene carbonate complexes, Las Negras and Í areas, southeastern Spain. Sedimentology 38, 871–898.

Franseen, E. K., Goldstein, R. H., Farr M. R., 1998. Quantitative controls on location and architecture of carbonate depositional sequences: Upper Miocene, Cabo de Gata region, SE Spain. Jour. of Sed. Res. 68, 283-298.

Frizon de Lamotte, D., Raulin, C., Mouchot, N., Wrobel-Daveau, J., Blanpied, C., Ringenbach, J., 2011. The southernmost margin of the Tethys realm during the Mesozoic and Cenozoic: Initial geometry and timing of the inversion processes. Tectonics 30, 1–22.

Freile, D., Hillis, L., 1997. Carbonate productivity of Halimeda incrassata in a land proximal lagoon, Pico Feo, San Blas, Panama: International Coral Reef Symposium, Proceedings, v. 8, p. 766–771.

Frydas, D., Keupp, H. & Bellas, S.M., 1999. Biostratigraphical research in Late Neogene marine deposits of the Chania Province, western Crete, Greece. Berliner Geowissenschafiliche Abhandlungen, E, 30, 55-67.

Gambini R., Tozzi M., 1996. Tertiary geodynamic evolution of the Southern Adria microplate. Terra Nova 8, 593-602.

Gautier, F., Clauzon, G., Suc, J.-P., Cravatte, J., Violanti, D., 1994. Age et durée de la crise de salinité messinienne. C.R. Acad. Sci. Paris 318, 1103-1109.

Ghosh, A.K., Chakraborty, A., Mazumder, A., 2017. *Halimeda* bioherms from the Serravallian (Middle Miocene) of Little Andaman Island, India. Micropaleontology 63, 67–75.

Gladstone, R., Flecker, R., Valdes, P., Lunt, D., Markwick, P., 2007. The Mediterranean hydrologic budget from a Late Miocene global climate simulation. Palaeogeogr. Palaeoclimatol. Palaeoecol. 251, 254–267.

Guilderson, T.P., Fairbanks, R.G., Rubenstone, J.L., 1994. Tropical temperature variations since 20,000 years ago: modulating inter- hemispheric climate change. Science 263, 663-665.

Guppy, H.B., 1887. The Solomon Islands: Their Geology, General Features, and Suitability for Colonization. S. Sonnenschein, Lowrey & Company.

Hay, M. E., Paul, V.J., Lewis, S., 1988. Can tropical seaweeds reduce herbivory by growing at night—diel patterns of growth, nitrogen-content, herbivory, and chemical versus morphological defenses. Oecologia 75, 233–245.

Haq, B.U., Hardenbol, J. and Vail, P.R., 1988. Mesozoic and Cenozoic chronostratigraphy and cycles of sea level change. In: Sea Level Changes: an Integrated Approach (C. K. Wilgus et al., eds). Spec. Publs. Soc. econ. Paleont. Miner., Tulsa, 42, 109–124.

Hardenbol, J., Thierry, J., Farley, M.B., Jacquin, Z., De Granciaski, P.C., Vail, P.R., 1998. Mesozoic and Cenozoic sequence stratigraphic framework of European Basins. In: De Granciaski, P.C., Hardenbol, J., Thierry, J., VAIL, P.R. (eds) Mesozoic and Cenozoic Sequence Stratigraphy of European Basins. Society of Economic Paleontologists and Mineralogists Special Publication 60, 3-14.

Heyward, A., Pinceratto, E., Smith, L., 1997. Big Bank shoals ofthe Timor Sea: An Environment Resource Atlas. Australian Institute of Marine Science and BHP Petroleum, 115 pp.

Hillis-Colinvaux, L., 1980. Ecology and taxonomy of *Halimeda*: primary producer of coral reefs. Adv. Mar. Biol. 17, pp. 327.

Hillis-Colinvaux, L., 1986. Halimeda growth and diversity on the deep fore-reef of Enewetak Atoll. Coral Reefs 5, 19–21.

Hillis, L., 1997. Coralgal reefs from a calcareous green alga perspective and a first carbonate budget. Proceedings of 8th International Coral Reef Symposium 1, 761-766.

Hillis, L.W., 2001. The calcareous reef alga Halimeda (Chlorophyta, Byropsidales): A cretaceous genus that diversified in the cenozoic. Palaeogeogr. Palaeoclimatol. Palaeoecol. 166, 89–100.

Hinde, J. G., 1904. Report on the materials from the borings at Funafuti Atoll, in The atoll of Funafuti. Borings into a coral reef and the results: London, Royal Society Coral Reef Committee Report, p. 186–361.

Hine, A.C., Hallock, P., Harris, M.W., Mullins, H.T., Belknap, D.F., Jaap, W.C., 1988. *Halimeda* bioherms along an open seaway: Miskito Channel, Nicaraguan Rise, SW Caribbean Sea. Coral Reefs 6, 173–178.

Insalaco, E., 1998. The descriptive nomenclature and classification of growth fabrics in fossil scleractinian reefs. Sedimentary Geology 118, 159-186.

Jiménez, A.P., Braga, J.C., 1993. Occurrence and taphonomy of bivalves from the Níjar reef (Messinian, Late Miocene, SE Spain). Palaeogeogr. Palaeoclimatol. Palaeoecol. 102, 239–251.

Johnston, T.M.S., Colin, P.L., 2022. Upwelling and Downwelling Driven by the North Equatorial Countercurrent and Internal Waves at Hatohobei Island and Helen Reef, Palau. J. Geophys. Res. Ocean. 127, 1–18.

Jolivet, L., Goffé, B., Monie, P., Truffert-Luxey, C., Patriat, M., Bonneau, M. 1996. Miocene detachment on Crete and exhumation P-T-t paths of high-pressure metamorphic rocks. Tec- tonics 15, 1129-1153.

Jolivet, L., and C. Faccenna (2000), Mediterranean extension and the Africa- Eurasia collision, Tectonics, 19, 1095–1106, doi:10.1029/2000TC900018.

Keupp, H., Bellas, S.M., Frydas, D., Kohring, R., 1994. Aghia Irini, ein Neogenprofil aufder Halbinsel Gramvoùssa/NW-Kreta. Berliner Geowiss. Abh. E 13, 469–481.

Kilias, A., Fassoulas, C., Mountrakis, D., 1994. Tertiary extension of continental crust and uplift of Psiloritis metamorphic core complex in the central part of the Hellenic Arc (Crete, Greece), Geol. Rundsch. 83, 417-430.

Kontakiotis, G., Butiseacă, G.A., Antonarakou, A., Agiadi, K., Zarkogiannis, S.D., Krsnik, E., Besiou, E., Zachariasse, W.J., Lourens, L., Thivaiou, D., Koskeridou, E., Moissette, P., Mulch, A., Karakitsios, V., Vasiliev, I., 2022. Hypersalinity accompanies tectonic restriction in the eastern Mediterranean prior to the Messinian Salinity Crisis. Palaeogeogr. Palaeoclimatol. Palaeoecol. 592, 110903.

Krijgsman, W., Fortuin, A.R., Hilgen, F.J., Sierro, F.J., 2001. Astrochronology for the Messinian Sorbas basin (SE Spain) and orbital (precessional) forcing for evaporite cyclicity. Sediment. Geol. 140, 43-60.

Kroeger, K.F. 2004. Sedimentary environments and climate change: a case study (late Miocene, central Crete). PhD thesis, Johannes Gutenberg-Universität, Mainz.

Lamb, K.G., 2014. Internal Wave Breaking and Dissipation Mechanisms on the Continental Slope/Shelf. Annu. Rev. Fluid Mech. 46, 231–254.

Laviano, A., 1996a. Late Cretaceous rudist lassemblages from the Salento peninsula (southern Italy). Geologica Romana 32, 1-14.

Leichter, J.J., Shellenbarger, G., Genovese, S.J., Wing, S.R., 1998. Breaking internal waves on a Florida (USA) coral reef: a plankton pump at work? Mar. Ecol. Prog. Ser. 166, 83–97.

Leichter, J.J., Stewart, H.L., Miller S.L., 2003. Episodic nutrient transport to Florida coral reefs. Limnol. Oceanogr. 48, 394–1407.

Leichter, J.J., Deane, G.B., Stokes, M.D., 2005. Spatial and Temporal Variability of Internal Wave Forcing on a Coral Reef. J. Phys. Oceanogr. 35, 1945–1962.

Littler, M.M., Littler, D.S., Blair, S.M., Norris, J.N., 1985. Deepest known plant life discovered on an uncharted seamount. Science 227, 57-59.

Lugli, S., Manzi, V., Roveri, M., 2008. New facies interpretation of the Messinian evaporites in the Mediterranean.In: F.Briand. CIESM 2008.The Messinian Salinity Crisis megadeposits to microbiology - A consensus report.vol. CIESM Workshop Monograph 33, p.67-72.

Mankiewicz, C., 1988. Coral Reefs Occurrence and paleoecologic significance of *Halimeda* in late Miocene reefs, southeastern Spain, Coral Reefs 6, 271-279.

Mann, T., Wizemann, A., Stuhr, M., Kappelmann, Y., Janßen, A., Jompa, J., Westphal, H., 2022. Shallow-marine carbonate cementation in Holocene segments of the calcifying green alga *Halimeda*. Sedimentology 69, 282–300.

Marshall, J.F., Davies, P.J., 1988. *Halimeda* bioherms of the northern Great Barrier Reef. Coral Reefs 6, 139–148.

Martín, J.M., Braga, J.C., 1994. Messinian events in the Sorbas Basin in southeastern Spain and their implications in the recent history of the Mediterranean. Sediment. Geol. 90, 257–268.

Martín, J.M., Braga, J.C., Riding, R., 1997. Late Miocene *Halimeda* algal-microbial segment reef in the marginal Mediterranean Sorbas Basin, Spain. Sedimentology 44, 441-456.

Martín, J.M., Braga, J.C., Betzler, C., 2003. Late Neogene - Recent uplift of the Cabo de Gata volcanic province, Almería, SE Spain. Geomorphology 50, 27–42.

Martín, J.M., Puga-Bernabéu, Á., Aguirre, J., Braga, J.C., 2014. Miocene Atlantic Mediterranean seaways in the Betic Cordillera (southern Spain). Rev. Soc. Geol. Esp. 27, 175–186

Martínez-Martínez, J.M., Azanon, J.M., 1997. Mode of extensional tectonics in the southeastern Betics (SE Spain): implications for the tectonic evolution of the peri-Alboran orogenic system. Tectonics 16, 205e225.

Martinis, B., 1962. Lineamenti strutturali della parte meridionale della Penisola Salentina. Geologica Romana 1, 11-23.

Martinis, B., Pieri, M., 1964. Alcune notizie sulla formazione evaporitica del Triassico Superiore nell'Italia centrale e meridionale. Memorie della Società Geologica Italiana 4, 649-678.

Mateu-Vicens, G., Hallock, P., & Brandano, M. (2008). A depositional model and paleoecological reconstruction of the lower Tortonian distally steepened ramp of Menorca (Balearic Islands, Spain). *Palaios, 23*(6), 465-481.

Mather, A.E., Martín, J.M., Harvey, A.M., Braga J.C. (Eds.), 2001.A Field Guide to the Neogene Sedimentary Basins of the Almeria Province, SE Spain.

McNeil, M.A., Webster, J.M., Beaman, R.J., Graham, T.L., 2016. New constraints on the spatial distribution and morphology of the *Halimeda* bioherms of the Great Barrier Reef, Australia. Coral Reefs 35, 1343–1355.

McNeil, M.A., Nothdurft, L., Erler, D., Hua, Q., Webster, J.M., 2021a. Variations in Mid- to Late Holocene Nitrogen Supply to Northern Great Barrier Reef *Halimeda* Macroalgal Bioherms. Paleoceanogr. Paleoclimatology 36, 1–18.

McNeil, M.A., Nothdurft, L.D., Dyriw, N.J., Webster, J.M., Beaman, R.J., 2021b. Morphotype differentiation in the Great Barrier Reef *Halimeda* bioherm carbonate factory: Internal architecture and surface geomorphometrics. Depositional Record 7, 176–199.

McNeil, M.A., Nothdurft, L.D., Hua, Q., Webster, J.M., Moss, P., 2022. Evolution of the inter-reef *Halimeda* carbonate factory in response to Holocene sea-level and environmental change in the Great Barrier Reef. Quat. Sci. Rev. 277, 107347.

Meulenkamp, J.E., Dermitzakis, M., Georgiadou-Dikeoulia, E., Jonkers, H.A., Bögerm, H., 1979. Field guide to the Neogene of Crete. Publications of the Department of Geology and Palaeontology. University of Athens, Athens 32.

Meulenkamp, J.E., van der Zwaan, G.J., van Wamel, W.A., 1994. On late miocene to recent vertical motions in the Cretan segment of the Hellenic arc. Tectonophysics 234, 1–2, 53-72,

Milia, A., 2017. Pliocene-Quaternary orogenic systems in Central Mediterranean: The Apulia-Southern Apennines-Tyrrhenian Sea example. Tectonics 36, 1431-1659.

Milliman, J., 1993. Production and accumulation of calcium carbonate in the ocean: budget of a nonsteady state. Global Biogeochemical Cycles 7, 927-957.

Moissette, P., Cornée, J.J., Antonarakou, A., Kontakiotis, G., Drinia, H., Koskeridou, E., Tsourou, T., Agiadi, K., Karakitsios, V., 2018. Palaeoenvironmental changes at the Tortonian/Messinian boundary: A deep-sea sedimentary record of the eastern Mediterranean Sea. Palaeogeogr. Palaeoclimatol. Palaeoecol. 505, 217–233.

Montenat, C., Ott d'Estevou, P., de La Chapelle, G., 1990. Le Bassin de Í-Carboneras et le couloir du Bas-Andarax. In: Montenat, C. (Ed.), Les Bassins Néogènes du domain Bétique oriental (Espagne). Tectonique et sédimentation dans un couloir de

décrochement. Première partie : étude régionale. IGAL, Paris, pp. 129–164.

Montgomery, P., Farr, M.R., Franseen, E.K., Goldstein, R.H., 2001. Constraining controls on carbonate sequences with high-resolution chronostratigraphy: Upper Miocene, Cabo de Gata region, SE Spain. Palaeogeography, Palaeoclimatology, Palaeoecology 176 (1–4), 11–45.

Moretti,I., Royden,L., 1988. Deflection, gravity anomalies and tectonics of doubly subducted continental lithosphere: Adriatic and Ionian seas. Tectonics 7, 875–893.

Morsilli, M., Hairabian, A., Borgomano, J., Nardon, S., Adams, E., Gartner, G.B., 2017. The Apulia Carbonate Platform-Gargano Promontory, Italy (Upper Jurassic-Eocene). Am. Assoc. Pet. Geol. Bull. 101, 523–531.

Morsilli, M., Hairabian, A., Borgomano, J., Nardon, S., Adams, E.W., Bracco Gärtner, G.L., 2022. A journey along the Gargano Promontory (Southern Italy): the Late Jurassic to Eocene Apulia Carbonate Platform evolution. IAS F. Guid. to Except. Expo. Carbonate Outcrops 395–480.

Multer, H.G., 1988. Growth rate, ultrastructure and sediment contribution of *Halimeda incrassata* and *Halimeda monile*, Nonsuch and Falmouth Bays, Antigua, W.I. Coral Reefs 6, 179–186.

Münch, P., Roger, S., Cornée, J.J., Saint Martin, J.P., Féraud, G., Moussa, A. Ben., 2001. Restriciton des communications entre l'Atlantique et la Méditerranée au Messinien : Apport de la téphrochronologie dans la plateforme carbonatée et le bassin de Mellilla-Nador (Rif nord-oriental, Maroc). Comptes Rendus de l'Academie de Sciences - Serie IIa: Sciences de la Terre et des Planetes 332, 569–576.

Muntaner-Gonzalez, C., Martin-Abadal, M., Gonzalez-Cid, Y., 2024. A Deep Learning Approach to Estimate *Halimeda incrassata* Invasive Stage in the Mediterranean Sea. J. of Mar. Sci. and Engineering 12, 1-20.

Mutti, M., Bernoulli, D., 2003. Early marine lithification and hardground development on a Miocene ramp (Maiella, Italy): key surfaces to track changes in trophic resources in non-topical carbonate settings. J. of Sed. Res. 73, 296–308.

Nardin, M., Rossi, D., 1966. Condizioni strutturali della zona compresa nel Foglio Otranto (Provincia di Lecce). Mem. Museo Civivico St. Nat. Verona, 14, 415–430.

Nicolai, C., Gambini, G., 2007. Structural architecture of the Adria platform-and-basin system. Italian Journal of Geosciences 7, 21-37.

Orme, G.R., Flood, P.G., Sargent, G.E.G., 1978. Sedimentation trends in the lee of the outer (ribbon) reefs, northern region of the Great Barrier Reef Province. R. Soc. London. A 291, 85-99.

Orme, R., 1985. The sedimentological importance of *Halimeda* in the development of back-reef lithofacies, northern Great Barrier Reef (Australia). Proc. 5th Int. Coral Reef Symp. 5, 31-37.

Orme, R., Riding, R., 1995. *Halimeda* Segment Reefs of the northern Great Barrier Reef. British Sedimentological Research Group, Annu. Meet. Abstr. Durham, p. 64.

Orme, G.R., Salama, M.S., 1988. Form and seismic stratigraphy of *Halimeda* banks in part of the northern Great Barrier Reef Province. Coral Reefs 6, 131–137.

Ott d' Estevou, P., 1980, Evolution dynamique du bassin néogène de Sorbas (Cordilleres Bétiques orientales, Espagne): Unpublished Ph.D. Thesis, Institut Géologique Albert Lapparent, Paris, 1, 264 p.

Ott d'Estevou, P. and Montenat, C., 1990. Le bassin de Sorbas- Tabemas. Dot. Trav. IGAL, 12-13: 101-128.

Overholtzer, K.L., P.J. Motta, 1999. Comparative resource use by juvenile parrotfishes in the Florida Keys. Mar. Ecol. Prog. Ser. 177, 177-187.

Panagopoulos, G., Vafidis, A., Soupios, P., Manoutsoglou, E., 2022. A study on the Gas-bearing Miocene Sediments of MESSARA Basin in Crete (Greece) by Using Seismic Reflection, Geochemical and Petrophysical Data. Arab. J. Sci. Eng. 47, 7449–7465.

Papanikolaou, D., Vassilakis, E., 2010. Thrust faults and extensional detachment faults in Cretan tectono-stratigraphy: Implications for Middle Miocene extension. Tectonophysics 488, 233–247.

Parente, M., 1994. A revised stratigraphy of the Upper Cretaceous to Oligocene units from southeastern Salento (Apulia, southern Italy). Boll. Soc. Paleontol. Ital. 33, 155–170.

Parente, M., 1997. Dasycladales from the Upper Maastrichtian of Salento Peninsula (Puglia,

Southern Italy). Facies 36, 91-122, Erlangen.

Passaseo, C., Morsilli, M., 2024. *Halimeda*-rich beds in a mixed carbonate system from a pre-evaporitic Messinian reef (Crete Island, Greece). AAPG Cross Regional Carbonates and Mixed Carbonate Systems Symposium, Palermo p. 82.

Passaseo, C., Morsilli, M., 2025. Characterization of *Halimeda* Bioherms of the Pre-Evaporitic Messinian of the Salento Peninsula (Southern Italy). Sedimentary Geology 475, 106- 782. https://doi.org/10.1016/j.sedgeo.2024.106782

Paul, V.J., Van Alstyne, K.L., 1988. Chemical defense and chemical variation in some tropical Pacific species of Halimeda (Halimedaceae; Chlorophyta). Coral Reefs 6, 263–269.

Pennings, S.C., Paul, V.J., 1992. Effect of plant toughness, calcification, and chemistry on herbivory by *Dolabella auricularia*. Ecology 73, 1606−1619.

Pérez-Asensio, J.N., Aguirre, J., Schmiedl, G., Civis, J., 2014. Messinian productivity changes in the northeastern Atlantic and their relationship to the closure of the Atlantic-Mediterranean gateway: Implications for Neogene palaeoclimate and palaeoceanography. J. of Geol. Soc. London. 171, 389–400.

Perry, C.T., Morgan, K.M., Salter, M.A., 2016. Sediment generation by *Halimeda* on atoll interior coral reefs of the southern Maldives: a census-based approach for estimating carbonate production by calcareous green algae. Sedimentary Geology 346, 17–24.

Phipps, C.V.G., Roberts, H.H., 1988. Seismic characteristics and accretion history of *Halimeda* bioherms on Kalukalukuang Bank, eastern Java Sea (Indonesia). Coral Reefs 6, 149–159.

Platt, J.P., Vissers, R.L.M., 1989. Extensional collapse of thickened continental lithosphere — a working hypothesis for the Alboran Sea and Gibraltar Arc. Geology 17 (6), 540–543.

Pomar, L., Mateu-Vicens, G., Morsilli, M., Brandano, M., 2014. Carbonate ramp evolution during the Late Oligocene (Chattian), Salento Peninsula, southern Italy. Palaeogeogr. Palaeoclimatol. Palaeoecol. 404, 109–132.

Pomar, L., Morsilli, M., Hallock, P., Bádenas, B., 2012. Internal waves, an under-explored

source of turbulence events in the sedimentary record. Earth-Science Rev. 111, 56–81.

Pomoni-Papaioannou, F., Drinia, H., Dermitzakis, M.D., 2002. Neogene non-tropical carbonate sedimentation in a warm temperate biogeographic province (Rethymnon Formation, Eastern Crete, Greece). Sediment. Geol. 154, 147–157.

Poncet, J., 1989. Présence du genre *Halimeda* Lamouroux, 1812 (algue verte calcaire) dans le Permien supérieur du Sud Tunisien. Rev. de Micropaléontologie 32, 40-44.

Popov S.V., Rögl F., Rozanov A.Y., Steininger F. F., Shcherba I. G., Kovac M., 2004. Lithological-paleogoegraphic maps of Paratethys. Courier Forschungsinstitut Senckenberg 250, 46.

Purdy, E.G., 1974. Reef configurations: cause and effect. In: Laport L (ed) Reefs in time and space, vol 18. Soc. Econ. Paleontol. Mineral. Spec. Publ. Tulsa pp 9–76.

Purdy, E.G., Winterer, E.L., 2006. Contradicting barrier reef relation- ships for Darwin's evolution of reef types. Int. J. Earth Sci. 95, 143–167.

Rahl, J.M., 2004. Exhumation of high-pressure metamorphic rocks within an active convergent margin, Crete, Greece. Field-trip guide book, 32nd International Geological Congress. 36

Rao, V.P., Veerayya, M., Nair, R.R., Dupeuble, P.A., Lamboy, M., 1994. Late Quaternary *Halimeda* bioherms and aragonitic faecal pellet-dominated sediments on the carbonate platform of the western continental shelf of India. Mar. Geol. 121, 293–315.

Rao, V.P., Mahale, V.P., Chakraborty, B., 2018. Bathymetry and sediments on the carbonate platform off western India: Significance of *Halimeda* bioherms in carbonate sedimentation. J. Earth Syst. Sci. 127, 1–16.

Read, J.F., 1985. Carbonate Platform Facies Models. AAPG Bulletin, 69, 1-21.

Rees S.A., 2006. Coral reefs of the Indo-Pacific and changes in global Holocene climate. PhD thesis, University of Southampton, UK, p 188.

Rees, S.A., Opdyke, B.N., Wilson, P.A., Henstock, T.J., 2007. Significance of *Halimeda* bioherms to the global carbonate budget based on a geological sediment budget for the Northern Great Barrier Reef, Australia. Coral Reefs 26, 177–188.

Reghizzi, M., Gennari, R., Douville, E., Lugli, S., Manzi, V., Montagna, P., Roveri, M., Sierro, F.J., Taviani, M., 2017. Isotope stratigraphy (87Sr/86Sr, δ18O, δ13C) of the Sorbas basin (Betic Cordillera, Spain): Paleoceanographic evolution across the onset of the Messinian salinity crisis. Palaeogeogr. Palaeoclimatol. Palaeoecol. 469, 60–73.

Rehault, J. P., Boillot, G., Mauffret, A., 1984. The Western Mediterranean Basin geological evolution. Marine Geology, v. 55, p. 447 – 478.

Reid, E.C., De Carlo, T.M., Cohen, A.L., Wong, G.T.F., Lentz, S.J., Safaie, A., Hall, A., Davis, K.A., 2019. Internal waves influence the thermal and nutrient environment on a shallow coral reef. Limnol. Oceanogr. 64, 1949–1965.

Reolid, J., Betzler, C., Braga, J.C., Martín, J.M., Lindhorst, S., Reijmer, J.J.G., 2014. Reef slope geometries and facies distribution: Controlling factors (Messinian, SE Spain). Facies 60, 737–753.

Reolid, J., Bialik, O.M., Lindhorst, S., Eisermann, J.O., Petrovic, A., Hincke, C., Beaman, R.J., Webster, J.M., Betzler, C., 2024. A new type of *Halimeda* bioherm on the Queensland Plateau, NE Australia. Coral Reefs 43, 801–821.

Ricchetti G., Ciaranfi N., Luperto Sinni E., Mongelli F., Pieri P., 1988. Geodinamica ed evoluzione sedimentaria e tettonica dell'Avampaese Apulo. Memorie della Società Geologica Italiana 41, 57- 82.

Ricchetti, G., Ciaranfi, N., Luperto Sinni, E., Mongelli, F., Pieri, P., 1992. Geodinamica ed evoluzione sedimentaria e tettonica dell'Avampaese apulo. Memorie Società Geologica Italiana 41, 57-82.

Riding, R., Martín, J.M., Braga, J.C., 1991. Coral-stromatolite reef framework, Upper Miocene, Almería, Spain. Sedimentology 38, 799–818.

Riding, R., Braga, J.C., Martín, J.M., Sánchez-Almazo, I.M., 1998. Mediterranean Messinian salinity crisis: constraints from a coeval marginal basin, Sorbas, southeastern Spain. Mar. Geol. 146, 1–20.

Riding, R., Braga, J.C., Martín, J.M., 1999. Late Miocene Mediterranean desiccation: topography and significance of the 'Salinity Crisis' erosion surface on-land in southeast Spain. Sediment. Geol. 123, 1-7.

Riding, R., 2000. Microbial carbonates: the geological record of calcified bacterial–algal mats and biofilms. Sedimentology 47 (Supplement 1), 179–214.

Riding, R., Braga, J.C., Martín, J.M., 2000. Late Miocene Mediterranean desiccation: topography and significance of the 'Salinity Crisis' erosion surface on-land in southeast Spain: reply. Sediment. Geol. 133, 175-184.

Ries, J.B., Cohen, A.L., McCorkle, D.C., 2009. Marine calcifiers exhibit mixed responses to CO2-induced ocean acidification. Geology 37, 1131−1134.

Roberts, H.H., Phipps, C.V., Effendi, L., 1987. *Halimeda* bioherms of the eastern Java Sea, Indonesia. Geology 15, 371–374.

Roberts, H.H., Phipps, C.V., 1988. Morphology and sedimentology of *Halimeda* bioherms from the eastern Java Sea (Indonesia). Coral Reefs 6, 161–172.

Roep, T.B., Dabrio, C.J., Fortuin, A.R., Polo, M.D., 1998. Late highstand patterns of shifting and stepping coastal barriers and washover-fans (late Messinian, Sorbas Basin, SE Spain). Sediment. Geol. 116, 27e56.

Roger, S., Munch, P.H., Cornée, J.J., Saint Martin, J.P., Féraud, G., Conesa, G., Pestrea, S., Ben Moussa, A., 2000. 40Ar/39Ar dating of the pre-evaporitic Messinian marine sequences of the Melilla basin (Morocco): a proposal for some biosedimentary events as isochrons around the Alboran Sea. Earth Planet. Sci. Lett. 179, 101–113.

Rouchy, J. M., Saint Martin J. P., 1992. Late Miocene events in the Mediterranean as recorded by carbonate-evaporite relations. Geology 20, 629-632.

Roveri, M., Gennari, R., Lugli, S., Manzi, V., 2009. The Terminal Carbonate Complex: the record of sea-level changes during the Messinian salinity crisis. GeoActa 8, 63–77.

Roveri, M., Lugli, S., Manzi, V., Reghizzi, M., Rossi, F.P., 2020. Stratigraphic relationships between shallow-water carbonates and primary gypsum: insights from the Messinian succession of the Sorbas Basin (Betic Cordillera, Southern Spain). Sedimentary Geolology 404, 105-678.

Ruegg, G.J.H., 1964. Geologische onderzoekingen in het bekken van Sorbas, S. Spanje, Amsterdam Geological Institute, Amsterdam pp. 1–64.

Saint Martin, J.P., 1992. Un dispositif particulier de plateforme carbonatée messinienne: la bordure meridionale du bassin du Bas-Chelif Algerie. Comptes Rendus - Academie des Sciences Serie II 315, 1365–1372.

Saint Martin, J.P., Cornée, J.J., 1996. The Messinian reef complex of Melilla, northeastern Rif, Morocco: Models for carbonate stratigraphy from Miocene reef complexes of Mediterranean regions. SEPM Concepts in Sedimentology and Paleontology 5, 227–237.

Sánchez-Almazo, I.M., 1999. Evolucíon paleoambiental de las Cuencas Neogenas de Almería en el Messiniense. PhD thesis. Univ. Granada, Spain, unpublished, 427 pp.

Sánchez-Almazo, I. M., Spiro, B., Braga, J.C., Martín, J.M., 2001. Constraints of stable isotope signatures on the depositional paleoenvironments of upper Miocene reef and temperate carbon- ates in the Sorbas Basin, SE Spain. Paleogeogr. Paleoclimatol. Paleoecol. 175, 153–172.

Sandstrom, H., Elliott, J.A., 1984. Internal tidae and solitons on the Scotian shelf: A nutrient pump at work. J. Geophys. Res. 89, 6415–6426.

Santarelli, A., Brinkhuis, H., Hilgen, F.J., Lourens, L.J., Versteegh, G.J.M., Visscher, H., 1998. Orbital signatures in a Late Miocene dinoflagellate record from Crete (Greece). Mar Micropaleontol 33, 273–297.

Sarkar, S., Singh, Y.P., Verma, P., 2024. Paleoecological and paleobiogeographic implications of a seagrass-indicating foralgal skeletal assemblage: Retracing the Burdigalian Quilon Limestone (Kerala Basin, SW India). Mar. Micropaleont. 187, 102-330.

Searle, D.F., Flood, P.G., 1988. *Halimeda* bioherms of the Swains reefs – southern Great Barrier Reef. 6th International Coral Reef Symposium 3, 139–144.

Seidel, E., Okrusch, M., Kreuzer, H., Raschka, H., Harre, W., 1981. Eo-alpine metamorphism in the uppermost unit of the Cretan nappe system, petrology and geochronology: part 2. Synopsis ofhigh temperaturemetamorphics and associatedophiolites. Contrib. Mineral. Petrol. 76, 351–361.

Schlager, W., Purkis, S., 2015. Reticulate reef patterns – antecedent karst versus self-organization. Sedimentology 62, 501–515.

Schlüter, M., Steuber, T., Parente, M., 2008. Chronostratigraphy of Campanian-Maastrichtian platform carbonates and rudist associations of Salento (Apulia, Italy). Cretac. Res. 29, 100–114.

Sierro, F.J., Flores, J.A., Civis, J., Gonzalez-Delgado, J.A., Frances, G., 1993. Late Miocene globorotaliid event- stratigraphy and biogeography in the NE-Atlantic and Mediterranean. Mar. Micropaleontol., 21, 143-168.

Smith, S.V., Kinsey, D.W., 1976. Calcium carbonate production, coral reef growth and sea level change. Science 194, 937–939.

Smith, J.E., Smith, C.M., Vroom, P.S., Beach, K.L., Miller, S., Buckley, J., Cooper, C., Rutten, O., Smith, M., Lounsbury, R., Florrent, M., Styron, J., Dunbar, T., Hulsbeck, M., Kessling, D., 2004. Nutrient and growth dynamics of *Halimeda tuna* on Conch Reef, Florida Keys: Possible influence of internal tides on nutrient status and physiology immense support of the entire NURC staff, including. Limn. Oceanogr. 49, 1923–1936.

Spakman, W., Wortel, R., 2004. A Tomographic View on Western Mediterranean Geodynamics. In: Cavazza, W., Roure, F., Spakman, W., Stampfli, G.M. and Ziegler, P. Eds., The TRANSMED Atlas, The Mediterranean Region from Crust to Mantle. Springer-Verlag, Berlin-Heidelberg, Berlin, 31-52.

Spalluto, L., Caffau, M., 2010. Stratigraphy of the mid-Cretaceous shallow-water limestones of the Apulia carbonate platform (Murge, Apulia, southern Italy). Ital. J. Geosci. 129, 335–352.

Stanley, S. M., Ries, J.B., Hardie, L.A., 2010. Increasing production of calcite and slower growth for the major sediment-producing alga *Halimeda* as the mg/Ca ratio of seawater is lowered to a “calcite sea” level. J. of Sed. Res. 80, 6-16.

Stokes, M.D., Leichter, J.J., Wing, S.R., 2020. Spatial variations in the stable isotope composition of the benthic algae, *Halimeda tuna*, and implications for paleothermometry. Scientific Reports 10, 1–14.

Szilagyi, Z., Husdell, M., Chua, K., Behrens, B., Zeng, Y., Borghi, S., Clements, M., Webb, M., s.d. Halo : Halimeda Bioherm Origins , Function , and Fate in the Northern Great Barrier Reef 12–16.

Takayanagi, H., Iryu, Y., Yamada, T., Oda, M., Yamamoto, K., Sato, T., Chiyonobu, S., Nishimura, A., Nakazawa, T., Shiokawa, S., 2007. Carbonate deposits on submerged seamounts in the northwestern Pacific Ocean. Island Arc 16, 394–419.

Tancredi, S., Margiotta, S., Grasso, S., Tentori, D., Milli, S., 2022. Depositional setting, paleogeography, and sequence stratigraphy of the Salento Peninsula from the Paleogene to the Pleistocene. J. Mediterr. Earth Sci. 14, 47–93.

Tella, T. O., Winterleitner, G., Morsilli, M., & Mutti, M. (2022). Testing sea-level and carbonate production effects on stratal architecture of a distally steepened carbonate ramp (Upper Miocene, Menorca): A 3D forward modelling approach. *Sedimentary Geology, 441*, 106267.

ten Veen, J.H., Postma, A., G., 1999. Neogene tectonics and basin fill patterns in the Hellenic outer arc (Crete, Greece). Basin Research 11, 223-242.

ten Veen, J.H., Kleinspehn, K.L., 2003. Incipient continental collision and plate-boundary curvature: late Pliocene–Holocene transtensional Hellenic forearc, Crete, Greece, J. Geol. Soc. Lond. 160, 161–181.

Teofilo, G., Antoncecchi, I., Caputo, R., 2018. Neogene-Quaternary evolution of the offshore sector of the Southern Apennines accretionary wedge, Gulf of Taranto, Italy. Tectonophysics v. 738–739, 16-32.

Tozzi, M., 1993. Assetto tettonico dell'Avampaese Apulo meridionale (Murge meridionali - Salento) sulla base dei dati strutturali. Geologica Romana 29, 95-11.

Tondi, E., Piccardi, L., Cacon, S., Kontny, B. and Cello, G. (2005) Structural and time constraints for dextral shear along the seismogenic Mattinata Fault (Gargano, southern Italy). J. Geodynamics, 40, 134–152.

Tropeano, M., Spalluto, L., Meloni, D., Moretti, M., Sabato, L., 2022. 'Isolated base-of-slope aprons': An oxymoron for shallow-marine fan-shaped, temperate-water, carbonate bodies along the south-east Salento escarpment (Pleistocene, Apulia, southern Italy). Sedimentology 69, 345-371.

van Hinsbergen, D.J.J., Meulenkamp, J.E., 2006. Neogene supradetachment basin development on Crete (Greece) during exhumation of the South Aegean core complex. Basin Res. 18, 103–124.

Vasiliev, I., Karakitsios, V., Bouloubassi, I., Agiadi, K., Kontakiotis, G., Antonarakou, A., Triantaphyllou, M., Gogou, A., Kafousia, N., de Rafélis, M., Zarkogiannis, S., Kaczmar, F., Parinos, C., Pasadakis, N., 2019. Large Sea Surface Temperature, Salinity, and Productivity-Preservation Changes Preceding the Onset of the Messinian Salinity Crisis in the Eastern Mediterranean Sea. Paleoceanogr. Paleoclimatology 34, 182–202.

Vertino, A., Stolarski, J., Bosellini, F.R., Taviani, M., 2014. Mediterranean Corals Through Time: From Miocene to Present, The Mediterranean Sea: Its History and Present Challenges. Springer Netherlands, Dordrecht.

Vescogni, A., 2000. Evoluzione delle costruzioni a vermetidi e loro utilizzo come “markers” paleobatimetrici e paleoclimatici. Giornale di Geologia 62, 55-61.

Vescogni, A., Bosellini, F.R., Reuter, M., Brachert, T.C., 2008. Vermetid reefs and their use as palaeobathymetric markers: New insights from the Late Miocene of the Mediterranean (Southern Italy, Crete). Palaeogeogr. Palaeoclimatol. Palaeoecol. 267, 89–101.

Vescogni, A., Vertino, A., Bosellini, F.R., Harzhauser, M., Mandic, O., 2018. New paleoenvironmental insights on the Miocene condensed phosphatic layer of Salento (southern Italy) unlocked by the coral-mollusc fossil archive. Facies 64, 7.

Vescogni, A., Guido, A., Cipriani, A., Gennari, R., Lugli, F., Lugli, S., Manzi, V., Reghizzi, M., Roveri., M. 2022. Paleoenvironmental settings and depositional model of Upper Messinian microbialites of the Salento Peninsula (Southern Italy): a central Mediterranean terminal carbonate complex. Paleogeography, Paleoclimatology, Paleoecology 595, 110-970.

Voelk H.R. and Rondeel H.E., 1964. Zur gliederung des Jung-tertiaers in becken von Vera, Suedost Spanien. Geol. Mijnbouw 43, 310-315.

Volpi, V., Accettella, D., Cuppari, A., 2011. Morphological features of the Apennines foreland/accretionary-wedge boundary in the Ionian Sea. Mar. Geophys. Res. 32, 481–492.

Volpi V., Del Ben A., Civile D., Zgur F., 2017. Neogene tectono-sedimentary interaction between the calabrian accretionary wedge and the apulian foreland in the northern Ionian Sea. Marine Petroleum Geology 83, 246-260.

Webb, S.D., Rind, D.H., Lehman, S.J., Healy, R.J., Sigman, D., 1997. Influence of ocean heat transport on the climate of the last glacial maximum. Nature 385, 695-699.

Webster, J.M., Beaman, R.J., Puga-Bernabéu, Á., Ludman, D., Renema, W., Wust, R.A.J., George, N.P.J., Reimer, P.J., Jacobsen, G.E., Moss, P., 2012. Late Pleistocene history of turbidite sedimentation in a sub- marine canyon off the northern Great Barrier Reef, Australia. Palaeogeogr Palaeoclimatol Palaeoecol 331-332, 75–89.

Webster, J., McNeil, M., Bostock, H., Nothdurft, L., Byrne, M., 2023. Making Sense of the Great Barrier Reef's Mysterious Green Donuts. Eos (Washington. DC). 104. https://doi.org/10.1029/2023eo230079.

Wei, Z., Zhang, Y., Yang, F., Long, L., 2022. Diurnal fluctuations in seawater pCO2 amplify the negative effects of ocean acidification on the biotic performance of the calcifying macroalga *Halimeda opuntia*. Frontiers in Marine Science 9, 1–14.

Weijermars, R., Roep, T.B., Van den Eeckhout, B., Postma, G., Kleverlaan, K., 1985. Uplift history of a Betic fold nappe inferred from Neogene-Quaternary sedimentation and tectonics (in the Sierra Alhamilla and Almeria, Sorbas and Tabernas Basins of the Betic Cordilleras, SE Spain). Geol. Mijnb. 64, 397-411.

Wilbur, K.M., Hillis-Colinvaux, L., Watabe N., 1969. Electron microscope study of calcification in the alga *Halimeda* (Order Siphonales). Phycologia 8, 27-35.

Wizemann, A., Meyer, F.W., Westphal, H., 2014. A new model for the calcification of the green macro-alga *Halimeda opuntia* (Lamouroux). Coral Reefs 33, 951–964.

Wolanski, E., Drew, E., Abel, K.M., O'Brien, J., 1988. Tidal jets, nutrient upwelling, and their influence on the productivity of the alga *Halimeda* in the Ribbon Reefs, Great Barrier Reef. Estuarine, Coastal and Shelf Science 26,169–201.

Wortel, M.J., Spakman, W., 2000. Subduction and slab detachment in the Mediterranean-Carpathian region. Science. 290, 1910-7.

Woodson, C.B., 2018. The Fate and Impact of Internal Waves in Nearshore Ecosystems. Ann. Rev. Mar. Sci. 10, 421–441.

Wray, J. L., 1977. Calcareous algae (Developments in Paleontology and Stratigraphy 4): Amsterdam, Elsevier, 185 p.

Xu, H., Zhao, X., Eberli, G.P., Liu, X., Zhu, Y., Cai, Y., Luo, W., Yan, G., Zhang, B., Wei, K., Shi, J., 2015. Biogenic carbonate formation and sedimentation in the Xisha Islands: evidences from living *Halimeda*. Acta Oceanologica Sinica 34, 62–73.

Zachariasse, W.J., van Hinsbergen, D.J.J., Fortuin, A.R., 2008. Mass wasting and uplift on Crete and Karpathos during the early Pliocene related to initiation of south Aegean left-lateral, strike-slip tectonics. GSA Bull. 120, 976–993.

Zachariasse, W.J., van Hinsbergen, D.J.J., Fortuin, A.R., 2011. Formation and fragmentation of a late Miocene supradetachment basin in central Crete: implications for exhumation mechanisms of high-pressure rocks in the Aegean forearc, Basin Res. 23, 678–701.

Acknowledgements

First and foremost, I am profoundly indebted to my supervisor, Professor Michele Morsilli, for his invaluable guidance and exceptional mentorship. His expertise, critical insights, and encouragement have been instrumental in shaping my research and academic growth. I am also deeply grateful for his patience and for the fantastic fieldwork across the Mediterranean, which was fundamental to this thesis. Above all, I thank him for immersing me, with the same passion he has always shown, in the fascinating world of carbonates.

Furthermore, I sincerely appreciate the external reviewers for their constructive feedback and evaluation of my work, which significantly improved the overall quality of this thesis.

A special thank you goes to Professor Piero Gianolla, whose humanity, and invaluable moments, when during breaks from the Messinian, he would share his knowledge of the Triassic with me, greatly enriched my understanding and experience.

I am grateful to all those who have contributed to the research in the area of my birthplace. Their invaluable dedication has been crucial in adding key pieces to this work.

Lastly, my sincere thanks go to all those who, in various ways, have accompanied me throughout this journey, offering their unwavering support and encouragement.